School of Medicine

Division of Cancer and Stem Cells

DNA repair Research Group

MRE11-RAD50-NBS1 COMPLEX BLOCKADE TO REVERSE PLATINUM RESISTANCE AND INDUCE SYNTHETIC LETHALITY IN EPITHELIAL OVARIAN CANCERS

Adel Alblihy, BSc., MSc.

Thesis submitted at University of Nottingham for degree of Doctor of Philosophy.

March 2020

DECLARATION OF AUTHENTICITY

I hereby declare that the work presented in this thesis is my own and has not been submitted previously for a higher degree to any other university.

ABSTRACT

Resistance to platinum drugs (carboplatin, cisplatin) negatively impacts patients' outcomes in ovarian cancer. Platinum-based chemotherapy cause intra-strand and inter-strand DNA adducts, which contribute to DSBs during replication. Proficient DNA repair is a critical mechanism that leads to resistance to platinating agents. Targeting DNA repair proteins is a promising strategy for ovarian cancer personalization therapy. The MRE11-RAD50-NBS1 (MRN) complex is a 'first responder' to DNA damage and is critical for repair of double strand breaks (DSBs) and stalled replication forks. Here we show that MRE11, RAD50 and NBS1 overexpression at the transcriptional and protein level is linked to poor survival outcomes in ovarian cancer patients treated with platinum chemotherapy. Pre-clinically, MRE11, RAD50 and NBS1 depletion promoted platinum sensitivity in ovarian resistance cell lines. Increased sensitivity was associated with accumulation of DSBs, cell cycle arrest and apoptosis. Mirin, a small molecular inhibitor of the 3' to 5' exonuclease activity of MRE11 was increased platinum sensitivity in ovarian resistance cell lines, was correlated with increased DSB accumulation, cell cycle arrest and apoptotic cells. Mirin was also synthetically lethal in BRCA2-deficient or XRCC1-deficient ovarian cancer cells including in 3D-spheroid models as evidenced by DSB accumulation, cell cycle arrest and increased apoptotic cells. We

generated a mirin resistant BRCA2-deficient PEO1R cell line which is cross-resistant to cisplatin and Olaparib (PARP inhibitor) including 3D-spheroid models. PEO1R cells have not restored BRCA2 protein expression but inactivated 53BP1 and activated DSB repair through upregulation of MRE11 and other components of HR, NER and MMR pathways at mRNA and protein levels. Interestingly, PEO1R cells also overexpressed OCT4 transcription factor which physically interacted with MRE11 promoting an aggressive cancer stem cell-like phenotype (characterised by overexpression of CD44, OCT4 & ZEB1), increased proliferation, spheroid formation, invasion, epithelial-to-mesenchymal transition (EMT), enhanced DNA repair expression and reduced apoptosis and increased tumorigenicity in mice xenograft models.

We conclude that MRE11, RAD50 and NBS1 are key predictive biomarkers in ovarian cancer, MRE11 is involved in cancer stem cell regulation and MRE11 targeting may be suitable for clinical application in DNA repair deficient ovarian cancers.

Key words: ovarian cancer; MRN complex; Mirin; platinum sensitization; synthetic lethality; stem cells; EMT.

PhD PUBLICATIONS

1. **ALBLIHY, A.**, MESQUITA, K. A., SADIQ, M. T. & MADHUSUDAN, S. 2019. Development and implementation of precision therapies targeting base-excision DNA repair in BRCA1-associated tumors. *Expert Review of Precision Medicine and Drug Development,* 4**,** 11-25.

2. ALI, R., ALABDULLAH, M., **ALBLIHY, A.**, MILIGY, I., MESQUITA, K. A., CHAN, S. Y., MOSELEY, P., RAKHA, E. A. & MADHUSUDAN, S. 2019. PARP1 blockade is synthetically lethal in XRCC1 deficient sporadic epithelial ovarian cancers. *Cancer Lett.*

3. MESQUITA, K. A., ALABDULLAH, M., GRIFFIN, M., TOSS, M. S., FATAH, T., **ALBLIHY, A.**, MOSELEY, P., CHAN, S. Y. T., RAKHA, E. A. & MADHUSUDAN, S. 2019. ERCC1-XPF deficiency is a predictor of olaparib induced synthetic lethality and platinum sensitivity in epithelial ovarian cancers. *Gynecol Oncol*, 153, 416-424.

4. ALI, R., **ALBLIHY, A.**, MILIGY, I., ALABDULLAH, M., TOSS, M S., FATAH, T., MOSELEY, P., CHAN, S. Y. T., RAKHA, E. A. & MADHUSUDAN, S. 2020. Targeting DNA polymerase β for platinum sensitization and synthetic lethality in epithelial ovarian cancers. SUBMITED IN ONCOGENE.

5. MESQUITA, K. A., ALI, R., DOHERTY, R., **ALBLIHY, A.**, TOSS, M., DORJSUREN, D., SIMEONOV, A., JADHAV, A., WILSON III, D., HICKSON, I., TATUM, N., RAKHA, E. A. & MADHUSUDAN, S.2020. Flap endonuclease 1 blockade for platinum chemo-sensitization and synthetic lethality in epithelial ovarian cancers. SUBMITED IN CELL REPORTS MEDICIENE.
6. ALI, R., **ALBLIHY, A.**, TOSS, M., RAKHA, E. A. & MADHUSUDAN, S. 2020. Targeting ATR, ATM and Wee1 either alone or in combination with PARP inhibitor Olaparib in XRCC1 deficient breast cancers. ACCEPTED AT BRITISH JOURNAL OF CANCER.
7. **ALBLIHY, A.**, ALI, R., RITCHIE, A., ALABDULLAH, M., TOSS, M., ALGETHAMI, M., MESQUITA, K. A., ORDONEZ-MORAN, P., ALLEGRUCCI, C., GRABOWSKA, A., RAKHA, E. A. & MADHUSUDAN, S. 2020. MRE11 has a role in cancer stem cell regulation and is a target for synthetic lethality in epithelial ovarian cancers. MANUSCRIPT.
8. **ALBLIHY, A.,** TOSS, M., ALABDULLAH, M., RAKHA, E. A. & MADHUSUDAN, S. 2020. Molecular disruption of NBS1 sensitized ovarian cancer cells to cisplatin-based chemotherapy. MANUSCRIPT.
9. **ALBLIHY, A.,** TOSS, M., ALABDULLAH, M., RAKHA, E. A. & MADHUSUDAN, S. 2020. Molecular disruption of RAD50

sensitized ovarian cancer cells to cisplatin-based chemotherapy. MANUSCRIPT.

ORAL AND POSTER PRESENTATIONS

1. **ALBLIHY, A.,** RAKHA, E. A. & MADHUSUDAN, S. Targeting MRN complex in ovarian cancer. Division of Cancer and Stem Cells Spring Meeting. Poster presentation. 2nd May 2017 (Nottingham).
2. **ALBLIHY, A.,** FATAH, T., RAKHA, E. A. & MADHUSUDAN, S. Targeting MRN complex in breast cancer. Nottingham breast cancer research centre. Oral presentation. 26 March 2018.
3. **ALBLIHY, A.,** TOSS, M., ALI, R., ALABDULLAH, M., RAKHA, E. A. & MADHUSUDAN, S. Clinicopathological and functional significance of meiotic recombination 11 (MRE11) in epithelial ovarian cancers: a target validation study. Poster presentation. NCRI, 2018.
4. ALABDULLAH, M., **ALBLIHY, A.,** ALI, R., MOSELEY, P., CHAN, S. Y. T., RAKHA, E. A. & MADHUSUDAN, S. Clinicopathological significance of ligase I, III & IV in Epithelial Ovarian Cancers. Poster presentation. NCRI, 2018.
5. ALABDULLAH, M., **ALBLIHY, A.,** ALI, R., MOSELEY, P., CHAN, S. Y. T., RAKHA, E. A. & MADHUSUDAN, S. Clinical and

outcome significance of positive AKT expression in epithelial ovarian cancer. Poster presentation. NCRI, 2018.

ACKNOWLEDGMENTS AND DEDICATION

I would like first to thank Allah for giving me the blessing to complete my PhD journey.

I would like to express my deepest appreciation to my supervisor Prof. Srinivasan Madhusudan for the inspiring guidance, support, invaluable comments throughout this project.

I also would like to thank the following people who have contributed in this project. Prof. Emad Rakha group for their contributions in clinical studies, Prof. Anna Grabowska and Alison Ritchie for their contributions in *in vivo* tumorigenicity studies and Dr. Cinzia Allegrucci for her contribution in EMT studies.

I also would like to thank my sponsor Kind Fahad Security College, Riyadh, Saudi Arabia for their generous funding and support.

I also would like to thank my friend Faris Alrumaihi for his support during my PhD journey.

Special thanks to Latifa (my mother), my wife Rana, my kids Yazn and Marh for the endless love, trust, support whenever I needed. Love you all.

TABLE OF CONTENTS

DECLARATION OF AUTHENTICITY i

ABSTRACT ii

PhD PUBLICATIONS iv

ORAL AND POSTER PRESENTATIONS vi

TABLE OF CONTENTS ix

LIST OF FIGURES xx

LIST OF TABLES xxxiii

LIST OF ABBREVIATIONS xxxiv

1. INTRODUCTION 2

1.1 OVARIAN CANCER 2

1.2 STAGING OF OVARIAN CANCER 4

1.3 PATHOLOGY OF OVARIAN CANCER 5

1.3.1 SEROUS CARCINOMA 7

1.3.1.1 HIGH GRADE SEROUS CARCINOMA 7

1.3.1.2 LOW GRADE SEROUS CARCINOMA 8

1.3.1.3 ENDOMETRIOID CARCINOMA 9

1.3.1.4 MUCINOUS CARCINOMAS 10

1.3.1.5 CLEAR CELL CARCINOMA 11

1.4 OVARIAN CANCER TREATMENT 12

1.4.1 SURGERY 12

1.4.2 CHEMOTHERAPY 13

1.5 RESISTANCE TO CHEMOTHERAPY 14

1.5.1 DECREASED DRUG ACCUMULATION 15

1.5.2 INCREASED DRUG INACTIVATION 16

1.5.3 EVASION OF APOPTOSIS 17

1.5.4 CHANGES IN SIGNALLING PATHWAYS 19

1.5.5 EPITHELIAL-MESENCHYMAL TRANSITION 22

1.5.6 CANCER STEM CELLS 23

1.5.7 INCREASED DNA REPAIR 24

1.5.7.1 DNA DAMAGE RESPONSE (DDR) 24

1.5.7.2 DNA REPAIR PATHWAYS 28

1.5.7.2.1 DIRECT REPAIR 29

1.5.7.2.2 BASE EXCISION REPAIR 30

1.5.7.2.3 MISMATCH REPAIR 32

1.5.7.2.4 NUCLEOTIDE EXCISION REPAIR 34

1.5.7.2.5 DOUBLE STRAND BREAKS REPAIR 38

1.6 TREATMENT OF RECURRENT DISEASES 49

1.6.1 TARGETED THERAPY 51

1.7 THE SELECTION OF DSBs REPAIR PATHWAY 56

1.8 THE MRN COMPLEX 59

1.8.1 STRUCTURE AND FUNCTION OF MRN COMPLEX 60

1.8.1.1 MRE11 60

1.8.1.2 RAD50 62

1.8.1.3 NBS1 63

1.8.2 THE ROLE OF MRN COMPLEX IN DDR 65

1.8.3 THE ROLE OF MRN COMPLEX IN DSB REPAIR 67

1.9 PROJECT RATIONALE AND HYPOTHESIS 72

1.10 PROJECT AIMS 73

2. MATERIAL AND METHOD 76

2.1 MATERIALS: 76

2.1.1 COMPOUNDS: 76

2.1.2 CELL LINES: 76

2.2 METHODS: 78

2.2.1 CLINICAL STUDY: 78

2.2.1.1 THE CONSTRUCTION OF TISSUE MICROARRAY 81

2.2.1.2 IMMUNOHISTOCHEMSTRY: 82

2.2.1.2.1 NOVOLINK DETECTION PROTOCOL FOR IMMUNOHISTOCHEMICAL ANTIBODY IDENTIFICATION..... 82

2.2.1.2.2 PRIMARY ANTIBODIES OPTIMISATION 84

2.2.1.2.3 IMMUNOHISTOCHEMICAL SCORING 86

2.2.1.2.4 STATISTICAL ANALYSIS 86

2.2.1.3 *MRE11*, *RAD50* AND *NBS1* TRANSCRIPT IN OVARIAN CANCER 89

2.2.2 PRE-CLINICAL STUDIES: 90

2.2.2.1 SUBCULTURING CELL LINES 90

2.2.2.2 CRYOPRESERVATION OF CELL LINES.....90

2.2.2.3 CELL LYSATE PREPARATION.....91

2.2.2.4 PROTEIN QUANTIFICATION.....91

2.2.2.5 WESTERN BLOT 92

2.2.2.5.1 SEPARATION OF PROTEINS 93

2.2.2.5.2 TRANSFER PROTIENS 93

2.2.2.5.3 BLOCKING..... 94

2.2.2.5.4 PRIMARY ANTIBODY INCUBATION 94

2.2.2.5.5 SECONDARY ANTIBODY INCUBATION 96

2.2.2.5.6 DETECTION AND ANALYSIS 96

2.2.2.6 TRANSIENT KNOCKDOWN OF MRN COMPLEX.....97

2.2.2.7 GENERATION OF XRCC1-KNOCKOUT USING CRISPR CAS-9…….. 98

2.2.2.8 CELL PROLIFERATION ASSAY 99

2.2.2.9 CLONOGENIC SURVIVAL ASSAY 100

2.2.2.9.1 PLATTING EFFICIENCY 100

2.2.2.9.2 CLONOGEINC ASSAY 101

2.2.2.10 FUNCTIONAL STUDIES..... 102

2.2.2.10.1 γH2AX ASSAY AND CELL CYCLE ANALYSIS....102

2.2.2.10.2 APOPTOSIS DETECTION 105

2.2.2.11 NUCLEAR AND CYTOPLASMIC EXTRACTION 107

2.2.2.12 DEVELOPMENT OF A MIRIN-RESISTANT CELL LINE 108

2.2.2.13 IMMUNOFLURESCENCE STAINING 108

2.2.2.14 SPHERES 110

2.2.2.15 INVASION ASSAY 111

2.2.2.16 DNA REPAIR GENE EXPRESSION PROFILING 113

2.2.2.16.1 RNA EXTRACTION 113

2.2.2.16.2 THE SYNTHESIS OF cDNA 114

2.2.2.16.3 RT^2 PROFILER^{TM} DNA REPAIR PCR ARRAY 115

2.2.2.16.4 QUANTITATIVE REAL TIME PCR 116

2.2.2.16.5 DATA ANALYSIS 118

2.2.2.17 IMMUNOPRECIPITATION 118

2.2.2.18 STABILITY PROTIEN 119

2.2.2.19 HA UBIQUITINATION ASSAY 119

2.2.2.20 TUMOUR XENOGRAFT STUDIES 120

2.2.2.21 STATISITCAL ANALYSIS 121

3. MRE11 BLOOKADE FOR PLATINUM CHEMO-SENSITIZATION IN EOC 124

3.1 INTRODUCTION 124

3.2 MRE11 INHIBITOR 124

3.3 CHAPTER AIMS 125

3.4 RESULTS 126

3.4.1 CLINICAL STUDY 126

3.4.1.1 MRE11 OVEREXPRESSION ASSOCIATES WITH PLATINUM RESISTANT IN EOC 126

3.4.2 PRE-CLINICAL STUDIES 133

3.4.3 THE DEPLETION OF MRE11 ENHANCES THE CHEMO-SENSITIVITY IN OC CELL LINES 133

3.4.4 MRE11 BLOCKADGE BY MIRIN PROMOTES PLATINUM SENSITIVITY 147

3.5 RESULTS SUMMARY 153

3.6 DISCUSSION 154

4. RAD50 BLOCKADE FOR PLATINUM CHEMO-SENSITIZATION IN EOC 161

4.1 INTRODUCTION 161

4.2 CHAPTER AIMS 163

4.3 RESULTS 165

4.3.1 CLINICAL STUDY 165

4.3.1.1 RAD50 OVEREXPRESSION ASSOCIATES WITH PLATINUM RESISTANT IN EOC 165

4.3.2 PRE-CLINICAL STUDIES 172

4.3.2.1 THE DEPLETION OF RAD50 PROMOTES THE CHEMO-SENSITIVITY IN OC CELL LINES 172

4.4 RESULTS SUMMARY 183

4.5 DISCUSSION 185

5. NBS1 BLOCKADE FOR PLATINUM CHEMO-SENSITIZATION IN EPITHELIAL OVARIAN CANCER 190

5.1 INTRODUCTION 190

5.2 CHAPTER AIMS 193

5.3 RESULTS 194

5.3.1 CLINICAL STUDY 194

5.3.1.1 NBS1 OVEREXPRESSION ASSOCIATES WITH PLATINUM RESISTANT IN EOC 194

5.3.2 PRE-CLINICAL STUDIES 201

5.3.2.1 THE DEPLETION OF NBS1 PROMOTES THE CHEMO-SENSITIVITY IN OC CELL LINES 201

5.4 RESULTS SUMMARY 214

5.5 DISCUSSION 215

6. EXPANDING THE SYNTHETIC LETHAL STRATEGY BEYOND PARP INHIBITORS 222

6.1 INTRODUCTION 222

6.2 SYNTHETIC LETHALITY 222

6.3 MIRIN RESISTANT IN PEO1 CELLS 224

6.4 CHAPTER AIMS 226

6.5 RESULTS 228

6.5.1 MIRIN IS SYNTHETICALLY LETHAL IN BRCA2-DEFECIENT CANCER CELLS 228

6.5.2 MIRIN IS SYNTHETICALLY LETHAL IN XRCC1-DEFICIENT CANCER CELLS 239

6.5.3 PEO1R CELLS OVEREXPRESSES MRE11 AND UP-REGULATE SEVERAL DNA REPAIR GENES 247

6.5.4 MRE11 PHYSICALLY INTERACTS WITH AND PROMOTES OCT4 STABILITY 260

6.5.5 THE OVEREXPRESSION OF MRE11-OCT4 ENHANCES A CANCER STEM CELL-LIKE AGGRESSIVE PHENOTYPE 268

6.6 RESULTS SUMMARY 279

6.7 DISCUSSION 281

7. GENERAL DISCUSSION AND FUTURE DIRECTION.....292

7.1 MRN COMPLEX ASSOCIATES WITH PLATINUM RESISTANT IN EOC 294

7.2 MOLECULAR DISRUPTION OF MRN COMPLEX ENHANCES PLATINUM CHEMO-SENSITIVITY IN OC CELL LINES 295

7.3 MRE11 BLOCKADE BY MIRIN INCREASES PLATINUM SENSITIVITY IN OC CELL LINES 296

7.4 MIRIN IS SYNTHETICALLY LETHAL IN BRCA2-DEFICENT CELLS 298

7.5 MIRIN IS SYNTHETICALLY LETHAL IN XRCC1-DEFICENT CELLS 300

7.6 MIRIN-RESISTANT PEO1R CELLS OVEREXPRESS MRE11 AND UPREGULATE SEVERAL DNA REPAIR GENES.....301

7.7 PEO1R CELLS OVEREXPRESS OCT4 AND MANIFEST AN AGGRESSIVE PHENOTYPE WITH CANCER STEM CELL-LIKE FEATURES 302

7.8 STRENGTHS AND WEAKNESSES OF THIS PROJECT 303

7.9 FUTURE DIRECTIONS 304

REFERENCES 299

LIST OF FIGURES

Figure 1.1: Various histopathological subtypes of epithelial ovarian cancer (EOC).. 6

Figure 1.2: Systematic representation of the molecular mechanism of cisplatin resistance. 16

Figure 1.3: Systematic representation of the proliferation signaling pathways. 21

Figure 1.4: Systematic representation of cellular response to DNA damage.. 27

Figure 1.5: Various DNA damaging agents, their effects and the response of DNA repair pathways... 29

Figure 1.6: Systematic representation of base excision repair.. 32

Figure 1.7: Systematic representation of the nucleotide excision repair. 37

Figure 1.8: Classical and alternative NHEJ mechanisms for repairing double strand breaks (DSBs). 44

Figure 1.9: A simplified view of Homologous recombination repair (HR). 47

Figure 1.10: Systematic representation of the concept of synthetic lethality. 53

Figure 1.11: The choice between DSB repair mechanisms. 58

Figure 1.12: Scheme of MRN complex protein domains...... 64

Figure 1.13: Systematic representation of the possible mode of interaction between MRN complex components in DSB site. 65

Figure 1.14: Systematic representation of the role of MRN complex in HR and NHEJ.. 69

Figure 1.15: Systematic representation of the role of MRN complex in replication forks dynamics.. 70

Figure 1.16: Systematic representation of the role of MRN complex in telomere dysfunction.. 71

Figure 2.1: Histogram charts showing the selection of immunohistochemical cut off scores for MRE11 nuclear and cytoplasmic expression........88

Figure 2.2: Histogram charts showing the selection of immunohistochemical cut off scores for RAD50 nuclear and cytoplasmic 88

Figure 2.3: Histogram charts showing the selection of immunohistochemical cut off scores for NBS1 nuclear and cytoplasmic expression........89

Figure 0.4: yH2AX analysis using Weasel softwear. 104

Figure 0.5: Cell cycle analysis using Weasel softwear.....104

Figure 0.6: Annexin V analysis using Weasel softwear.....106

Figure 3.1: Immunohistochemical expression of MRE11 (nuclear and cytoplasmic) in ovarian cancers. 127

Figure 3.2: Kaplan Meier survival curves for MRE11 nuclear expression.. 130

Figure 3.3: Kaplan Meier survival curves for MRE11 cytoplasmic expression.. 131

Figure 3.4: The correlation of MRE11 mRNA expression and PFS and OS survivals...... 132

Figure 3.5: Clonogenic assay showing cisplatin sensitivity in A2780, A2780cis, PEO1 and PEO4. 134

Figure 3.6: Western blot for MRE11 protein levels in A2780, A2780cis, PEO1 and PEO4 cells.. 135

Figure 3.7: Representative western blot of nuclear and cytoplasmic levels of MRE11.. 137

Figure 3.8: The quantification of MRE11 nuclear and cytoplasmic expression levels. 138

Figure 3.9: MRE11 knockdown in A2780cis cells using siRNA. 139

Figure 3.10: Clonogenic assay showing cisplatin sensitivity in A2780cis and MRE11_KD_A2780cis cells. 140

Figure 3.11: Functional studies of A2780cis cells using flow cytometry. 141

Figure 3.12: MRE11 knockdown in PEO4 cells using siRNA. 142

Figure 3.13: Clonogenic assay showing cisplatin sensitivity in PEO4 and MRE11_KD_PEO4 cells. 143

Figure 3.14: Functional studies of PEO4 cells using flow cytometry..... 144

Figure 3.15: MRE11 knockdown in A2780cis cells using a second siRNA construct.. 145

Figure 3.16: Clonogenic assay showing cisplatin sensitivity in A2780cis and MRE11_KD_A2780cis cells.. 146

Figure 3.17: Mirin toxicity in PEO4 cells using MTS Cell proliferation assay.. 148

Figure 3.18: Clonogenic assay showing mirin treatment sensitized A2780cis cells to cisplatin.. 149

Figure 3.19: Functional studies of A2780cis cells using flow cytometry.. 150

Figure 3.20: Clonogenic assay showing mirin treatment sensitized PEO4 cells to cisplatin. 151

Figure 3.21: Functional studies of PEO4 cells by flow cytometry. 152

Figure 4.1: Immunohistochemical expression of RAD50 (nuclear and cytoplasmic) in ovarian cancers.. 166

Figure 4.2: Kaplan Meier survival curves for RAD50 nuclear expression.. 169

Figure 4.3: Kaplan Meier survival curves for RAD50 cytoplasmic expression. 170

Figure 4.4: The correlation of RAD50 mRNA expression and PFS and OS survivals...... 171

Figure 4.5: Western blot for RAD50 protein levels in A2780, A2780cis, PEO1 and PEO4 cells. 172

Figure 4.6: Representative western blot of nuclear and cytoplasmic levels of RAD50. 174

Figure 4.7: The quantification of RAD50 nuclear and cytoplasmic expression levels. 175

Figure 4.8: RAD50 knock down in A2780cis cells using siRNA.. 176

Figure 4.9: Clonogenic assay showing cisplatin sensitivity in A2780cis and RAD50_KD_A2780cis cells.. 177

Figure 4.10: Functional studies of A2780cis cells using flow cytometry.. 178

Figure 4.11: RAD50 knock down in PEO4 cells using siRNA. 179

Figure 4.12: Clonogenic assay showing cisplatin sensitivity in PEO4 and NBS1_KD_PEO4 cells. 180

Figure 4.13: Functional studies of PEO4 cells using flow cytometry.. 181

Figure 4.14: RAD50 knock down in A2780cis cells using a second siRNA construct. 182

Figure 4.15: Clonogenic assay showing cisplatin sensitivity in A2780cis and RAD50_KD_A2780cis cells.. 183

Figure 5.1: Immunohistochemical expression of NBS1 (nuclear and cytoplasmic) in ovarian cancers.. 195

Figure 5.2: Kaplan Meier survival curves for NBS1 nuclear expression. 198

Figure 5.3: Kaplan Meier survival curves for NBS1 cytoplasmic expression.. 199

Figure 5.4: The correlation of NBS1 mRNA expression and PFS and OS survivals.. 200

Figure 5.5: Western blot for NBS1 protein levels in A2780, A2780cis, PEO1 and PEO4 cells.. 202

Figure 5.6: Representative..... 203

Figure 5.7: The quantification of NBS1 nuclear and cytoplasmic expression levels. 204

Figure 5.8: NBS1 knock down in A2780cis cells using siRNA. 205

Figure 5.9: Clonogenic assay showing cisplatin sensitivity in A2780cis and NBS1_KD_A2780cis cells.. 207

Figure 5.10: Functional studies of A2780cis cells using flow cytometry... 208

Figure 5.11: NBS1 knock down in PEO4 cells using siRNA.. 209

Figure 5.12: Clonogenic assay showing cisplatin sensitivity in PEO4 and NBS1_KD_PEO4 cells. 210

Figure 5.13: Functional studies of PEO4 cells using flow cytometry. 211

Figure 5.14: NBS1 knock down in A2780cis cells using a second siRNA construct.. 212

Figure 5.15: Clonogenic assay showing cisplatin sensitivity in A2780cis and NBS1_KD_A2780cis cells.. 213

Figure 6.1: Effects of mirin on PEO1 and PEO4 cells...... 229

Figure 6.2: The percentage of γH2Ax positive cells in mirin-treated PEO1 and PEO4 cells using FACS.. 230

Figure 6.3: Immunofluorescence staining for 53BP1 and γH2AX in PEO1 and PEO4 cells untreated (UT) and treated with mirin (18μMol/L) for 24 hours... 231

Figure 6.4: Functional studies of PEO4 and PEO1 cells using FACS. 232

Figure 6.5: Spheroids of PEO1 and PEO4 cells untreated (UT) and treated with 18μM mirin for 48 hours. 234

Figure 6.6: Effects of mirin on BRAC2-deficient HeLa cells. 235

Figure 6.7: Functional studies of mirin-treated and untreated (UT) control and BRCA2-deficient HeLa cells.. 236

Figure 6.8: Spheroids of HeLa control and BRCA2-deficient HeLa cells untreated (UT) and treated with 18μM mirin for 48 hours. 237

Figure 6.9: Kaplan Meier survival curves for BRCA2 and MRE11 co-expression. 238

Figure 6.10: Mirin sensitivity in XRCC1 knockout cells. 240

Figure 6.11: Functional studies of A2780 control and A2780_XRCC1-KO cells using FACS.. 241

Figure 6.12: Spheroids of A2780 control and A2780_XRCC1-KO cells untreated (UT) and treated with 25μM mirin for 48 hours.. 242

Figure 6.13: Mirin sensitivity of XRCC1-deficient cells. 243

Figure 6.14: Functional studies of HeLa control cells and XRCC1-deificent HeLa cells using FACS. 244

Figure 6.15: Spheroids of HeLa control and XRCC1-deficient HeLa cells untreated (UT) and treated with 25μM mirin for 48 hours. 245

Figure 6.16: Kaplan Meier survival curves for XRCC1 and MRE11 co-expression. 246

Figure 6.17: Clonogenic assays showing sensitivity to mirin and cisplatin in PEO1 and PEO1R cells.. 247

Figure 6.18: Spheroids of PEO1 and PE01R cells untreated (UT) and treated with 18μM mirin or 5μM cisplatin for 48 hours. 248

Figure 6.19: Clonogenic assay for Olaparip sensitivity in PEO1 and PEO1R cells. 249

Figure 6.20: BRCA2 and 53BP1 baseline proteins levels in PEO1 and PEO1R cells. 250

Figure 6.21: Functional studies of mirin-treated PEO1 and PEO1R cells using FACS...... 251

Figure 6.22: Functional studies of cisplatin-treated PEO1 and PEO1R cells using FACS...... 251

Figure 6.23: MRE11 levels in PEO1 and PEO1R cells...... 253

Figure 6.24: RAD50 and NSB1 levels in PEO1 and PEO1R cells.. 254

Figure 6.25: MRE11, RAD50 and NBS1 levels in PEO1R and PEO1R_MRE11_KD cells.. 255

Figure 6.26: Clonogenic assays showing cisplatin and mirin sensitivity in PEO1, PEO1R and PEO1R_MRE11_KD cells.. 257

Figure 6.27: Expression of DNA repair genes.. 258

Figure 6.28: DNA repair protein levels in PEO1 and PEO1R cells. 259

Figure 6.29: Physical interaction between MRE11 and OCT4. 261

Figure 6.30: MRE11 and OCT4 protein levels in PEO1, PEO1R, PEO1R_MRE11-KD and PEO1_scramble cells.. 262

Figure 6.31: MRE11, CD44, RPA1, ATM, PARP1, LIG3 and ERCC1 protein levels in PEO1R and PEO1R_MRE11_KD cells. 263

Figure 6.32: Proteasome mediated OCT4 degradation in PEO1R control and PEO1R_MRE11_KD cells...... 265

Figure 6.33: Ubiquitination assay in PEO1R control and PEO1R_MRE11_KD cells...... 266

Figure 6.34: Kaplan Meier survival curve for OCT4 and MRE11 co-expression.. 267

Figure 6.35: SOX2, ALDH1, NANG, CD44 and OCT4 protein levels in PEO1 and PEO1R cells. 269

Figure 6.36: FACS analysis of CD44 expression in PEO1 and PEO1R cells. 270

Figure 6.37: Immunofluorescence staining for OCT4 in PEO1 and PEO1R cells. 270

Figure 6.38: Proliferation capacity of PEO1 and PEOR cells. 272

Figure 6.39: Representative photomicrographic images of PEO1 and PEO1R spheroids. 272

Figure 6.40: PEO1 and PEO1R Morphology...... 273

Figure 6.41: Invasion assay showing of PEO1 and PEO1R cells. 273

Figure 6.42: E-cadherin and N-cadherin levels in PEO1 and PEO1R cells...... 274

Figure 6.43: Gene expression analysis of EMT markers assessed by RT-PCR. 275

Figure 6.44: PEO1 and PEO1R tumors in immunodeficient mice. 277

Figure 6.45: Gene expression analysis of E-cadherin, Vimentin, ZEB1 and OCT4 assessed by RT-PCR.. 278

LIST OF TABLES

Table 1.1 Second-line systemic treatment for OC. 51

Table 1.2 DNA repair inhibitors in clinical trials. 55

Table 2.1: Cell lines and culture media. 77

Table 2.2: Patient demographics and pathological characteristics in EOC. 79

Table 2.3: Antibodies for Immunohistochemistry. 84

Table 2.4: Primary antibodies for western blot. 95

Table 2.5: Antibodies for immunofluorescence staining. .. 110

Table 2.6: PCR reaction mix. 115

Table 2.7: RT-QPCR reaction mix. 117

Table 3.1: The association between MRE11 expression and clinicopathological variables in EOC. 129

Table 4.1 The association between RAD50 expression and clinicopathological variables in EOC. 168

Table 5.1: The association between NBS1 expression and clinicopathological variables in EOC. 197

LIST OF ABBREVIATIONS

14-3-3	A family of homologous proteins that contain seven isoforms	C-NHEJ	Classical non-homologous end-joining
ACTION	Adjuvant Cytotoxic Chemotherapy in Older Women	CTIP	C-terminal binding protein interacting protein
ALDHA1	Aldehyde dehydrogenase 1 family, member A1	DNA2	DNA Replication Helicase/Nuclease 2
Alt-NHEJ	Alternative pathway of non-homologous end-joining	DNAase 2	Deoxyribonuclease-2-alpha
APE1	Apurinic/apyrimidinic (AP) endonuclease 1	DNA-PKcs	DNA-dependent protein kinase
ART1	ADP-Ribosyltransferase 1	E2F1	Retinoblastoma-Binding Protein 3
ART2	ADP-Ribosyltransferase 2	E-cadherin	Epithelial-calcium-dependent adhesion
ATLD	Ataxia Telangiectasia like disorder	ERCC1	Excision Repair Cross-Complementation Group 1
ATM	Ataxia telangiectasia mutated	ERK	Extracellular-signal-regulated kinase
ATR	ATM related kinase	EXO1	Exo1 exonuclease 1
AURELIA	A Study of Bevacizumab Added to Chemotherapy in Platinum-resistant Ovarian Cancer patients	FA pathway	Fanconi anaemia pathway
BAD	BCL2 associated agonist of cell death	FEN1	Flap Structure-Specific Endonuclease 1
BARD	BRCA1-associated RING domain protein	FKHR	Forkhead protein FKHR
BER	Base excision repair	GAPDH	Glyceraldehyde 3-phosphate dehydrogenase
BLM	Bloom syndrome protein	GSH	Glutathione
BRAF	B-Raf proto-oncogene serine/threonine kinase	GSK3B	Glycogen synthase kinase 3 beta
BRCA1	Breast cancer susceptibility gene 1	HBOC	hereditary breast-ovarian cancer syndrome
BRCA2	Breast cancer susceptibility gene 2	HER 2	Human epidermal growth factor receptor 2
CDC25	cell division cycle 25	HISTON H1	One of the histone protein families
CDK	Cyclin-dependent kinases	HNOCC	hereditary nonpolyposis colorectal cancer
CHK1	Checkpoint kinase 1	HNFIB	Hepatocyte Nuclear Factor-1 Beta
CHK2	Checkpoint kinase 2	HR	Homologous recombination
CK7	Cytokeratin 7	ICON1 1	International Collaborative Ovarian Neoplasm trial
CK20	Cytokeratin 20	IR	Ionizing radiation
C-MYC	Master Regulator of Cell Cycle Entry and Proliferative Metabolism	KD	Kilodalton

KRUS	Ki-ras2 Kirsten rat sarcoma viral oncogene homolog	PNKP	Polynucleotide Kinase 3'-Phosphatase
KU70	X-ray repair complementing defective repair in Chinese hamster cells	RAD50	DNA repair protein
KU80	X-ray repair complementing defective repair in Chinese hamster cells	RAD51	RAD51 homolog (S. cerevisiae)
LIG1	DNA Ligase 1	RAD51B	RAD51 paralog B
LIG3	DNA Ligase 3	RAD51C	RAD51 paralog C
LIG4	DNA Ligase 4	RAD52	RAD52 homolog (S. cerevisiae)
MAPK	Mitogen-activated protein kinase	RAF	Rapidly Accelerated Fibrosarcoma
MEK	Mitogen-activated protein kinase	RAP1	Ras-proximate-1 or Ras-related protein 1
MDR	Multiple drug resistant	RPA1	Replication protein A1
MDM2	Mouse double minute 2 homolog	RFC	Reconstitution of recombinant human replication factor C
MLH1	MutL protein homolog 1	RNAP1	RNA polymerase 1
MRE11	Meiotic recombination 11 homolog A	SLUG	Zinc finger transcriptional factor
MSH2	MutS homolog 2	SNAIL	A family of transcriptional factors
MSH6	MutS homolog 6	SMC	Structural maintenance of chromosome
MMGMT	O(6)-Methylguanine-DNA methyltransferases	SOX2	Sex determining region Y-box 2
MOTR	Mammalian target of rapamycin	TARF1	Telomeric Repeat Factor 1
NBS1	Nijmegen Breakage Syndrome 1	TARF2	Telomeric Repeat Factor 2
NER	Nucleotide excision repair	TBS	Tris Buffered Saline
N-cadherin	Neural- calcium-dependent adhesion	TDT	Terminal deoxynucleotidyl transferase
OCT4	octamer-binding transcription factor	TDP1	Tyrosyl-DNA phosphodiesterase 1
P16	Tumour suppressor protein	TIN2	TERF1-interacting nuclear factor 2
PALB2	Partner and localizer of BRCA2	TP53	Tumour protein p53
PARP1	Poly [ADP-ribose] polymerase 1	TPP1	Tripeptidyl Peptidase 1
PAX8	Paired box gene 8	TWIST1	Twist-related protein 1transcriptional factor
PCNA	Proliferating cell nuclear antigen	TWIST2	Twist-related protein 2
PI3K	Phosphoinositide 3-kinases	XPG	Xeroderma Pigmentosum Complementation Group G
PI3KCB	Phosphatidylinositol-4,5-bisphosphate 3-kinase catalytic subunit beta	WNT	A group of signal transduction pathways
POLB	DNA polymerase beta	WT1	Wilms tumour protein

POT1	Protection of telomeres 1	XLF	XRCC4-like factor
XPA	DNA repair protein complementing XP-A	XRCC2	X-ray repair complementing defective repair in Chinese hamster cells 2
XPD	Xeroderma pigmentosum D	XRCC3	X-ray repair complementing defective repair in Chinese hamster cells 3
XPG	Xeroderma Pigmentosum Complementation Group G	ZEB1	Zinc finger E-box-binding homeobox 1
XRCC1	X-ray repair complementing defective repair in Chinese hamster cells 2	ZEB2	Zinc finger E-box-binding homeobox 2

CH 1

INTRODUCTION



1. INTRODUCTION

1.1 OVARIAN CANCER

Ovarian cancer (OC) is one of the main gynecologic cancers that comes the third after cervical and uterine cancers. OC has the worst prognosis and the highest mortality rate (Momenimovahed et al., 2019). In 2018 alone, there were 22,240 cases of OC diagnosed and 14,070 OC deaths in the United States (USA) (Siegel et al., 2018). In the United Kingdom (UK), between 2014 until 2016, there were 7,470 cases of OC every year, and 4,116 OC deaths in 2017 in the UK (Cancer Research UK, 2019). The lifetime risk of developing OC among women worldwide is 1.3%, and their rate of mortality due to the disease is 1 in 100 (Reid et al., 2017). The exact cause of OC is unknown, but there are some risk factors that may increase the chances of developing OC, such as increased age. Most cases of OC occur after menopause and half of all OC cases are in women of age greater than 63 years (Moorman et al., 2008). Pregnancy was found to decrease the risk of OC by 30%-60% compare to that for nulliparous women, and each additional pregnancy reduce the risk by an additional 15% (Reid et al., 2017). Moreover, there is a strong protective correlation between the use of oral contraceptive pills and OC risk. Pregnancy and oral contraceptives as factors reducing the

risk of OC support the notion that the risk of OC is related to ovulation, with inhibition of ovulation decreasing the incidence of OC (Treviño et al., 2012).

Family history is an important risk factor for OC, with the risk increasing to 5% when one first-degree relative has OC and to 7% when two such relatives have been diagnosed with OC (Reid et al., 2017). About 23% of ovarian carcinomas have been linked to inherited mutations, notably 65–85% of heredity OC due to germline mutation in *BRCA* genes. Carriers of *BRCA1* and *BRCA2* mutations have high lifetime risks of developing breast and OC by 85% and 54%, respectively (Toss et al., 2015).

However, there are two clinically syndromes that are associated with OC. The most common is the hereditary breast-ovarian cancer syndrome (HBOC), which results from mutations in *BRCA1* and *BRCA2*. Another one is hereditary nonpolyposis colorectal cancer (HNPCC), or Lynch syndrome, which is caused by mutations in mismatch repair genes, such as *MLH1, MSH2, MSH6* and *PMS1*. Several DNA repair genes, including *TP53*, *BARD1*, *CHEK2*, *RAD51* and *PALB2,* have also been shown to be associated with inherited OC (Steinke et al., 2013, Toss et al., 2015). Because of the vagueness of symptoms and lack of affective screening tests for OC, about 75%

of women diagnosed with OC at stage III or IV of the disease (Doubeni et al., 2016).

1.2 STAGING OF OVARIAN CANCER

The Federation International of Gynaecology and Obstetrics (FIGO) staging for OC is as follows:

1- **Stage I:** Tumour is only in the ovaries.

A. Tumour limited to one ovary.

B. Tumour limited to both ovaries.

C. Tumour identified as either Stage IA or IB but with tumour on the surface of one or both ovaries; or ruptured capsule(s); or ascites with malignant cells.

2- **Stage II:** Tumour has grown in one or both ovaries, with pelvic extension.

A. Extension into the fallopian tubes or the uterus.

B. Extension to other pelvic tissue such as the bladder or rectum.

3- **Stage III:** Tumour has spread outside the pelvis to the peritoneum or inguinal nodes.

A. 1) Cancer has spread to the lymph node (LN) in the back of the abdomen; or 2) Tumour has spread to the peritoneum and it may also be in the LN.

B. Tumour size is 2cm or smaller on the peritoneum and it might be in the LN

C. Tumour size is larger than 2cm on the peritoneum and it might be in the LN

4- **Stage IV:** Distant metastases.

A. Cancer can be associates with caused Pleural effusion.

B. Cancer can spread to liver, spleen, LN and lung.

The survival rates are based on the stage at diagnosis as it follows:

- Stage I – 90% five-year survival.
- Stage II – 70% five-year survival.
- Stage III – 21% five-year survival.
- Stage IV – 6% five-year survival (Cancer Research UK, 2019).

1.3 PATHOLOGY OF OVARIAN CANCER

Primary ovarian tumours are classified according to the classification of World Health Organization (WHO) into three main categories: sex-cord stromal tumours (8%), germ cell (30%) and epithelial (60%). Epithelial ovarian cancer (EOC) accounts for 90% of all malignant primary ovarian tumours and will be the focus of the current research (Devouassoux-Shisheboran and Genestie, 2015, Prat, 2012). These tumours are heterogeneous and primarily subdivided based on cell

type into serous (30–70%), endometrioid (10–20%), mucinous (5–20%), clear cell (3–10%), transitional (1.7%) and undifferentiated (1%). The microscopic morphological features of those tumours are shown in Figure 1.1. These subtypes differ regarding the biological behaviour, treatment response and overall prognosis (Ricci et al., 2018, Chen et al., 2003).

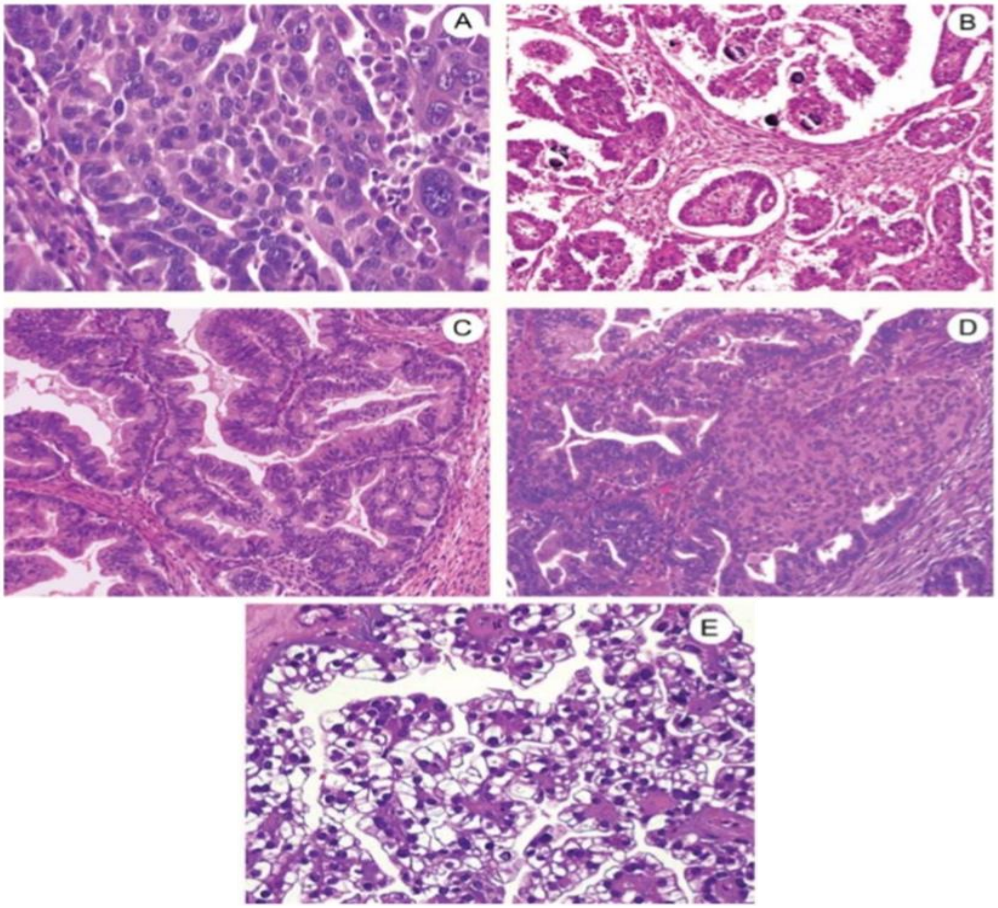

Figure 1.1: Various histopathological subtypes of epithelial ovarian cancer (EOC). A) High-grade serous carcinoma (HGSC). B) Low-grade serous carcinoma (LGSC). C) Mucinous carcinoma (MC). D) Endometrioid carcinoma (EC). E) Clear cell carcinoma (CCC). From (Prat, 2012).

1.3.1 SEROUS CARCINOMA

The overwhelming majority of primary malignant ovarian tumours are serous carcinomas. These tumours are classified into two types: high grade and low grade (Prat, 2012, Vang et al., 2009). Details are described below.

1.3.1.1 HIGH GRADE SEROUS CARCINOMA

High grade serous carcinoma (HGSCs) account for over two-thirds of serous carcinomas and are associated with higher OC mortality rate. HGSCs is often bilateral and mainly solid, multiloculated cystic areas signified by necrosis, haemorrhage and friability (Rosen et al., 2010). Microscopically, HGSCs show heterogeneous morphology whereas the papillary fronds and solid sheets of malignant cells are the most common. The tumour cells are pleomorphic with prominent nucleoli and frequent mitotic figures. Lymph vascular invasion and extra capsular extension are common features alongside with extensive necrosis. Most of HGSCs show immunoreactivity with BRCA1, p53, p16 and WT1. They also demonstrate a high proliferation index, as elucidated by high nuclear expression of Ki-67. Two-thirds of HGSC cases exhibit oestrogen receptor (ER) expression (Prat, 2012). Genomically, HGSCs are unstable and

aneuploid, and almost 10% of HGSC have a germ-line mutation in *BRCA1* or *BRCA2*.

Moreover, *TP53* has been shown to be mutated in 95% of HGSCs. Furthermore, *BRCA1/2* inactivation are found to be a consistent genetic mutation in HGSCs (Prat, 2012, Devouassoux-Shisheboran and Genestie, 2015, Neff et al., 2017). As evident from genome-based analysis approximately half of HGSCs have defects in homologous recombination (HR), and this deficiency is main determinant of platinum sensitivity. As a result, the treatment of HGSC with poly (ADP-ribose) polymerase inhibitors (PARPi) has been exploited (Lheureux et al., 2019).

1.3.1.2 LOW GRADE SEROUS CARCINOMA

Low grade serous carcinoma (LGSCs) are uncommon and account for 10%-15% of serous carcinoma. LGSCs regularly have non-invasive borderline components and represent serous borderline tumours progression beyond microinvasion. The existence of stromal microinvasion in a serous borderline tumour is correlated with an excellent prognosis. Microscopically, LGSCs demonstrate micro-papillae with minimal nuclear atypia and low mitotic activity. The expression of biomarker profile is similar to HGSC; however, Ki-67 expression differs significantly, with median Ki-67 labelling index of

2.5% in LGSC compare to 22.4% in HGSC. LGSCs have been demonstrated genomic mutation in *KRAS* (38%) and *BRAF (*19%) but do not show either chromosomal instability or complex genetic abnormalities. They are also not linked with BRCA germline alterations (Prat, 2012, Devouassoux-Shisheboran and Genestie, 2015, Lalwani et al., 2011).

1.3.1.3 ENDOMETRIOID CARCINOMA

Endometrioid carcinoma (ECs) represents 10% of all ovarian carcinomas and are commonly found as unilateral solid tumours with a smooth outer surface. EC section shows cystic areas that contain friable soft masses and bloody fluid. ECs also have features of haemorrhage and necrosis (Rosen et al., 2009). Immunohistochemical analysis demonstrated that ECs exhibit positive staining in PAX8, CK7 and hormone (progesterone and oestrogen) receptor. ECs are classified into three grades according to FIGO system, depending on the amount of solid areas and cytological atypia. ECs grade 3 are morphologically similar to HGSC, and both harbour *TP53* mutations as well. However, there are some immunohistochemical markers that can be used to differentiate between them. 80-90% of HGSC show positive staining for WT1, whereas ECs are mostly negative (Shimizu et al., 2000). P16 reveals

positive staining in most HGSCs while ECs show patchy staining (O'Neill et al., 2007). HGSCs show aberrant staining with p53 while ECs exhibit "wild type" staining. HGSCs exhibit positive staining of PTEN whereas ECs are mostly negative for PTEN (Devouassoux-Shisheboran and Genestie, 2015, Murali et al., 2019, Han et al., 2013). Genomically, ECs harbour *PIK3CA* (20%), *CTNNB-1* (48%), *ARID1A* (30%) mutations. ECs are mostly observed with Lynch syndrome. Additionally, sporadic cases have microsatellite instabilities (Devouassoux-Shisheboran and Genestie, 2015).

1.3.1.4 MUCINOUS CARCINOMAS

Mucinous carcinomas (MCs) represents 10%-15% of all primary OCs as approximately 80% of mucinous tumours are benign and most of the rest are borderlines. Microscopically, MCs consist of cysts and variable size of glands, with a confluent pattern and back to back glands. They also show a complex papillary architecture. The cells are columnar, tall and stratified with basophilic cytoplasmic that contains mucin. Invasive MCs are subdivided according to expansile and infiltrative pattern. The expansile type is usually stage 1 and shows a very good prognosis. It composed of confluent glands with small or no interposed stroma and is mostly identified in young patients. The infiltrative type exhibits a constructive invasion with

desmoplastic stromal reaction. Immunohistochemical studies suggest the positive expression in CK7, CK20 and PXA8 and negative expression for WT1 in MCs. The frequencies of *KRAS* alterations in normal ovary, benign and malignant tumours were 0%, 57%, and 76%, respectively, indicating that *KRAS* could have role in the progression of MCs. Additionally, *HER2* amplification was found in 18% of invasive MCs and 6% of borderline mucinous tumours (Prat, 2012, Ricci et al., 2018, Lee et al., 2016).

1.3.1.5 CLEAR CELL CARCINOMA

Clear cell carcinoma (CCC) accounts for 10% of all OC and it presents with stage I or II of the disease. CCCs are rarely bilateral and correlated with unfavourable prognosis, particularly at advanced stage. Microscopically, CCCs typically consist of papillae with a hyalinized core, although tubulocystic, solid and glandular pattern are common. CCC cells are large with clear or eosinophilic cytoplasm. The nuclei are irregular, hyperchromatic and pleomorphic. As evident from immunohistochemical analysis, a positive staining for CK7, CK20, HNF1B and Napsin. Genomically, these tumours do not show BRCA mutations, instability of chromosome or *TP53* mutations, but half of all CCCs carry *ARID1A* mutations (Skirnisdottir et al., 2013, Prat, 2012).

1.4 OVARIAN CANCER TREATMENT

The majority of women are diagnosed with stage III / IV. The gold standard for advanced EOC treatment is the combination of cytoreductive surgery and platinum-based chemotherapy (Della Pepa et al., 2015).

1.4.1 SURGERY

Surgery plays a vital role in EOC management. The importance of optimal resection is well-known, and maximal cytoreduction is one of the most importance determinants of survival among EOC patients (Elattar et al., 2011, Al Rawahi et al., 2013). Surgery can be either primary debulking, which is performed before the initiation of six cycles of platinum-based chemotherapy, or interval debulking, which is preformed after three cycles of neoadjuvant platinum-based chemotherapy and then followed by three cycles of platinum-based chemotherapy. However, recent clinical trials have shown that there was no difference in survivals rates between patients having primary surgery or interval debulking surgery for advanced EOC (Vergote et al., 2010).

1.4.2 CHEMOTHERAPY

Platinum-based chemotherapy (cisplatin/carboplatin) is the cornerstone of OC treatment. The chemotherapeutic agents are transported inside the cell by either passive diffusion or a copper transport (CTR1) mediation. Once these agents inter the cell, they become active and bind to DNA, which leads to formation of monoadducts. DNA adducts (intra- or inter-stand) are then formed, leading to impaired replication, conformational DNA changes and inhibiting DNA synthesis (Jamieson and Lippard, 1999, Siddik, 2003). The International Collaborative Ovarian Neoplasm Trial 1 (ICON1) and the Adjuvant Chemo Therapy in Ovarian Neoplasm (ACTION) trial demonstrated that platinum-based chemotherapy after surgery improves overall survivals (OS) and delays recurrence (Colombo et al., 2003, Trimbos et al., 2003).

Numerous studies have investigated the patient benefits of adding further agents. Several randomized clinical trials (RCT) have highlighted the significance of the addition of paclitaxel to platinum agents in terms of improving the OS and progression free survival (PFS) (Piccart et al., 2000, Bookman et al., 2003). However, ICON3 randomised trial in 2002 showed that there were no significant differences in survival benefit between single platinum agent

treatment or treatment with additional of paclitaxel. The option of single or double agent is currently tailored to the patients. To date, the standard OC treatment is offered to all patients regardless of stage, histological subtype or surgical outcomes.

1.5 RESISTANCE TO CHEMOTHERAPY

Although initial responsiveness to platinum-based treatment is high (60-80%) in EOC, more than 70% of advanced stage EOC patients relapse, and even in stage I or II the relapse rate is 20%-25% due to platinum resistant (Huntoon et al., 2013, van Zyl et al., 2018, Ushijima, 2010b). This resistance remains the major obstacle to EOC treatment. This resistance is classified as intrinsic, which presents at the time of diagnosis, or acquired. Thus, it is crucial to understand the chemoresistance molecular mechanism to aid identifying novel therapeutic approaches for treatment of EOC (Galluzzi et al., 2012, Zheng, 2017). The platinum molecular resistance mechanisms include decreased drug accumulation, increased drug inactivation, evasion of apoptosis, alterations in signalling pathways, epithelial–mesenchymal transition, stemness and increase DNA repair.

1.5.1 DECREASED DRUG ACCUMULATION

One of the mechanisms of drug resistance is decreased drug accumulation. This can be due to defects in transport system that contribute to decrease influx of chemotherapeutic agent, or increase drug efflux or inhibition of drug intake (Sodani et al., 2012). CTR1 controls cellular influx of platinum. Additionally, the copper transporters ATP7A and ATP7B have been shown to play roles in cisplatin resistance, and high expression of ATP7A is associated with lower survival in ovarian patients (Song et al., 2004, Holzer et al., 2006, Samimi et al., 2004). Overexpression of drug efflux ATP-binding cassette (ABC) family transporters is often associated with multidrug resistance (MDR). For example, overexpression of P-glycoprotein (known also as MDR1) has been linked with variable kinds of solid and haematological tumours, such as neuroblastomas, leukaemia, breast and ovarian cancers, indicating its role in chemoresistance (Higgins, 2007, Sharom, 2008). A recent study has revealed that P-glycoprotein inhibitors increased chemotherapeutic accumulation, reduced cell viability, decreased cell migration and increased cell death in 2-dimensional (2D) and 3D cell culture studies (Nanayakkara et al., 2018).

1.5.2 INCREASED DRUG INACTIVATION

Glutathione (GSH) plays key role in cell differentiation, proliferation and apoptosis. It also leads to detoxification and inactivation of many chemotherapeutic agents such as cisplatin and its analogues. High GSH levels increase the capacity of antioxidant and resistance to oxidative stress of cancer cells. Furthermore, the content of GSH in some cancer cells is correlated with higher levels of GSH enzymes, including γ-glutamyl-transpeptidase (GGT) and γ-glutamyl cysteine ligase (γ-GC) activities (Figure 1.2) (Traverso et al., 2013, Estrela et al., 2006).

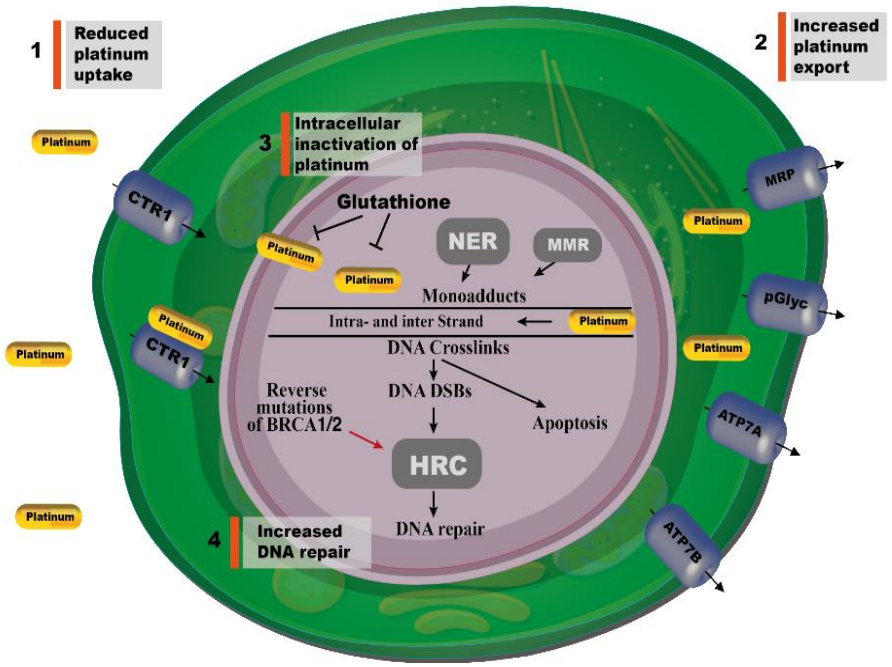

Figure 1.2: Systematic representation of the molecular mechanism of cisplatin resistance. Original diagram. Information from (Zhu et al., 2016).

1.5.3 EVASION OF APOPTOSIS

TP53 is a tumour suppressor gene that has a pivotal role in maintaining the genome integrity by controlling cell cycle, activating DNA repair proteins and regulating apoptosis. The level of P53 increases rapidly after DNA damage, leading to the activation of genes implicated in arresting cells from entering S phase until the DNA damage is repaired. If the damage cannot be repaired, then apoptosis is induced by p53. P53 plays a key role in regulating the apoptosis pathway through the activation of pro-apoptotic BH3-only proteins such as PUMA and NOXA. These proteins bind to anti-apoptotic BCL-2 proteins and prevent them from inhabiting the pro-apoptotic BCL-2 proteins such as BAX and BAK. BAX and BAK form aggregates in the outer membrane of mitochondria generating channels. These channels release cytochrome C to cytoplasm contributing to the recruitment of caspases enzymes and then triggers apoptosis in the unhealthy cell (Fernald and Kurokawa, 2013, Aubrey et al., 2018). *TP53* is found to be mutated in nearly 50% of human cancers. The vast majority of these mutations are missense in the DNA binding domain leading to lose of capability to activate p53 target genes, causing impairment of tumour suppression function and decreasing apoptosis (Hientz et al., 2016, Khoury and Domling, 2012, Mantovani et al., 2019).

Tumours harbouring *TP53* mutations are commonly associated with aggravated metastasis, genomic instability, increased drug resistant and treatment failure when compared to wild type *TP53* (Mantovani et al., 2019). Several researchers have investigated the possibilities of restoration the function of p53 to treat cancers. Several novel molecules have been identified that restore p53 tumour suppression function, and these molecules have revealed promising results when combined with conventional chemotherapeutic agents. For instance, APR-246 has been studied in a phase I/IIa trials in haematological malignancies and prostate cancer patients, and it is currently investigated in a phase II trial in HGSC (NCT02098343) (Hientz et al., 2016, Zhang et al., 2018, Lehmann et al., 2012). Approximately 50% of all cancers express wild type *TP53* proposing the role of other proteins within the p53 pathway. Small molecules have been recently identified that can inactivate MDM2, which is a negative regulator of p53. One such molecule, RO5045337, has been studied in a phase I trial in acute myelogenous leukaemia patients (NCT01635296) and in phase I trial in soft tissue sarcoma (NCT01605526).

1.5.4 CHANGES IN SIGNALLING PATHWAYS

The PI3K/AKT/mTOR pathway has important role in the regulation of normal cell physiology and integrating extracellular growth signals into an intracellular cascade promoting cellular metabolism, growth and cell proliferation (Cheaib et al., 2015). This pathway is commonly altered in OC as copy number changes of *PIK3CA* and *PIK3CB* subunits of *PI3K* have been linked with poor prognosis in OC patients. Several studies suggest that PIK3CA and AKT expression level were correlated with decreased survival and activation of PI3K/AKT/mTOR pathway, as measured by the phosphorylation level of AKT or mTOR (Musa and Schneider, 2015, Cheaib et al., 2015). PX-866 is a PI3K inhibitor that is being examined in phase I/II trial in combination with cetuximab for treatment of metastatic colorectal carcinoma and squamous cell carcinoma (NCT01252628). Additional phase I/II trials of PI3K inhibitors are ongoing in (NCT01587040, NCT01629615 and NCT01540253).

AKT1 overexpression and *AKT2* gene amplification resulted in paclitaxel resistant in OC cells. MK2206 is an AKT inhibitor that can inhibit both AKT1 and AKT2 and might be one of the most effective inhibitors in clinical trials (NCT01283035) (Musa and Schneider, 2015, Mabuchi et al., 2015).

PTEN is tumour suppressor gene that inhibits PI3K/Akt pathway. *PTEN* mutations cause activation of the PI3K/Akt pathway and play a key role in tumorigenesis and tumour development. In fact, these mutations have the second-highest frequency of alterations in cancers, following only that of *TP53* (Georgescu, 2010, Chalhoub and Baker, 2009).

The Ras/Raf/MAPK pathway is another signalling pathway that controls various downstream cascades in increase survival, cell proliferation and malignant transformation. This pathway is prevalently upregulated in HGSC (Figure 1.3) (Smolle et al., 2013). However, RAS has been viewed to be undruggable target due to it is lack of appropriate surface for binding small inhibitors molecules (O'Bryan, 2019).

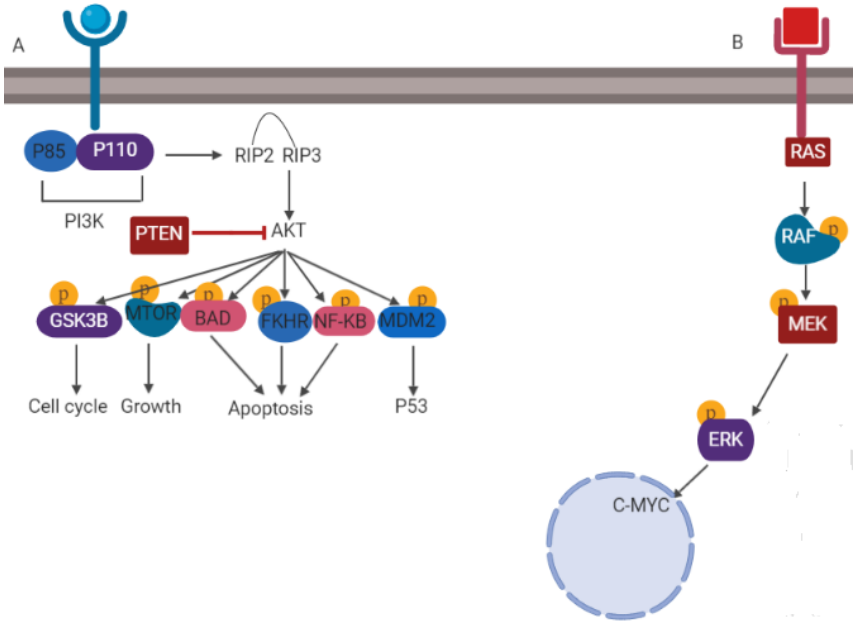

Figure 1.3: Systematic representation of the proliferation signaling pathways. A) The PI3K pathway: P85 and P110 are usually mutated in human cancer, and these mutations increase kinases activation. PI3Ks activation leads to phosphate PIP2 to produce PIP3. RIP3 phosphorylates AKT on threonine 308 (T308), which allows AKT to phosphates a cascade of downstream proteins. B) The RAS pathway: this pathway is frequently activated in human cancer. The activation of RAS by SOS. The activation of RAS causes the phosphitylation of RAF which in turn phosphate a cascade of downstream proteins. Modified from (Zheng, 2017). The small yellow orange circle on the top of a proteins means these proteins become phosphorylated.

1.5.5 EPITHELIAL-MESENCHYMAL TRANSITION

Epithelial mesenchymal transition (EMT) is a process in which epithelial cells undergo multiple process changes, including loss of polarity and cell-cell adhesion, followed by transition into the cells with a mesenchymal phenotype. A mesenchymal phenotype is correlated with an increased the capacity of migration, extracellular matrix (ECM) degrading enzymes production, proclivity for invasiveness and chemoresistance and resistance to apoptosis as well (Deng et al., 2016, Alblihy et al., 2019). During the process of EMT, cells show downregulation of several markers, such as E cadherin, which is a key player in cell adhesion, and claudins, occludins, laminin1 and cytokeratin's that are vital for the stability of desmosomes.

Simultaneously, N-cadherin, vimentin, matrix metalloproteinases (MMPs) and fibronectin are upregulated. A complex network of transcriptional factors regulates EMT and leads to suppression of epithelial genes and activation of mesenchymal genes. The main EMT transcriptional factors are ZEB1/2, SNAIL, SLUG, and TWIST1/2. ZEB1 and SNAIL bind to *CDH1* (the gene that encodes E-cadherin) and eventually repress it is expression. Increasing evidence reveals that there is a strong relationship between EMT and platinum

resistant. It has been reported that the exposure to continuously increasing levels of paclitaxel induces chemoresistance and EMT. Moreover, gene expression and proteomic analysis demonstrated that resistance OC cell lines (A2780cis) exhibit high level of EMT markers compared to sensitive OC cell line (A2780) (Loret et al., 2019, Deng et al., 2016, Alblihy et al., 2019).

1.5.6 CANCER STEM CELLS

Cancer stem cells (CSCs) are the subpopulation of cancer cells, identified by their tumour forming capacity, multiple differentiation, self-renewal, drug resistant, growth of cancer and recurrence (Zheng, 2017). Chemotherapy or radiation contribute to the enrichment of CSCs in several cancers. The CSCs demonstrate phenotype changes as well as high expression of stem cell markers, including CD133, NANOG, ALDH, SOX2 and OCT4. High OCT4 expression is associated with resistance to cisplatin, paclitaxel, etoposide and doxorubicin in lung cancer. High expression level of OCT4 protein or mRNA was also correlated with poor clinical outcome for various cancer, including OC. Cumulative evidence has showed that CSC markers, including CD117, CD44, ALDH1 and CD133, can be a valuable prognostic factor in OC (Tao et al., 2018, Mohiuddin et al., 2019). Agents that target CSC-associated signalling pathways,

such as WNT, Notch and hedgehog, and cell surface receptors in OC including CD117, CD44, CD133 and ALDH have produced promising pre-clinical data and now undergo clinical trials (Annett and Robson, 2018).

1.5.7 INCREASED DNA REPAIR

The main target of platinum agents is DNA, and the sensitivity or resistance to these agents is affected or modulated by the capability of cells to sense and repair the DNA damage that is induced by platinating agents. DNA damage response (DDR) and DNA repair pathways will be discussed in detail below.

1.5.7.1 DNA DAMAGE RESPONSE (DDR)

To maintain genomic integrity, cells have evolved efficient DDR mechanisms in order to sense, signal and repair DNA damage as impaired processing of DSBs can contribute to mutations, chromosome rearrangements and loss of heterozygosity and cancer.

Cells activate their cell-cycle checkpoints as a response to various types of DNA damage or stalled replication forks. This checkpoints arrest progression of cell cycle at various phases. This process initiates a step-by-step the activation of multiple proteins, including

sensors, transducers and effectors that regulate the progression of cell cycle and facilitate DNA repair (Figure 1.4) (Pardo et al., 2009, Jackson and Bartek, 2009). Specifically, cells immediately activate sensor proteins, such as DNA-PKcs and MRN complex, as result of DSBs. These sponsors operate a signal transduction cascade that is implicated in activation of main checkpoint regulators, including ATM and ATR (Maréchal and Zou, 2013, Awasthi et al., 2015).

When the three kinases DNA-PKS, ATM and ATR become activated, they phosphorylate several downstream mediators, transducers and effectors, such as CHK1 and CHK2. These effector kinases play key roles in activating cell cycle checkpoints that contribute to the arrest of cell cycle in G1- or G2-phases, thus facilitating DNA repair (Awasthi et al., 2015).

Cumulative evidences have shown that the DNA repair machinery can differentiate between several types of damages and translates them into various modes of activation of checkpoints in G1- and S/G2-phase (Barlow et al., 2008). The classical view of the DDR is that the ATM-CHK2 pathway becomes activated in response to ionizing radiation induce DNA lesions and acts in the initial stages, whereas ATR-CHK1 pathway is often activated as a response to DNA damage that results from ultraviolet (UV) light or single-strand DNA

(ssDNA) regions that might evolve during chromosomal lesions process or be generated from stalled DNA replication (Maréchal and Zou, 2013). Although, the vast majority of RPA-coated ssDNA is usually present in S-phase (Fanning et al., 2006), ATR activation is not restricted only to S-phases. Several studies have demonstrated that ATM and ATR do not work in an independent manner during the DDR but cooperate to initiate and maintain DDR. There is overlap in their substrate specificity, suggesting the possibility of a crosstalk between ATM and ATR pathways to maintain genomic stability (Helt et al., 2005, Yajima et al., 2006).

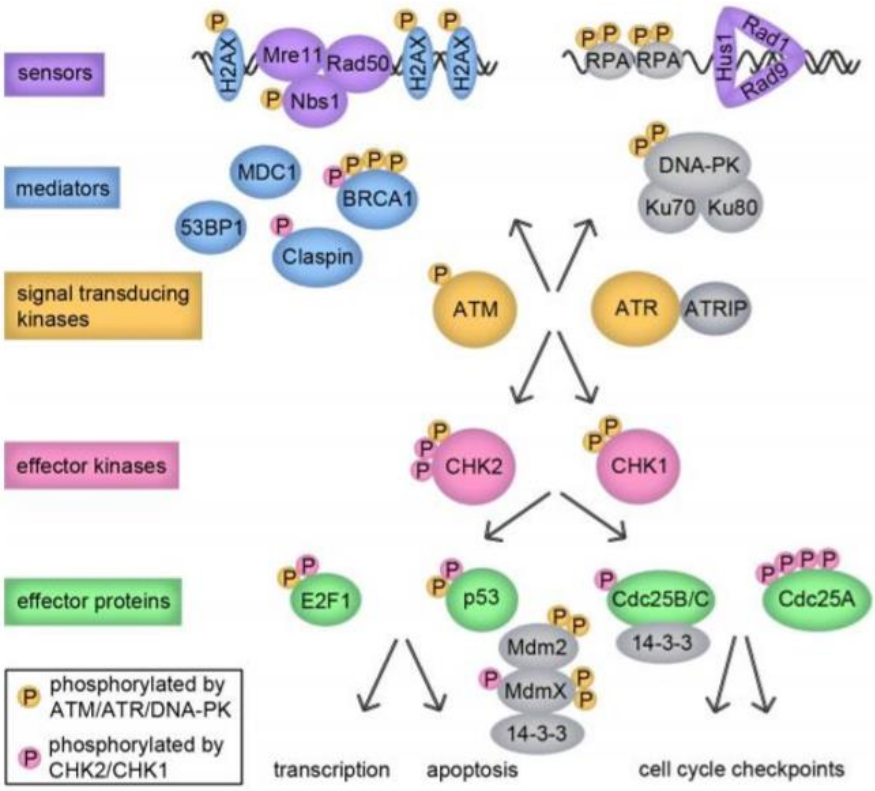

Figure 1.4: Systematic representation of cellular response to DNA damage. Sensors are shown in purple sense single or double strand breaks. Mediators are shown in blue signal the transducing kinase that are shown in orange. These kinases phosphorylate effectors kinases shown in pink and effector proteins shown in green contributing to gene transcription, apoptosis and cell cycle arrest. The phosphorylation by ATM, ATR and DNA-pks are shown by a yellow phosphorylate group. The phosphorylation by CHK1 and CHK2 are shown by a pink phosphorylate group. From (Freeman and Monteiro, 2010).

1.5.7.2 DNA REPAIR PATHWAYS

DNA is constantly subjected to attacks from various endogenous and exogenous agents. Each mutagen can lead to either direct or indirect damage to the genome. Each agent shows a predilection for damaging particular nucleotides, which can contribute to distinguishable patterns of mutations. Endogenous factors include enzymatic conversions, replication errors, deamination and free radical species (Lindahl, 1993, Gates, 2009). Exogenous factors include X-rays, UV light, thermal disruption and chemical exposure (e.g., to platinum-based compounds) (Harris, 2013).

DNA damage includes bases modification, intra- or inter-strand crosslinks, 6-4 photoproducts, pyrimidine dimers and single or double strand breaks (Figure 1.5) (Ghosal and Chen, 2013). There are six main pathways responsible for the DNA lesions repair: direct repair, base excision repair (BER), mismatch repair (MMR), nucleotide excision repair, hon-homologous and joining repair (NHEJ), homologous recombination (HR) and alternative non-homologous and joining (Bernstein et al., 2002).

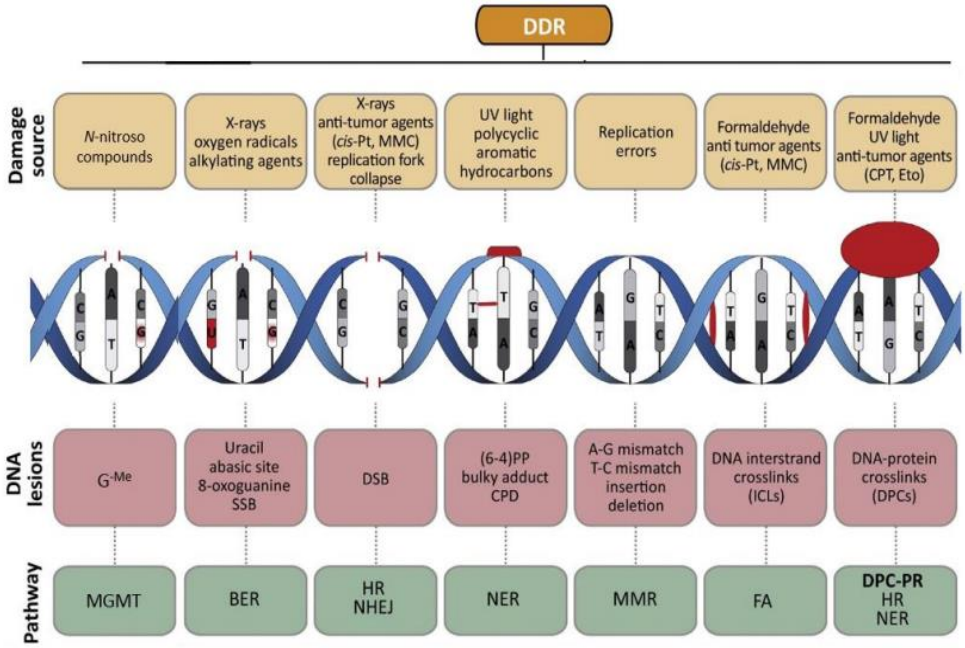

Figure 1.5: Various DNA damaging agents, their effects and the response of DNA repair pathways. From (Vaz et al., 2017).

1.5.7.2.1 DIRECT REPAIR

Direct repair by O^6-methylguanine-DNA methyltransferase (MGMT) remove the methyl group of the O^6 of guanine, which causes the guanine to base-pair to thymine instead of cytosine during replication. The cancer chemotherapeutic agents' dacarbazine, temozolomide and nitrosoureas causes alkylation of O^6-methylguanine, which causes persistent mismatching of bases during DNA replication if MGMT is deficient. The MMR pathway attempts to repair this damage; however, these attempts are unsuccessful due to the alkylated DNA base that is permanently

bound with the template DNA, thus triggering futile cycles of excision and repair which eventually leads to apoptosis (Fan et al., 2013, Luo et al., 2010).

1.5.7.2.2 BASE EXCISION REPAIR

Base excision repair (BER) is an evolutionarily conserved mechanism, which is considered the "workhorse" repair pathway of the cell. It corrects the spontaneous production of hydrolytic decay in DNA and the daily bases modification caused by oxidation and alkylation (Kim and Wilson, 2012). BER is initiated by damage DNA glycosylases that remove` corrupted DNA bases by hydrolysis of N-glycosylic bond, yielding an apurinic/apyrimidinic (AP) site in the DNA, which is further processed by APE1 (Dianov, 2011). APE1 cleaves the phosphodiester bond 5'-to the AP-site, leading to a single strand break (SSB) with a 5'-sugar phosphate. This SSB is thereafter repaired by complex proteins, including XRCC1, DNA ligase IIIα (LIG III) and POLβ (Abbotts and Madhusudan, 2010). POLβ removes the 5'sugar phosphate, acts as DNA polymerase and adds a single nucleotide at the 3'end of the arising single-nucleotide gap.

LIG III eventually seals the DNA ends and thus accomplishes the repair of DNA. This pathway is called the short patch BER pathway (Dianov, 2011). However, if POLβ fails to remove the 5'sugar phosphate, then after POLβ adds the first nucleotide, a switch is made to Pol δ/ε, which adds two to eight more nucleotide in the repaired gap. Subsequently, a flap structure is generated, which is removed by FEN-1 in a PCNA-dependent fashion. DNA ligase I eventually seals the remaining nick in the backbone of DNA and this pathway is referred to as long patch (LP-BER) (Figure 1.6) (Dianov, 2011, Abbotts and Madhusudan, 2010).

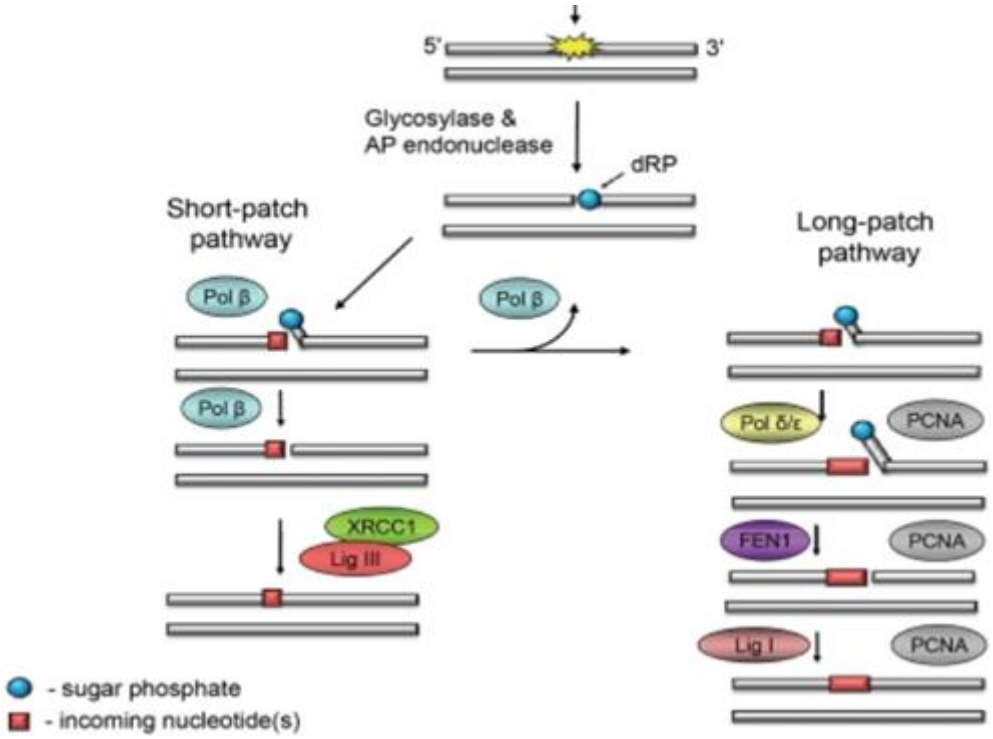

Figure 1.6: Systematic representation of base excision repair. DNA damage was removed by glycosylase and then generates an AP site. APE1 cleaves the phosphodiester bond 5'-to the AP-site and recruits complex proteins including XRCC1, DNA ligase IIIα (LIG III) and Pol β. In LP-BER, Pol δ/ε is recruited and a flap structure is generated which is removed by FEN-1 in a PCNA-dependent mode. Finally, ligation is done by DNA ligase I. From (Dianov, 2011).

1.5.7.2.3 MISMATCH REPAIR

During DNA replication lesions may result, which is processed through mismatch repair (MMR). When the mismatch is recognized by an MSH2 and MSH6 complex, this pathway is triggered. The kind of mismatch acknowledged is stipulated through the different MSH3/MSH6 combinations produced with MSH2. Following this MSH

proteins play role in recruiting MLH1 and its partners: post–meiotic-segregation increased by 1 (PMS1) protein and post–meiotic-segregation increased 2 (PMS2). Ultimately, the restoration is finished by DNA Ligase, following the DNA lesion being eliminated by the exonuclease and a new strand being synthesised by a DNA polymerase. Vulnerability to cancer is a result of a mutator phenotype being produced by an MMR defect.

Apoptosis, DNA damage signalling, mitotic and meiotic recombination are all influenced by MMR status (Jiricny, 2006, Li, 2008).Turcot syndrome, Muir-Torre syndrome and HNPCC syndrome are three clinical disorders typically linked to MMR deficiency. Small intestinal, kidney, stomach, ovarian and endometrial tumours, in addition to colon cancer, are common risks for HNPCC patients. Mutations in hPMS2, hMSH2, hMSH6 and hMLH1 MMR gene are present in 80% of HNPCC patients.

Small intestinal, kidney, stomach, ovarian, endometrial and colon visceral tumours, as well as sebaceous carcinomas are an increased risk for Muir-Torre syndrome patients, who have hMSH1 and hMSH2 genetic mutations. hMSH1 and hPMS2 genetic mutations result in Turcot syndrome. Small intestinal, stomach, kidney, ovarian, endometrial and colon visceral tumours, in addition to lymphomas

and gliomas, are risks typically related to Turcot syndrome (Chung and Rustgi, 2003, Peltomaki, 2003, Thoms et al., 2007).

1.5.7.2.4 NUCLEOTIDE EXCISION REPAIR

Oxidative damage and contact with genotoxic agents can cause an array of structurally un-associated DNA lesions. For example, bulky adducts and huge chemical adducts, cross-links of intra-strand, cyclobutane pyrimidine dimers and photo-lesions are caused by ultraviolent light. Nucleotide excision repair (NER) is critically involved in processing these types of DNA lesions (Buschta-Hedayat et al., 1999, Wood, 1999). There are two sub-pathways by which NER can process DNA damage namely a transcription coupled repair (TCR) and Global genome repair (GG-NER).

A TCR is a sub-pathway that can be produced by combining NER with transcription, thus facilitating the transcribed strand (TS) rather than non-transcribed strand (NTS) inactive genes, which is the preferred restorative mechanism. Although when a blocking lesion is found within the TS the RNA polymerase II (RNAPII) is typically considered to be a damage indicator triggering the NER pathway, uncertainty still characterises TCR's mechanical characteristics (Hanawalt,

2002). Consequently, in response to the lesion, DNA-Damage Binding (DDB) complexes and XPC can swiftly alter to RNAPII.

Moreover, the preservation of TCR by XP group C subjects also occurs, which are those who lack global genomic repair (GGR). The transcribed strand of active genes can cause lesions that are thus eradicated by TCR, while the genome's repair of the non-transcribed domain is controlled by GGR. Typically, RPA, XPA, 9 subunits of transcription factor-IIH (TFIIH) and XPC-hHR23B (human RAD23B homolog) are all utilised to create a small bubble structure including damaged bases or otherwise in the preliminary stage of NER, in addition to damaged residue realisation.

ERCC1- XPF and XPG are the two endonucleases that conduct the double incision in relation to the lesion's 3' and 5' damaged DNA strands. Employing the DNA ligase I (Lig I), pentameric clamp loader, PCNA and sliding clamp can be used to integrate DNA POLδ and POLε (Figure 1.7). The created gap's lesion, synthesis and litigation is all comprised within the oligonucleotide which is produced as a result (Christmann et al., 2003, Gillet and Schärer, 2006).

These genes are also essential for TCR as they are for GGR, apart from XPC-hHR23B. Moreover, Cockayne syndrome type B (CSB) and Cockayne syndrome type A (CSA) are also necessary genes for TCR.

Cockayne Syndrome and an array of different genetic diseases may result from TCR pathway insufficiencies. With this syndrome, since early years of development grave neurological issues and developmental problems may occur, although vulnerability to cancer is not worsened (Christmann et al., 2003, Scharer, 2003).

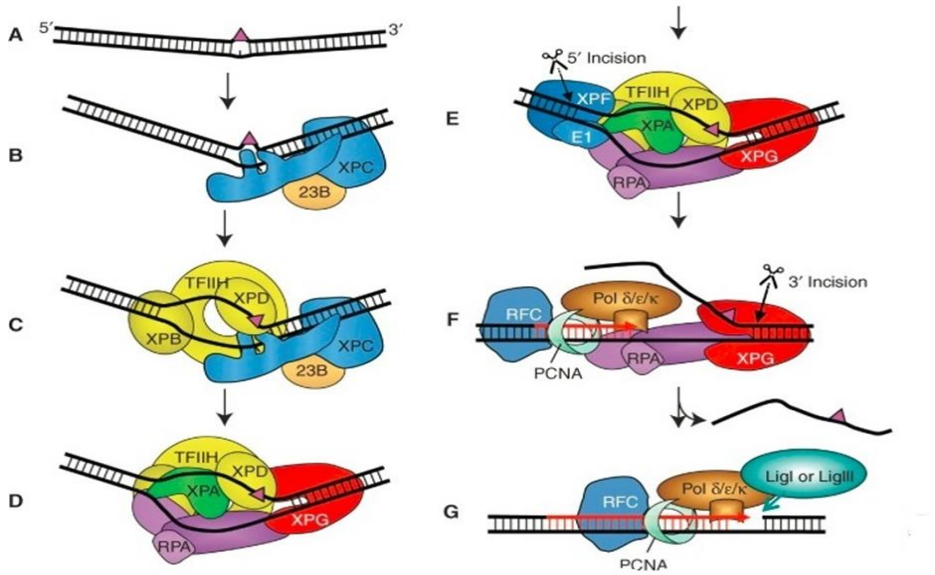

Figure 1.7: Systematic representation of the nucleotide excision repair. A) Bulky damages lead to destabilize DNA. B) In GGR, DNA lesions are directly identified by XPC-RAD23B which in turns bind to the strand opposite side of the lesions. C) The interaction between TFIIH and XPC-RAD23B contributes to open DNA with the help of XPB subunit to allow XPD to track DNA until stalls at the DNA lesion and confirms the bulkiness of the lesion. D) The next step is to form the preincision complex through the recruitment of PRA, XPG and XPA. However, at this point the endonuclease activity of XPG does not able to do an incision. E) The incision 5′ is made when ERCC1-XPF interacts with XPA to the complex. F) Repair synthesis is initiated by Pol δ and Pol ε or Pol κ or related factors, after that XPG does the 3′ incision. G) DNA ligase I or DNA ligase IIIα/XRCC1 completes the repair and nick sealing. From (Schärer, 2013).

1.5.7.2.5 DOUBLE STRAND BREAKS REPAIR

Double strand breaks (DSBs) are most cytotoxic lesions that threaten genomic stability. Failure to repair DSBs can have deleterious consequences including chromosomal translocation, loss of heterozygosity, large or small deletions, chromosome loss, evasion of cell death all of which are drivers of cancer (Jackson and Bartek, 2009, McKinnon, 2009). Two main repair mechanisms are used to repair DSBs namely non-homologous end joining (NHEJ) and homologous recombination (HR). The essential difference between these two mechanisms is their reliance on DNA homology and the accuracy of repair (Essers et al., 2000). HR requires a homologous sequence as a template for repair. This sequence must either be an undamaged sister chromatid or homologous chromosome that contributes to the reconstitution of the original DNA sequence (error free pathway).

On the other hand, NHEJ just joins the two DNA broken ends without need for a homologous sequence which results in deletions or extensive additions of nucleotides during the ligation process (error prone pathway). Even though, NHEJ does not have the ability to restore the sequence information at a damaged site, it can restore the molecular integrity (Mao et al., 2008, Lieber, 2010a). The

relative extent of these two pathways in repairing DSBs is determined by the abundance of repetitive DNA sequences and the phase of cell cycle.

As NHEJ does not require a DNA template, it can operate at any phase of the cell cycle. Indeed, NEHJ is believed to be the dominant in G1 phase of cell cycle, whereas HR cannot be operated during this time. In contrast, HR is limited to S and G2 phases, during which a sister chromatid is available and it can be used as template for the repair (Kruger et al., 2004, Moynahan and Jasin, 2010).

1.5.7.2.5.1 NON-HOMOLOGOUS AND JOINING

NHEJ is the main pathway for cells of higher eukaryotes to repair DSBs. This pathway has four main stages: set of enzymes (1) pinpointing and (2) overseeing the takeover of the damaged DNA molecule's ends, followed by (3) the establishment of a molecular bridge cross the two DNA ends and (4) the re-ligation of the broken DNA. In most cases, proteins such as DNA-PKcs, ARTEMIS, KU, XRCC4, LIG4, XLF/CERNUNNOS and DNA polymerase are utilized for NHEJ. There are two NHEJ sub-pathways include distinct sets of proteins: classical NHEJ (C-NHEJ) uses DNA-PK, KU, 53BP1 and XRCC4/Lig IV, whereas alternative and joning (Alt-EJ) utilizes

several SSBR proteins, such as Lig IIIα/XRCC1 and PAPR1, and co-opts multiple proteins that involved in the repair of DSB through the HR pathway (Chakraborty et al., 2016). Interestingly, C-NHEJ mutants exclude a significant section of DSBs from their genome through Alt-NHEJ. As a result, this repair mechanism can act as a backup in cases where C-NHEJ is not activated (Riha et al., 2006, Lieber, 2010a, Cortizas et al., 2013).

1.5.7.2.5.1.1 CLASSICAL NHEJ

A substantial number of components within C-NHEJ are conserved from yeast to humans. Mammals employ DNA-PKcs for DSB repair purposes through NHEJ, but a homolog of this enzyme in yeast, or in lower eukaryotes, is not currently known to exist (Pannunzio et al., 2014). In C-NHEJ within a few minutes, chromosome integrity is re-established via an efficient synapses mechanism occurring through a series of protein-protein interactions within the context of chromatin and of nuclear matrix chromatin (Iliakis et al., 2004). Furthermore, C-NHEJ is also crucial when it comes to utilising DSB intermediates produced throughout V(D)J recombination, during which defects within C-NHEJ can contribute to chromosomal abnormalities, sensitivity to IR and immunodeficiency (Couedel et al., 2004). The heterodimeric KU70/80 complex is made up of 70kDa

and 80kDa and it is an abundant cellular protein (Davis and Chen, 2013). In initial step of C-NHEJ mediated DSB repair, the KU heterodimer recognized DNA ends and then binds to DNA ends (blunt, 5'- or 3'-overhangs). The DNA helix is enveloped by the KU heterodimer asymmetric ring structure (Walker et al., 2001) and DNA-PKcs are then recruited to DNA ends to bring kinase activity. The DNA-PKcs create a synaptic complex and join the two DNA ends. Certain conformational alterations are made that dimerize to produce a platform for further processing to occur for non-ligatable DNA termini prior to the final relegation. After the two DNA ends are caught and tied by the DNA-PK, the C-NHEJ repair process can be initiated which allows for the phosphorylation of a number of downstream substrate proteins such as WRN helicase, RPA2, XLF/CERNUNNOS, ARTEMIS, XRCC4 and DNA LIG4 in addition to auto-phosphorylation of DNA-PKcs (Cruet-Hennequart et al., 2008, Yu et al., 2008).

A number of enzymes have been found, which can remove non-compatible overhangs, such as PNKP, TDT, TDP1, nucleases such as ARTEMIS or polymerases. At this point in the C-NHEJ activity, nucleotides occasionally can be lost (Valerie and Povirk, 2003). Lastly, following the release of DNA-PK from DNA ends, ligation complex (XRCC4/LIG4 /XLF) start processing DNA ends with the

assistance of polymerase μ (mu) or Pol λ (lambda) (Figure 1.8) (Mahajan et al., 2002, Capp et al., 2006).

1.5.7.2.5.1.2 ALTERNATIVE NHEJ

Alt-NHEJ displays a unique type of end-joining and is an earlier evolutionarily pathway that does not have as much optimization in its synapsis mechanisms. Alt-NHEJ joins DNA ends with less rapid kinetics at half-times of 2-10 hours. The faster DNA end-joining of C-NHEJ is considered to kinetically restrict this slower pathway (DiBiase et al., 2000, Khanna and Jackson, 2001). Alt-NHEJ is nonetheless considered to crucially contribute to genome maintenance and reliability, and thus has significant role in the general repair of DSBs. Furthermore, Alt-NHEJ is thought to be involved in telomere maintenance (Rai et al., 2010, Wu et al., 2008) with the ability to replace C-NHEJ in CSR inLIG4-deficient mice. In turn, it is understood to be able to stand in for V(D)J recombination in C-NHEJ deficient cells, in which mutations throughout recombination activating genes (RAG1/RAG2) mean that proteins produce DNA ends without the ability to hold them (Lee et al., 2004).

Even taking the possible outcomes of the Alt-NHEJ function into account, there is limited information known about this fundamental

mechanism, how it is controlled, how it is implemented in cellular DSB processing apparatus and how it interacts with the various parts of C-NHEJ and HR. Biochemical and Genetic experiments have revealed that proteins like PARP1, PARP2, WRN, MRN, LIG3, histone H1, and XRCC1 are involved in Alt-NHEJ (Jazayeri et al., 2008, Haince et al., 2008, Rosidi et al., 2008).

After the induction of DNA damage, PARP1 and MRN are recruited for DSBs. Before ligation, histone H1 assists in the alignment of DNA ends. It is noteworthy that MRN is critical for end-joining by Alt-NHEJ, as the inhibition for C-NHEJ mutants decrease the frequency of end-joining (Rass et al., 2009). LIG3 is thought to work in a complex with XRCC1 which is controlled by PARP1 (Robert et al., 2009). Previous study showed that PARP1 may compete with the KU heterodimer for DNA ends. KUs have greater affinity for DNA ends, and so offer a kinetics basis for backup character in Alt-NHEJ (Wang et al., 2006). Additionally, this backup property could stem from other types of lesions such as SSBs or base damages, are in competition for PARP1 as well and LIG3 as the PARP1/ XRCC1/ LIG3complex is involved in repairing base damages and SSBs (Figure 1.8) (Audebert et al., 2004).

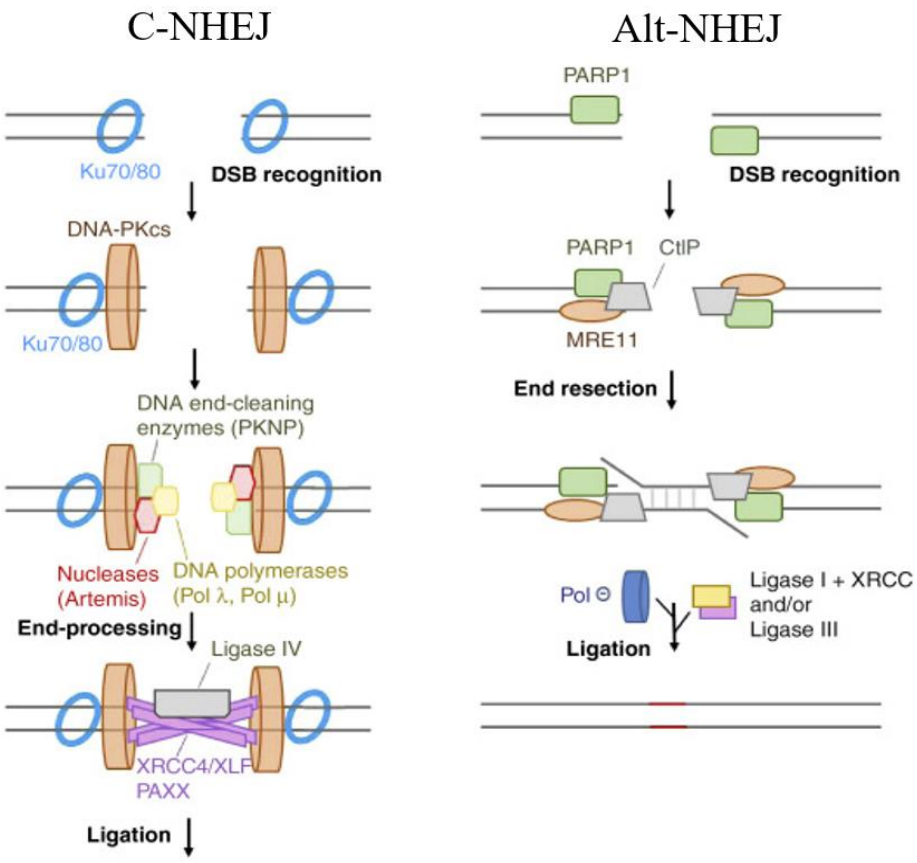

Figure 1.8: Classical and alternative NHEJ mechanisms for repairing double strand breaks (DSBs). From (Setton *et al*, 2016).

1.5.7.2.5.2 HOMOLOGOUS RECOMBINATION

HR provides high-fidelity for repairing DNA lesions, including DNA inter-strand crosslinks, DNA gaps and DSBs, in an error free manner. HR machinery and its regulation are conserved among all eukaryotes. Null mutations in main HR genes such as *BRCA1*, *BRCA2*, *NBS1*, *MRE11* and *RAD51* are lethal (Thompson and Schild, 2002).

Mutations in HR genes lead to reduction in HR levels, and as a result, increase the level of miss-segregation at mitosis and chromosomal aberrations (Bishop and Schiestl, 2002). The main steps in HR are as follows: 1) the process of DNA ends, 2) the search for homology sequence, the invasion of strand and holliday junction formation, 3) the synthesis of DNA and branch migration (Figure 1.9) (Wu et al., 2008). MRN complex senses the initial DNA damage and binds to the DNA damage site, thus prompting an intracellular DNA damage signal, which contribute to the recruitment of several proteins to DNA damage ends, such as, ATM, BRCA1, CTIP, BLM, EXO1 and DNA2 (Lou et al., 2006). MRN, CTIP, DNA2 and activated EXO1 promote the DSB resection in order to form recombinogenic 3'-ssDNA overhangs. The resulted 3'-ssDNA tail is covered by RPA which in turns protect the DNA ends from degradation and prevent the secondary structure formation (Nimonkar et al., 2011).

Interestingly, the formation of 3'-ssDNA tail may regulate the transition from NHEJ pathway to HR due to NHEJ utilizes preferentially the unprocessed DNA ends for the process of ligation (Yun and Hiom, 2009). Accordingly, the ATR-CHK1 pathway is activated by the ssDNA ends, which may also promote the repair of DSB by HR mechanism (Sorensen et al., 2005).

With the help of RAD52 epistasis group such as RAD51 paralogs (RAD51C, RAD51B, RAD51D, XRCC3 and XRCC2), RAD54 and BRCA2 (Symington, 2002), RAD51 displaces RPA and as a result generates RAD51 nucleoprotein filaments. The role of RAD51 nucleoprotein filaments are to bind to ssDNA and begin searching for homology duplex sequence by invading homologous DNA segments for polymerase mediated DNA synthesis (Mazin et al., 2010). The 3' end from the invading strand is utilized to prime a leading strand DNA synthesis via the donor complex, while the other end interacts with the displaced strand to form what is called "holliday junction". The resolution of holiday junction could lead to crossover or non-crossover products. However, the chance of a crossover event during somatic HR is very rare (Figure 1.9) (Mazin et al., 2010, Nagaraju et al., 2006).

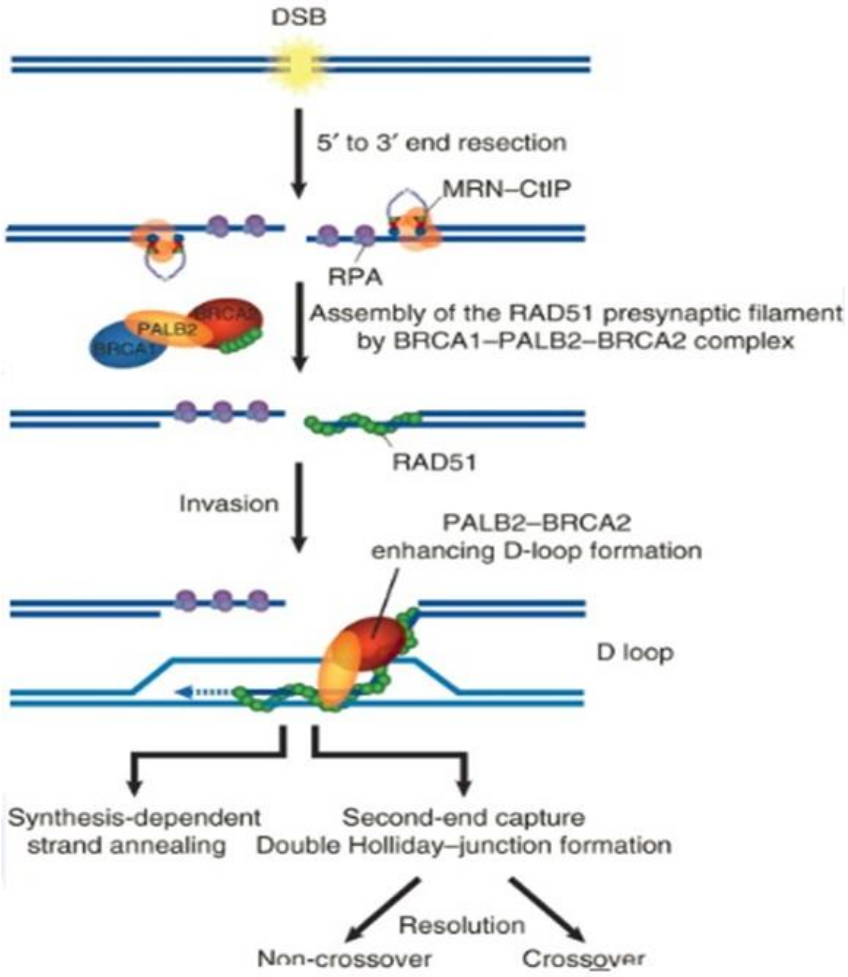

Figure 1.9: A simplified view of Homologous recombination repair (HR). MRN senses the DSB and recruits many proteins, leading to the binding of CtIP to MRN complex and the initialisation of the resection process. RAD51 is activated by PALB2–BRCA2, which leads to strand invasion of undamaged homologous template. This contribute to either SDSA or the formation of holiday junction to allow the repair of DSB. From (Buisson et al., 2010).

Back to the role of DNA repair capacity in resistance to platinum agents. Preclinical evidences strongly suggests that the presence or absence of DNA repair capacity is correlated with either sensitivity or resistance to platinum drugs (Damia and Broggini, 2019). NER plays a key role in repairing platinum induced DNA damage. ERCC1 is a key player in NER. Overexpression of ERCC1 has been shown to be significantly linked with HGSC, poor PFS and OS. Pre-clinically, the depletion of either XPF, or ERCC1 in platinum resistance A2780cis cell line increased sensitivity to platinum (Mesquita et al., 2019). Cisplatin induces DNA inter-strand crosslinks (ICLs) that lead to blocked DNA replication and transcription eventually contribute to generation of DSB. ATM and DNA-PK are mainly activated in response to DSBs. High ATM expression is associated with serous cystadenocarcinoma and platinum resistant. Overexpression of DNA-PK is correlated with serous cystadenocarcinomas, high-grade and advanced stage (Abdel-Fatah et al., 2014b). Although deficiency in homologous recombination has been associated with increased platinum sensitivity, restoration of *BRCA1/2* mutation has been reported to lead to platinum resistant (Mylavarapu et al., 2018).

Emerging evidences also suggests a possible role of base excision repair (BER) pathway in influencing sensitivity to cisplatin (Kothandapani et al., 2011). POLβ plays a vital role in BER and

overexpression of POLβ is significantly correlated with serous cystadenocarcinomas, poor PFS, poor OS and platinum resistant. XRCC1 is also a key player in BER. High expression of XRCC1 has been reported to be linked with serous cystadenocarcinomas, high grade, platinum resistant, poor OS and poor PFS. Pre-clinically, the depletion of XRCC1 promotes platinum sensitivity in ovarian resistance cell lines in 2D and 3D models (Ali et al., 2019). APE1 expression has also been overexpressed in 71.9 % of OC and is associated with optimal debulking, tumour type and OS (Al-Attar et al., 2010). Moreover, the overexpression of FEN1 was associated with high grade, high stage and poor survival in OC (Abdel-Fatah et al., 2014a).

1.6 TREATMENT OF RECURRENT DISEASES

The treatment of recurrent OC mostly relies on chemotherapy, which is used to improve survival and quality of life. The benefit of secondary cytoreductive surgery is controversial, but recent studies indicate that it may have a role in well-selected population (Lorusso et al., 2012, Hennessy et al., 2009). The second surgery was shown to improve survival of patients whose recurrence was at least six months after the first-line treatment. However, it remains unclear

whether these survival benefits were because of the surgical procedure or the biology of tumour (Bhat et al., 2015).

The major prognostic factor for success in the first-line treatment is the progression-free interval (PFI), which is the period from completion of chemotherapy until recurrence. There is a positive correlation between a long PFI and the response to the second-line treatment. Moreover, the PFI determines the selection of a chemotherapeutic regimen in cases of recurrence patients. Patients with a PFI less than six months are defined as having platinum resistant, while patients with disease progress during the initial treatment or with a PFI less than three months are identified as having platinum-refractory disease (Ushijima, 2010a). ICON4 has revealed increase in PFS and OS in recurrent OC in combination between paclitaxel plus carboplatin treatment (Parmar et al., 2003). Several second line agents are now available and shown in table 1.

Table 1.1 Second-line systemic treatment for OC.

Agents	Definition	Mechanism of action	Reference
Doxorubicin	Anthracycline antibiotic with cytotoxic and antimitotic activity	Inhibits topoisomerase II activity	(Strauss et al., 2008)
Etoposide	A semi-synthetic derivative of podophyllotoxin	Inhibits topoisomerase II activity	(Thavaramara et al., 2009)
Bevacizumab	Monoclonal antibody	Binds to VEGF and prevents angiogenesis	(Monk et al., 2013)
Gemcitabine	A nucleoside analogue	Inhibits DNA synthesis and induce apoptosis	(Kodaz et al., 2015)
Tamoxifen	A nonsteroidal triphenylethylene derivative	Binds to oestrogen and alter the regulation of its dependent genes	(Markman et al., 2004)
Topotecan	A synthetic camptothecin derivative	Inhibits topoisomerase I	(Markman et al., 2000)

1.6.1 TARGETED THERAPY

There is an urgent need for identifying novel biological therapies that target specific molecular abnormalities in tumour cells. Several signalling components are altered in OC, leading to activation of key oncogenic pathways implicated in process such as angiogenesis, DNA repair, cell proliferation and migration. Angiogenesis is key component in the growth of tumour and metastasis. Bevacizumab is

a monoclonal antibody target Vascular Endothelial Growth Factor (VEGF). Two randomised phase III trials (GOG 0218 and ICON7) have shown an improvement in PFS when bevacizumab was added to the combination of paclitaxel and carboplatin, followed by maintenance therapy, as the first-line therapy for advanced OC (Burger et al., 2011, Perren et al., 2011). Moreover, the addition of bevacizumab to chemotherapeutic agents in cases with platinum sensitive (OCEANS) and platinum resistant (AURELIA) recurrent disease improved PFS (Aghajanian et al., 2012, Pujade-Lauraine et al., 2014). Several angiogenesis inhibitors have also been investigated in clinical trials (Yoo and Kwon, 2013).

Targeted therapy using PARPi in *BRCA* mutated OC via the concept of synthetic lethality (SL) is well-established. SL is a phenomenon where two non-lethal genetic alterations can contribute to lethality together. This lethality may be from genes in the same pathways or related pathway, indicating that a deficiency in both genes significantly impacts their signalling and functions. SL has recently been applied in cancer treatment, whereby cancerous cells harbouring specific genetic mutations could be challenged by targeting the synthetic lethality genes or pathways, resulting in killing selective tumour cells (Figure 1.10) (Hosoya and Miyagawa, 2014, Helleday et al., 2008, Minchom et al., 2018).

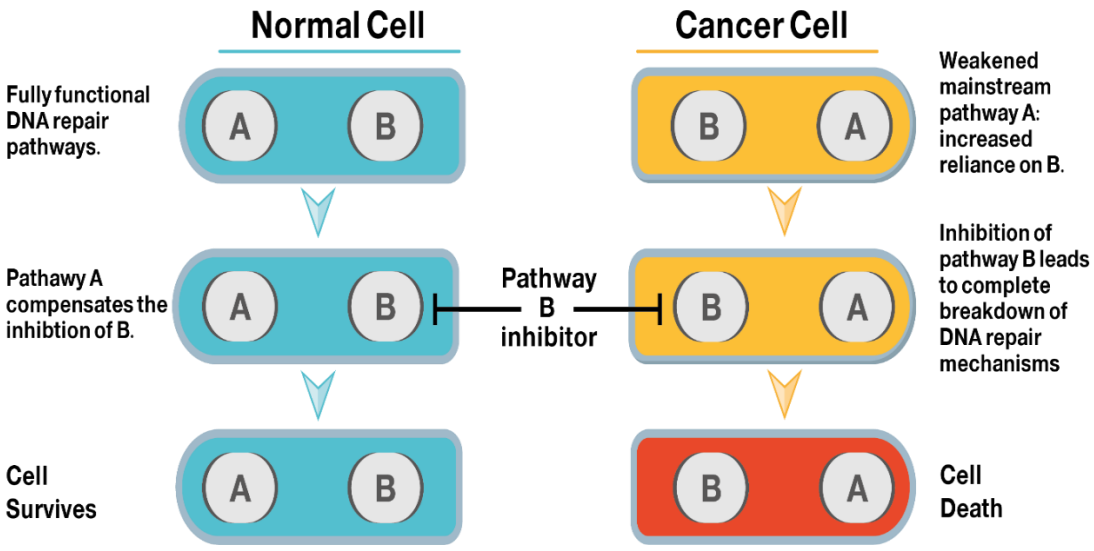

Figure 1.10: Systematic representation of the concept of synthetic lethality. DNA lesion is often repaired by multiple repair mechanism. A and B pathways are functional in normal cells; thus, DNA breaks will be repaired, and cell survives. In cancer cells: Pathway A is not functioned because of mutations, while Pathway B will be blocked due to the treatment of pathway B inhibitors, leading to cancer cell death, but normal cell is not affected. Modified from (Hosoya and Miyagawa, 2014).

The classic example of SL employed in OC therapy is that the relationship between BRCA genes and PARP. PARP inhibitors (PARPi) are the first DNA repair targeted therapy approved by Food and Drug Administration (FDA) for OC that based on personalized molecular background (Musella et al., 2018). PARP1 plays vital role in BER and NER repair pathways. It rapidly reaches DNA damage sites and get activated, which leads to poly-ADP-ribose (PAR) synthesis. PARP1

auto-PARylation recruits several DNA repair proteins (Morales et al., 2014). BRCA1/2 proteins are critically engaged in DSBs via HR. Women carrying harmful germline alterations in the *BRCA1/2* genes have a high risk of developing OC (Walsh, 2015). PARPi block PARP1 catalytic activity leading to prevent auto-PARylation, which disrupts BER and progression replication fork leading to DSB accumulation and cell dead (Ali et al., 2019a). PARPi in *BRCA* germline deficient OC patients was revealed to considerably improve progression-free survival (Lord and Ashworth, 2017, Walsh, 2015, Farmer et al., 2005, Bryant et al., 2005). There are currently three approved PARPi namely Olaparib, Niraparib and Rucaparib for OC treatment in USA and Europe (Musella et al., 2018). Talazoparib is also potent PARP1/2 inhibitor that was shown a significant clinical activity as a single agent in BRCA-deficient patients (Alblihy et al., 2019). However, 40-70% of BRCA1/2-mutated OC patients do not respond to PARPi treatment (Jiang et al., 2019), and the development of resistance recently abbreviated the clinical use of these inhibitors. Thus, the development of alternative SL approach targeting other DNA repair pathways is a high priority. Other DNA repair inhibitors, such as ATM inhibitors, ATR inhibitors and Wee1 inhibitors are also in early phase in clinical trials (Table 1.2). More importantly, whether a combination of DNA repair inhibitors can be used in certain

biological background, such as patients with HR deficiency, is currently an area of intense investigations. Targeting DNA repair pathways has true Potential to transform personalization therapy for cancer (Alblihy et al., 2019).

Table 1.2 DNA repair inhibitors in clinical trials. Modified from (Alblihy et al., 2019). * clinicaltrials.gov

DSB repair	Inhibitor	Clinical trial identifier
ATM	AZD1390 AZD0156	NCT03423628* NCT02588105*
ATR	AZD6738 VX970	NCT036682289* NCT02487095*
WEE1	AZD1775 (MK1775)	NCT02513563*
DNA-PKS	MSC2490484A M3814	NCT02316197* NCT03770689*
CHK1/2	SRA737 LY2606368	NCT02797977* NCT02873975*
BER		
PARP	Talazoloparib Olaparib Rucaparib Niraparib Veliparib	NCT01945775* NCT01874353* NCT01968213* NCT01847274* NCT02470585*
APE1	APX-3330	NCT03375086*

1.7 THE SELECTION OF DSBs REPAIR PATHWAY

Both HR and NHEJ are required for DNA double strand breaks repair. DSB end structure, end resection and the cell cycle phase are the main factors determining the choice between DSBs repair pathways (Figure 1.11). The cell cycle is the most important factor that regulates these repair pathways. The activity of HR occurs in post replicative stage of S phase due to the availability of the DNA homologous template or the generation of replication related one-ended DSB which are exclusively repaired by HR. In addition, the structure of condensed chromatin makes the homology search in G2-M phase difficult, thus leading to HR restriction. The dependency of DSB repair mechanisms on the cell cycle is thought to be dependent upon CDKs, which are able to regulate the DNA end resection (Tomimatsu et al., 2014). In G1 phase, DSB activates PI3KKs, ATM and DNA-PKcs. Unrepaired DSBs in G1 can contribute to fork collapse of replication stall, which upon resection activates the ATR-mediated checkpoint (Branzei and Foiani, 2008).

These PI3KKs functions as a sensor and initiate the signalling cascade which plays vital role in the DNA repair proteins recruitment. As a result, the generating long stretches of ssDNA leads to the commitment of cells to the HR (Shibata et al., 2014). DSB repair

kinetics by HR are believed to be slow and the turnover of DSBs indicates the repair choice of HR or NHEJ. More recent works show that NHEJ is the dominant DSB repair mechanism in G0, G1 and early S phases, and it also continues to have a minor role in late S and G2 phases. The phosphorylation of 53BP1 and it its interaction factor RIF1 inhibits the recruitment of BRAC1 at G1 phase, thus contributing to the end resection inhibition and HR (Zimmermann and de Lange, 2014). This inhibition is removed in S and G2 phases when CDK1- mediated the phosphorylation of Ctlp and then promoting HR (Yun and Hiom, 2009).

Cancerous cells are believed to have mutations in several checkpoint proteins, thus lending them with survival benefits. Therefore, understanding defects in DNA repair mechanisms and their selection in different cell cycle phases can open a great benefit for the field of targeted therapy. Alt-NHEJ shows slower kinetics repair compare to C-NHEJ, which confirms why the former, when active, is the dominant part of DNA end joining. Moreover, the KU heterodimers are abundant in nuclei and very quickly bind to the DNA broken ends and as a consequence, commit the repair towards NHEJ (Fattah et al., 2010).

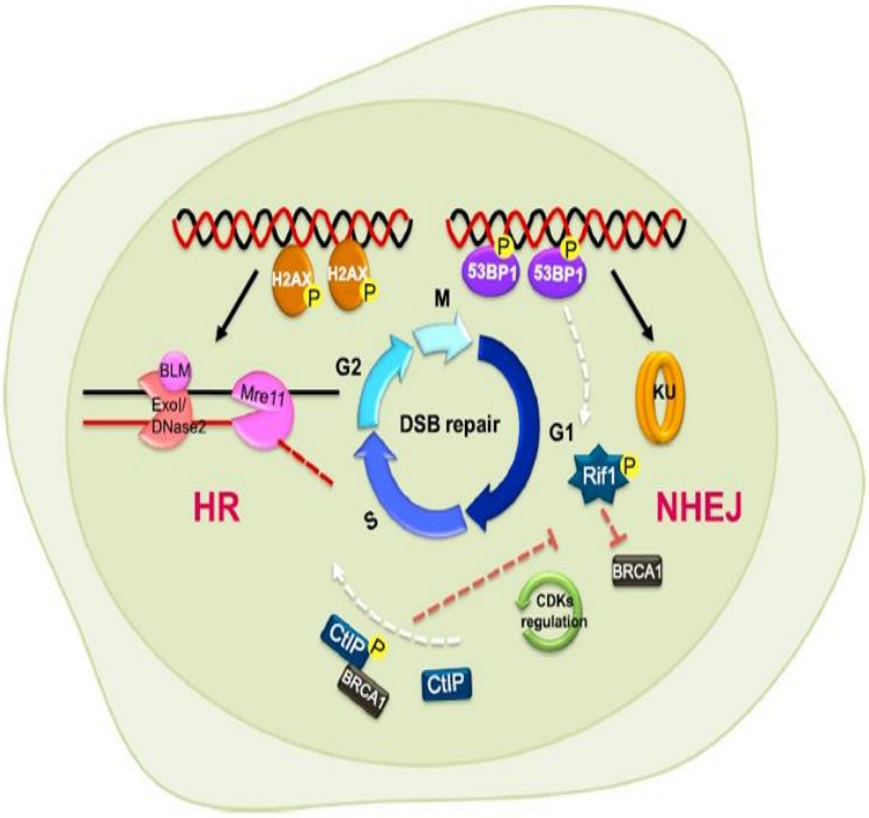

Figure 1.11: The choice between DSB repair mechanisms. HR and NHEJ are determined by many regulatory factors. HR is the dominated pathway in S and G2 phases due to the availability of a homologous template. While NEHJ operates throughout the cell cycle, NEHJ plays a main role in G1 and M phases. The negative regulation between RIF1 and 53BPI can also commit the repair choice to HR or NHEJ. The nuclease activity of MRE11 and EXO1/ *BLM* provide long starches of ssDNA tail that facilitate HR. The binding of the KU heterodimer to DNA ends can lead to direct commitment to NHEJ. The phosphorylation of Ctlp occurs in S phase and interacts with *BRAC1*, thus contributing to facilitate HR. The repair outcome also influences by CDKs. From (Srivastava and Raghavan, 2015).

1.8 THE MRN COMPLEX

Eukaryotic MRN consists of three subunits: MRE11, RAD50 and NBS1. MRE11 and RAD50 are strongly conserved across archaea to humans, while NBS1 (homolog of Xrs2 in yeast) does not have the same level of conservation as a eukaryotic-specific protein (Williams et al., 2007, D'Amours and Jackson, 2002). MRN has several enzymatic functions and so is categorised as a fundamental complex rather than a straightforward component existing in a linear pathway. MRN is involved in DNA damage sensing, the repair of DNA (Tauchi et al., 2002), DNA replication, mitosis, meiosis, the maintenance of telomere and apoptosis (Lamarche et al., 2010a). Furthermore, MRN is needed for V(D)J recombination (Helmink et al., 2009). Cells that are deficient in MRN components have similar phenotypes to those seen in ATM-deficient cells, such as impaired the activation of checkpoints in cell cycle, inefficient DNA repair, gene conversion, exchanges of sister chromatid, limited ss-annealing and apoptosis. While ATM loss does not have any embryonic lethality, null mutations for any of MRN proteins can contribute to embryonic lethality (Demuth et al., 2004).

Mutations in MRN subunits lead to cancer-prone diseases such as Nijmegen breakage syndrome (NBS) or Ataxia Telangiectasia like

disorder (ATLD) (Syed and Tainer, 2018b).There have been few reports of mutations in the RAD50 gene but have not been linked to specific human phenotypes. However, recent studies have shown a patient to have had heterozygous mutations in the RAD50 gene with low level of the unstable protein of RAD50. This patient's cells were characterized by a deficiency in RAD50 displayed a phenotype similar to NBS cells (Waltes et al., 2009a). These three diseases have common cellular and clinical phenotypes, including cerebellar degeneration, immunodeficiency, defects in DNA damage-induced activation of checkpoints, lack of ability to create DNA damage-induced MRN foci, increase the instability of chromosomes, premature aging and radiation sensitivity (Waltes et al., 2009a).

1.8.1 STRUCTURE AND FUNCTION OF MRN COMPLEX

1.8.1.1 MRE11

It is a highly conserved 70-90 KDa protein and it consists of 708 amino acids (aa). MRE11 contains several domains, which are involved in multiple functions (Figure 1.12) (Williams et al., 2007). The C-terminal has two DNA binding domains and a RAD50 binding domain, while the amino-terminal includes a NBS1- binding domain

and four phosphoesterase motifs which provides the ability to bind to duplexed and ssDNA- ends (Borde and Cobb, 2009). Nuclease domain in MRE11 is responsible for several enzymatic activities, such as the endonuclease activity against ssDNA on 5'- overhang and the exonuclease activity against dsDNA on 3'-5' which is manganese (Mn2+), NBS1 and ATM dependent. Moreover, MRE11 has DNA annealing and DNA unwinding activities that have shown to be regulated via the interaction with NBS1 and RAD50 (Jazayeri et al., 2008, Buis et al., 2008). The nuclease activity of MRE11 does not play vital role in the resection of clean DSBs, however, it is required to process DNA ends with covalent adducts (Llorente and Symington, 2004). It is likely that the nuclease activity of MRE11 is necessary for the resection 5'-3' of DNA ends appropriate for HR (Mimitou and Symington, 2009).

The biochemical and structural data shows generation of 3'-ssDNA tails for HR in vivo requires additional factors with reverse direction of nuclease activity in comparison with MRE11, such as EXO1 or CtIp (Schaetzlein et al., 2007). Consequently, one possible mechanism for the resection of DNA end may be a mechanism that has two steps, the involvement of a helicase such as BLM in conjunction with ssDNA endo- or exo- nuclease activity for DSBs resection (Mimitou and Symington, 2009). Certain studies in yeast show that the first

step relies on Sae2 and Mrx, which leads to endonucleolytic removal from the 5'end about 50-100 nucleotides, which generate an intermediate with 3'-ssDNA tails that is quickly processed in the second stage by a specific nuclease such as Sgs1 or EXO1 (Niu et al., 2009).

1.8.1.2 RAD50

RAD50 is a 150KDa protein and an ATP- dependent member of MRN related to the structural maintenance of chromosome (SMC) family member that regulate the dynamics of chromatin and the higher-order structure. Walker A and Walker B nucleotide triphosphate (NTP) binding motifs divided by two coil coiled regions holding two binding sites for MRE11 and central zinc-hook domains (CXXC motif) (Figure 1.12). The latter contains 14 residues, which is non-helical (440-453aa) and contain two major chain hydrogen bonds that are critical for the assembly of MRN complex and recombinational repair. RAD50 ATPase motifs are vital for all known functions of MRN including the activation of ATM through DSBs in vitro. ATPase and Adenylate kinase (AK) activities competitively act and control RAD50 conformation (allosteric) changes. These activities are critical for different functions of MRN in vivo, for example, unwinding, DNA tethering and DNA binding. Nonetheless, the main function of RAD50

is to bind to DNA damage ends and holding them in close proximity (Bhaskara et al., 2007, Hopfner et al., 2000, Lee and Paull, 2005, Lee and Paull, 2007).

1.8.1.3 NBS1

NBS1 is a 65-85KDa protein and contains 754aa. It consists of two vital phosphorylation sites for ATM which are Ser-278 and Ser-343 and three functional domains. These three domains are: The N-terminal fork-head associated domain (FHA), The BRCT domain and the C-terminal that has ATM and MRE11 interacting sites (Figure 1.12) (Williams et al., 2007). The FHA domain has role in mediating phospho-specific protein-protein interaction and hence it is vital for the efficient DNA damage signalling. It both identifies a phosphorylated target, such as γ-H2AX and interact with it, which contributes to MRN recruitment to DNA damage site. The BRCT domain leads to the formation of nuclear foci, the association of chromatin and is involved in S-phase checkpoint regulation (Bhaskara et al., 2007, Lloyd et al., 2009). The site where NBS1 interact with MRE11 in C-terminal is critical for viability due to the truncation in this region leads to interrupted MRE11 binding, and embryonic lethality. NBS1 patient cells with a deletion on N-terminal show abrogated phosphorylation of MRE11 and lack of recruitment

of nuclear focal of MRE11, which suggests that the formation of MRE11 foci and the phosphorylation are both NBS1 dependent. However, other studies indicate that half a C-terminal is enough to the localization of RAD50-MRE11 (MR complex) to nucleus. However, this interaction does not have enough stimulation to the ATM interaction and/ or formation of nuclear focus. The catalytic functions in MR complex are regulated via NBS1 by joining them to form MRN complex. The main function of NBS1 is to drive MR complex to nucleus and activate ATM (Difilippantonio et al., 2005, Syed and Tainer, 2018b). The interaction between MRN components at the DSB site is shown in Figure 1.13.

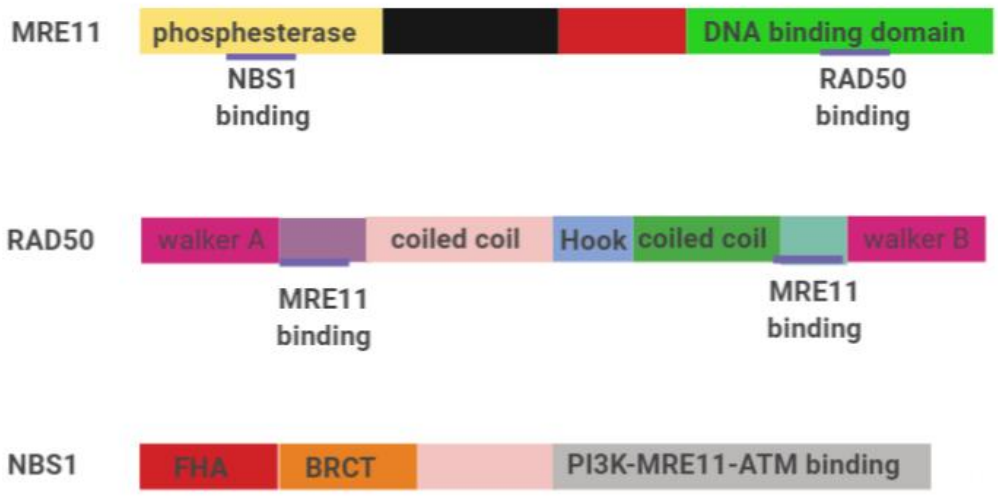

Figure 1.12: Scheme of MRN complex protein domains. Interaction domains are demonstrated in purple. CXXC hook: zink domain, BRCT: BRCA1 carboxyl terminal domain, FHA: forkhead associated domain. Modified from (Lamarche et al., 2010a).

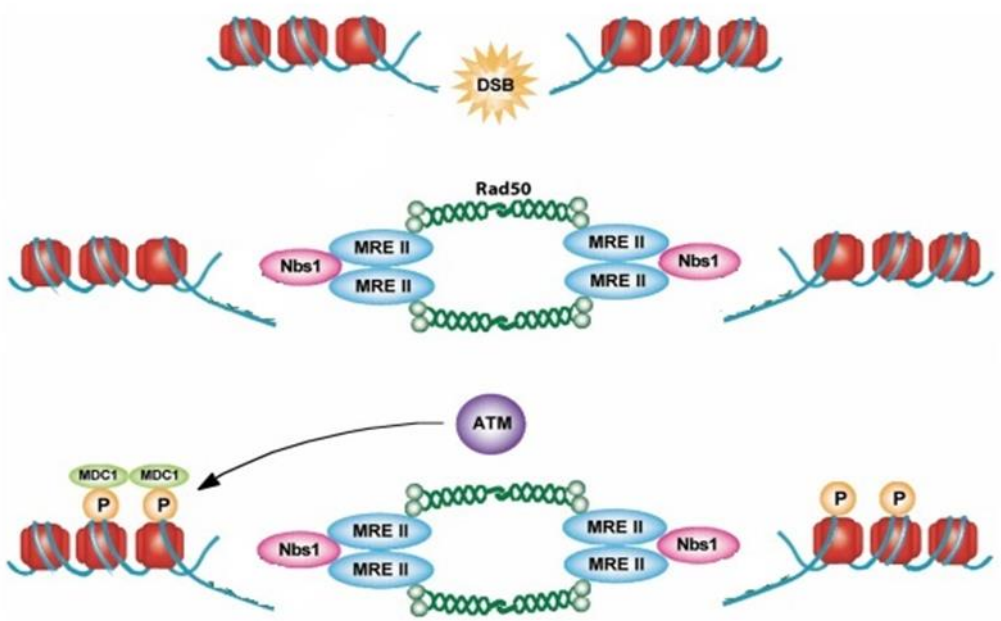

Figure 1.13: Systematic representation of the possible mode of interaction between MRN complex components in DSB site. Modified from (Richard et al., 2011).

1.8.2 THE ROLE OF MRN COMPLEX IN DDR

After the induction of DNA damage, MRN very rapidly localize to DSBs. NBS1 then recruits ATM to the site of damage, leading to the autophosphorylation of ATM on Ser-1981. ATM is thus converted from an ATM inactive dimer to active monomer (Berkovich et al., 2007), and its kinase activity is initiated. ATM also phosphorylates NBS1 and MRE11, thus activates cascades of downstream of DNA damage signalling, DNA repair mechanisms and cell cycle responses (Syed and Tainer, 2018a).

The function of MRN is not only to play a vital role in ATM activation, but also it can be a target for the kinase activity of ATM to amplify the cell cycle checkpoints signals. The signals of cell cycle checkpoints can be activated by the binding of NBS1 to γ-H2AX, which contributes to a second wave of recruitment of MRN to the damage site. Several in vitro studies have demonstrated that mutations in *NBS1* at Ser-343 indicates no checkpoints response due to the failure in stimulating the phosphorylation of CHK2 via ATM (Difilippantonio et al., 2005, Lee and Paull, 2007, Lavin, 2007).

The nuclease activity of MRE11 in mammals is involved in ATM activation through variable approaches, such as the impact on replication fork stability, cell cycle checkpoints initiation and repair processes (Hashimoto et al., 2010). Consequently, there is a putative role for the nuclease activity of MRE11 in the continued activation of ATM. Although the initial activation of ATM does not require MRE11 nuclease activity, MRE11 nuclease activity plays role in the maintenance of ATM checkpoints signalling (Jazayeri et al., 2008, Dimitrova and de Lange, 2009). The processing of DSBs to ss-DNA finally inhibits ATM and leads to the switch from ATM to ATR. MRN might function to control the activity of ATM through ongoing DSB signalling by regulating the production of appropriate DNA substrates at various stages in the response of DSB. Furthermore,

the nuclease activity of MRE11 is a critical function in the DNA repair that is distinct from MRN regulation of ATM signalling (Buis et al., 2008, Shiotani and Zou, 2009).

Taken together, these studies show that MRN functions not only as a sensor for DNA damage and upstream regulator for ATM activity, but that it also has an important role in downstream ATM kinase activity in signalling and repairing DSBs.

1.8.3 THE ROLE OF MRN COMPLEX IN DSB REPAIR

As mentioned earlier, the MRN complex activates cell cycle checkpoints in response to DNA breaks and has critical role in all DSB repair mechanisms (normally HR, C-NHEJ and Alt-NHEJ). There are multiple distinct models for the role of MRN complex in DNA end-tethering and processing during DSB repair. For example, HR repair needs architecture, structural and enzymatic elements. Architecture elements are required for tethering DSB-ends in close proximity to avoid inappropriate recombination and to pair the DSB ends with homologous sequence (Figure 1.14). Enzymatic activities are needed for processing DNA ends and repairing process (Lieber, 2010b, Shin et al., 2004). MRN complex appears to be a linker for DNA

homologous stretches and/or broken ends, whereas MRE11 resecting activity is needed for RAD51 nucleoprotein filament formation during the presynaptic step of recombination (Hopfner et al., 2002, Hopkins and Paull, 2008).

MRN complex involvement in HRR is supported by data revealing that a deletion of MRE11 or NBS1 in chicken DT40 cells led to a reduction in HR and the exchange of sister chromatid without impacting end-joining frequencies in plasmid-based assays (Yang et al., 2006c). Other studies demonstrated that the deficiency of MRN confers a strong defect in class switch recombination (CSR) affecting both C-NHEJ and Alt-NHEJ (Helmink et al., 2009). Other results revealed that depletion of RAD50, MRE11 or CTIP decreased NHEJ, possibly because MRE11 can regulate end-joining via both ATM dependent and ATM independent pathways (Rass et al., 2009). MRN plays also an important role in replication fork dynamics (Figure 1.15) and dysfunctional telomeres (Figure 1.16).

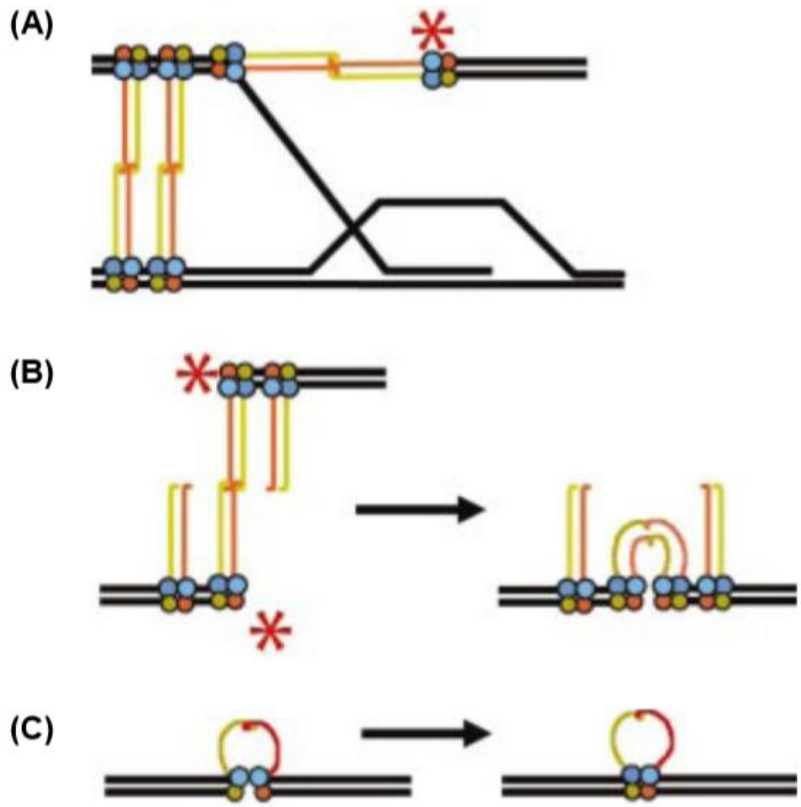

Figure 1.14: Systematic representation of the role of MRN complex in HR and NHEJ. A) MRE11 nuclease activity process DSB end for the next repair step. The tail-tail architecture-linked MRN complex indicates a mechanism to bridge sister chromatids, initiate and stabilize displacement loop formation, break-induced replication and the maintenance of telomere. B) In NHEJ, head domains of M2R2 complexes bind to separate broken DNA ends to align and tether them after a structural transition. C) Circularization of a single M2R2 complex can potentially lead to productive repair of broken DNA ends. From (Hopfner et al., 2002).

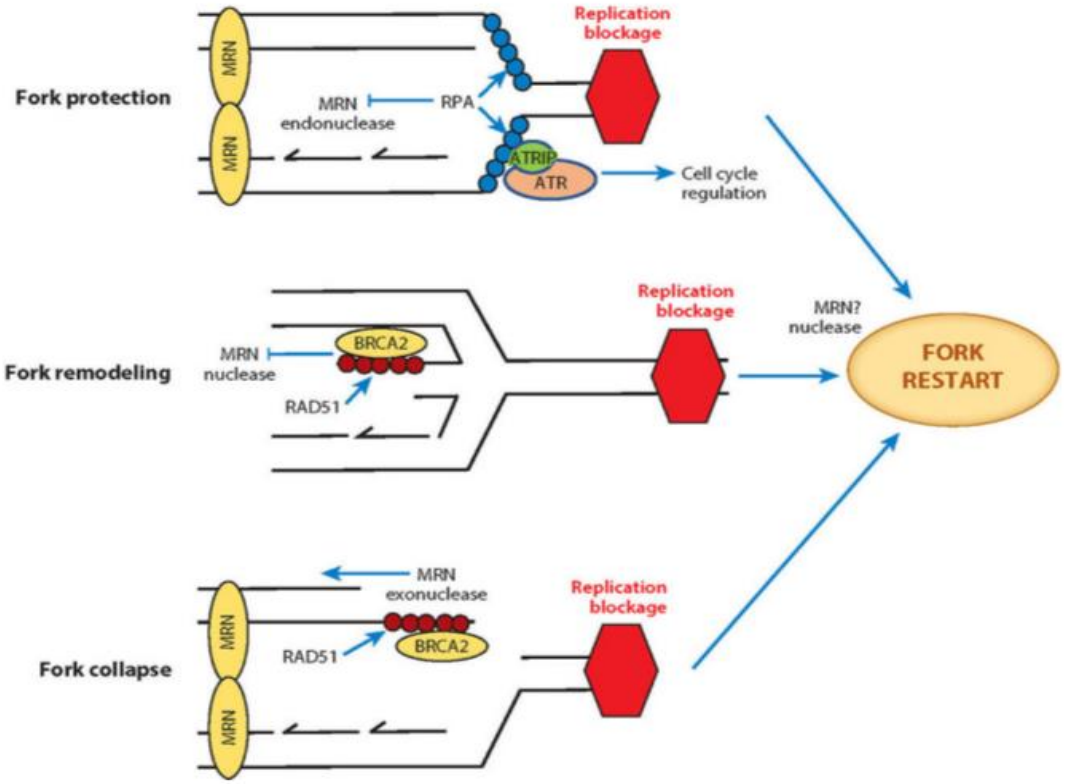

Figure 1.15: Systematic representation of the role of MRN complex in replication forks dynamics. MRN, with help of ATR and RPA, orchestrates replication fork protection, remodelling and restart HR rescue of collapsed forks. At stalled forks, MRN plays role through its DNA tethering function, while its nuclease activity is suppressed by RPA. RPA-coated ssDNA promotes ATR checkpoint signalling that give cells enough time to repair and restart. The barriers of replication are removed by remodelling via fork reversal, which must be then processed for fork restart. RAD51 protects the nascent ssDNA at reversed fork against the exonuclease activity of MRN. The excision of MRE11 of one strand can facilitate fork reversal and restart. Unrepaired collapsed fork becomes DSBs where MRN is key player in repairing DSBs. From (Syed and Tainer, 2018b).

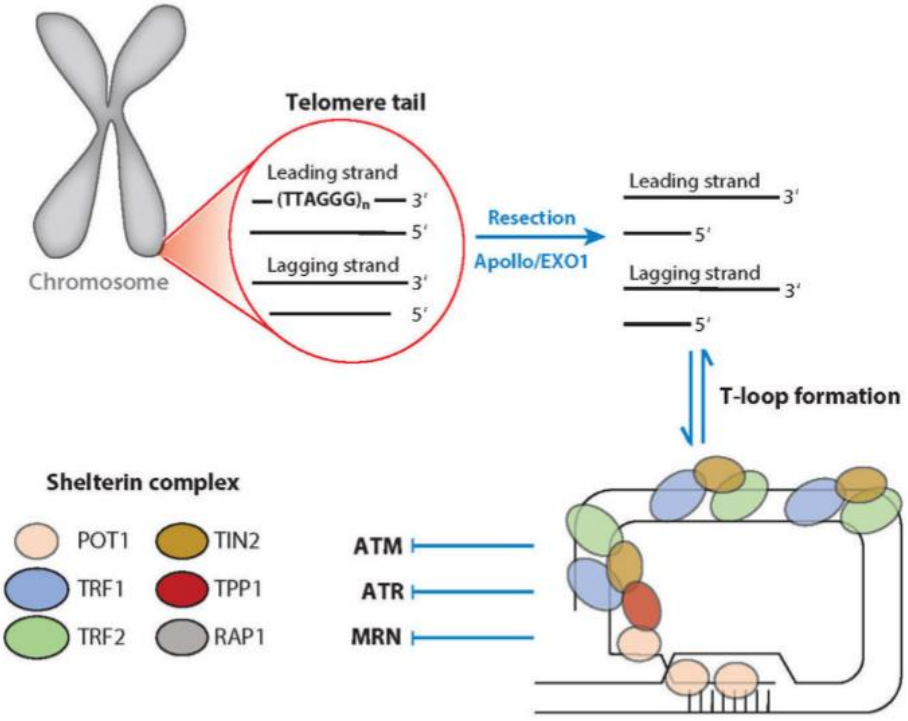

Figure 1.16: Systematic representation of the role of MRN complex in telomere dysfunction. Telomere structure and dynamics control MRN interaction and differentiate the ends of chromosome from breaks. Human telomeres composed of repetitive sequence (TTAGGG) and interacting proteins. Telomeres forming from the replication of a leading DNA strand, resulting in tails with blunt ends, while the lagging DNA strand replication generates telomeres with 3’ overhang. The 5’ resection of a blunt-ended telomere leads to inhibit the fusion of telomere via NHEJ with the assistance of MRN complex. The 3’ overhang in a telomere form transient T-loop structure. The sheltering complex helps in protecting the telomere ends. MRN complex aids the sheltering complex to avoid the repair of DSB at functional telomeres and recruiting telomerase to telomers. From (Syed and Tainer, 2018a).

1.9 PROJECT RATIONALE AND HYPOTHESIS

Platinum resistance is a formidable clinical problem in OC. The DNA repair mechanism is the key regulator in the formation and removal of platinum adducts. Thus, targeting DNA repair proteins is a promising strategy for OC personalization therapy. The recent approval of PARPi for the use in clinical setting in *BRCA* mutated OC has re-energised the DNA repair targeted therapy field. However, 40%-70% of patients do not respond to PARPi, which makes an adverse clinical impact. Therefore, the development of alternative DNA repair targets is crucial. MRN complex has several functions; a 'first responder' to DNA damage, activation of ATM and ATR, a DSB repair effector in both NHEJ and HR, stalled replication fork and dysfunctional telomeres. In the light of this our hypothesis is that MRN complex could be a promising drug target for chemo-sensitization and synthetic lethality application.

1.10 PROJECT AIMS

The main aims of this project were 1) to clinically assess the association between MRN complex expression and platinum resistant in EOC, 2) To determine the role of MRN complex in mediating therapeutic response to cisplatin in cell lines models and

3) Generating mirin (MRE11 inhibitor) resistance cell line (PEO1R) form parental PEO1 cell line. The strategies for achieving these aims were:

- Evaluate the clinicopathological significance of MRN complex expression by immunohistochemistry in 331 human OC.
- Investigate MRN mRNA expression in a publicly available online gene expression dataset of 1259 OC patients to determine the correlation between MRN mRNA expression and patients' survivals.
- Study the effectiveness of MRN complex depletion in enhancing platinum sensitivity.
- Investigate whether MRE11 inhibitor (mirin) would sensitize resistance ovarian cell lines models.
- Study whether mirin treatment could be synthetically lethal in BRCA2-deficient and XRCC1-deficent OC cells lines models and 3D spheroids models.

- Develop a mirin resistant cell line model (PEO1R) from a parental cell (PEO1) to evaluate the mechanism of resistance to MRE11 inhibitor.
- Investigate the role of MRE11 in invasion, EMT and ovarian stem cells like phonotype.

CH. 2

MATERIALS AND METHODS



2. MATERIAL AND METHOD

2.1 MATERIALS:

2.1.1 COMPOUNDS:

Cisplatin was kindly provided as a 3.3 mM solution from the pharmacy at Nottingham University City Hospital (Nottingham, UK), and it was stored at room temperature. Mirin inhibitor (M9948) was purchased from Sigma Aldrich, UK. Mirin is stored at 4°C. Olaparib (AZD2281) was provided by AstraZeneca Pharmaceuticals, and it stored at -20°C. Mirin and olaparib were each suspended in 100 % v/v dimethyl sulphoxide (DMSO) (276855-250ML, Sigma Aldrich, UK). The Proteasome inhibitor (MG-123) (M7449-200UL) was purchased form Sigma Aldrich, UK. The Protein synthesis inhibitor (Cycloheximide) was purchased form Sigma Aldrich, UK.

2.1.2 CELL LINES:

A2780 and A2780cis cells were purchased from Sigma Aldrich (Gillingham, UK). PE01 (BRCA2-deficient) and PE04 (BRCA2-proficient) were purchased from American Type Culture Collection (ATCC, Manassas, USA). Control Hela SilenceX , BRCA2 hela SilenciX and XRCC1 hela SilenciX were purchased from tebu-bio, Peterborough, UK. Cell lines characteristics and culture media are

presented in Table 2.1. Authentication of cell lines were done by ATCC company using Promega Powerplex® 17 short tandem repeat (STR) system to ascertain there was no cross-contamination or misidentification of cell lines. Mycoplasma test was routinely preformed almost every six months using MycoProbe Mycoplasma Detection Kit (R&D systems; Abingdon, UK). Cell lines were used up to 16 passages.

Table 2.1: Cell lines and culture media.

Cell line *	Characteristic	Culture media
A2780	Human ovarian carcinoma, endometrioid isolated from primary tumours of untreated patient	1% penicillin/streptomycin +10% FBS + RPMI (1640)
A2780cis	Cisplatin-resistant cell line developed by continuous expose of A2780 to cisplatin doses	1% penicillin/streptomycin +10% FBS + RPMI (1640)
PEO1	Isolated from malignant effusion from peritoneal ascites of a patient with very poor differentiated serous adenocarcinoma having BRCA2 mutation [5193C>G (Y1655X)]	1% penicillin/streptomycin +10% FBS + RPMI (1640)
PEO4	Derived from the same PEO1 patient as PEO1 cells after the patient developing resistance to chemotherapy in clinic due to the restoration of BRCA2 mutation	1% penicillin/streptomycin +10% FBS + RPMI (1640)
Control hela SilenciX	Monoclonal Hela control engineered to deliver a stable siRNA designed to not match a human gene	1%penicillin/streptomycin +10%FBS + Dulbecco's Modified Eagle Medium (DMEM)
BRCA2 hela SilenciX	Cell line has a stable and efficient *BRCA2* gene knockdown	DMEM +125 µg/ml Hygromycin B+ 1%penicillin/streptomycin +10%FBS
XRCC1 hela SilenciX	Cell line has a stable and efficient *XRCC1* gene knockdown	DMEM +125 µg/ml Hygromycin B+ 1%penicillin/streptomycin +10%FBS

*Data about all ovarian cell lines adapted from (Stordal et al., 2013, Beaufort et al., 2014). Data about control hela silenceX, BRCA2 hela SilenciX and XRCC1 hela SilenciX obtained from tebu-Bio, UK, https://www.tebu-bio.com/.

2.2 METHODS:

2.2.1 CLINICAL STUDY:

Evaluation of the expression of MRE11, RAD50 and NBS1 in Epithelial ovarian cancer (EOC) was performed on tissue microarrays of 331 consecutive EOC cases treated at Nottingham University Hospitals between 1997 and 2010. Tumour stages were determined according to the International Federation of Obstetricians and Gynaecologists (FIGO) Staging System for Ovarian Cancer. Overall survival (OS) was calculated between the day of diagnosis or time of treatment initiation and time where patients still alive. Progression free survival (PFS) is the time between treatment initiation and tumour progression again. The patient demographics and pathological characteristics in EOC is shown in table 2.2. This study was carried out in accordance with the declaration of The Helsinki and ethical approval which was obtained from the Nottingham Research Ethics Committee (REC Approval Number 06/Q240/153).

Table 2.2: Patient demographics and pathological characteristics in EOC.

Characteristics	Number	Percentages
Pathology		
Serous cystadenocarcinoma	178	53.9%
Endometrioid	44	13.2%
Clear cell carcinoma	24	7.2%
Mucinous cystadenocarcinoma	46	13.8%
Others	15	4.5%
Mixed	17	5.1%
missing	7	2.3%
Grade		
1	46	13.8%
2	60	18%
3	171	51.5%
missing	54	16.7%
Residual tumors		
None/Microscopic	205	61.7%
<1cm	34	10.2%
>1-2 cm	15	4.5%
>2cm	40	12%
Missing	37	11.6%
FIGO Stage		
I	123	37%
II	49	14.7%
III	128	38.5%
IV	11	3.3%
Missing	20	6.5%
Chemotherapy		
Carboplatin monotherapy	100	30%
Carboplatin + Paclitaxel	110	33%
Other regimens *	26	8%
No chemo	23	7 %
unknown	72	22%
Platinum sensitivity		
Sensitive *	250	75.3%
Resistant	26	7.8%
Unknown	55	16.5%
Relapse status		
Progression-free *	169	50.9%
Progressed/relapsed	118	35.5%
Unknown	44	13.2%

Other Regimens included: 3= CAP (Cyclophosphamide, Adriamycin and Cisplatin) 4 = ICON5 Trial 5 = SOCTROC Trial 6 = Carboplatin and Endoxan. 7 = Chlorambucil. For the unknown category, the majority received platinum-

based chemo but because the exact regimen was not mentioned clearly in the database, they were considered as unknown. However, for these cases the platinum sensitivity status were clearly mentioned / recorded.

*Platinum resistance was defined as patients who had progression during first-line platinum chemotherapy or relapse within 6 months after completion of platinum treatment.

* Progression-free survival was calculated from the date of the initial surgery to disease progression or from the date of the initial surgery to the last date known to be progression-free at the end of follow-up. All the patients' dates of disease recurrence were recorded in the main sheet where we used to perform the analysis.

Clinical study was performed by. Dr. Muslium alabdullah form Prof. Emad Rakha pathology group. University of Nottingham.

2.2.1.1 THE CONSTRUCTION OF TISSUE MICROARRAY

A tissue sample was preserved by fixing it in formalin, to protect the proteins and essential structures within the tissue. Sample was then embedded in a paraffin wax block; to facilitate the cut slices of needed sizes to mount on a microscopic slide for investigation. Formalin-Fixed Paraffin-Embedded (FFPE) blocks with abundant tumour and suitable thickness were chosen for TMA construction. Cores of 0.6 mm thickness were taken from the most representative tumour areas in the donor blocks and then arrayed into a recipient paraffin block. Only one sample from each case was used in each TMA. An automated TMA puncher/arrayer (Beecher Instruments, Silver Spring, MD, USA) was used to load 60 donor blocks at a time into the recipient blocks. Core orientation on the slide is very important, because uncertainty in core orientation can threaten the assessment of the experiments. Therefore, in each block, three normal kidney cores were used at the start of the first row and three normal liver cores were used at the end of the last row. Before sectioning, TMA blocks were incubated at 37°C for 15 minutes to allow the surrounding paraffin and cores to hybridize. For immunohistochemistry, 4 μM thickness were cut by microtome from each TMA block and placed on clean glass slides (Kononen et al., 1998).

2.2.1.2 IMMUNOHISTOCHEMSTRY:

Immunohistochemistry (IHC), a well-versed method for diagnosis and research purposes, was employed here to enable the identification of antigens in tissue cells through the process of specific antigen-antibody reactions. Here, the antigen in question was a protein. IHC achieves rapid results without high costs and permits the colocalization of proteins with any lesions they have formed, resulting in increased the accuracy of diagnosis.

2.2.1.2.1 NOVOLINK DETECTION PROTOCOL FOR IMMUNOHISTOCHEMICAL ANTIBODY IDENTIFICATION

The glass slides with the tissue samples were incubated at 60°C on hotplate for 10 minutes to ensure binding of the TMA cores to the slides. The slides were then allowed to cool and de-waxing by immersion in two xylene baths for 5 minutes in room temperature. The samples were rehydrated by immersion in Industrial Methylated Spirits (IMS) (3 × 2 min), and the slides were rinsed for 5 min in water. These steps were carried out via the use of the IHC Leica Autostainer XL (ST5010).

Antigen retrieval was conducted by heating the slides at 95°C in a microwave (Whirlpool JT359 Jet Chef 1000W) for 20 minutes while

the slides were submerged in a pH 6.0 1M sodium citrate buffer. The slides were cooled under flowing tap water for 5 minutes. The slides were dried and then an ImmeEdgeTM pen (H-4000) was used to make two hydrophobic barriers, one above and one below TMA cores. Slides were then washed with TBS-Tween (500ml 1X TBS of pH 7.6 with 500µl Tween20), followed by addition of 300µl Peroxidase Block (Novolink Max Polymer DS (1250) - RE7280-CE, Lecia, US) for 5 minutes to inhibit internal peroxidise production. Slides were washed three times with TBS-Tween each time for 5 minutes. 300µl of anti MRE11, anti RAD50 and anti NBS1 primary antibodies were diluted in BONDTM antibody diluent (AR9352, Lecia, US) for 60 minutes at room temperature (optimized staining time). Information about the antibodies are shown in (Table 2.3). Slides were then washed with TBS-Tween (3 × 5 min). 300µl of post primary was added for half hour, and then slides were washed with TBS-Tween (3 × 5 min). 300µl polymer was added for 30 minutes and then slides were washed with TBS-Tween (3 × 5 min). DAB working solution was prepared using DAB chromogen and DAB substrate buffer in 1:20 ratio. 300µl of DAB was added to the slides for 5 minutes, and then slides were washed with TBS-Tween (3 × 5 min). Slides were then counterstained with 300µl of Haematoxylin stain for 6 minutes. Slides were then dehydrated in the Leica autostainer. Samples on the slides were then covered by coverslips and left in a hood to dry overnight. Negative controls (with primary

antibody and IgG-matched serum omitted) and positive controls were used in each run.

Table 2.3: Antibodies for Immunohistochemistry. RT=room temperature.

Anti-human Ab.	Clone	Conc. used	Incubation condition	Source
Anti-MRE11	Ab214	1:800	1hour/RT	Abcam
Anti-RAD50	Ab89	1:400	1hour/RT	Abcam
Anti-NBS1	N3162-200UL	1:200	1hour/RT	Sigma

2.2.1.2.2 PRIMARY ANTIBODIES OPTIMISATION

Optimisation of antibodies was performed by incubating at least four different concentrations of each antibody with TMA slides. The concentration was chosen based on the supplier recommendation. The specificity of MRE11 antibody was tested by applying positive and negative controls. Negative control was ovarian TMA section used without adding MRE11 antibody which revealed no staining. MRE11 antibody was examined for optimization. 1:100, 1:200 and 1:300 dilutions overnight, and 1:100, 1:200, 1:400 and 1:800

dilutions for one hour. The 1:800 dilution section for one hour provided the optimal staining with very clear nuclear staining without background staining. The specificity of MRE11 antibody was also tested by western blotting in four ovarian cell lines. MRE11 antibody specificity was also confirmed by the knockdown studies.

The specificity of RAD50 antibody was tested by applying positive and negative controls. Negative control was ovarian TMA section used without adding RAD50 antibody which revealed no staining. RAD50 antibody was examined for optimization. 1:100, 1:200, 1:300 and 1:400 dilutions for one hour. The 1:400 dilution section for one hour provided the optimal staining with very clear nuclear staining without background staining. The specificity of RAD50 antibody was also tested by western blotting in four ovarian cell lines.

The specificity of NBS1 antibody was tested by applying positive and negative controls. Negative control was ovarian TMA section used without adding NBS1 antibody which revealed no staining. NBS1 antibody was examined for optimization. 1:50, 1:100 and 1:200 dilutions for one hour. The 1:200 dilution section for one hour provided the optimal staining with very clear nuclear staining without background staining. The specificity of NBS1 antibody was also tested by western blotting in four ovarian cell lines.

2.2.1.2.3 IMMUNOHISTOCHEMICAL SCORING

TMA cores was scored by the author and pathologists in collaboration with Prof. Emad Rakha group at the University of Nottingham, using a Nikon Eclipse 80i Microscope. TMA cores that had several replicates were averaged and allowed for further intra-rater reliability. The scoring was preformed using histochemical scores (H-score). H-score calculates both the percentage of immune staining and the intensity of staining and combine them into one score. The staining intensity was assessed as follow: negative staining was 0; weak = 1; moderate = 2; and strong = 3. The percentage of positive tumour cells was estimated in a range of 0-100%. The H-score was calculated using this formula: (percentage of strongly staining nuclei x3 + (percentage of moderately staining nuclei x2 + (percentage of weakly staining). TMA cores that were missing because of TMA construction, antigen retrieval, benign or contained less than 15% tumours cells were excluded from scoring.

2.2.1.2.4 STATISTICAL ANALYSIS

Statistical Package for the Social Science (SPSS), version 22, Chicago, IL, USA) software for windows, was used for statistical analysis. The cut-off points for all MRN complex markers were chosen using the median of the H-score according to the distribution

pattern of data. Low/negative nuclear MRE11 expression was identified by the median H score of ≤110. Low cytoplasmic MRE11 staining was identified by the median H score of ≤60 (Figure 2.1). Low/negative nuclear RAD50 staining was identified by the median H score of ≤120. Low/negative cytoplasmic RAD50 staining was identified by the median H score of ≤0 (Figure 2.2). Low/negative nuclear NBS1 staining was identified by the median H score of ≤0. Low/negative cytoplasmic NBS1 staining was identified by the median H score of ≤90 (Figure 2.3). Univariate correlation between markers expression and pathological parameters was determined using Chi-squared test. Survivals rates were calculated using Kaplan–Meier survivals and compared by the log-rank test. The P value less than 0.05 was considered as statistically significant. The statistical analyses were performed by Dr. Muslium alabdullah form Prof. Emad Rakha group.

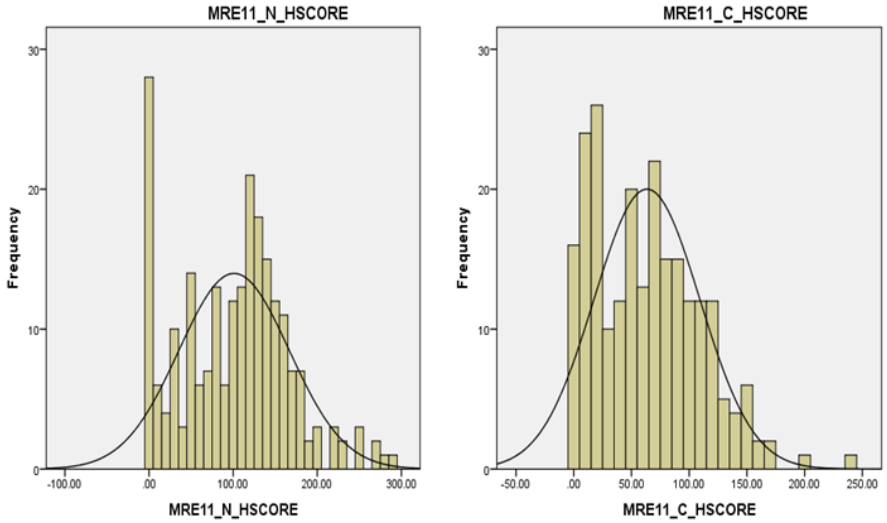

Figure 2.1: Histogram charts showing the selection of immunohistochemical cut off scores for MRE11 nuclear and cytoplasmic expression. Low/negative nuclear MRE11 expression was identified by the median H score of ≤110. Low cytoplasmic MRE11 expression was identified by the median H score of ≤60.

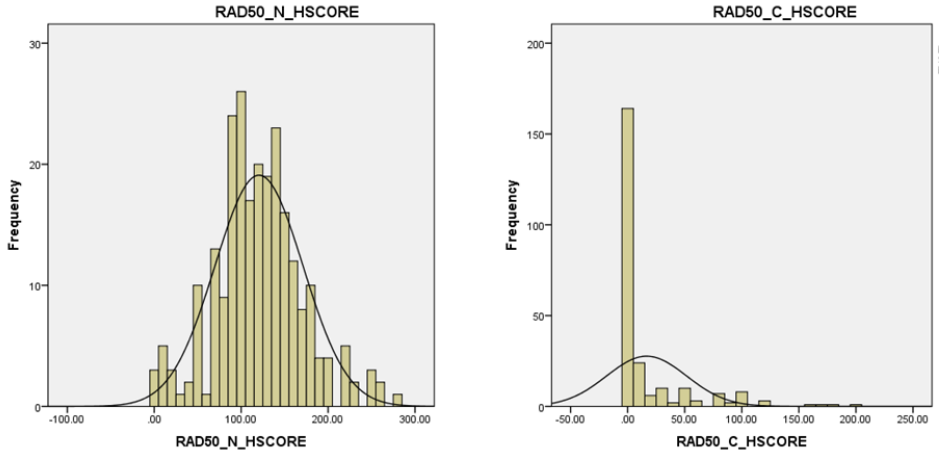

Figure 2.2: Histogram charts showing the selection of immunohistochemical cut off scores for RAD50 nuclear and cytoplasmic. Low/negative nuclear RAD50 expression was identified by the median H score of ≤120. Low cytoplasmic RAD50 expression was identified by the median H score of ≤0.

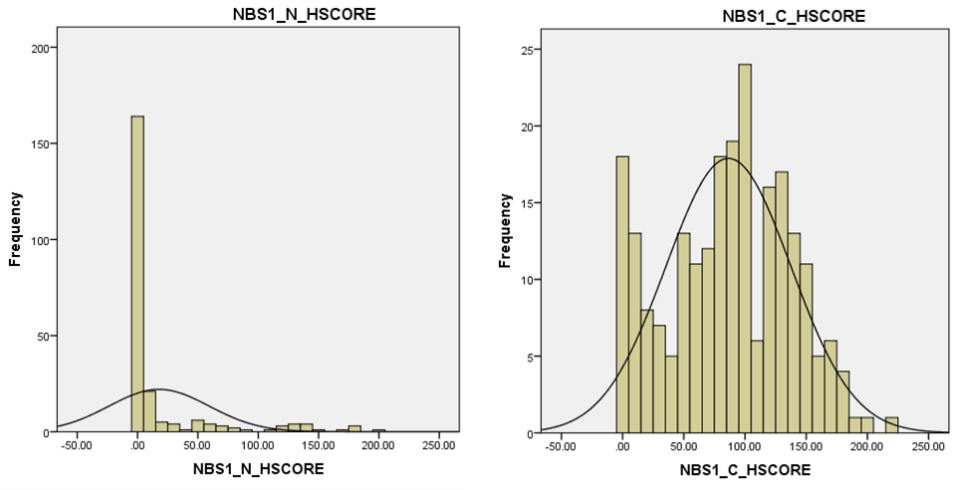

Figure 2.3: Histogram charts showing the selection of immunohistochemical cut off scores for NBS1 nuclear and cytoplasmic expression. Low/negative nuclear NBS1expression was identified by the median H score of ≤0. Low cytoplasmic NBS1expression was identified by the median H score of ≤90.

2.2.1.3 *MRE11*, *RAD50* AND *NBS1* TRANSCRIPT IN OVARIAN CANCER

MRN complex mRNA expression was evaluated in a publically available online gene expression dataset of 1287 ovarian cancer patients treated with platinum-based chemotherapy from 15 previously published studies and available at 'http://kmplot.com/analysis/index.php?p=service&cancer=ovar'.

For more details about the database setup (Gyorffy et al., 2012).

2.2.2 PRE-CLINICAL STUDIES:

2.2.2.1 SUBCULTURING CELL LINES

Cell lines were cultured at 37ºC with 5% CO_2/95% air. To trypsinise cells, each cell line was separately handled under sterile conditions with its own reagents. First, cell media was removed by pipetting, and cells then washed PBS (without Mg2+ and Ca2+). This was followed by adding 0.5mg/ml trypsin- EDTA (Sigma Aldrich, UK) to disrupt cell monolayers. Cells were then incubated for 3-5 minutes at 37ºC. Medium was then added to the flask 4:1 to trypsin to deactivate the effect of trypsin. Cells were then centrifuged at 1000 rpm for 5 minutes. Cell pellet was re-suspended in fresh media, which was then mixed well. This mixture was put into a new flask.

2.2.2.2 CRYOPRESERVATION OF CELL LINES

Cells at a low passage number were cryopreserved for future use. Cells were collected by trypsin as described above. Approximately 1 x 10^6 cells were re-suspended in 1ml of cell line-specific media+ 10% DMSO (9:1) and stored in freezing container (CLS432000-1EA, Sigma Aldrich, UK) at -80ºC. Next day, cells were stored in liquid nitrogen for long-term storage. For re-use cells, they were taken from the liquid nitrogen and thawed in a water bath at 37°C. The cells were then re-suspending in 9 ml of cell-specific medium and

transferred to T25 flask to adhere overnight. The following day media was discarded, and fresh media was added.

2.2.2.3 CELL LYSATE PREPARATION

Cell lysates were prepared for western blot. Cells were collected as previously described and counted. A minimum of 1×10^6 cells per sample were lysed by resuspension in 100 µl of lysis buffer, consisting of RIPA buffer (R0278-500ML, Sigma Aldrich, UK), 1% of Cocktail 2 (P5726-1ML , Sigma Aldrich; UK), 1% of Cocktail 3 (P0044-1ML, Sigma Aldrich; UK) and 1% of protease inhibitor (Sigma; UK). The cell lysate was stored at -20 °C. Before using the lysate for western blot, the lysates were repeatedly aspirated with a fine-gauge needle in order to break cell membranes. Lysates then were centrifuged at 13000 rpm for 20 minutes at 4 °C to remove cell debris.

2.2.2.4 PROTEIN QUANTIFICATION

The bovine serum albumin (BSA) protein quantification assay was used to calculate protein concentrations in cell lysates by generating protein strand curves, in this case for BSA. The BCA kit (A7906, Sigma Aldrich, UK) is a colorimetric detection kit using the reduction of Cu+2 to Cu+1 by protein in an alkaline medium (the biuret reaction) with high sensitivity. The colorimetric detection of the

cuprous cation (Cu+1) using bicinchoninic acid is highly sensitive producing purple coloured product that can be strongly detected at 562 nm absorbance. The colour intensity of the product is nearly linear with increasing protein concentrations over a broad working range (20–2000 µg/mL). BSA was diluted in nuclease-free water to the following concentrations: 2000 µg/ml, 1500 µg/ml, 1000 µg/ml, 750 µg/ml, 500 µg/ml, 250 µg/ml, 125 µg/ml, 25 µg/ml and 0. Samples were diluted in nuclease free water in 1:5, and 8 µl of diluted protein samples were pipetted in triplicate in a 96-well plate. Then 200 µl of working solution (reagent A+ regent B) was added to each of the 96 well plate and the plates were then incubated at 37°C for 30 minutes. The 96-well plates were read by FLUOstar OPTIMA, UK/ Infinite® F50 (UK) microplate reader at 590 wavelengths.

2.2.2.5 WESTERN BLOT

Western blot (WB) is a semi-quantitative method that used to determine the level of proteins in various cell lysates. The technique consists of six steps:

separation of protein according to their molecular weight on a sodium dodecyl sulfate (SDS)-polyacrylamide gel, electrophoretic transfer of proteins into polyvinylidene difluoride (PVDF) or a nitrocellulose membrane to enable detection of targeted proteins by

labelled antibodies, blocking, primary antibody incubation, secondary antibody incubation, detection and analysis.

2.2.2.5.1 SEPARATION OF PROTEINS

A ready-made, SDS 4X sample buffer (B0008, Thermo Fisher, UK) was used. SDS is an anionic detergent that can break the hydrogen bond between molecules and help protein unfolding. 10x Dithiothreitol (DTT) reducing agent (B0009, Thermofisher, UK) was added to the sample to aid the reduction of disulfide linkages between cysteine molecules. Cell lysates (20 µg) were added to 2.5 µL sample buffer and 1 µL reducing agents and then denaturation was performed by heating at 100°C for 5 minutes. Protein samples were loaded into Precast SDS 4-12% gels (NW04125BOX, Thermofisher; UK) at 125 V for 1 hour.

2.2.2.5.2 TRANSFER PROTIENS

Proteins were transferred from gels to nitrocellulose membrane (Whatman, GE Healthcare). Gels were removed from their casing, sandwiched between filter paper and transfer sponges that had pre-soaked in a transfer buffer (20% (v/v) methanol, 50 mM Tris-HCl, and 380 mM glycine), and placed in a transfer model mini bolt Module (B1000, Thermofisher, UK). The transfer process was performed at 11 volts for 90 minutes.

2.2.2.5.3 BLOCKING

The aim of this step is to block unreacted sites on membranes to decrease subsequent non-specific binding with the antibodies. Blocking was done by soaking membranes 5% non-fat milk in phosphate buffered saline/0.05% tween20 (PBS-T) for 1 hour at room temperature.

2.2.2.5.4 PRIMARY ANTIBODY INCUBATION

The primary antibodies (Table 2.4) were diluted in 1% BSA. Membranes were incubated with the primary antibodies at room temperature for one hour or at 4°C overnight. The membranes were then washed with PBS-T (3 × 5 min) to remove non-bound primary antibodies. The washed membranes were incubated with a housekeeper antibody (beta-actin or GAPDH) for 1 hour at room temperature to normalise the levels of proteins of interest by determining that protein loading was the same across the gel. After incubation with the housekeeper antibody, the washing procedure was repeated.

Table 2.4: Primary antibodies for western blot. RT= room temperature.

Anti-human Ab.	Clone	Conc. used	Incubation condition	Source
53BP1	Ab175933	1:2000	1hour/RT	Abcam
ALDHA1	D4R9V	1:1000	Overnight at 4°C	Cell signalling
ATM	Ab23420	1:1000	1hour/RT	Abcam
Beta-actin	Ab8226	1/2000	1hour/RT	Abcam
BRCA2	Ab123491	1:2000	1hour/RT	Abcam
CD44	Ab157107	1:2000	Overnight at 4°C	Abcam
E-CAD	4A2C7	1:1000	Overnight at 4°C	Thermofisher
ERCC1	M3648	1:2000	1hour/RT	DAKO
GAPDH	Ab8245	1/5000	1hour/RT	Abcam
LIG3	HPA006723	1/1000	1 hour/RT	Sigma
MRE11	Ab214	1:500	1hour/RT	Abcam
NBS1	N3162-200UL	1:500	1hour/RT	Sigma
OCT4	2750S	1:1000	Overnight at 4°C	Cell signalling
PARP1	Ab32138	1/2000	1 hour/RT	Abcam
RAD50	Ab89	1:500	1hour/RT	Abcam
RPA1	Ab79398	1:1000	1hour/RT	Abcam
SOX2	2748S	1:1000	Overnight at 4°C	Cell signalling
NANAG	D73G4	1:2000	Overnight at 4°C	Cell signalling
N-CAD	Ab18203	1:1000	Overnight at 4°C	Abcam
YY1	Ab109228	1/1000	1hour/RT	Abcam

2.2.2.5.5 SECONDARY ANTIBODY INCUBATION

The membranes were incubated with horseradish peroxidase (HRP)-conjugated secondary antibodies to detect the primary antibodies. The secondary antibodies were used as follow: IRDye® 680RD Donkey anti-Mouse IgG (LI-COR, USA) and IRDye® 800CW Donkey anti-Rabbit IgG (LI-COR, USA). Each antibody was diluted 1:10,000 in 1% BSA. The incubation was for 1 hour at room temperature, following by washing with PBS-T as described above.

2.2.2.5.6 DETECTION AND ANALYSIS

The LI-COR Odyssey Imaging System was utilized for protein detection. For quantifying the bands, the Image Studio Lite software (Ver 3.1) (Li-Cor, USA) was used. The detected band intensity for the proteins of interest as well as housekeeper gene band intensity were quantified in LI-COR software. The readings for proteins of interest were normalised to the reading for housekeeper proteins. Western blot was performed in three independent experiments. Differences between samples was calculated using student t-test. Graphs and statistical analysis were performed using GraphPad Prism software version 7.

2.2.2.6 TRANSIENT KNOCKDOWN OF MRN COMPLEX

MRE11 (ID S8960), RAD50 (ID S792), NBS1 (ID S9292) siRNAs oligonucleotides, and the validation construct of MRE11 (ID 8959), RAD50 (ID S793) and NBS1 (ID S9293) were obtained from Invitrogen, UK. Negative scrambled control constructs (catalogue no. 4390843) were purchased from Invitrogen, UK. Constructs were diluted in 50 µL nuclease-free water to make a stock solution of 100 µM, and then diluted 10 µM working solution in the experiment day. Lipofectamine 3000 transfection reagent (L3000015, Thermofisher; UK) was applied to deliver siRNA to the cells in Opti-MEM reduced serum medium (11058021, Thermofisher, UK). The proportions of Lipofectamine used were according to the manufacturer's recommendation. Cells were seeded at 50-60% confluency in T25 flasks and incubated overnight. 20.8 µl Lipofectamine was diluted in 0.75 ml of the Opti-MEM, and 9.4 µl of the working SiRNA solution or negative control was diluted in 0.75 ml of the Opti-MEM for 5 minutes. The diluted lipofectamine was then added to the diluted siRNA to make the transfection master mix, which was incubated for 15 minutes at room temperature. Cells were washed by the Opti-MEM before the transfection master mix was added. The transfected cells were incubated at 37°C overnight. The following day, the Opti-MEM was removed by pipetting and fresh cells-specific media was

added. The transfection efficiency was checked at day 3 and 5 using western blot. Knocking down procedures were performed in three independent experiments. Differences between samples were calculated using the student t-test.

2.2.2.7 GENERATION OF XRCC1-KNOCKOUT USING CRISPR CAS-9

Oligonucleotides carry silencing gRNA for XRCC1 cloned into a Plv-U6g-EPCG plasmid expressing Cas-9 and carry gene that resistance to puromycin were obtained from Sigma (UK). Cells were plated at 60% confluency in 6 well-plates overnight. 7.5 µL lipofectamine 3000 (L3000015, Thermofisher, UK) was diluted into 400µl Opti-MEM medium (11058021, Thermofisher, UK) and 3 µg of CRISPR plasmid was then diluted in 400µl Opti-MEM medium and p3000 reagent. Diluted lipofectamine was added to dilute DNA and then incubated at room temperature for 15 minutes. The transfection mixture was added to the cells and then incubated overnight. In the following day, the transfection medium was removed, and fresh media was added. After two days, the selection of desired clones was started with puromycin. A2780 was selected in 5µg/ml of puromycin. The selection doses were identified before conducting the transfection experiments using the puromycin kill curve experiments. After 14 days, stable transfected colonies were

amplified, and western blot was performed to check the transfection efficiency.

2.2.2.8 CELL PROLIFERATION ASSAY

The MTS assay is commonly used to screen various compounds to determine whether they impact cell proliferation or display direct cytotoxic consequences that contribute to apoptosis. The constituents of the MTS solution are an electron coupling reagent (phenazine methosulfate [PMS]) and a tetrazolium compound [3-(4,5-dimethylthiazol-2-yl)-5-(3-carboxymethoxyphenyl)-2-(4-sulfophenyl)-2Htetrazolium, inner salt; MTS]. A soluble formazan product that can be dissolved in tissue culture medium is generated because cells facilitate the reduction of MTS. Formazan is generated from dehydrogenase enzymes that are present exclusively in cells that are actively engaged in metabolism (Cory et al., 1991).

For assessing the degree to which several inhibitor dosages are cytotoxic, MTS assays were applied by seeding 500 to 2,000 cells in 100 µl of cell-specific medium into every well of a 96-well plate (according to the instructions of the manufacturer). The plate was incubated at 37°C, 5% CO_2 for 1 day to allow cells to adhere.

The following day, drugs were added at several concentrations. Each concentration was applied in three wells and cells were incubated. On day 6, the MTS reagent (CellTiter 96® AQueous One Solution,

Promega, UK) was added. 20 µl of the MTS reagent was placed into the tested wells. Next, the plate was incubated in dark conditions for 1 to 4 hours at 37 °C. The FlUOstar Optima plate reader was employed 490 nm to evaluate formazan absorbance. The absorbance percentage was identified in relation to a control group of untreated cells. The MTS experiment was conducted three times, each in triplicate. Microsoft Excel 2010 was used to establish normalization between average readings of treated cells and average readings of control cells. Survival curves were plotted and the differences between samples were calculated using the student t-test (GraphPad Prism, version 7).

2.2.2.9 CLONOGENIC SURVIVAL ASSAY

The clonogenic survival assay is utilized to test the capability of cells to divide and form colonies following the treatment with a drug. This method measures the efficacy of drug cytotoxicity after allowing time for the cells to perform at least five to six replication rounds. Colonies can be seen by naked eye at the end of the experiment and can be stained by crystal violet and counted.

2.2.2.9.1 PLATTING EFFICIENCY

Plating efficiency is the ability of each cells to form a colony. Plating efficiency of each cell line should be determined before starting the

clonogenic experiment. To preform plating efficiency, cells were plated at various seeding densities in six-well plates in triplicate and left to grow under normal incubation condition for two weeks. Subsequently, media were aspirated, and cells were washed with PBS and were then fixed with fixation solution (10% acetic acid, 10% methanol, 80% H2O) for 10 minutes. Plates were then stained with crystal violet and colonies were manually counted. The calculation of plating efficiency is number of colonies formed/number of cells seeded) x 100, using Microsoft Excel 2010.

2.2.2.9.2 CLONOGEINC ASSAY

The clonogenic assay was conducted three times, each in triplicate. Cells were seeded in six-well plates and left to adhere overnight at 37°C, 5% CO2. The next day, the cell medium was removed, cells were washed with PBS and 2ml of fresh media containing the treatment doses were added. Plates were incubated at 37°C, 5% CO2 for 14 days. The same steps, fixation and staining in plating efficiency were applied. Following this incubation, the cells were fixed, stained and counted as described above. The survival fraction was calculated as (number of colonies formed after treatment/number of cells seeded) × plating efficiency, using Microsoft Excel 2010. Survival curves were plotted using GraphPad

Prism, version 7. Differences between samples were calculated using the student t-test.

2.2.2.10 FUNCTIONAL STUDIES

2.2.2.10.1 γH2AX ASSAY AND CELL CYCLE ANALYSIS

There are three types of histone H2A protein. H2AX is the variant most sensitive to double-strand breaks (DSBs). Phosphorylated histone γH2AX is a key component that is activated in response to DSBs. ATM, DNA-PK or ATR phosphorylate H2AX on serine 139 residue, leading to the formation of γH2AX foci. Each focus is believed to correspond to a DSB within the nucleus. The number of DSB can be detected by labelling the cells with γH2AX-antibody Ser139 (16202A, Millipore, UK).

2.2.2.10.1.1 ASSAY PROTOCOL

$1x10^5$ cells per well were seeded in six-well plates and incubated overnight at 37°C in a 5% CO2 atmosphere. The next day, the cells were treated with indicated doses of drugs and then incubated for 24 hours. Media were discarded, and cells were then washed twice with PBS and collected by trypsinization. Fresh media were added to the cells, followed by centrifugation at 1000rpm for 5 minutes. The

cells were then washed by PBS and centrifuged at 1000rpm for 5 minutes. The cells were fixed with 70% ethanol for 1hour at -20°C or for weeks at -20°C. The 70% ethanol was removed, and the cells were then washed twice with cold PBS and centrifuged. The cells were then resuspended by 50 µl of 1X permeabilization solution. 0.7 µl of fluorescein isothiocyanate (FITC)-conjugated anti-phospho-histone (γH2AX) Ser139 antibody, (JBW301, Merck; UK) was added, and the cells were incubated for 15 minutes on ice. After incubation, the cells were washed with 100 µl 1X saponin wash solution to remove non-bound FITC. The cells were pelleted by centrifugation at 1000rpm for 5 minutes and resuspended in 5µg/ml RNAase solution (12091021, Invitrogen, UK) for 15 minutes in room temperature. The cells were then stained with 400 µl of 1 µg/ml propidium iodide solution (PI) (P4170, Sigma Aldrich, UK). PI stains DNA in each phase of the cell cycle, thus allowing assessment of cell cycle progression. The cells were analysed on a Beckman-Coulter FC500 flow cytometer using a 488nm laser for excitation and emission data for PI, collected using a 620 nm bandpass filter (FL3) and a 525nm bandpass filter (FL1) for FITC-anti-phospho-Histone H2A.X (Figure 2.4). Data was analysed using Weasel software (Walter and Elisa Hall, Australia) (Figure 2.5). The presentation of data was done by GraphPad Prism, version 7. Each experiment was performed in triplicate. Differences between samples were calculated by one way-ANOVA.

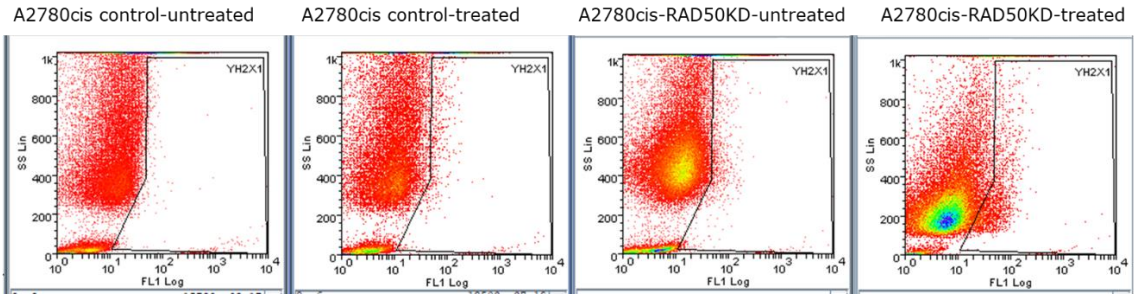

Figure 2.4: yH2AX analysis using Weasel softwear. yH2AX analysis in A2780cis control untreated, A2780cis control treated with cisplatin, A2780cis_RAD50KD untreated and A2780cis_RAD50KD treated with cisplatin. A2780cis_RAD50KD treated cells revelaed significant accumulation of yH2AX positive cells. FL1 Log: FACS fluorescence channel used to measure yH2AX staining.

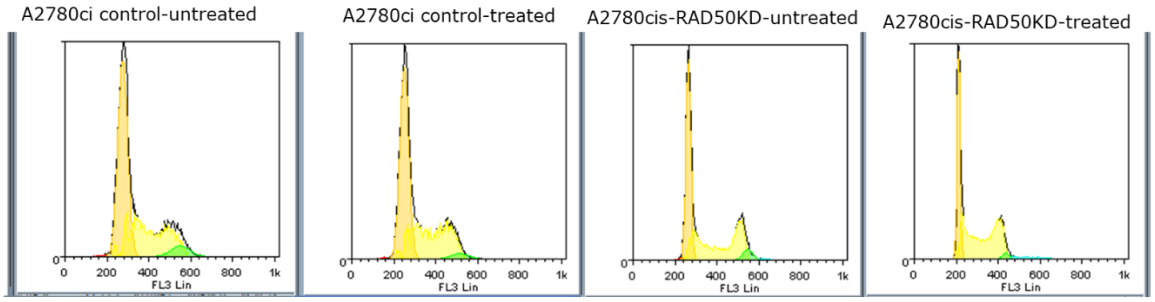

Figure 2.5: Cell cycle analysis using Weasel software. Representative images of cell cycle analysis in A2780cis control untreated, A2780cis control treated with cisplatin, A2780cis_RAD50KD untreated and A2780cis_RAD50KD treated with cisplatin. A2780cis_RAD50KD treated cells showed S-phase cell cycle arrest. FL3 Lin: FACS fluorescence channel used for measuring PI staining.

2.2.2.10.2 APOPTOSIS DETECTION

Apoptosis is a genetically regulated mechanism that is vital to help in maintaining tissue homeostasis. Apoptosis is identified by several morphologic characteristics, including loss of cellular membrane asymmetry, chromatin condensation and translocation of the membrane phospholipid phosphatidylserine (PS) from inside to the outside (Koopman et al., 1994). Annexin V is a 35 kDa Ca2+ dependent phospholipid-binding protein that possesses high affinity for PS. Annexin V staining can be combined with other dye, such as PI, which helps in detecting cells that undergo apoptosis. Viable cells with intact membrane will not be stained by PI or Annexin V. Early apoptotic cells will be stained with Annexin V but not PI, while late apoptotic cells will have positive staining for both Annexin V and PI (Figure 2.6) (Riccardi and Nicoletti, 2006).

2.2.2.10.2.1 ANNEXIN V ASSAY PROTOCOL

1x 10^{5} cells per well were seeded into six-well plates overnight. The cells were then not treated or treated with indicated doses of cisplatin or mirin for 24 hours. The cells were then trypsinized, washed twice with cold PBS and centrifuged at 1000 rpm for 5 minutes. Annexin V detection kit (556547, BD Pharmingen, USA) was used to measure apoptotic cells. The cells were incubated with

100 µl 1X Annexin V binding buffer. 2.5µl FITC conjugated Annexin V antibody and 2.5 µl PI were added and the cells were incubated on ice in a dark room for 15 minutes. 300 µl of 1x Annexin binding buffer was then added to the cells. Samples were analysed with a FC500 flow cytometer (Beckman Coulter, USA) using a 488nm laser for excitation and a 575nm bandpass filter. Weasel software (Walter and Elisa Hall, Australia) was used for quantifying fluorescence intensity of PI and Annexin V for cells in each sample. Unstained cells were used for gating of negative cell population. The presentation of data was done using GraphPad Prism, version 7. Each experiment was performed in triplicate. Differences between the samples were calculated by two-ANOVA.

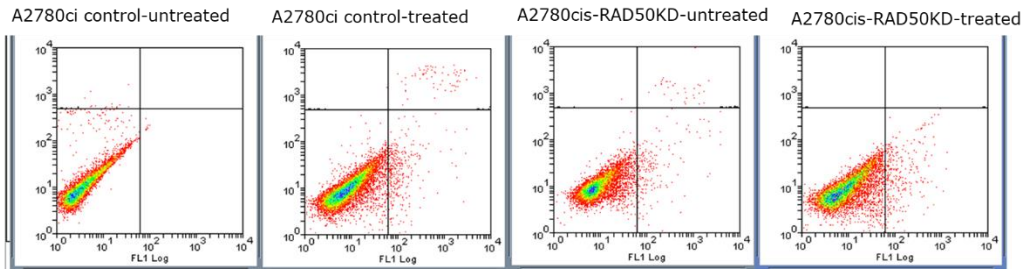

Figure 2.6: Annexin V analysis using Weasel softwear. Representitive images of Annexin V analysis in A2780cis control untreated, A2780cis control treated with cisplatin, A2780cis_RAD50KD untreated and A2780cis_RAD50KD treated with cisplatin. A2780cis_RAD50KD treated cells demonstrated significant apoptotic cells. FL1 Log: FACS fluorescence channel used to measure Annexin V staining (horizontal) and FL3 lof to measure PI staining (vertical).

2.2.2.11 NUCLEAR AND CYTOPLASMIC EXTRACTION

2 × 10^6 cells were seeded in T25 flasks overnight. The cells were then treated with 5μM of cisplatin for 24 and 48 hours. The cells were collected by trypsinization, centrifuged at 1000 rpm for 5 minutes at room temperature. The cells were then transferred to 1.5ml Eppendorf tubes. Separation of nuclear and cytoplasmic fractions was done with the Thermo Scientific NE-PER Nuclear and Cytoplasmic Extraction Kit according to the manufacturer's instructions (78833, Thermo Fisher; UK). The cells were washed with cold PBS and the PBS was carefully discarded, leaving the cell pellet as dry as possible. The cells were then incubated with 200 μl of CER I and vigorously vortex the tubes for 15 seconds, then incubated on ice for 10 minutes. 11 μl of cold-CER II was added to the tubes and the cells were vortexed vigorously for 5 sec and incubated on ice for 1 minute. After that, the cells were vortexed for 5 second and centrifuge for 5 minutes at maximum speed in a microcentrifuge. The supernatants were immediately transferred to clean Eppendorf tubes and placed on ice. The cell pallet containing the nuclei were incubated with 100 μl cold-NER, vortexed for 15 seconds and placed on ice. The cell pallet vortexed for 15 seconds every 10 minutes for a total of 40 minutes. The pellets were centrifuged for 10 minutes at maximum speed in a microcentrifuge. The nuclear extracts were

immediately transferred to clean tubes and placed on ice. Extracts were quantified using BCA protein quantification kit, and protein levels were checked by western blot. Nuclear and cytoplasmic extracts were blotted against YY1 as a nuclear marker and GADPH as a cytoplasmic abundant marker in order to verify the purity of the extractions. Proteins of interest in the nuclear extractions were normalised to YY1 levels. Proteins of interest levels in cytoplasmic extracts were normalised to GADPH levels.

2.2.2.12 DEVELOPMENT OF A MIRIN-RESISTANT CELL LINE

PEO1 cells were exposed to stepwise increasing concentration of mirin (5 μM -45 μM). A starting dose of 5 μM of mirin was chosen based on IC50 of mirin in PEO1 cells. At each dose level, the cells were maintained for three generations. Mirin-resistant PEO1 cells (PEO1R) were established over a period of seven months. The mirin resistant of the cell line was determined by clonogenic assays. Briefly, the IC50 values of the treated cells were calculated and compared to that of the parental cell line.

2.2.2.13 IMMUNOFLURESCENCE STAINING

$1x10^5$ cells per well were plated into autoclaved coverslips pre-layered in six-well plates overnight. Cells were then treated with

mirin for 24 hours. The cells were then stained according to the described protocol (Ibrahim et al., 2012b), and fixed with 4% paraformaldehyde (8187085000, Sigma Aldrich, UK) for 30 minutes. After that, the cells were permeabilised with 300 µL per well of 0.1% Triton (85111, Thermo Fisher Scientific) for 30 minutes and incubated with 3% BSA (A7906, Sigma) for 1 hour. The cells were then incubated with 300 µL of diluted primary antibody at 4° C overnight (Table 2.5). The cells were then washed with washing buffer (1 %BSA and 0.1% Tween-20 in PBS) (3 × 5 minutes). Secondary antibodies diluted in 1% BSA were added and cell were incubated in the dark for 1 hour at room temperature. The cells were then washed with washing buffer (3 × 5 minutes). Next, the coverslips were removed using tweezers and placed on clean slides that contains one drop of DAPI (H1200, Vector Laboratories). The coverslip edges were sealed with a colourless nail varnish. Imaging was conducted using a Leica SP2 confocal laser scanning microscope. The analysis of images was performed by ImageJ software. A minimum of 100 cells per slide were counted for analysis. Data were presented using in GraphPad Prism 7 software. The statistical analysis was performed using student t-test.

Table 2.5: Antibodies for immunofluorescence staining. RT=room temperature.

Anti-human Ab.	Clone	Conc. used	Incubation condition	Source
53BP1	4937S	1:200	Overnight at 4° C	Cells signalling
Alexa fluor 488 goat anti-Mouse secondary antibody	A-11029	1:200	1 hour /RT	Thermofisher
Goat anti-rabbit secondary antibody, TRITC.	T-2769	1:500	1 hour /RT	Thermofisher
MRE11	Ab214	1:200	Overnight at 4° C	Abcam
OCT4	2750S	1:100	Overnight at 4° C	Cells signalling
YH2X	JBW301	1:500	Overnight at 4° C	Sigma

2.2.2.14 SPHERES

Cells were seeded at $4x10^4$ cells/well in in ultra-low attachment six-well plates (174932, Thermo Fisher Scientific, UK). The cells were cultured in 3D Tumorsphere Medium (C28070, PromoCell, UK) at 37°C in a 5% CO_2 atmosphere. Cells were then topped off with fresh medium every three days until speriods structures were formed. Spheroid fixation was preforemd using 37% formaldehyde at a 1:10 ratio for 30 minutes. Spheroid were then stained with 2μM of calcein AM and 1.5μM of ethidium homodimer-1 (LIVED/DEAD assay kit, Thermofisher, UK) (Debnath et al., 2003). The polyanionic dye calcein is well retained within live cells, producing an intense uniform green fluorescence. Ethidium homodimer-1 enters cells with damaged membranes and in dead cells produces a bright red

fluorescence. Ethidium homodimer-1 is excluded by the intact plasma membrane of live cells.

A Leica SP2 confocal laser scanning microscope (CLSM) was used to acquire images of the spheroids. spheroid images were analysed using ImageJ software (NIH, USA). At least 30 spheroids were analysed were measured. For cell viability quantification, the spheroids were trypsinised, washed with PBS and centrifuged at 1000×g for 5 minutes. The light-protected cellular pellets in PBS were incubated with 0.1μM of Calcein-AM and 1 μM of Ethidium homodimer-1 for 20 minutes at room temperature. Samples were analysed using Beckman-Coulter FC500 flow cytometer using a 495nm laser for excitation and a 515nm laser for emission data for Calcein AM and a 495nm laser for excitation and emission at 635nm for Ethidium Homodimer-1. Data analysis was performed using Weasel software.

2.2.2.15 INVASION ASSAY

The CytoSelect cell invasion assay kit (catalogue no. CBA-110) was used to investigate the invasive ability of tumour cells. This kit has polycarbonate membrane inserts (8 μm pore size) in a 24-well plate. The upper surface of this membrane is coated with a basal matrix to differentiate invasion cell from non-invasion cells. Invasion cells can degrade this matrix and pass via the pores of polycarbonate

membrane. Non-invasive cells can be removed from the top of the membrane and invasive cell can be then stained and quantified. To perform the invasion assay, suspensions 0.6- 1x10^{6} of cell were prepared in in serum-free culture media. 250 µL of cell suspension was then loaded into each of the inserts. 500 µL of cell- specific culture media with 10% FBS were then added to the lower well of invasion plate. Cells were then incubated for 24 hours at in the incubator. All media with non-invasive cells were removed. The inside of the inserts was wiped using wetted cotton swaps to remove all remaining non-invasive cells. The invasive cells that were in the bottoms of the inserts were stained in crystal violet for 10 minutes and imaged using a Nikon microscope camera at 20X magnification. For invasive cells quantification, the stained inserts were placed into a clean 24-well plate that contains 200 µL in each well of the cell extraction solution and incubated for 10 minutes on a shaker. 100 µL of each samples of dissociated cells were then transferred to a 96-well plate to quantify the optical density at 560 nm by a microtiter plate reader. Data were presented using in GraphPad Prism 7 software. The statistical analysis was performed using student t-test.

2.2.2.16 DNA REPAIR GENE EXPRESSION PROFILING

DNA repair RT^2 profiler^{TM} PCR Array (Qiagen, UK) was used to study 84 key human DNA repair genes.

2.2.2.16.1 RNA EXTRACTION

The RNeasy Mini Kit (74104, Qiagen, UK) was used to extract RNA according to the manufacturer's recommendation. 350 µL of RTL buffer were added to 2 x 10^6 pelleted cells and cells lysates then vortexed for 10 seconds. Cell lysates were then incubated with 350 µL of 70% ethanol and 700 µL of each cell lysate were transferred to a RNeasy spin column. Samples were then centrifuged for 15 seconds at 10.000 rpm. The flow-through was removed and 350 µL of RWI were added to the RNeasy spin column. Samples were then centrifuged for 15 seconds at 10,000 rpm. DNA digestion was preformed using the DNase digestion kit (79254, Qiagen, UK). 10 µL of DNase I stock and 70 µL of buffer RDD were added in a 0.5 ml eppendorf tube. This mixture was centrifuged for 14 seconds at 10,000 rpm. 80 µL of this mixture were added to each RNeasy spin column and incubated at room temperature for 15 minutes. 350 µL of RWI buffer were then added to the RNeasy spin column and centrifuged at 10,000 rpm for 14 seconds. The flow-through was then removed and 500 µL of RPE Buffer were added to the RNeasy

spin column. The samples were centrifuged as before. To wash, 50µl of RPE Buffer were added to each RNeasy spin column. Samples were then centrifuged for 2 minutes at 10,000 rpm. The RNeasy column was placed carefully to clean 1.5ml Eppendorf tubes. 40 µl of RNase-free water were added to the spin column membrane. To elute the RNA, the samples were centrifuged for 60 seconds at 10,000 rpm. The eluted RNA was quantified using a Nanodrop 2000c (Thermo Fisher Scientific, UK).

2.2.2.16.2 THE SYNTHESIS OF cDNA

The RT^2 First Strand Kit (330404, Qiagen, UK) was used to reverse transcribed 0.5µg for total RNA to cDNA. Variable amount of nuclease-free water and 2µl DNA elimination buffer (GE) were added to each RNA sample to bring the total volume of genomic DNA (gDNA) to 10µl. This DNA mixture was centrifuged at 10,000 rpm for 10 seconds, incubated for 5 minutes at 42° C, and the mixture placed on ice for 60 seconds. A room temperature cocktail was prepared as follow: 1 µl of Primer & External Control Mix (P2), 4 µl of 5X RT Buffer 3 (BC3), 3 µl of nuclease-free water and 2 µl of RT Enzyme Mix 3 (RE3) were added to a clean 1.5 ml Eppendorf tube. 10 µl of this reverse-transcription mix were added to the 10 µl gDNA mixture. This mixture was incubated for 15 minutes and then this reaction was stopped by incubating at 95°C for 5 minutes. 91 µl nuclease-

free water was then added to cDNA and placed on ice unit next step or stored at -80ºC.

2.2.2.16.3 RT² PROFILER™ DNA REPAIR PCR ARRAY

To assess 84 DNA repair expression, the cDNA samples were incubated with RT² SYBR Green master mix (Qiagen, UK) according to the manufacturer's guidelines. Briefly, the PCR reaction mix was prepared as shown in table 2.6.

Table 2.6: PCR reaction mix.

Reagent	Volume
RT² SYBR Green mastermix	1350 µl
cDNA synthesis reaction	102 µl
RNase-free water	1248 µl
Total	2700 µl

25 µl of the reaction mix was added to each well of PCR array plate (PAHS-042ZC, Qiagen, UK). Optical Adhesive sealing Film was used to cover the plate and then centrifuged for 60 seconds. Applied Biosystems 7500 FAST cycler was used to perform RT-PCR.

2.2.2.16.4 QUANTITATIVE REAL TIME PCR

RT-QPCR was performed to confirm the expression of some DNA repair proteins and to evaluate stem cells markers expression. The reaction mix was prepared as shown in table 2.7.

Table 2.7: RT-QPCR reaction mix.

Reagent	Volume
cDNA from RT² first strand synthesis	2 µl
10x QuantiTec primer	1 µl
SYBR Green Mastermix	5 µl
RNase-free water	2 µl
Total	10 µl

The reaction mix was added to each well of PCR plate (Applied Biosystems®, UK*).* Optical adhesive sealing film was used to cover the plate, which was then centrifuged for 60 seconds*.* RT-PCR was performed using Applied Biosystems 7700 using SYBR green detection. The cycle conditions were incubation for 10 minutes at 95 ºC, followed by 40 cycles of 95 ºC for 15 seconds and for 1 minute at 60 ºC. The product was then heated form 60ºC to 95ºC for 20 minutes. This allow the determination of meting curve analysis, the specificity of products and confirmed the absence of primers-dimers. GAPDH was used for normalization.

2.2.2.16.5 DATA ANALYSIS

The data was analysed using the template that available at https://dataanalysis.sabiosciences.com/pcr/arrayanalysis.php?wuid=8fa7191b-bb49-409d-b896-8ce28966b04e&logindata=&customerdata=&customeremail=&platform=customArray&format=X. This web-based software preformed automatically the threshold cycle-based fold calculation form the data. The relative gene expression was averaged for the two samples and normalised to the expression of GAPDH. The software uses delta CT normalised to reference housekeeper genes expression available in the plate layout. Then delta delta CT method is used to calculate fold change in gene expression between samples.

2.2.2.17 IMMUNOPRECIPITATION

PureProteome Protein A/G Mix magnetic beads (LSKMAGA10, Millipore,UK) were preformed per the manufacturer's recomindation. Briefly, PEO1R and PEO1R_MRE11_KD lyastes were inubated with anti-MRE11 antibody at 4° overnight on an orbitalshaker. The buffer from the suspended beads was then removed. The beads were then washed four times using washing buffer (PBS, 0,1% Tween 20, pH 7.4). The washing buffer was revomed from the beads and then the antibody-antigen complex was added to the dry beads and incubated at room temperature for 2 hours. The beads were washed again. The

native and denaturing elutions were assessd to confirm the appropriate elution buffer. The beads were re-engaged to the magnet stand and the supernatant was collected. The samples were tested using western blot.

2.2.2.18 STABILITY PROTIEN

$2x10^{6}$ cells were plated overnight in T25 flasks. The following day, cycloheximide (Sigma Aldrich, UK) was added to concentration of 100 µg/ml for 4 hours. The proteasome inhibitor MG132 (Sigma Aldrich, UK) was then added to the cells to a concentration of 100 µM. Lysates were then collected at different time points: 0-hour, 1 hour and 3 hours. The samples were tested using western blot.

2.2.2.19 HA UBIQUITINATION ASSAY

PEO1R_control and PEO1R_MRE11_KD Cells were transfected with 2-3 µg a plasmid carrying ubiquitin tagged HA for 48 hours (Ali et al., 2019b). OCT4 and HA antibodies were used, and the results were shown by western blot.

2.2.2.20 TUMOUR XENOGRAFT STUDIES

This *In vivo* tumorgenicity experiments were conducted to evaluate the growth rate of PEO1 and PEO1R cells, at different cell concentrations. The experiments were conducted under the UK Home Office Project Licence number PPL P435A9CF8. LASA good practice guidelines, FELASA working group on pain and distress guidelines and ARRIVE reporting guidelines were also followed.18 female immunodeficient CD-1 NuNu mice at 7-8 weeks old were purchased from Charles River (UK). Mice were maintained in Individually Ventilated Cages (Tecniplast UK) within a barriered unit, illuminated by fluorescent lights set to give a 12-hour light-dark cycle. The room was air-conditioned in order to maintain an air temperature range of 21 ± 2 ºC. Mice were housed in social groups, 3 per cage, during the study, with irradiated bedding and autoclaved nesting materials and environmental enrichment (Datesand UK). Sterile irradiated 5V5R rodent diet (IPS Ltd, UK) and irradiated water was offered ad libitum. The condition of the animals was monitored throughout the study by an experienced animal technician. After a week's acclimatisation, the mice were initiated with tumours as follows: The cells *in vitro* were maintained in RPMI medium (Sigma, UK) + 10% (v/v) heat inactivated FBS (Sigma, Poole, UK) and 2 mM L-glutamine (Sigma, UK) at 37 ºC in 5% CO2. Cells were harvested with 0.025% EDTA, washed and counted. Cells were re-suspended

and plated at $2x10^6$ cells in T150 flask and then incubated for two days. On the day of experiment, cells were harvested, washed and counted. Cells were re-suspended, for *in vivo*, in standard matrigel at 2e5, 1e6 and 2e6/100ul for subcutaneous injection into the left flank. Three mice were implanted per cell concentration for each of the two cell lines.

Tumour establishment and growth was measured by Vernier calipers (Camlab) twice weekly and animals weighed weekly. The mice were also photographed weekly to record tumour development.

The scientific end point was determined to be when the first tumour reached maximum allowable size under the PPL i.e.1.2cm diameter. At this point, all mice were culled by cervical dislocation, tumours were dissected out and were photographed ex vivo. Tumours were preserved by snap freezing, fixation (NBF) 50:50 and by freezing in RNA later. This work was done in a collaboration with Prof. Anna Grabowska, cancer biology group, University of Nottingham.

2.2.2.21 STATISITCAL ANALYSIS

Statistical analysis was conducted as on GraphPad Prism7 software. To compare between two groups such as the quantification of western blot, MTS, clonogenic assays and the quantification of immunofluorescence, the data were normally distributed therefore, student- T-tests analysis was performed but not the Mann Whitney

test student- T-tests analysis was performed. One-way ANOVA was performed to compare between more than two groups (variances analyses) as γH2AX assay. ANOVA was used but not Kruskall- Wallis test because ANOVA is suitable for normally distributed variances. Two-way ANOVA was used to analyse two variables such as Annexin V analysis and cell cycle analysis. All experiments were expressed as means ± standard deviation S.D. of three independent experiments. P-values <0.05 =*, p-value <0.01 =** & p-value <0.001=***. All the pre-clinical statistical analyses were performed by the author.



MRE11 BLOCKADE FOR PLATINUM CHEMO-SENSITIZATION IN EPITHELIAL OVARIAN CANCER



3. MRE11 BLOOKADE FOR PLATINUM CHEMO-SENSITIZATION IN EOC

3.1 INTRODUCTION

The human *MRE11* gene is situated in chromosome 11q21 and encodes for 70-90KDa protein. MRE11 is a central protein of MRN complex, which encodes a nuclear protein involved in sensing and repairing DSBs and telomere length maintenance. In many cancers, including breast, colon, bladder, gastric and prostate, high MRE11 protein expression has been reported to be associated with either poor prognosis, radio-resistant or chemoresistance (Ho et al., 2018, Wang et al., 2019, Yuan et al., 2012). Dysfunction of MRE11 impairs the cell cycle checkpoints and DNA repair proteins, which contributes to hypersensitivity to DNA-damaging agents (Stracker and Petrini, 2011).

3.2 MRE11 INHIBITOR

Mirin (6-(4-hydroxyphenyl)-2-thioxo-2,3 dihydro-4 (1H)-pyrimidinone) is a MRE11 inhibitor isolated from a forward chemical genetic screen of compounds that inhibit MRN complex (Dupre et al., 2008). Mirin binds to the active site of MRE11 leading to block DNA phosphate backbone rotation, which inhibits the exonuclease activity. Mirin also inhibits the activation of ATM by MRN complex

without affecting the kinase activity of ATM, inhibits the autophosphorylation of ATM at ser 1982 in response to DSBs and abolishes G2/M checkpoint in cells (Dupre et al., 2008, Shibata et al., 2014).

Hypothesis, whether MRE11 expression relates to clinicopathological parameters and influence response to platinum therapy EOC. We also hypothesized that MRE11 could be a novel target for personalization of EOP therapy.

3.3 CHAPTER AIMS

- Evaluate the clinicopathological significance of MRE11 expression by immunohistochemistry (IHC) in 331 human EOC.
- Investigate MRE11 mRNA expression in a publicly available online gene expression dataset of 1259 OC patients to determine the correlation between MRE11 mRNA expression and patients' survivals.
- Profile a panel of OC cell lines to identify MRE11 protein level in OC cell lines.
- Evaluate MRE11 protein levels in nuclear and cytoplasmic extracts from OC cell lines before and after 24 and 48 hours of cisplatin treatment.

- Investigate whether MRE11 depletion can sensitize OC resistance cell lines to platinum treatment.
- Assess the effectiveness of MRE11 inhibitor (mirin) in enhancing sensitivity to platinum agents in OC resistance cell lines.
- Conduct functional studies to examine the effect of MRE11 depletion or mirin treatment on DSBs, cell cycle and apoptosis.

3.4 RESULTS

3.4.1 CLINICAL STUDY

3.4.1.1 MRE11 OVEREXPRESSION ASSOCIATES WITH PLATINUM RESISTANT IN EOC

To evaluate the association between MRE11 expression and the clinicopathological parameters in EOC, we conducted IHC staining to detect MRE11 expression in 331 human EOC. MRE11 nuclear expressions is shown in Figure 3.1a, b and c. Cytoplasmic expression is demonstrated in figure 3.1d and F. The patient demographics and pathological characteristics in EOC is shown in chapter two (p.79).

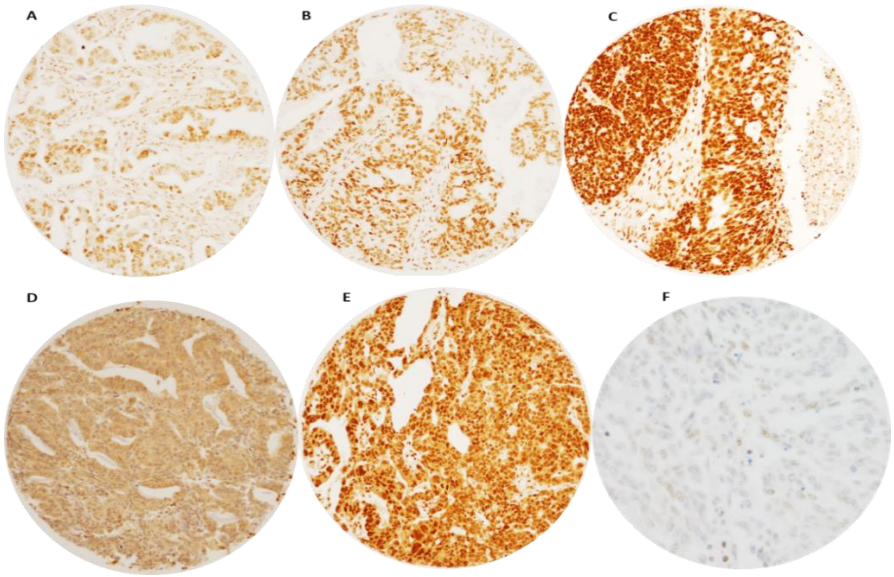

Figure 3.1: Immunohistochemical expression of MRE11 (nuclear and cytoplasmic) in ovarian cancers. A) Week nuclear expression of MRE11. B) Moderate nuclear expression of MRE11. C) Strong nuclear expression of MRE11. D) Week cytoplasmic expression of MRE11. E) Strong cytoplasmic with nuclear expression of MRE11. F) Negative expression which was TMA without adding MRE11 antibody. Magnification 20x.

We then studied the association between MRE11 expression and clinicopathological features. The expression of MRE11 was evaluable in 226 tumours. Intense nuclear staining of MRE11 was seen in 103/226 (51.7%) tumours and linked to serous cystadenocarcinoma ($p<0.001$), high FIGO stage ($p=0.002$), platinum resistance (0.022) and optimal debulking (0.002). Optimal debulking is a judgment made by the operating surgeon whether the tumour was completely excised or not. So optimally debulked cancer means complete removal of cancerous tissue. However, non-optimally debulked means that some tumour tissue was left behind as it was difficult / risky to excise the whole mass.

High MRE11 cytoplasmic expression was associated with serous cystadenocarcinoma (0.000046) and high tumour grade (0.007) (Table 3.1) High nuclear MRE11 expression was associated with poor progression free survival (PFS) ($p=0.002$) and a worse overall survival (OS) ($p=0.002$) (Figure 3.2). However, high MRE11 cytoplasmic expression did not influence patient survivals (Figure 3.3).

Table 3.1: The association between MRE11 expression and clinicopathological variables in EOC.

	MRE11 _C -	MRE11 _C +	P- value	MRE11_N -	MRE11 _N +	P- value
Pathological Type			***0.000046***			***0.00007***
Serous adenocarcinoma	25 (38.2%)	84 (61.8%)		49 (36%)	87 (64%)	
Mucinous adenocarcinoma	22 (78.6%)	6 (22.4%)		23 (82.1%)	5 (17.9 %)	
Endometrioid carcinoma	11 (36.7%)	19 (63.3%)		15 (50%)	15 (50%)	
Clear cell carcinoma	12 (92.3%)	1 (7.7%)		10 (76.9%)	3 (23.1%)	
Mixed	6 (50%)	6 (50%)		4 (33.3 %)	8 (66.7 %)	
FIGO Stage			0.113			***0.020***
I	48 (56.5%)	37 (43.5%)		50 (58.8%)	35 (41.2%)	
II	17 (48.6%)	18 (51.4%)		13 (37.1%)	22 (62.9%)	
III	36 (38.3%)	58 (61.7%)		37 (39.4%)	57 (60.6%)	
IV	4 (50%)	4 (50%)		2 (25%)	6 (75%)	
Tumour Grade			***0.007***			0.118
Grade 1	19 (70.4%)	8 (29.6%)		17 (63%)	10 (37%)	
Grade 2	23 (53.5%)	20 (46.5%)		17 (39.5%)	26 (60.5%)	
Grade 3	49 (38.9%)	77 (61.1%)		54 (42.9%)	72 (57.1%)	
Surgical Optimal Debulking			0.072			***0.002***
Optimally Debulked	89 (53%)	79 (47%)		87 (51.8%)	81 (48.2%)	
Not Optimally Debulked	15 (38.5%)	24 (61.5%)		10 (25.6%)	29 (74.4%)	
Residual tumour			0.137			0.16
None/Microscopic	76 (56.3%)	59 (43.7%)		71 (22.7%)	64 (47.4%)	
<1cm	10 (34.5%)	19 (65.5%)		12 (41.4%)	17 (58.6%)	
1-2 cm	5 (34.5%)	7 (58.3%)		5 (41.7%)	7 (58.3%)	
>2cm	13 (44.8%)	16 (55.2%)		9 (31%)	20 (69%)	
Measurable Disease Before ChemoTherapy **			0.19			0.06
Non	73 (52.9%)	65 (47.1%)		69 (50%)	69 (50%)	
Measurable	29 (45.3%)	35 (54.7%)		24 (37.5%)	40 (62.5%)	
Platinum sensitivity			***0.036***			***0.022***
Sensitive	81 (45.3%)	98 (54.7%)		91 (50.8%)	88 (49.2%)	
Resistance	11 (73.3%)	4 (26.7%)		3 (20%)	12 (80%)	

* MRE11_C= MRE11 cytoplasmic expression, MRE11_N= MRE11 nuclear expression. + = high expression, -= low expression. The $P < 0.05$ was considered significant. Some cases were lost in the analysis, as we could not find their records. They have most probably been referred from another trust to be treated in NUH with limited access to their pathological reports. Others are old cases where the pathological reports were not written in a clear template like the recent ones. Therefore, in order to avoid bias, the grades were stated as unknown. The same rule was applied to the other clinicopathological characteristics. **Measurable disease before ChemoTherapy: As a routine, all the patients after surgical resection of tumours get a scan before the initiation of chemotherapy. If any cancer tissue was detected, then will be recorded as measurable disease.

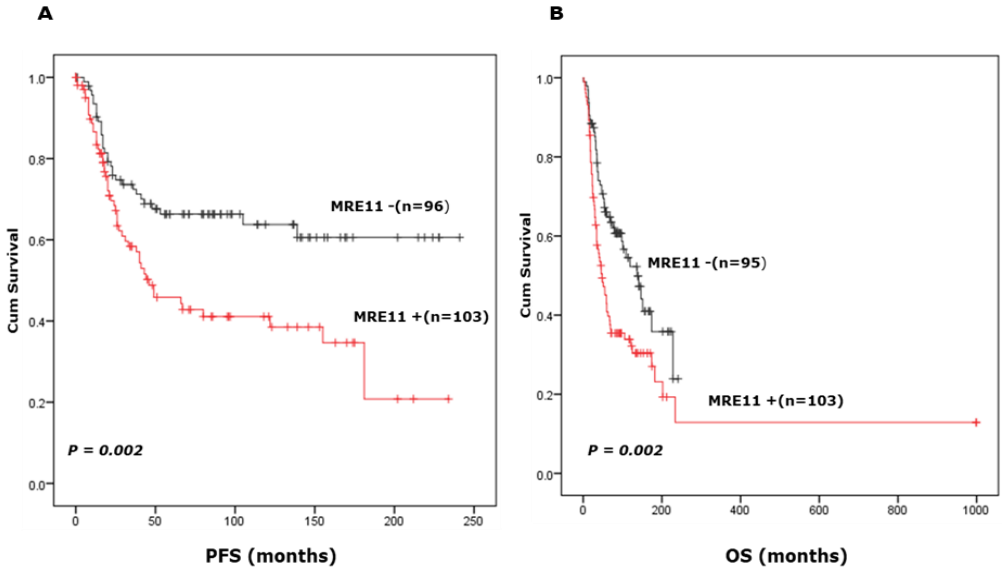

Figure 3.2: Kaplan Meier survival curves for MRE11 nuclear expression. Kaplan Meier statistical analysis was used to conduct a univariate analysis of OS and PFS against MRE11 expression. A) High nuclear MRE11 expression (Red lines) was significantly associated with poor PFS (P=0.002). PFS is the time between treatment initiation and tumour progression again. B) High nuclear MRE11 expression (Red lines) was significantly correlated with worse OS (p=0.002). OS is calculated between the day of diagnosis or time of treatment initiation and time where patients still alive. MRE11-= low MRE11 level, MRE1+= high MRE11 level and n= number of cases.

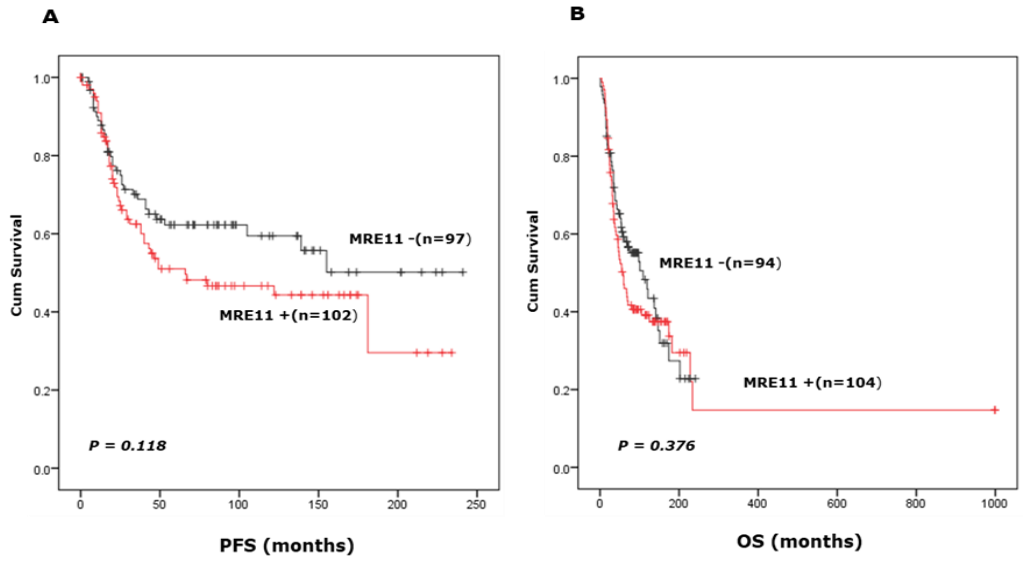

Figure 3.3: Kaplan Meier survival curves for MRE11 cytoplasmic expression. A) High MRE11 cytoplasmic expression (Red line) did not influence PFS (P=0.118). B) High MRE11 cytoplasmic expression (Red line) did not influence OS survival curves (0.376).

For alternative validation, the transcriptomic level of MRE11 in EOC patients who received platinum agents was investigated. High mRNA expression of MRE11 significantly associated with poor PFS (p=0.00036) while with broadline no significant (p=0.068) with OS (Figure 3.4).

Taken together, the data shows that the protein and transcriptional expression levels of MRE11 has predictive and prognostic significance in human EOC. We then moved to detailed preclinical examinations in platinum-sensitive and resistance OC cell lines to validate our clinical observation.

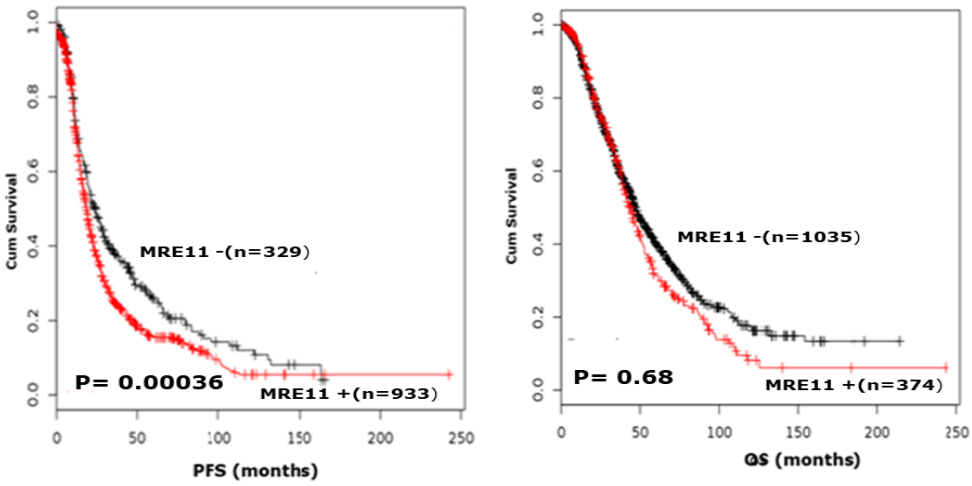

Figure 3.4: The correlation of MRE11 mRNA expression and PFS and OS survivals. A) High MRE11 mRNA expression (Red lines) was significantly associated with a worse PFS (p=00036). B) High MRE11 mRNA expression is associated with broadline no significant (p=0.068) with OS.

3.4.2 PRE-CLINICAL STUDIES

3.4.3 THE DEPLETION OF MRE11 ENHANCES THE CHEMO-SENSITIVITY IN OC CELL LINES

We first examined the sensitivity of four OC cell lines A2780, A2780cis, PEO1 and PEO4 to cisplatin (Figure 3.5). Details about these OC cell lines are described in chapter 2 (p.77).

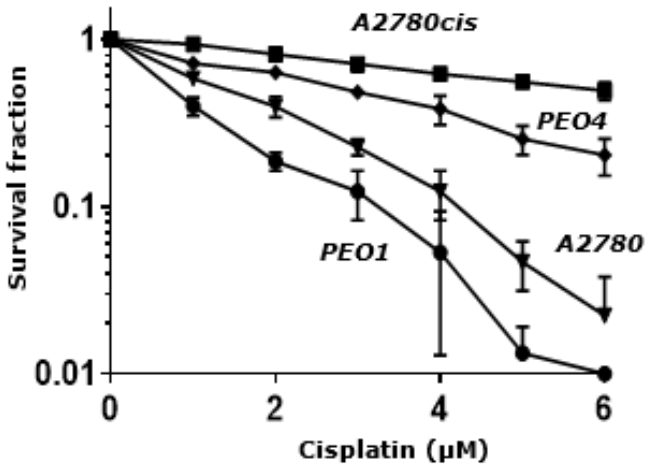

Figure 3.5: Clonogenic assay showing cisplatin sensitivity in A2780, A2780cis, PEO1 and PEO4. A2780 and A2780cis cells 200 cells/per well were seeded in six-well plates overnight. PEO1 cell line 1000 cells/per well were plated, while PEO4 cell line 300 cell/ per well were seeded overnight. In the following day, cells were treated with increased dose of cisplatin. Cells were left in the incubator for two weeks (Ali et al., 2019a). Microsoft Excel 2010 was used to determine plating efficiency and survival fraction. The calculation of plating efficiency and survival fraction were shown in chapter two page (p.101). A2780cis and PEO4 cells were resistance to ؤisplatin, while A2780 and PEO1 cells were sensitive. Data presentation and statistical analysis in were performed by GraphPad Prism, version 7. All results in this chapter are expressed as means ± standard deviation S.D. of three independent experiments.

We then screened the baseline level of MRE11 in A2780, A2780cis, PEO1 and PEO4 cell lines. In whole lysate, MRE11 baseline protein level was significantly high in A2780cis cells compared to A2780 cells. Similarly, MRE11 baseline protein level was significantly high in PEO4 cells in comparison with PEO1 cells (Figure 3.6). Thus, the MRE11 baseline level was high in cisplatin-resistance cells lines

A2780cis and PEO4 cells compared to cisplatin-sensitive cell lines A2780 and PEO1 cells.

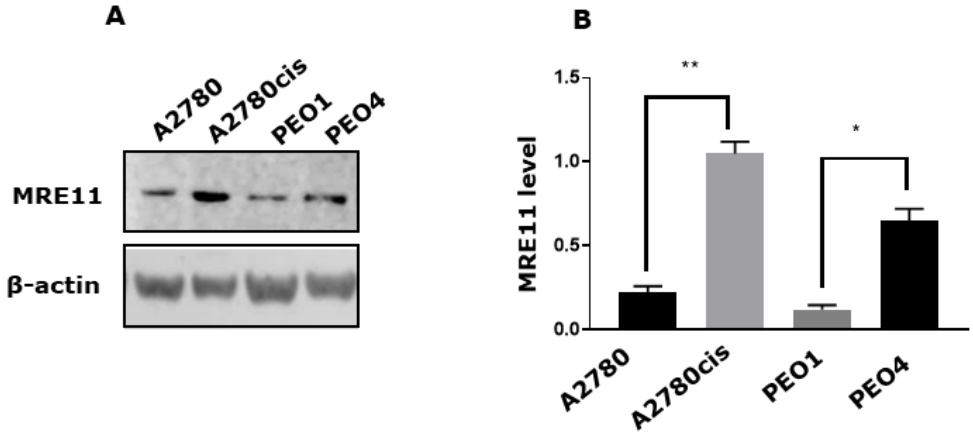

Figure 3.6: Western blot for MRE11 protein levels in A2780, A2780cis, PEO1 and PEO4 cells. A) High MRE11 protein level in cisplatin-resistant A2780cis and PEO4 cells compared to platinum-sensitive A2780 and PEO1 cells. β-actin level was used as a loading control. B) The quantification of MRE11 levels in four ovarian cell lines. The detected band intensity for MRE11 as well as B-actin band intensity were quantified in LI-COR software. The readings for MRE11 were normalised to B-actin reading. Microsoft Excel 2010 was used for normalization. Data presentation and statistical analysis were performed using GraphPad Prism, version 7. The P value was calculated by student's t-test, * $p<0.05$ and ** $p<0.01$.

To investigate the alteration in sub-cellular localization of MRE11, we took nuclear and cytoplasmic extracts from A2780, A2780cis, PEO1 and PEO4 cell lines before and after 5 μM cisplatin treatment (IC50 for ovarian resistance cell lines). Although after 24 hours of cisplatin treatment, there was no significant differences, at 48 hours, significantly increased MRE11 nuclear sub-cellular localisation

A2780cis cells and PEO4 cells were evident compared to A2780 cells and PEO1 cells. No significant changes were seen for MRE11 cytoplasmic level (Figure 3.7-3.8). The data suggests that MRE11 nuclear accumulation could stimulate repair of platinum induced DNA damage and contribute to resistance in A2780cis and PEO4 cells.

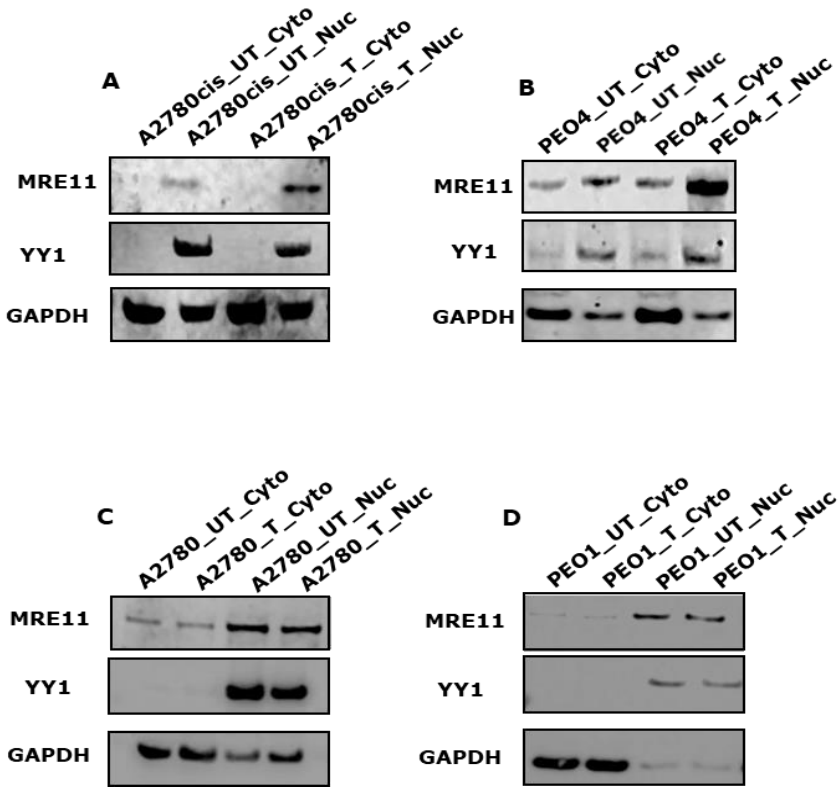

Figure 3.7: Representative western blot of nuclear and cytoplasmic levels of MRE11. For nuclear and cytoplasmic extraction protocol see chapter two (P.107-108). MRE11 nuclear expressions were normalised to YY1 levels. MRE11 cytoplasmic expressions were normalised to GADPH levels. Microsoft Excel 2010 was used for normalization. A) MRE11 nuclear expression in A2780cis cells was significantly increased after 5 μM cisplatin therapy for 48 hours, while no significant difference was observed in MRE11 cytoplasmic level after cisplatin treatment. B) MRE11 nuclear expression in PEO4 cells was significantly increased after 5 μM cisplatin treatment for 48 hours, while no significant difference was seen in MRE11 cytoplasmic level. C) MRE11 nuclear and cytoplasmic expression in A2780 cells did not change after 48 hours of 5 μM cisplatin therapy. D) 5 μM cisplatin treatment for 48 hours did not change MRE11 nuclear and cytoplasmic levels in PEO1 cells (Mesquita et al., 2019).

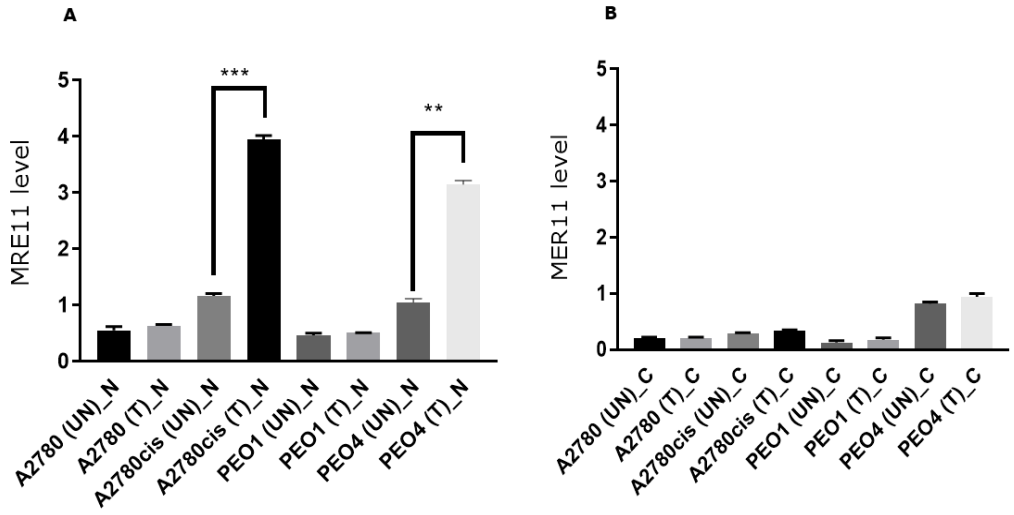

Figure 3.8: The quantification of MRE11 nuclear and cytoplasmic expression levels. A) MRE11 nuclear levels in A2780, A2780cis, PEO1 and PEO4. MRE11 nuclear expression level in untreated A2780cis and PEO4 cells was high compared with untreated A2780 and PEO1. MRE11 nuclear expression level was significantly increased after cisplatin treatment in A2780cis and PEO4 cells compared the same cells before treatment. B) MRE11 cytoplasmic levels in A2780, A2780cis, PEO1 and PEO4. Data presentation and statistical analysis were performed using GraphPad Prism, version 7. The P value was calculated by student's t-test, ** p>0.01 and *** p>0.001.

We then investigated MRE11 depletion in A2780cis and PEO4 cells for platinum sensitivity. Downregulation of genes that are overexpressed in resistance cell lines using siRNA is a useful approach to study the resistance mechanism (Ganesh et al., 2013). We first generated transient knockdown (KD) of MRE11 using siRNA in A2780cis cells. MRE11 was successfully knocked down by day three and persistent on day five in A2780cis cells (Figure 3.9).

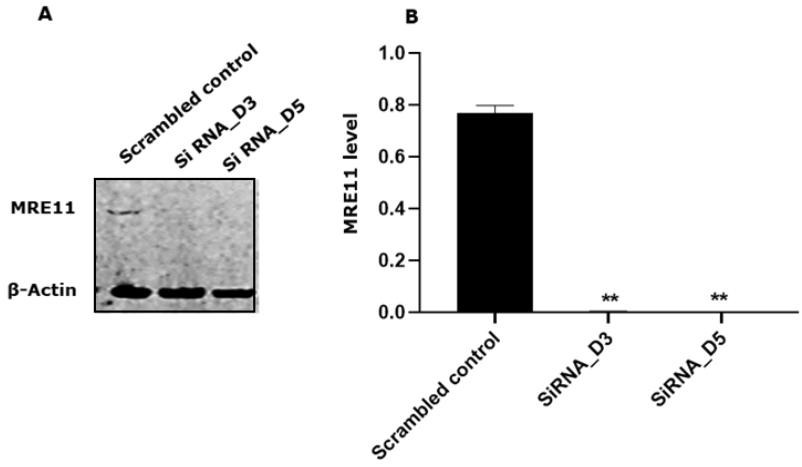

Figure 3.9: MRE11 knockdown in A2780cis cells using siRNA. Cells were seeded at 60-70% confluency in T25 flasks overnight. Cells were transfected with mMRE11 siRNA oligonucleotide or scrambled siRNA oligonucleotide control in Opti-MEM media. Transfection process was preformed using lipofectamine 3000 regent (Mesquita et al., 2019). See chapter two (p.97) for more details. Transfection efficiency was confirmed using western blot. A) Representative western blot which shows MRE11 protein level in A2780cis control and silenced cells. MRE11 was successfully knocked down in day 3 and day 5 in A2780cis cells. B) The quantification analysis of MRE11 reduction in A2780cis scrambled control and silenced cells. Data presentation and statistical analysis were performed using GraphPad Prism, version 7. The P value was calculated by student's t-test, ** $p<0.01$. D3=day 3, D5=day 5.

In clonogenic assays, MRE11_KD_A2780cis cells were significantly sensitive to cisplatin treatment compared to scrambled control cells (Figure 3.10). We then procced to functional studies using fluorescence-activated cell sorting (FACS) in MRE11 KD and scrambled control cells. After 24 hours of 5 μM cisplatin treatment, MRE11 depleted cells showed a significant accumulation of γH2AX, which is a surrogate marker of DSB accumulation in nucleus (Figure

3.11). Accumulation of DSBs induce cell cycle checkpoint activation leading on cell cycle arrest to allow time for cells to repair DNA damage. If the DSBs are extensive, cells undergo apoptosis. Therefore, we investigated the cell cycle and apoptosis after 24 hours of 5 μM cisplatin treatment in MRE11-deficient and proficient cells. S-phase cell cycle arrest and increased apoptosis was evident in MRE11_KD cells compared with scrambled controls (Figure 3.11).

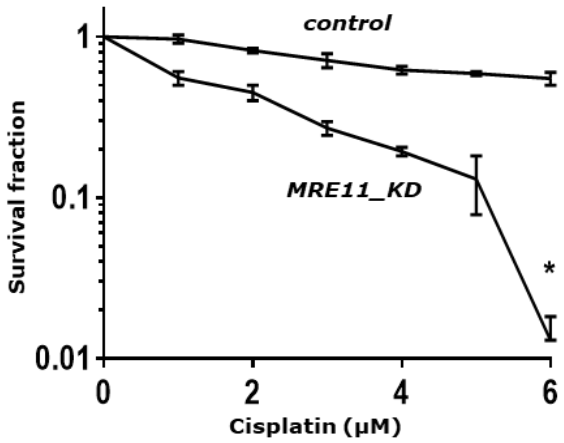

Figure 3.10: Clonogenic assay showing cisplatin sensitivity in A2780cis and MRE11_KD_A2780cis cells. Cells transfected as described in figure 3.9. Control cells and transfected cells (MRE11_KD) were seeded in six-well plates and left in the incubator overnight. The following day, increased doses of cisplatin were added. Cells were then left in the incubator for two weeks (Ali et al., 2019a). Microsoft Excel 2010 was used to determine plating efficiency and survival fraction, see chapter two page (100-101) for more details. MRE11 depletion increased cisplatin sensitivity in A2780cis cells. The P value was calculated by student's t-test, * $p<0.050$. Data presentation and statistical analysis were performed by GraphPad Prism, version 7.

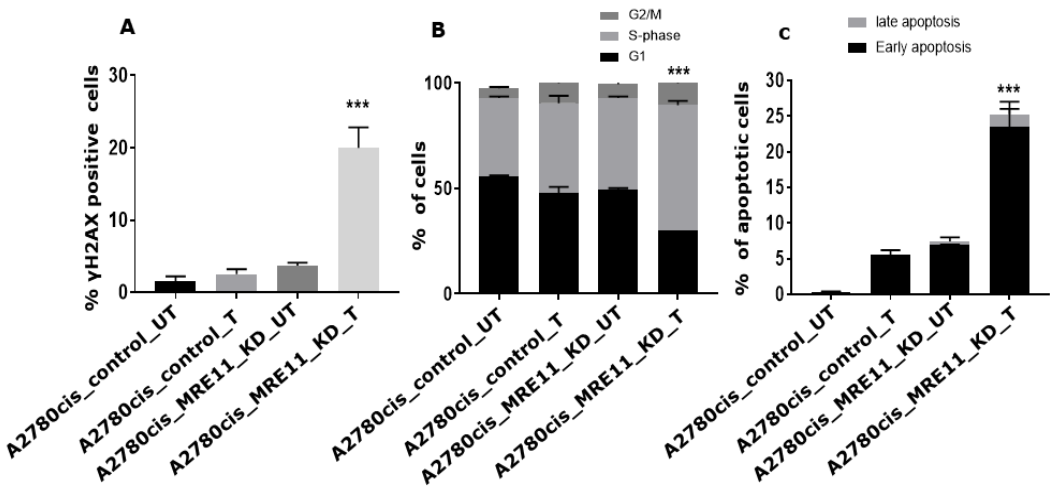

Figure 3.11: Functional studies of A2780cis cells using flow cytometry. Cells transfected as described in figure 3.9. On day two, A2780cis siRNA control and transfected MRE11 siRNA cells were trypsinized and re-plated in six-well plates. The following day, 5 μM of cisplatin was added for 24 hours. Cells were then collected (Ali et al., 2018); Protocols are described in chapter 2 (p.102-106). A) The percentage of γH2Ax positive cells; statistical analysis determined by one-way ANOVA. A2780cis_MRE11_KD treated revelaed significant accumulation of yH2AX positive cells. B) Cell cycle analysis in UT and treated cells, from two way-ANOVA. A2780cis_MRE11_KD showed S-phase cell cycle arrest. C) Annexin V analysis in UT and treated cells, from two way-ANOVA. A2780cis_MRE11_KD treated cells demonstrated significant increased apoptotic cells. Weasel Software Version 3.0.2 (The Walter and Eliza Hall Institute of Medical Research, Australia) was used for all flow cytometry analyses. Data presentation and statistical analysis were performed using GraphPad Prism, version 7. *** $P < 0.001$. UT= untreated cells, T= treated cells.

We next generated transient knockdown (KD) of MRE11 using siRNA in another platinum resistant PEO4 cells (Figure 3.12). MRE11 was successfully knocked down by day three and persistent on day five in PEO4 cells. In clonogenic assay, MRE11_KD_PEO4 cells were significantly more sensitive to cisplatin treatment compared to

scrambled controls (Figure 3.13). We then conducted functional studies in MRE11_ KD_PEO4 cells and PEO4 scrambled control cells. DSB accumulation, S-phase cell cycle arrest and apoptosis ware evident in MRE11 KD cells compared to scrambled controls (Figure 3.14).

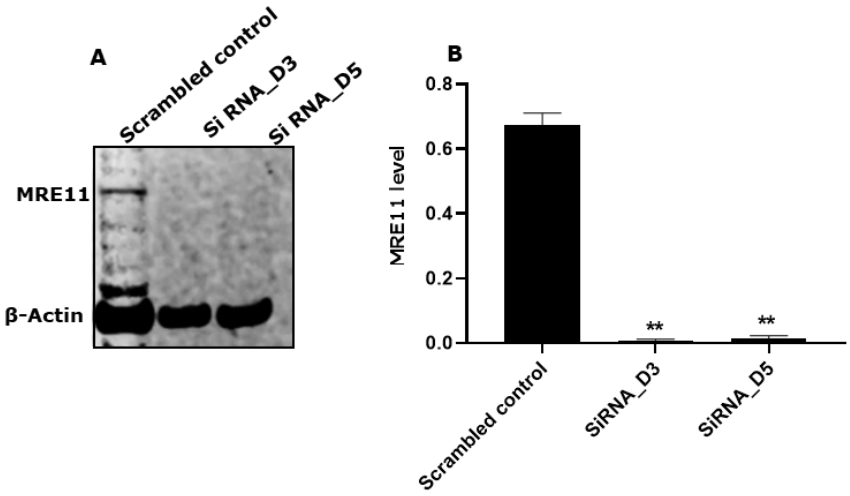

Figure 3.12: MRE11 knockdown in PEO4 cells using siRNA. A) Representative western blot which shows MRE11 protein level in PEO4 scrambled control and silenced cells. MRE11 was successfully knocked down in day 3 and day 5 in PEO4 cells. B) The quantification analysis of MRE11 reduction in PEO4 scrambled control and silenced cells. Data presentation and statistical analysis were performed using GraphPad Prism, version 7. The P value was calculated by student's t-test, ** $p<0.01$. D3=day 3, D5=day 5.

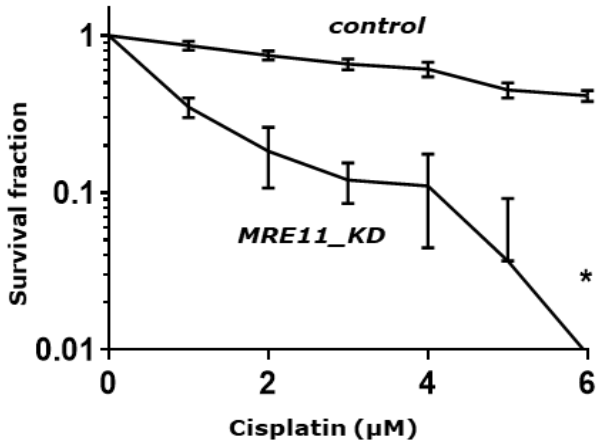

Figure 3.13: Clonogenic assay showing cisplatin sensitivity in PEO4 and MRE11_KD_PEO4 cells. Cells transfected as described in figure 3.9. Control cells and transfected cells (MRE11_KD) were seeded in six-well plates and left in incubator overnight. The following day, increased doses of cisplatin were added. Cells were then left in the incubator for two weeks (Ali et al., 2019a). Microsoft Excel 2010 was used to determine plating efficiency and survival fraction, see chapter two page (100-101) for more details. MRE11 depletion increased toxicity of PEO4 cells to cisplatin. Data presentation and statistical analysis were performed using GraphPad Prism, version 7. The P value was calculated by student's t-test, * $p<0.050$.

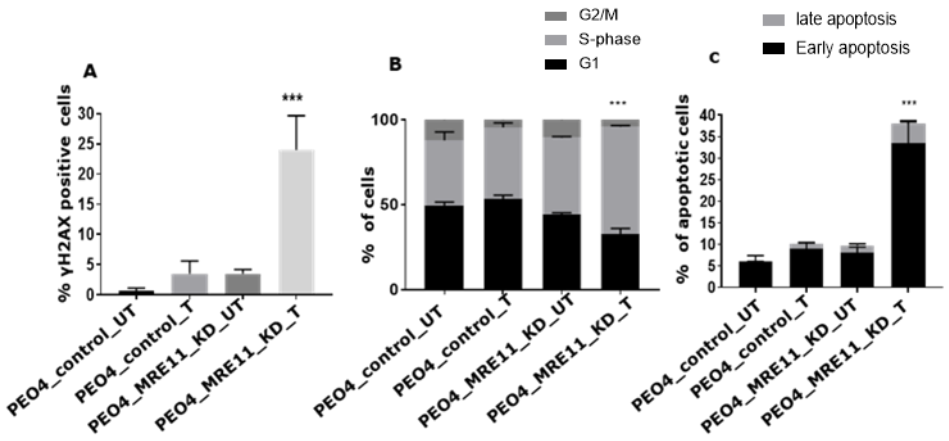

Figure 3.14: Functional studies of PEO4 cells using flow cytometry. A) The percentage of γH2Ax positive cells in UT and treated cells. PEO4_MRE11_KD_T cell showed significant accumulation of γH2AX positive cells. B) Cell cycle analysis in UT and treated cells. PEO4_MRE11_KD_T cells revealed S-phase arrest. C) Annexin V analysis of UT and treated cells. PEO4_MRE11_KD_T cells show significant accumulation of apoptotic cells. The P-value was calculated by one way-ANOVA or two way-ANOVA, ***P < 0.001. Weasel Software Version 3.0.2 (The Walter and Eliza Hall Institute of Medical Research, Australia) was used for all flow cytometry analyses. Data presentation and statistical analysis were performed using GraphPad Prism, version 7.

The results were then validated using another siRNA construct for MRE11 (Figure 3.15). Cisplatin sensitization was evident in MRE11_KD_A2780cis cells compared to scrambled control cells (Figure 3.16).

Taken together, the clinical and pre-clinical results provide evidence that MRE11 is a biomarker of platinum sensitivity in EOC.

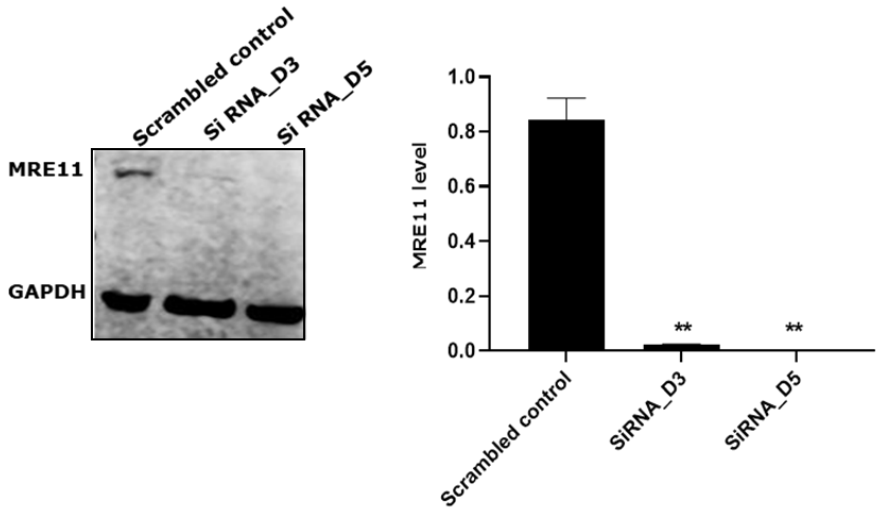

Figure 3.15: MRE11 knockdown in A2780cis cells using a second siRNA construct. A) Representative western blot which revels MRE11 protein level in A2780cis control cells and silenced cells. MRE11 was successfully knocked down in day 3 and day 5 in A2780cis cells. B) The quantification analysis of MRE11 reduction in A2780cis scrambled control and silenced cells. Data presentation and statistical analysis were performed using GraphPad Prism, version 7. The P value was calculated by student's t-test, ** $p<0.01$. D3=day 3, D5=day 5.

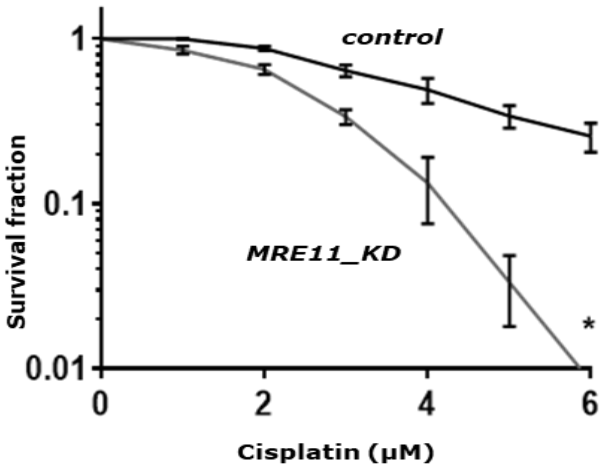

Figure 3.16: Clonogenic assay showing cisplatin sensitivity in A2780cis and MRE11_KD_A2780cis cells. A second siRNA was used as a construct to validate our previous results. See chapter two (p.97) for transfection methods. Scrambled control cells and transfected cells (MRE11_KD) were seeded in six-well plates overnight. The following day, increased dose of cisplatin was added. Cells were then left in the incubator for two weeks (Ali et al., 2019a). Microsoft Excel 2010 was used to determine plating efficiency and survival fraction, see chapter two page (100-101) for more details. MRE11 depletion increased cisplatin sensitivity in A2780cis cells. Data presentation and statistical analysis were performed using GraphPad Prism, version 7. The P value was calculated by student's t-test, * $p<0.050$.

3.4.4 MRE11 BLOCKADGE BY MIRIN PROMOTES PLATINUM SENSITIVITY

Mirin is a small molecular inhibitor of the 3’ to 5’ exonuclease activity of MRE11. We initially investigated whether the treatment of mirin would sensitize A2780cis and PEO4 cells to cisplatin. MTS cell proliferation assay was preformed to determined mirin dose that kills 50% of cells in PEO4 cells (Figure 3.17). In clonogenic assays, we showed that mirin pre-treatment (18μM) leads to cisplatin sensitization in A2780cis cells (Figure 3.18). We then preformed functional studies. Treatment of mirin in A2780cis cells was associated with DSB accumulation, S-phase arrest and increased apoptotic cells (Figure 3.19). Similarly, in PEO4 cells, mirin treatment increased platinum sensitivity (Figure 3. 20), was associated with increased DSB accumulation, S-phase arrest and apoptotic cells (Figure 3.21).

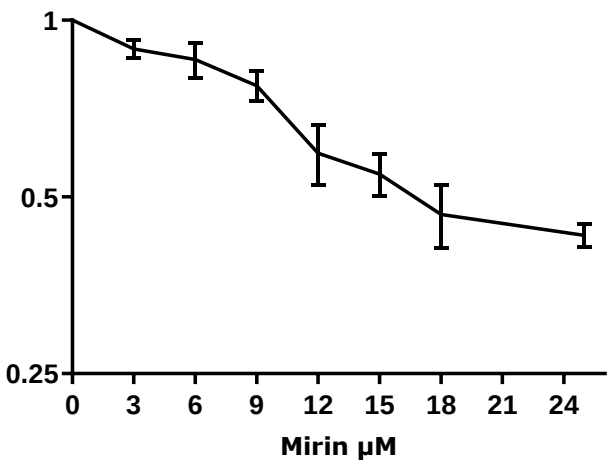

Figure 3.17: Mirin toxicity in PEO4 cells using MTS Cell proliferation assay. Cells were plated in 96-well plates at density of 1000 cells per well and then left in the incubator overnight. Cells were then treated with increased doses of mirin and incubated for 5 days according to the manufacturer's instructions (Al-Subhi et al., 2018). See cahpter two (p.99) for more detalis. 18uM of mirin killed 50% of PEO4 cells. MTS analysis was done using Microsoft Excel 2010. Survival curve was plotted using GraphPad Prism, version 7.

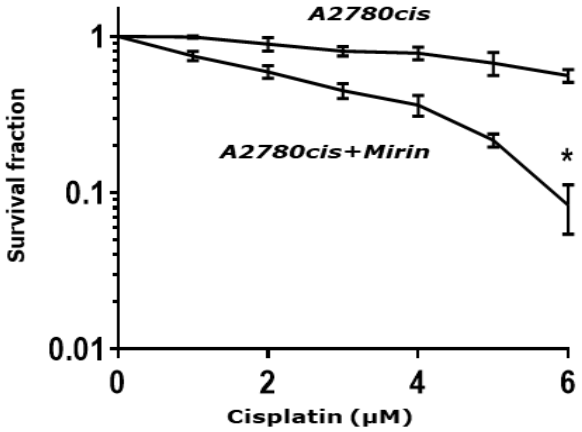

Figure 3.18: Clonogenic assay showing mirin treatment sensitized A2780cis cells to cisplatin. Cells were plated in six-well plates overnight. A2780cis cells were treated with increasing concentration of cisplatin. While A2780cis+mirin cells were treated with increasing concentration of cisplatin and in the following day 18μM of mirin was added. Cells were then left in the incubator for two weeks (Ali et al., 2019a). Microsoft Excel 2010 was used to determine plating efficiency and survival fraction. The treatment of mirin increased cisplatin toxicity in A2780cis cells. The plotting of survival curve and statistical analysis were preformed using GraphPad Prism, version 7. The P value was calculated by student's t-test, * $p<0.050$.

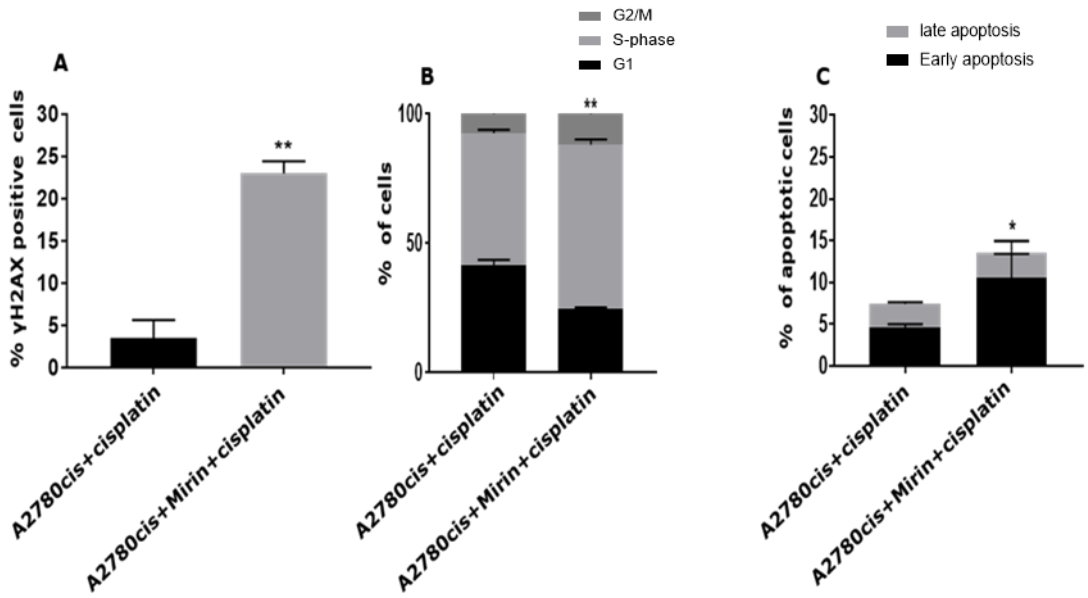

Figure 3.19: Functional studies of A2780cis cells using flow cytometry. A2780cis+cisplatin cells were treated with 5 μM cisplatin for 24 hours. A2780cis + mirin + cisplatin cells were treated with 5 μM cisplatin for 24 hours, and the following day 18 μM/L of mirin were added for 24 hours (Ali et al., 2018). A) The percentage of γH2Ax positive cells, evaluated by one way-ANOVA. A2780cis+ mirin+ cisplatin cells revealed significant accumulation of γH2AX positive cells. B) Cell cycle analysis, using two way-ANOVA. A2780cis+ mirin+ cisplatin cells showed S-phase arrest. C) Annexin V analysis, using two way-ANOVA. A2780cis+ mirin+ cisplatin cells demonstrated significant accumulation of apoptotic cells. *P < 0.050, **P < 0.01.

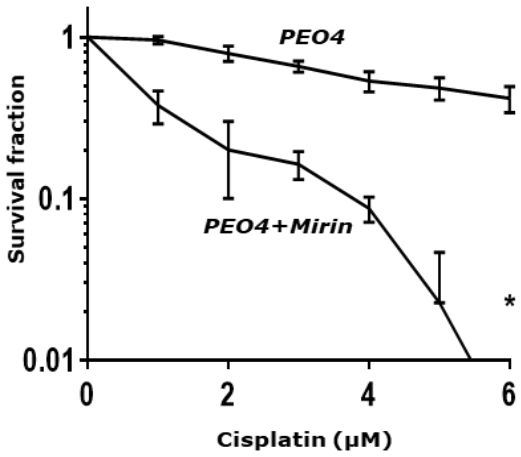

Figure 3.20: Clonogenic assay showing mirin treatment sensitized PEO4 cells to cisplatin. Cells were plated in six-well plates overnight. PEO4 cells were treated with increasing concentration of cisplatin. While PEO4+mirin cells were treated with increasing concentration of cisplatin and in the following day 18μM of mirin was added. Cells were then left in the incubator for two weeks (Ali et al., 2019a). Microsoft Excel 2010 was used to determine plating efficiency and survival fraction. The treatment of mirin increased cisplatin toxicity in PEO4 cells. The P value was calculated by student's t-test, * $p<0.050$.

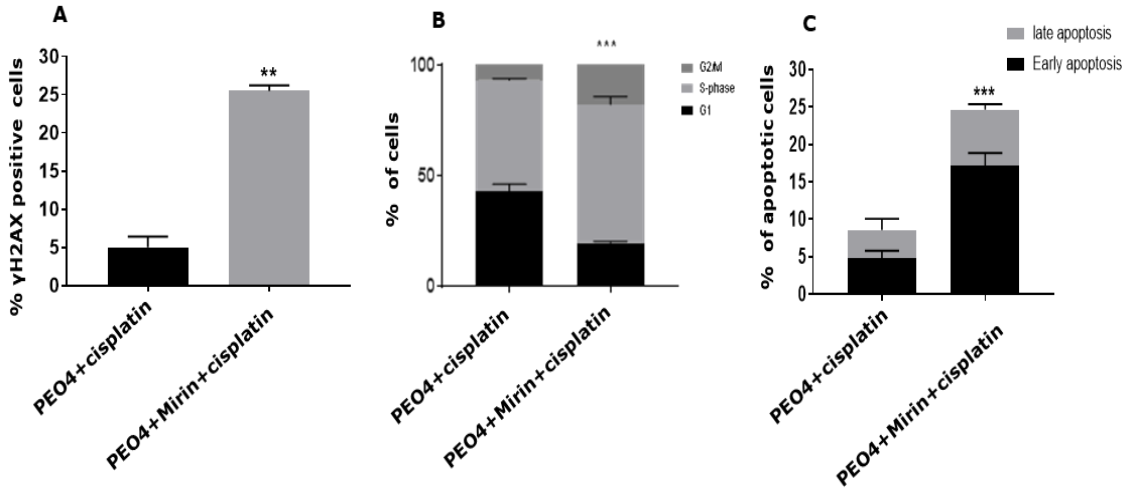

Figure 3.21: Functional studies of PEO4 cells by flow cytometry. PEO4+cisplatin cells were treated with 5 μM cisplatin for 24 hours. PEO4 + mirin + cisplatin cells were treated with 5 μM cisplatin for 24 hours, and the following day 18 μM/L of mirin were added for 24 hours (Ali et al., 2018). A) The percentage of γH2Ax positive cells, evaluated by one way-ANOVA. PEO4+ mirin+ cisplatin cells revealed significant accumulation of γH2AX positive cells B) Cell cycle analysis, using two way-ANOVA. PEO4+ mirin+ cisplatin cells showed S-phase arrest. C) Annexin V analysis, using two way-ANOVA. PE04+ mirin+ cisplatin cells demonstrated significant accumulation of apoptotic cells. **P < 0.01, ***P < 0.001.

3.5 RESULTS SUMMARY

- Clinical data showed that high MRE11 protein levels were significantly associated with serous cystadenocarcinoma ($p<0.001$), high FIGO stage ($p=0.002$), optimal debulking (0.002), poor PFS ($p=0.002$) and a worse OS ($p=0.002$). High MRE11 cytoplasmic expression associated with serous cystadenocarcinoma (0.000046) and high grade (0.007) but did not influence survival.
- Clinical data revealed that high MRE11 mRNA expressions was significantly associated with poor PFS ($p=0.00036$) but has no influence on OS.
- Preclinical studies demonstrated that MRE11 depletion sensitized A2780cis and PEO4 cells to platinum therapy. Increased sensitivity was correlated with DSB accumulation, S-phase cell cycle arrest and apoptosis when compared with scrambled controls
- Preclinical studies showed that mirin treatment increased platinum sensitivity A2780cis and PEO4 cells. Increased sensitivity was linked with DSB accumulation, S-phase cell cycle arrest and increased apoptosis.

3.6 DISCUSSION

Resistance to platinum drugs (carboplatin, cisplatin) negatively impacts patients' outcomes in OC. These agents cause intra-strand and inter-strand DNA adducts, which contribute to DSBs during replication. Proficient DNA repair is a critical mechanism that leads to resistance to platinating agents (Rabik and Dolan, 2007). MRE11 has an important role in sensing DSBs, DSBs repair, DNA recombination, telomere maintenance and apoptosis (Lamarche et al., 2010a). In this study, we provided comprehensive clinical and preclinical evidence that MRE11 could be a predictor of platinum resistant and could also be a promising drug target for chemo-sensitization. We clinically demonstrated that MRE11 overexpression was associated with aggressive clinicopathological features in EOC. High MRE11 protein expression also predicted platinum resistance and it was correlated with poor survivals outcomes in EOC patients an evident by poor PFS. Previous studies showed that MRE11 is highly expressed in various tumours types, including breast cancer (BC)(Yuan et al., 2012), gastric cancer (Altan et al., 2016), prostate cancer (Wang et al., 2019) and rectal cancer (Ho et al., 2018). Elevated MRE11 expression has been correlated with more malignant behaviour in BC (Yuan et al., 2012). High expression of MRE11 was also associated with poor prognosis and chemoresistance in breast and colon cancers (Pavelitz et al., 2014, Yuan et al., 2012).

Overexpression of MRE11 in gastric cancer patients was significantly associated with lymph node metastasis and distal metastasis (Altan et al., 2016). In prostate cancer, high MRE11 expression was also significantly linked to progression of poor OS and poor disease free survival (DFS)(Wang et al., 2019). Overexpression of MRE11 was associated with a worse OS in rectal cancer patients (Ho et al., 2018). A recent study has demonstrated that low MRE11 expression was observed in low grade EOC (Brandt et al., 2017). Additionally, next generation sequencing analysis revealed that germline MRE11 variant (rs1805363) can be used as a marker for radiotherapy outcomes in bladder cancer (Teo et al., 2014).

Interestingly, high MRE11 protein levels are associated with better outcomes in some cancers. For examples, in early BC, patients with elevated MRE11 expression showed a reduction in recurrence from radiotherapy (Soderlund et al., 2007). Two studies in bladder cancer demonstrated that overexpression of MRE11 was correlated with better cancer-specific survival (CSS) in patients who received radiotherapy rather than a cystectomy (Choudhury et al., 2010, Laurberg et al., 2012).

The possible explanation for these different observations could be that; 1) MRE11 may play different roles in cancers arising from different tissues, 2) These studies used tissue microarrays (TMA),

which provide a robust platform to analyse several markers, but might not represent the heterogeneity of the entire tumour (Matos et al., 2010), 3) It might be the prognostic value of MRE11 expression relied on certain combinations of surgery, chemotherapy and radiotherapy, which differ between the treatment modalities preferred for different cancers, 4) It could also be due to issues with antibody specificity, 5) The determination of cut-off values between negative or positive results (Soderlund et al., 2007).

One mechanism that might contribute to altered MRN complex gene expression is mutations in mismatch repair (MMR) genes. Previous study showed that *MRE11* was mutated in MMR-deficient tumours and cell lines compare to tumours /cells that had normal MMR function. However, these observations that link MRN complex expression with MMR deficiency are a subject for further investigation (Giannini et al., 2002, Ho et al., 2018).

We observed some cytoplasmic expression of MRE11. This might be due to the altered nuclear localization of MRE11. MRE11 interacts with NBS1 which is responsible for nuclear localization of MRN complex, and NBS1 physically interacts with KPNA2 (importin alpha1). The disruption of NBS1 and KPNA2 interaction could lead to accumulation of MRE11 cytoplasmic expression (Kim et al., 2017a, Tseng et al., 2005). Another possibility could be the possible role of

MRE11 in mitochondrial DNA (mtDNA) repair. Dmitrieva et al reported that MRE11 binds to mtDNA and the amount of MRE11 expression in the mitochondria varies based on cellular stress and differentiation. Moreover, MRE11 has a role in the maintenance of genomic integrity in mitochondria (Dmitrieva et al., 2011).

Our pre-clinical data showed that basal levels of MRE11 was high in A2780cis and PEO4 cells compared to A2780 and PEO1 cells. We also revealed that MRE11 nuclear accumulation could promote repair of platinum induced DNA damage and contribute to resistance in A2780cis and PEO4 cells. The MER11 levels either in whole lysate or in nuclear and cytoplasmic extracts were tested using western blot (WB). WB as all biological assays, has some limitations: 1) The loading concentration, transfer process and the detection method could affect WB results. 2) The low specificity and selectivity of primary antibodies could cause a cross-reactivity which influences results. 3) The concentration of primary and secondary antibodies might cause variation in interpretation of results (Ghosh et al., 2014). As a result, WB data can be validated using alternative techniques such as ELISA and FACS analysis.

Upregulation of MRE11 in resistance cell lines may increase DNA repair capacity and promote resistance to platinum therapy.

We also reported that MRE11 depletion or mirin caused a substantial platinum sensitization in A2780cis and PEO4 cells. Increased sensitivity was correlated with increased DSB accumulation, S-phase arrest and apoptotic cells.

Loss of MRE11 impairs homologous recombination pathway (HR), which sensitises cancer cells to chemotherapeutic agents (Konstantinopoulos et al., 2015). Similarly, MRE11 deficiency leads to increase the sensitivity to PARP inhibitors in colorectal (Vilar et al., 2011, McPherson et al., 2014), myeloid malignancies (Gaymes et al., 2013), breast (Daemen et al., 2012) and endometrial cancers (Koppensteiner et al., 2014) *in vitro*. Additionally, MRE11 depletion in endometrial and ovarian cancers predicts sensitivity to PARP inhibitors in vitro (Brandt et al., 2017).

Previous study demonstrated that mirin can effectively increase radio-sensitivity in human glioblastoma cells, suggesting that mirin could be a potent radiosensitizer for glioma cells treatment (Mishima et al., 2014).

In conclusion, our clinical and pre-clinical data showed that MRE11 inhibition could be a promising approach for personalization of EOC therapy. However, there are some limitations in this work. For example, only two resistance ovarian cancer cell lines were used

(A2780cis and PEO4 cells), the functional studies were not repeated on the second siRNA construct, CRISPER-cas9 can be used to validate siRNA results and Comet assay or other DNA damage makers could be performed to measure DNA damage. Further pre-clinical and xenograft studies of mirin are required.



RAD50 BLOCKADE FOR PLATINUM CHEMO-SENSITIZATION IN EPITHELIAL OVARIAN CANCER



4. RAD50 BLOCKADE FOR PLATINUM CHEMO-SENSITIZATION IN EOC

4.1 INTRODUCTION

The human *RAD50* gene is situated in chromosome 5q31 and encodes for 153KD protein. RAD50 plays a critical role in non-homologous and joining (NHEJ) and homologous recombination (HR) (Wang et al., 2018). RAD50 is an ATP-modulated DNA cross-linker that has three vital domains: ATP-binding cassette (ABC), zink hook region and MRE11 interaction site (Chang et al., 2016), and the integrity of these domains is crucial for the process of DSBs by MRN complex (Abuzeid et al., 2009). RAD50 act as a bridge at the junction of DNA damage, facilitating the recognition and processing of DNA ends by the exonuclease activity of MRE11 to initiate DNA repair. MRE11 endo- and exo- nuclease activities are stimulated upon correlation with RAD50 (Waltes et al., 2009b). RAD50 deficiency reduces MRE11 nuclear localization and it is interaction with NBS1. Moreover, *RAD50* mutations lead to some reduction in expression levels of MRE11 and NBS1, similar to what was seen in MRE11 mutations (Waltes et al., 2009b). RAD50 dysfunction directly reduced DSBs repair performed by MRN complex. It is reported that RAD50 mutation in the phosphor-site-specific (S635G) abrogates RAD50 activating phosphorylation by ATM, and that RAD50- deficient

cells impair the cell cycle checkpoints and DNA repair proteins (Gatei et al., 2011).

RAD50 also plays role in the maintenance of telomere. MRN complex generates a 3' overhang in the chromosome ends that preform as replication primers for telomerase, which expressed in most cancer to prevent the loss of telomeric DNA (Chai et al., 2006). The generation of 3' overhang in the chromosome ends by MRN complex is based on the molecular bridging of DNA through RAD50. As a result, disruption of RAD50 function leads to severe telomere shorting and cell death. RAD50 is physically correlated with key shelterins proteins. Key shelterins protect telomeres form being identified as DSBs but also prevent telomerase from accessing telomere ends. RAD50 downregulates the telomeric correlation of key shelterins, increasing the activity of telomerase and telomere lengthening. (Abuzeid et al., 2009, Wu et al., 2007).

RAD50 has been described as a risk gene linked to genomic instability in hereditary breast cancer (Heikkinen et al., 2006). Mutations in *RAD50* are correlated with increased cancer risk, including familial and sporadic cancers (Rein and Stracker, 2014), and It has been shown that *RAD50* polymorphisms are correlated with risk of breast and ovarian cancer (OC)(Flores-Perez et al., 2014). Previous studies have demonstrated RAD50 as a potential

therapeutic target in nasopharyngeal, head and neck, breast and non–small cell lung cancers (NSCLC) (Chang et al., 2016, Flores-Perez et al., 2014, Abuzeid et al., 2009, Wang et al., 2018). Hypothesis, whether RAD50 expression relates to clinicopathological parameters and influence response to platinum therapy EOC. We also hypothesized that RAD50 could be a promising target for personalization of EOC therapy.

4.2 CHAPTER AIMS

- Evaluate the clinicopathological significance of RAD50 expression by immunohistochemistry (IHC) in 331 human EOC.
- Investigate RAD50 mRNA expression in a publicly available, online gene expression dataset of 1259 OC patients to assess the association between RAD50 mRNA expression and patients' survivals.
- Profile a panel of OC cell lines to identify RAD50 protein level in OC cell lines.
- Monitor RAD50 protein levels in nuclear and cytoplasmic extracts from OC cell lines before and after 24 and 48 hours of cisplatin treatment.
- Investigate whether RAD50 depletion can sensitize OC resistance cell lines to platinum treatment.

- Conduct functional studies to study the effect of RAD50 depletion in DSBs, cell cycle and apoptosis.

4.3 RESULTS

4.3.1 CLINICAL STUDY

4.3.1.1 RAD50 OVEREXPRESSION ASSOCIATES WITH PLATINUM RESISTANT IN EOC

To assess the association between RAD50 expression and the clinicopathological parameters in EOC, we conducted IHC staining to detect RAD50 expression in 331 human EOC (Figure 4.1). RAD50 nuclear expressions is shown in Figure 3.1a, b and c. Cytoplasmic expression is demonstrated in figure 3.1d and F. The patient demographics and pathological characteristics in EOC is shown in chapter two (P.79).

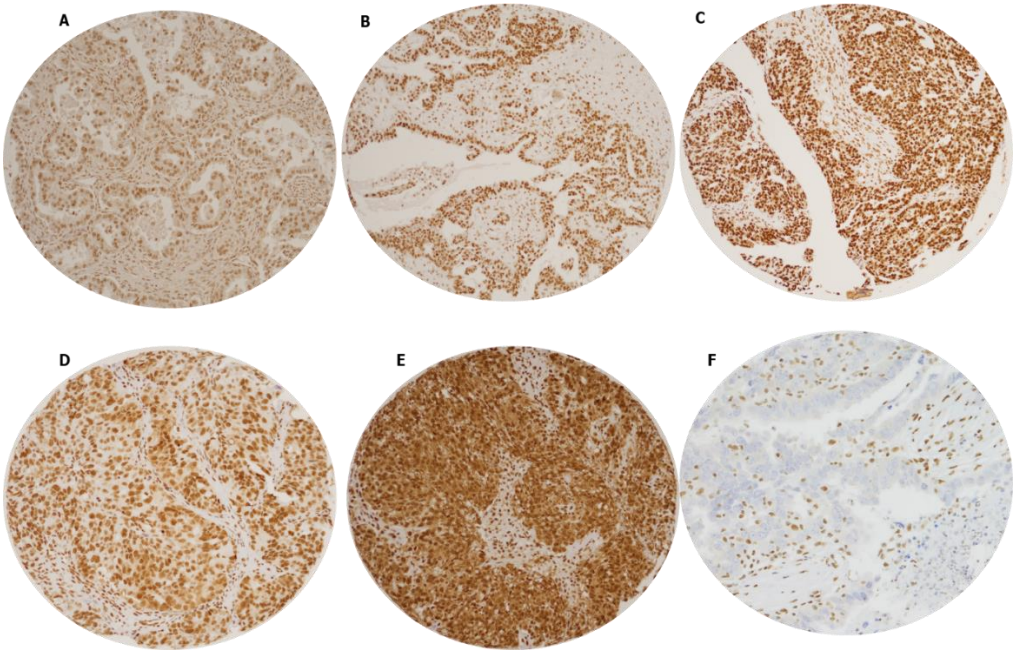

Figure 4.1: Immunohistochemical expression of RAD50 (nuclear and cytoplasmic) in ovarian cancers. A) Week nuclear expression of RAD50. B) Moderate nuclear expression of RAD50. C) Strong nuclear expression of RAD50. D) Week cytoplasmic expression of RAD50. E) Strong cytoplasmic with nuclear expression of RAD50. F) Negative expression of RAD50. Magnification 20x.

We then evaluated the relationship between RAD50 expression and clinicopathological parameters. RAD50 protein expression was evaluable in 239 tumours. Intense nuclear RAD50 was observed in 90/239 (42.6%) tumours and associated with serous cystadenocarcinoma (p=0.033), high grade 3 tumours (P=0.004) (Table 4.1). High nuclear RAD50 was linked to poor PFS (p=0.006) and poor OS (p=0.003) (Figure 4.2). High RAD50 cytoplasmic expression did not influence PFS survival (p=0.866), while was borderline non-significant with OS (p=0.078) (Figure 4.3).

Table 4.1 The association between RAD50 expression and clinicopathological variables in EOC.

	RAD50 _C -	RAD50_C +	P- value	RAD50_N -	RAD50 _N+	P- value
Pathological Type			0.153			***0.033***
Serous adenocarcinoma	88 (63.3%)	51 (36.7%)		64 (46%)	75 (54%)	
Mucinous adenocarcinoma	20 (64.5%)	11 (35.5%)		22 (71%)	9 (29%)	
Endometrioid carcinoma	23 (74.2%)	8 (25.8%)		21 (67.7%)	10 (32.3%)	
Clear cell carcinoma	17 (94.4%)	1 (5.6%)		12 (66.7%)	6 (33.3%)	
Mixed	8 (66.7%)	4 (33.3%)		6 (50%)	6 (50%)	
FIGO Stage			0.433			0.572
I	62 (70.5%)	26 (29.5%)		51 (58%)	37 (42%)	
II	25 (75.8%)	8 (24.2%)		15 (45.5%)	18 (54.5%)	
III	66 (62.9%)	39 (37.1%)		59 (59.2%)	46 (43.8%)	
IV	4 (57.1%)	3 (42.9%)		3 (42.9%)	4 (57.1%)	
Tumour Grade			0.274			***0.004***
Grade 1	22 (73.3%)	8 (26.7%)		24 (80%)	6 (20%)	
Grade 2	33 (73.3%)	12 (26.7%)		26 (57.8%)	19 (42.2%)	
Grade 3	81 (62.3%)	44 (37.7%)		61 (46.9%)	69 (53.1%)	
Surgical Optimal Debulking			0.377			0.134
Optimally Debulked	120 (68.2%)	56 (31.8%)		103 (58.5%)	73 (41.5%)	
Not Optimally Debulked	27 (64.3%)	56 (31.8%)		20 (47.6%)	22 (52.4%)	
Residual tumour			***0.013***			0.08
None/Microscopic	103 (72%)	40 (28%)		186 (60.1%)	57 (39.9%)	
<1cm	12 (42.9%)	16 (57.1%)		11 (39.3%)	17 (60.7%)	
1-2 cm	8 (61.5%)	5 (38.5%)		5 (38.5%)	8 (61.5%)	
>2cm	28 (77.4%)	7 (22.6%)		20 (46.5%)	11 (35.5%)	
Measurable Disease Before ChemoTherapy			0.333			0.245
Non	101 (68.7%)	46 (31.3%)		86 (58.5%)	61 (41.5%)	
Measurable	42 (46.6%)	23 (35.4%)		34 (52.3%)	31 (47.7%)	
Platinum sensitivity			0.052			0.228
Sensitive	124 (66.7%)	62 (33.3%)		110 (59.1%)	76 (40.9%)	
Resistance	16 (88.9%)	2 (11.1%)		8 (44.4%)	10 (55.6%)	

* RAD50_C= RAD50 cytoplasmic expression, RAD50_N= RAD50 nuclear expression. + = high expression, -= low expression. The $P < 0.05$ was considered significant. Some cases were lost in the analysis, as we could not find their records. They have most probably been referred from another trust to be treated in NUH with limited access to their pathological reports. Others are old cases where the pathological reports were not written in clear template like the recent ones. Consequently, to avoid bias, the grade was stated as unknown. Same rule was applied to the other clinicopathological characteristics.

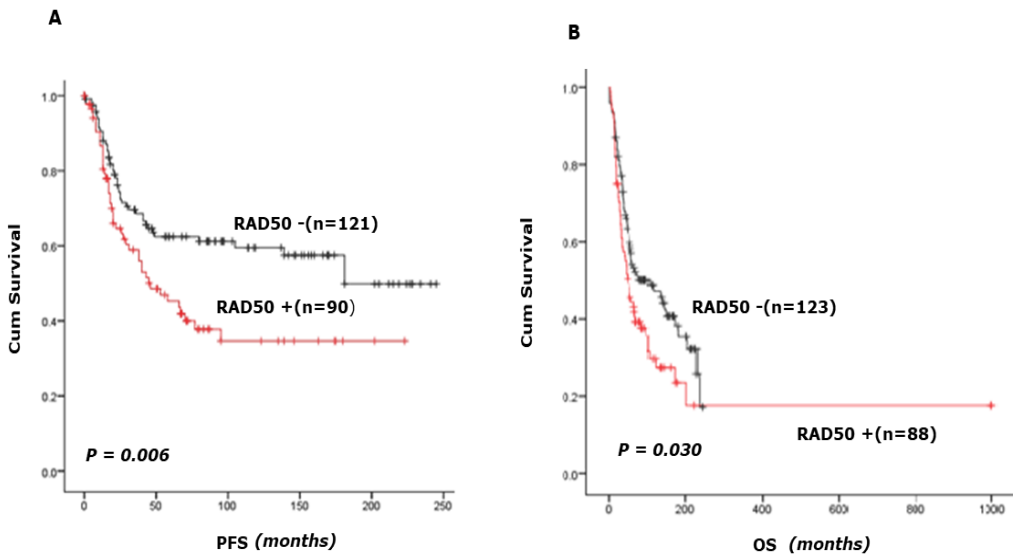

Figure 4.2: Kaplan Meier survival curves for RAD50 nuclear expression. Kaplan Meier statistical analysis was used to conduct a univariate analysis of OS and PFS against RAD50 expression. A) High nuclear RAD50 expression (Red lines) was significantly associated with poor PFS (P=0.006). PFS is the time between treatment initiation and tumour progression again. B) High nuclear RAD50 expression (Red lines) was significantly associated with worse OS (P=0.030). OS is calculated between the day of diagnosis or time of treatment initiation and time where patients still alive. RAD50-= low RAD50 level, RAD50+= high RAD50 level and n= number of cases.

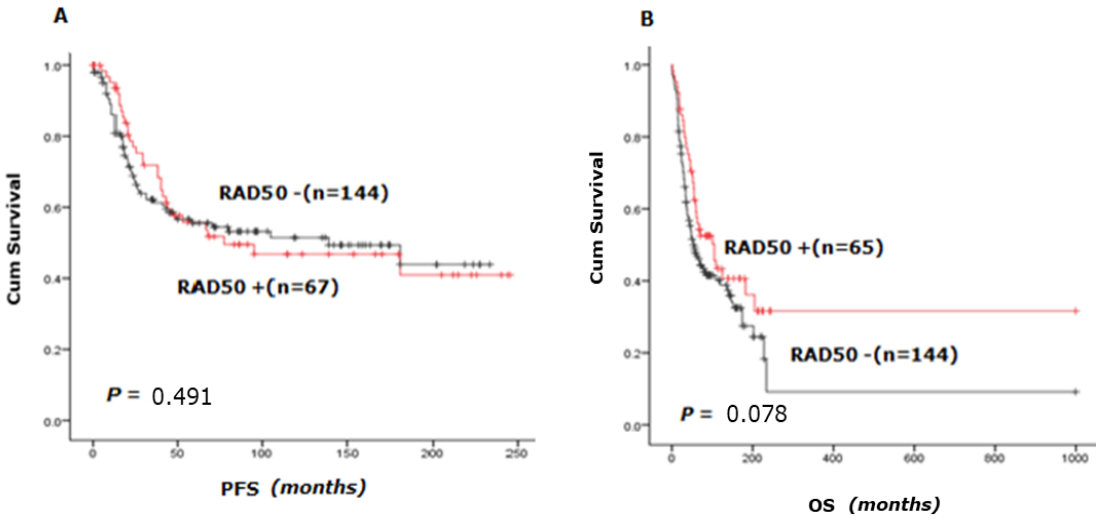

Figure 4.3: Kaplan Meier survival curves for RAD50 cytoplasmic expression. A) High RAD50 cytoplasmic expression (Red line) did not influence PFS (p=0.866). B) High RAD50 cytoplasmic expression (Red line) was borderline non-significant with OS (p=0.078).

To validate further, the transcriptomic level of RAD50 in EOC patients who received platinum agents was investigated. High mRNA expression of RAD50 significantly associated with poor PFS (p=0.001) but has no influence on OS (p=0.22) (Figure 4.4). Altogether, the results demonstrate that the protein and transcriptional expression levels of RAD50 have predictive and prognostic significance in human EOC. We then moved to detailed preclinical examinations in platinum-sensitive and resistance OC cell lines.

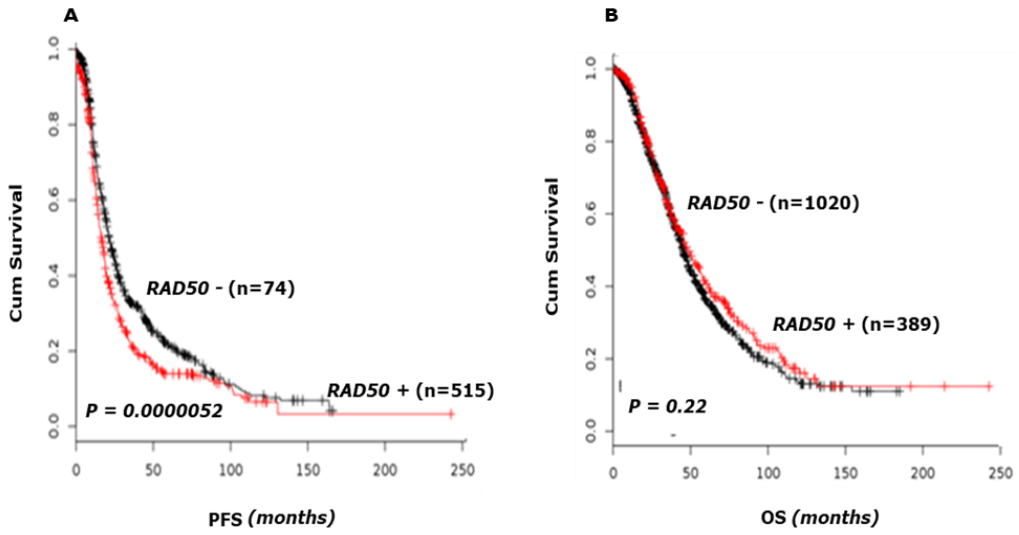

Figure 4.4: The correlation of RAD50 mRNA expression and PFS and OS survivals. A) High RAD50 mRNA expression (Red lines) was significantly associated with poor PFS. B) No significant correlation was associated with OS.

4.3.2 PRE-CLINICAL STUDIES

4.3.2.1 THE DEPLETION OF RAD50 PROMOTES THE CHEMO-SENSITIVITY IN OC CELL LINES

We first screened the baseline level of RAD50 in A2780, A2780cis, PEO1 and PEO4 cell lines. In whole lysate, RAD50 baseline protein level was significantly high in A2780cis cells compared to A2780 cells. Similarly, RAD50 baseline protein level was significantly high in PEO4 cells compared to PEO1 cells (Figure 4.5). Hence, the RAD50 baseline level is high in OC resistance cell lines (A2780cis and PEO4) compare to that were sensitive cells (A2780 and PEO1).

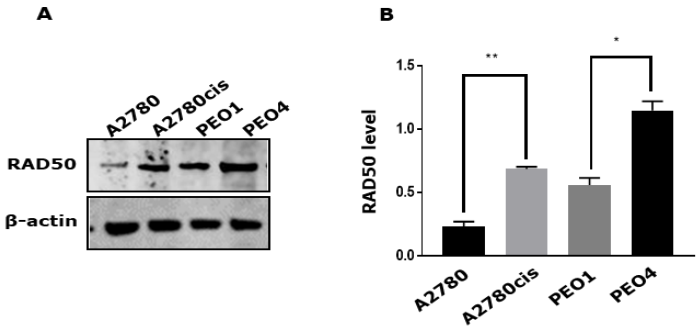

Figure 4.5: Western blot for RAD50 protein levels in A2780, A2780cis, PEO1 and PEO4 cells. A) High RAD50 protein level in cisplatin-resistant A2780cis and PEO4 cells compared to platinum-sensitive A2780 and PEO1 cells. B) The quantification of RAD50 levels in four ovarian cancer cell lines. The detected band intensity for RAD50 as well as β-actin band intensity were quantified in LI-COR software. The readings for RAD50 were normalised to β-actin reading. Microsoft Excel 2010 was used for normalization. Data presentation and statistical analysis were performed using GraphPad Prism, version 7. The P value was calculated by student's t-test, * $p<0.05$ and ** $p<0.01$.

To evaluate the alteration in sub-cellular localization of RAD50, we took nuclear and cytoplasmic extracts from A2780, A2780cis, PEO1 and PEO4 cell lines before and after 5 μM cisplatin treatment. Although after 24 hours of cisplatin treatment, there was no significant differences, at 48 hours, significantly increased RAD50 nuclear sub-cellular localisation in A2780cis and PEO4 cells were evident compared to A2780 and PEO1 cells. No significant changes were observed for RAD50 cytoplasmic expression (Figure 4.6-4.7). The data suggests that RAD50 nuclear accumulation could promote repair of platinum induced DNA damage and contribute to resistance in A2780cis and PEO4 cells.

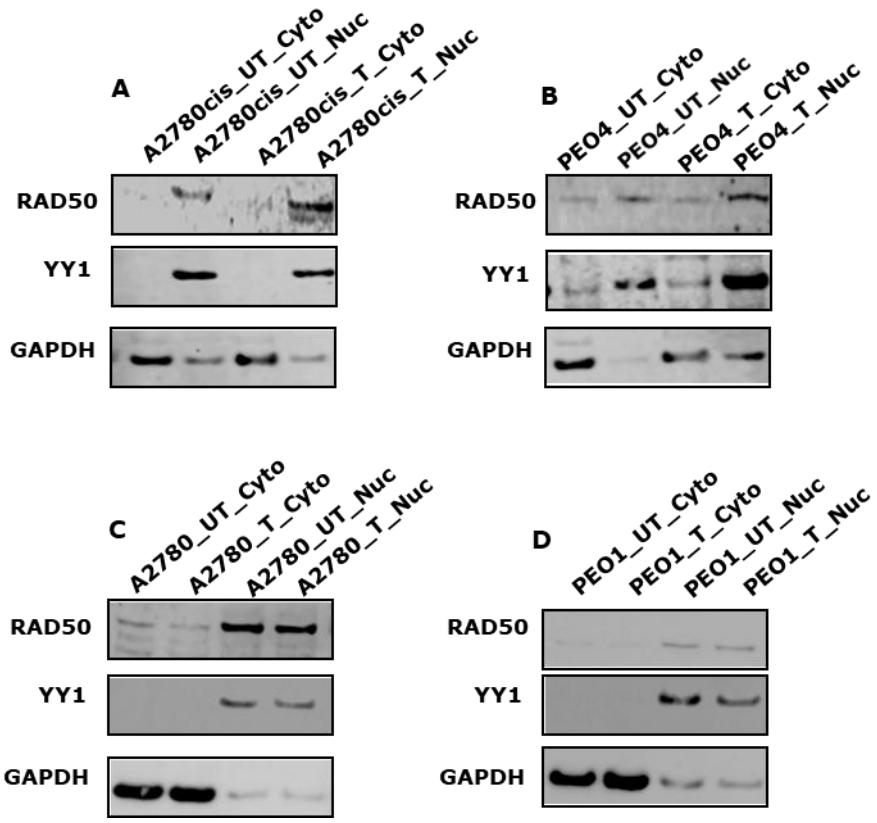

Figure 4.6: Representative western blot of nuclear and cytoplasmic levels of RAD50. For nuclear and cytoplasmic extraction protocol see chapter two (P.107-108). RAD50 nuclear expressions were normalised to YY1 levels. RAD50 cytoplasmic expressions were normalised to GADPH levels. Microsoft Excel 2010 was used for normalization. A) RAD50 nuclear expression in A2780cis cells was significantly increased after 5 μM cisplatin therapy for 48 hours, while no difference was observed in RAD50 cytoplasmic expression before and after cisplatin treatment. B) RAD50 nuclear expression in PEO4 cells was significantly increased after 5 μM cisplatin treatment for 48 hours, while no significant difference was seen in RAD50 cytoplasmic expression. C) RAD50 nuclear and cytoplasmic expression in A2780 cells did not change after 48 hour of cisplatin therapy. D) Cisplatin treatment for 48 hours did not change RAD50 nuclear and cytoplasmic levels in PEO1 cells (Mesquita et al., 2019).

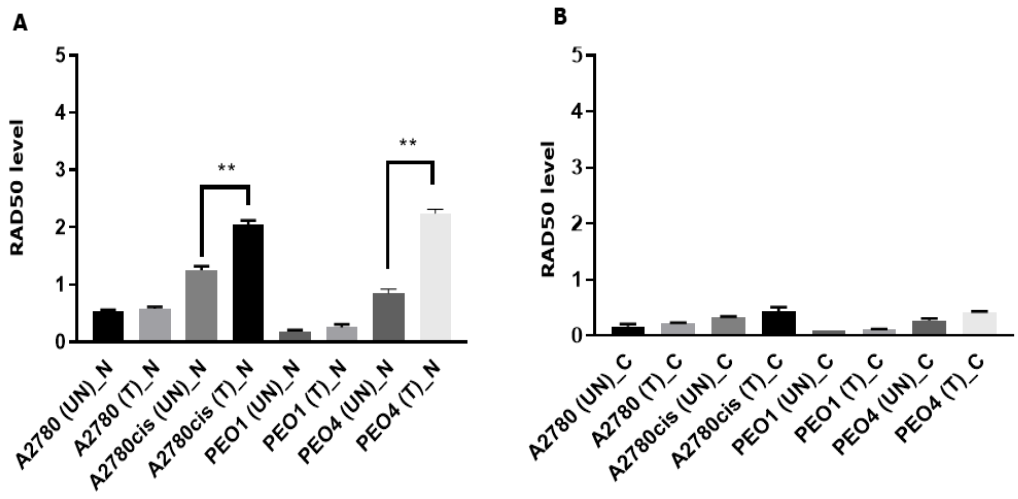

Figure 4.7: The quantification of RAD50 nuclear and cytoplasmic expression levels. A) RAD50 nuclear levels A2780, A2780cis, PEO1 and PEO4. RAD50 expression level in untreated A2780cis and PEO4 cells was high compared with untreated A2780 and PEO1. RAD50 nuclear expression level was significantly increased after cisplatin treatment in A2780cis and PEO4 cells compared the same cells before treatment. B) RAD50 cytoplasmic levels in A2780, A2780cis, PEO1 and PEO4. The P value was calculated by student's t-test, ** p>0.01. Data presentation and statistical analysis were performed using GraphPad Prism, version 7.

We then evaluated RAD50 depletion in A2780cis and PEO4 cells for platinum sensitivity. Downregulation of genes that are upregulated in resistance cell lines using siRNA is a useful strategy to study resistance mechanism (Ganesh et al., 2013). We initially generated transient knockdown (KD) of RAD50 by siRNA in A2780cis. RAD50 was successfully knocked down by day three and persistent on day five in A2780cis cells (Figure 4.8).

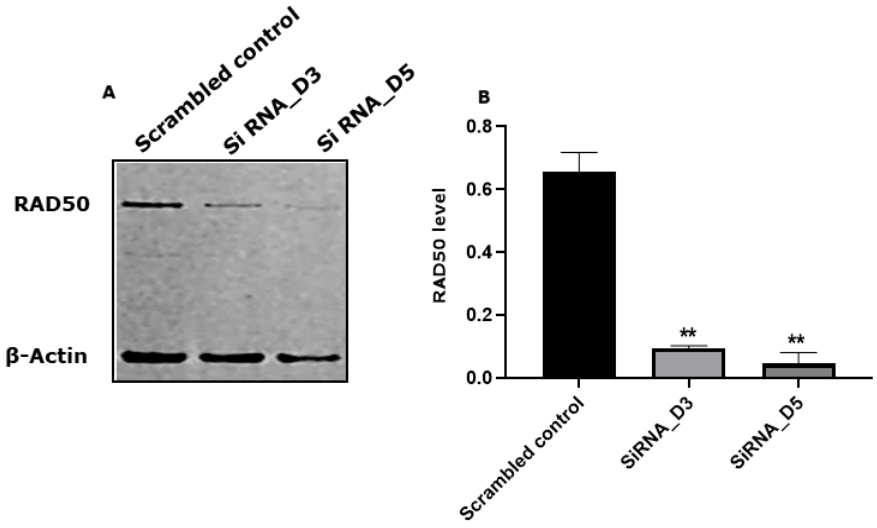

Figure 4.8: RAD50 knock down in A2780cis cells using siRNA. Cells were seeded at 60-70% confluency in T25 flasks overnight. Cells were transfected with mRAD50 siRNA oligonucleotide or scrambled siRNA oligonucleotide control in Opti-MEM media. Transfection process was preformed using lipofectamine 3000 regent (Mesquita et al., 2019). See chapter two (P.97) for more details. Transfection efficiency was confirmed using western blot. A) Representative western blot which shows RAD50 protein level in A2780cis control and silenced cells. RAD50 was successfully knocked down in day 3 and day 5 in A2780cis cells. B) The quantification analysis of RAD50 depletion in A2780cis scrambled control and silenced cells. The P value was calculated by student's t-test, ** $p<0.01$. D3=day 3, D5=day 5. Data presentation and statistical analysis were performed using GraphPad Prism, version 7.

In clonogenic assays, RAD50_KD_A2780cis cells were significantly sensitive to cisplatin treatment compared to scrambled control cells (Figure 4.9). We then moved to functional studies using fluorescence-activated cell sorting (FACS) in RAD50 KD and scrambled control cells. After 24 hours of 5 μM cisplatin treatment, RAD50 depleted cells showed a significant accumulation of γH2AX,

which is a surrogate marker of DSB accumulation in nucleus (Figure 4.10). Accumulation of DSBs induce cell cycle checkpoint activation leading on cell cycle arrest to allow time for cells to repair DNA damage. If the damages were unrepairable, cells undergo apoptosis. Therefore, we investigated the effect of RAD50 KD on cell cycle and apoptosis after 24 hours of 5 μM cisplatin treatment in RAD50-deficient and proficient cells. S-phase cell cycle arrest and increased apoptotic cells population was evident in RAD50_KD cells compared with scrambled controls (Figure 4.10).

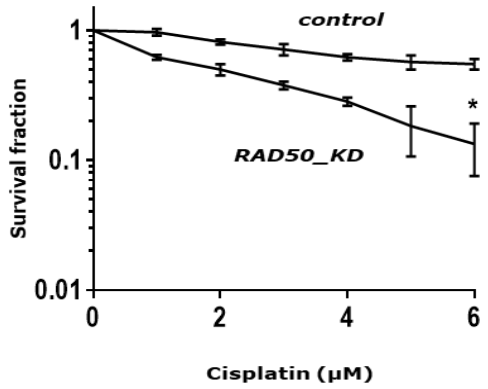

Figure 4.9: Clonogenic assay showing cisplatin sensitivity in A2780cis and RAD50_KD_A2780cis cells. Cells transfected as described in figure 4.8. Control cells and transfected cells (RAD50_KD) were seeded in six-well plates and left in the incubator overnight. The following day, increased doses of cisplatin were added. Cells were then left in the incubator for two weeks (Ali et al., 2019a). Microsoft Excel 2010 was used to determine plating efficiency and survival fraction, see chapter two page (100-101) for more details. RAD50 depletion increased cisplatin sensitivity in A2780cis cells. The P value was calculated by student's t-test, * $p<0.050$. Data presentation and statistical analysis were performed using GraphPad Prism, version 7.

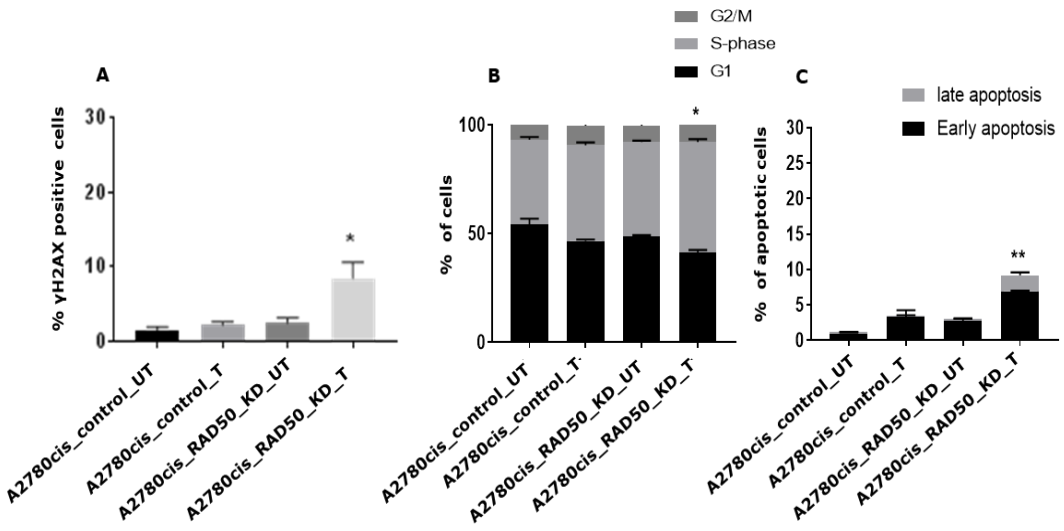

Figure 4.10: Functional studies of A2780cis cells using flow cytometry. Cells transfected as described in figure 4.8. On day two, A2780cis siRNA control and transfected RAD50 siRNA cells were trypsinized and re-plated in six-well plates. The following day, 5 μM of cisplatin was added for 24 hours. Cells were then collected (Ali et al., 2018); Protocols are described in chapter 2 (P.102-106). A) The percentage of γH2Ax positive cells, statistical analysis determined by one-way ANOVA. A2780cis_RAD50_KD treated cells revealed significant accumulation of γH2AX positive cells. B) Cell cycle analysis in UT and treated cells, from two way-ANOVA. A2780cis_RAD50_KD treated cells showed S-phase cell cycle arrest. C) Annexin V analysis in UT and treated cells, from two way-ANOVA. A2780cis_RAD50_KD treated cells demonstrated significant increased apoptotic cells. Weasel Software Version 3.0.2 (The Walter and Eliza Hall Institute of Medical Research, Australia) was used for all flow cytometry analyses. * $p<0.050$ and ** $P < 0.01$. UT= untreated cells, T= treated cells, T= treated cells.

We then generated transient knockdown (KD) of RAD50 using siRNA in another platinum-resistant PEO4 cells (Figure 4.11). RAD50 was successfully knocked down by day three and persistent on day five in PEO4 cells. In clonogenic assays, RAD50_KD_PEO4 cells were significantly more sensitive to cisplatin treatment compared to

scrambled controls (Figure 4.12). We then preformed functional studies in RAD50_KD_PEO4 cells and PEO4 scrambled control cells. DSB accumulation, S-phase cell cycle arrest and apoptosis was evident in RAD50_KD cells compared to scrambled controls (Figure 4.13).

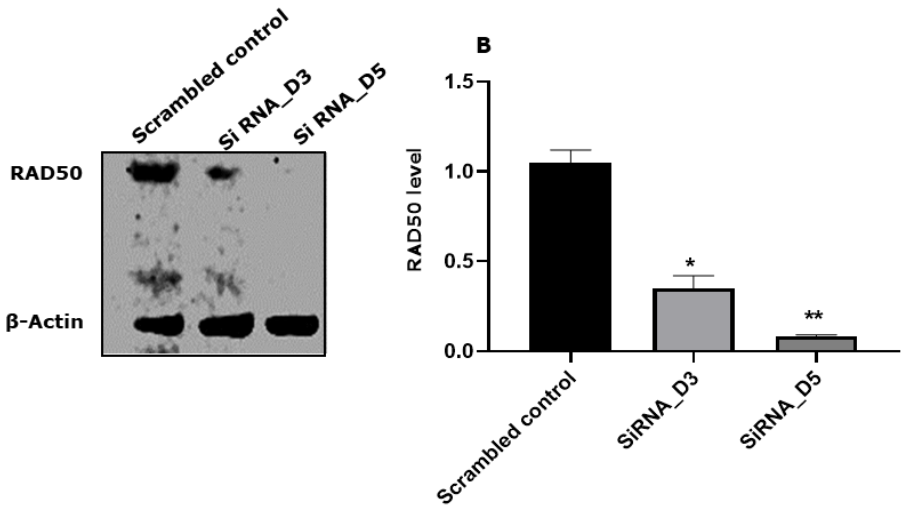

Figure 4.11: RAD50 knock down in PEO4 cells using siRNA. A) Representative western blot which shows RAD50 protein level in PEO4 scrambled control and silenced cells. RAD50 was successfully knocked down in day 3 and day 5 in PEO4 cells. B) The quantification analysis of RAD50 reduction in PEO4 scrambled control and silenced cells. The P value was calculated by student's t-test, * $p<0.050$ and ** $p<0.01$. D3=day 3, D5=day 5. Data presentation and statistical analysis were performed using GraphPad Prism, version 7.

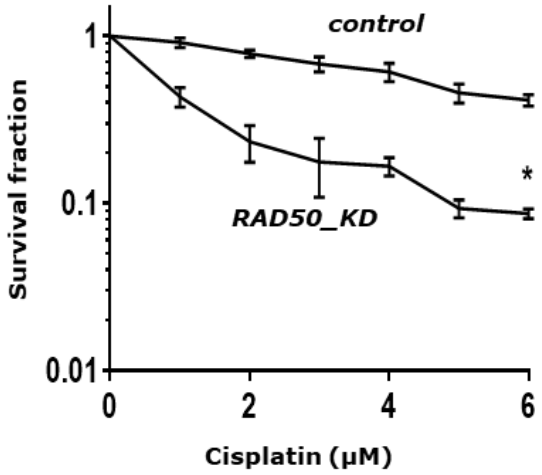

Figure 4.12: Clonogenic assay showing cisplatin sensitivity in PEO4 and NBS1_KD_PEO4 cells. Cells transfected as described in figure 4.8. Control cells and transfected cells (RAD50_KD) were seeded in six-well plates and left in incubator overnight. The following day, increased doses of cisplatin were added. Cells were then left in the incubator for two weeks (Ali et al., 2019a). Microsoft Excel 2010 was used to determine plating efficiency and survival fraction, see chapter two page (100-101) for more details. RAD50 depletion increased toxicity of PEO4 cells to cisplatin. The P value was calculated by student's t-test, * $p<0.050$.

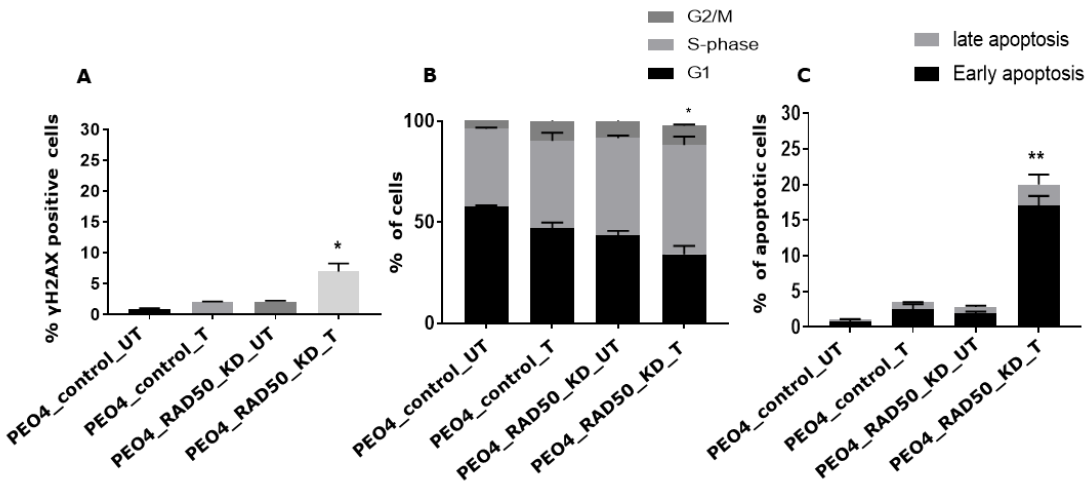

Figure 4.13: Functional studies of PEO4 cells using flow cytometry. A) The percentage of γH2Ax positive cells in UT and treated cells. A2780cis_RAD50_KD treated cells revealed significant accumulation of yH2AX positive cells. B) Cell cycle analysis in UT and treated cells. A2780cis_RAD50_KD treated cells showed S-phase cell cycle arrest. C) Annexin V analysis of UT and treated cells. A2780cis_RAD50_KD treated cells demonstrated significant increased apoptotic cells. The P-value was calculated by one way-ANOVA or two way-ANOVA, * $p<0.05$ and **$P < 0.01$.

The data were then validated using another siRNA construct for RAD50 (Figure 4.14). Cisplatin sensitization was evident in RAD50_KD_A2780cis cells compared to scrambled control cells (Figure 4.15).

Altogether, the clinical and pre-clinical results provide evidence that RAD50 is a biomarker of platinum sensitivity in EOC.

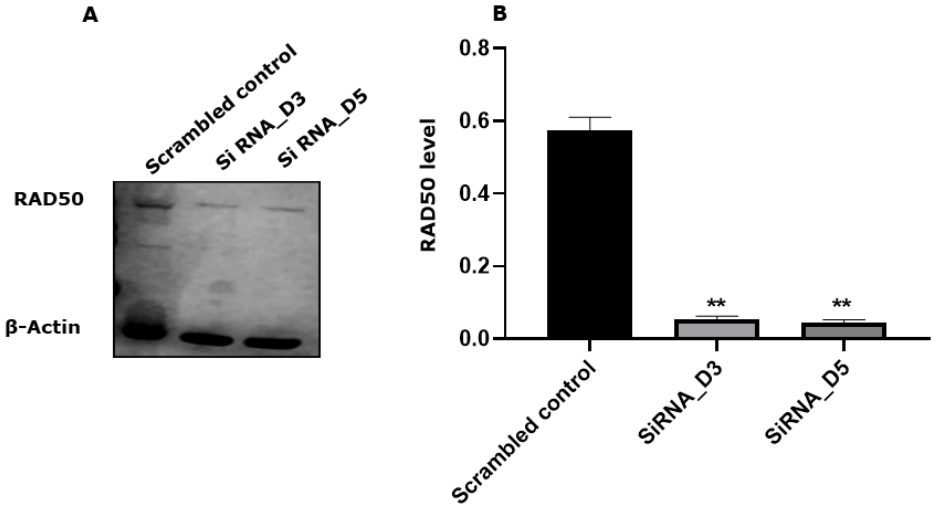

Figure 4.14: RAD50 knock down in A2780cis cells using a second siRNA construct. A) Representative western blot which showed RAD50 protein level in A2780cis control cells and silenced cells. RAD50 was successfully knocked down in day 3 and day 5 in A2780cis cells B) The quantification analysis of RAD50 reduction in A2780cis scrambled control and silenced cells. The P value was calculated by student's t-test, ** $p<0.01$. D3=day 3, D5=day 5.

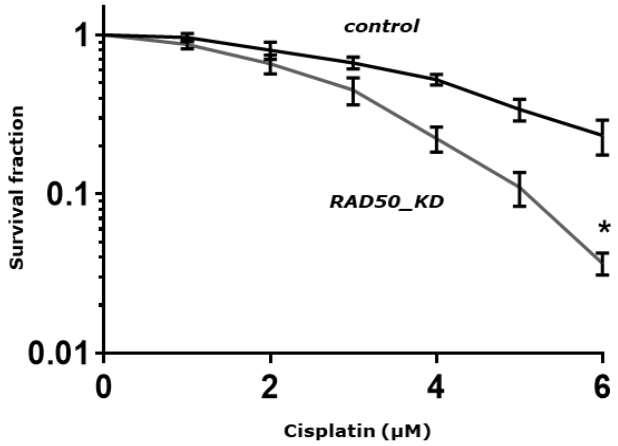

Figure 4.15: Clonogenic assay showing cisplatin sensitivity in A2780cis and RAD50_KD_A2780cis cells. We used a second siRNA construct to validate our previous results. See chapter two (P.97) for transfection methods. Scrambled control cells and transfected cells (RAD50_KD) were seeded in six-well plates overnight. The following day, increased dose of cisplatin was added. Cells were then left in the incubator for two weeks (Ali et al., 2019a). Microsoft Excel 2010 was used to determine plating efficiency and survival fraction, see chapter two page (100-101) for more details. RAD50 depletion increased cisplatin sensitivity in A2780cis cells. The P value was calculated by student's t-test, * $p<0.050$.

4.4 RESULTS SUMMARY

- Clinical data showed that high nuclear RAD50 protein levels were significantly associated with serous cystadenocarcinoma (p=0.033), high grade 3 tumours (P=0.004), poor PFS (p=0.006) and poor OS (p=0.003). Cytoplasmic expression of RAD50 borderline non-significant with OS (p=0.078).

- Clinical data revealed that High RAD50mRNA expressions was associated significantly with PFS (p=0.001) but has no influence on OS.
- Preclinical studies demonstrated that the depletion of RAD50 sensitized A2780cis and PEO4 cells to platinum therapy. Increased sensitivity was correlated with DSB accumulation, S-phase cell cycle arrest and apoptosis when compared with scrambled controls.

4.5 DISCUSSION

The ultimate goal of cancer treatment is to improve patients' survivals, so a current challenge in cancer research is to identify molecular targets that enhance the sensitization of cancer cells to current chemotherapy and radiotherapy. Platinum drugs (carboplatin, cisplatin) are commonly used as a first-line treatment in several malignancies including OC. However, the development of acquired platinum resistant is a major obstacle to cure of OC. Platinum agents cause intra-strand and inter-strand DNA adducts, which contribute to DSBs during replication (Damia and Broggini, 2019, Flores-Perez et al., 2014). Proficient DNA repair is a critical mechanism that leads to resistance to platinating agents. RAD50 has vital role in NHEJ, HR and telomere maintenance (Abuzeid et al., 2009). Thus, RAD50 targeting may disturb DBSs repair, and it might contribute to the sensitization of resistance OC cells to platinum agents.

In the current study, we provided a comprehensive clinical and preclinical evidence that RAD50 could be a predictor of platinum resistant and could also be a promising drug target for platinum sensitization. We clinically demonstrated that high nuclear RAD50 was correlated with aggressive clinicopathological characteristics in EOC.

RAD50 nuclear overexpression also predicted platinum resistant and it is associated with poor survivals outcomes in EOC patients an evident by poor PFS. Previous study showed that high RAD50 expression in tumour cells was correlated with increased DNA repair capacity, high recombination rates and increased radio- and chemotherapy resistance. RAD50 overexpression was linked to poor survival in non-small-cell lung cancer (NSCLC) patients (Qiao et al., 2005). Additionally, high RAD50 expression was associated with poor clinical outcomes after post-operative radiotherapy for NSCLC patients. Elevated RAD50 might be a predictor of radio-resistant in lung cancer patients who received radiotherapy (Wang et al., 2018). Overexpression RAD50 in gastric cancer patients was significantly associated with lymph node metastasis and significantly low expression of γH2AX, so RAD50 may function to reduce DNA damage in gastric cancer patients (Altan et al., 2016). High RAD50 expression was correlated with poor patients survival in colorectal cancer (Chen et al., 2018). A recent study showed that Upregulation of RAD50 was linked to poor patient survival, and to radiotherapy-resistant colorectal cancer cells (Situ et al., 2019). A previous study has shown that low RAD50 expression was observed in low grade EOC (Brandt et al., 2017).

Interestingly, low RAD50 protein levels are correlated with worse outcomes in some cancers. For instance, in early breast cancer,

patients with low RAD50 expression showed poor response to radiotherapy (Soderlund et al., 2007). Ho et al also showed that low postoperative RAD50 expression was correlated with poor OS and disease free survival (DFS) in early tumour and low-grade patient subgroups, supporting the notion that RAD50 could be an early prognostic biomarker in rectal cancer (Ho et al., 2017). The possible explanations for these different findings were mentioned in the chapter three discussion (page 155-156).

Our pre-clinical data showed that base levels of RAD50 was high in A2780cis and PEO4 cells compared to A2780 and PEO1 cells. Overexpression of RAD50 in resistance cell lines may increase DNA repair capacity and promote resistance to platinum therapy. We also demonstrated that RAD50 depletion caused a substantial platinum sensitization in A2780cis and PEO4 cells, and was associated with increased DSB accumulation, S-phase arrest and apoptotic cells.

Similarly, a Previous study designed an adenoviral vector that containing a gene sequence encodes for RAD50 zink hook region, but missing ATPase and MRE11 interaction regions. Interestingly, the resulting mutant RAD50 markedly impaired MRN functions in human squamous cell carcinoma cells (SCS). A combination of mutant RAD50 and cisplatin therapy significantly increased tumour cytotoxicity in vitro, which correlated with enhanced DNA damage

and shortening of telomere. Moreover, cisplatin resistance SCS xenografts studies revealed that this combination treatments resulted in a dramatic regression and increased apoptosis (Abuzeid et al., 2009). A recent study demonstrated that RAD50 depletion increased radiation-sensitivity in NSCLC cells and RAD50 overexpression enhanced radio-resistant in vitro experiments (Wang et al., 2018). Moreover, RAD50 reduction sensitizes human breast cancer cells to cisplatin treatment (Flores-Perez et al., 2014). Additionally, the disruption of RAD50 promoted radiation sensitivity in human nasopharyngeal carcinoma cells (NPC), and the combination of IR and a recombinant adenovirus (Ad-RAD50) produced substantial regression in human NPC xenografts (Chang et al., 2016).

In conclusion, our clinical and pre-clinical data shows that RAD50 inhibition could be a promising approach for personalization of OC therapy. Modulating the activity of DNA repair pathways with PARP inhibitors might be a promising approach to tailored therapy of EOC. However, further pre-clinical validation is required, particularly with more resistance OC cell lines, CRISPER-cas9 can be used to validate siRNA results, the functional studies can be performed on a second RAD50 siRNA construct and also comet assay or other DNA damage makers could be performed to measure DNA damage. The development of potent compounds to inhibit RAD50 is warranted.

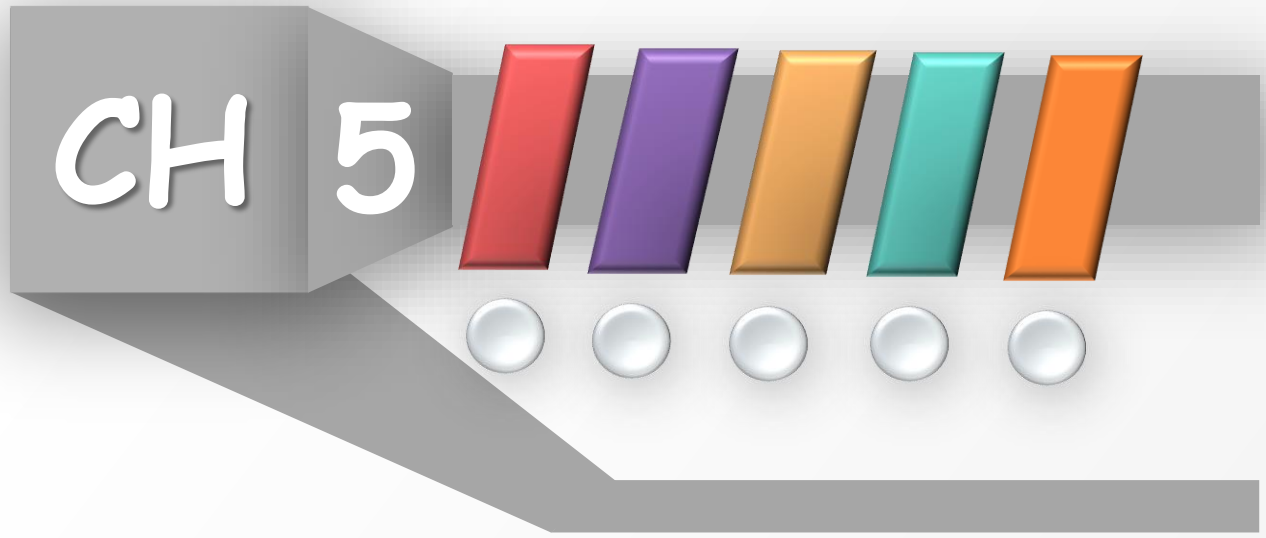

NBS1 BLOCKADE FOR PLATINUM CHEMO-SENSITIZATION IN EPITHELIAL OVARIAN CANCER



5. NBS1 BLOCKADE FOR PLATINUM CHEMO-SENSITIZATION IN EPITHELIAL OVARIAN CANCER

5.1 INTRODUCTION

The human *NBS1* gene is located in chromosome 8q21 and encodes for 80KD protein. *NBS1* null mutations in mice is embryonic lethal (Zhang et al., 2006). The hypomorphic alterations that contribute to reduced NBS1 function which lead to Nijmegen breakage syndrome (NBS). NBS is a rare autosomal recessive disorder related to the predisposition to cancer, microcephaly, growth retardation, immunodeficiency and radio sensitivity (Chrzanowska et al., 2012). NBS1 protein plays a key role in sensing and repairing Double strand breaks (DSBs). NBS1 modulates DNA damage response (DDR) by recruiting ATM, ATR and possibly DNA-PKs to DNA damage sites and activating their functions. NBS1 also recruits RDA50 and MRE11 to the proximity of DSB sites by the interaction with yH2AX via the FHA/BRCT domains and its C-terminal region; consequently, NBS1 plays role in both HR and NHEJ pathways. NBS1 has role in the telomere maintenance and integrity via its ability to generate 3' overhang on the chromosome end that acts as a replication primer for telomerase (Stavridi and Halazonetis, 2005, Difilippantonio et al., 2005, Zhang et al., 2006).

NBS1 is a main player in controlling intra-S-Phase checkpoints through the activation of ATM and CHK2 after ionizing radiation (IR). NBS1 downregulation by siRNA leads to a reduction in CHK2 activation after exposure to IR (Zhang et al., 2005). *NBS1* mutations and polymorphisms are correlated with risk of quite a few types of cancer, including malignant melanoma, non-Hodgkin's lymphoma, lung, breast and ovarian cancer (Lu et al., 2009). Several studies have demonstrated a correlation of homozygous E185Q with lung cancer and acute lymphoblastic leukaemia in China and between homozygous E185Q and breast cancer in the USA (Saito et al., 2013).

Yang et al showed that c-MYC directly regulates NBS1 expression and that NBS1 overexpression increases cell proliferation. It is also reported that elevated NBS1 expression leads to transformation via the activation of PI3K/AKT, suggesting that NBS1 plays a role in cell proliferation and tumorigenesis (Yang et al., 2006a).

Previous studies have demonstrated high nuclear NBS1 expression is associated with increased tumour size and metastases in oral squamous cell carcinoma (OSCC) (Hsu et al., 2010), aggressive head and neck cancer (Yang et al., 2006b), tumour severity and metastases in uveal melanoma (Ehlers and Harbour, 2005) and high

grade tumours and poor overall survival (OS) in colorectal cancer (Situ et al., 2019).

Hypothesis, whether NBS1 expression relates to clinicopathological parameters and influence response to platinum therapying EOC. We also hypothesized that NBS1 could be a novel target for personalization of EOP therapy.

5.2 CHAPTER AIMS

- Evaluate the clinicopathological significance of NBS1 expression by immunohistochemistry (IHC) in 331 human EOC.
- Investigate NBS1 mRNA expression in a publicly available online gene expression dataset of 1259 OC patients to determine the correlation between NBS1 mRNA expression and patients' survivals.
- Profile a panel of OC cell lines to identify NBS1 protein level in OC cell lines.
- Examine NBS1 protein levels in nuclear and cytoplasmic extracts from OC cell lines before and after 24 and 48 hours of cisplatin treatment.
- Investigate whether NBS1 depletion can sensitize OC-resistance cell lines to platinum treatment.
- Preformed functional studies to study the effect of NBS1 depletion in DSBs, cell cycle and apoptosis.

5.3 RESULTS

5.3.1 CLINICAL STUDY

5.3.1.1 NBS1 OVEREXPRESSION ASSOCIATES WITH PLATINUM RESISTANT IN EOC

To assess the association between NBS1 expression and the clinicopathological parameters in EOC, we conducted IHC staining to detect NBS1 expression in 331 human EOC (Figure 5.1). NBS1 nuclear expressions is shown in Figure 5.1a, b and c. Cytoplasmic expression is demonstrated in figure 5.1d and F. The patient demographics and pathological characteristics in EOC is shown chapter two (P.79).

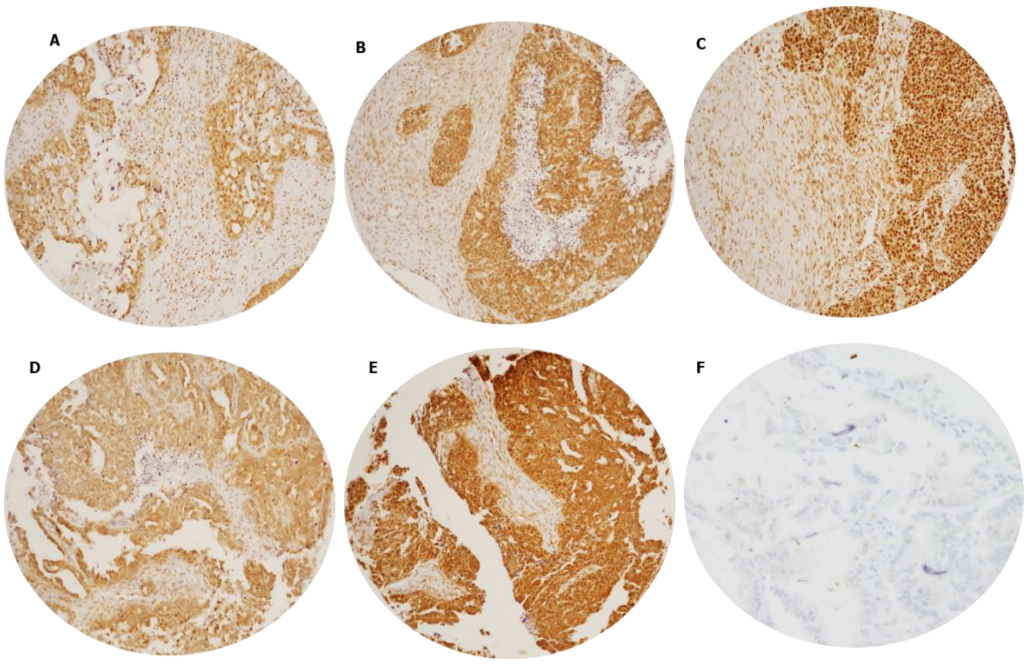

Figure 5.1: Immunohistochemical expression of NBS1 (nuclear and cytoplasmic) in ovarian cancers. A) Week nuclear expression of NBS1. B) Moderate nuclear expression of NBS1. C) Strong nuclear expression of NBS1. D) Week cytoplasmic expression of NBS1. E) Strong cytoplasmic with nuclear expression of NBS1. F) Negative expression which was TMA without adding NBS1 antibody. Magnification 20x.

We then investigated the association between NBS1 expression and clinicopathological features. NBS1 protein expression was evaluable in 225 tumours. Intense nuclear NBS1 was seen in 56/225 (28.5%) tumours and showed significant association with platinum resistance. High cytoplasmic NBS1 expression was linked to serous cystadenocarcinoma (p=0.00004) (Table 5.1). High nuclear NBS1 was associated with shorter PFS (p=0.003) and poor OS (p=0.035) (Figure 5.2). However, High cytoplasmic expression of NBS1 did not influence survival (Figure 5.3).

Table 5.1: The association between NBS1 expression and clinicopathological variables in EOC.

	NBS1_C-	NBS1_C+	P- value	NBS1_N-	NBS1_N+	P- value
Pathological Type			***0.00004***			0.27
Serous adenocarcinoma	58 (42.6%)	78 (57.4%)		92 (67.6%)	44 (32.4%)	
Mucinous adenocarcinoma	24 (88.9%)	3 (11.1%)		23 (85.2%)	4 (14.8%)	
Endometrioid carcinoma	16 (57.1%)	12 (42.9%)		22 (78.6%)	6 (21.4%)	
Clear cell carcinoma	13 (81.3%)	3 (18.8%)		11 (68.8%)	5 (31.3%)	
Mixed	4 (40%)	6 (60%)		8 (80%)	2 (20%)	
FIGO Stage			0.528			0.312
I	49 (57.6%)	36 (42.4%)		64 (75.3%)	21 (24.7%)	
II	15 (42.9%)	20 (57.1%)		21 (60%)	14 (40%)	
III	49 (53.3%)	43 (46.7%)		65 (70.7%)	27 (29.3%)	
IV	4 (57.1%)	3 (42.9%)		8 (80%)	2 (20%)	
Tumour Grade			0.148			0.374
Grade 1	13 (48.1%)	14 (51.9%)		22 (81.5%)	5 (18.5%)	
Grade 2	27 (65.9%)	14 (34.1%)		27 (65.9%)	14 (34.1%)	
Grade 3	61 (48.8%)	64 (51.2%)		89 (71.2%)	36 (28.8%)	
Surgical Optimal Debulking			0.427			0.539
Optimally Debulked	94 (55.6%)	75 (44.4%)		121 (71.6%)	48 (28.4%)	
Not Optimally Debulked	21 (52.5%)	19 (47.5%)		29 (72.5%)	11 (27.5%)	
Residual tumour			0.759			0.525
None/Microscopic	74 (54%)	63 (46%)		102 (74.5%)	35 (25.5%)	
<1cm	17 (63%)	10 (37%)		17 (63%)	10 (37%)	
1-2 cm	6 (46.2%)	7 (53.8%)		8 (61.5%)	5 (38.5%)	
>2cm	16 (53.3%)	14 (46.7%)		22 (73.3%)	8 (26.7%)	
Measurable Disease Before ChemoTherapy			0.543			0.252
Non	77 (55%)	63 (45%)		102 (72.9%)	38 (27.1%)	
Measurable	35 (54.7%)	29 (45.3%)		43 (67.2%)	21 (32.8%)	
Platinum sensitivity			0.676			**0.0001**
Sensitive	97 (55.4%)	78 (44.6%)		131 (74.9%)	44 (25.1%)	
Resistance	8 (50%)	8 (50%)		5 (31.3%)	11 (68.8%)	

* NBS1_C= NBS1 cytoplasmic expression, NBS1_N= RAD50 nuclear expression. + = high expression, -= low expression. $P < 0.05$ was considered significant. We lost some cases in the analysis, as we could not find their records. They have most probably been referred from another trust to be treated in NUH with limited access to their pathological reports. Others are old cases where the pathological report was not written in clear template like the recent ones. Therefore, the grade was written in no clear cut, unlike the more recent ones in which the grade was clearly stated. Therefore, and in order to avoid bias, the grade was stated as unknown. Same rule was applied to the other clinicopathological characteristics.

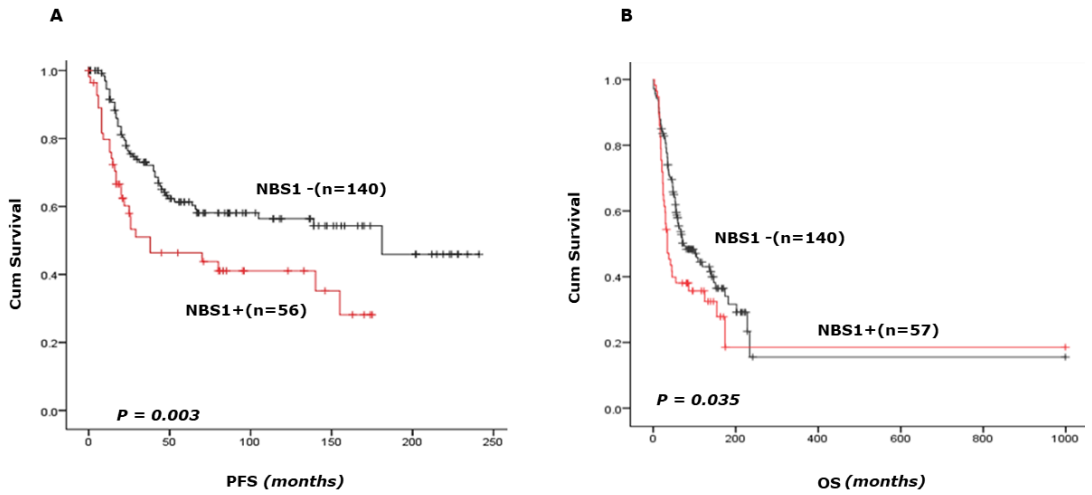

Figure 5.2: Kaplan Meier survival curves for NBS1 nuclear expression. Kaplan Meier statistical analysis was used to conduct a univariate analysis of OS and PFS against NBS1 expression. A) High NBS1 expression (Red lines) was significantly associated with shorter PFS (p=0.003). PFS is the time between treatment initiation and tumour progression again. B) High nuclear NBS1 expression (Red lines) was significantly associated with worse OS (P=0.035). OS is calculated between the day of diagnosis or time of treatment initiation and time where patients still alive. NBS1-= low NBS1 level, NBS1+= high NBS1 level and n= number of cases.

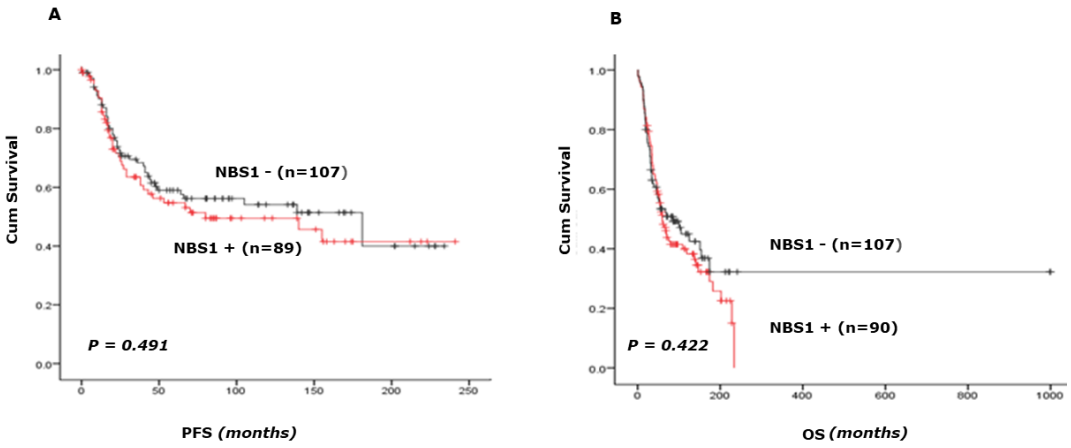

Figure 5.3: Kaplan Meier survival curves for NBS1 cytoplasmic expression. A) High NBS1 cytoplasmic expression (red line) did not influence PFS (p=0.491). B) High NBS1 cytoplasmic expression (Red line) did not influence OS (P=0.422).

For alternative validation, the transcriptomic level of NBS1 in EOC patients who received platinum agents was investigated. High mRNA expression of NBS1 significantly associated with poor PFS (p=0.011) but has no influence on OS (Figure 5.4).

Collectively, the clinical data shows that the protein and transcriptional expression levels of NBS1 have predictive and prognostic significance in human EOC. We then looked at pre-clinical examinations in platinum-sensitive and resistance OC cell lines.

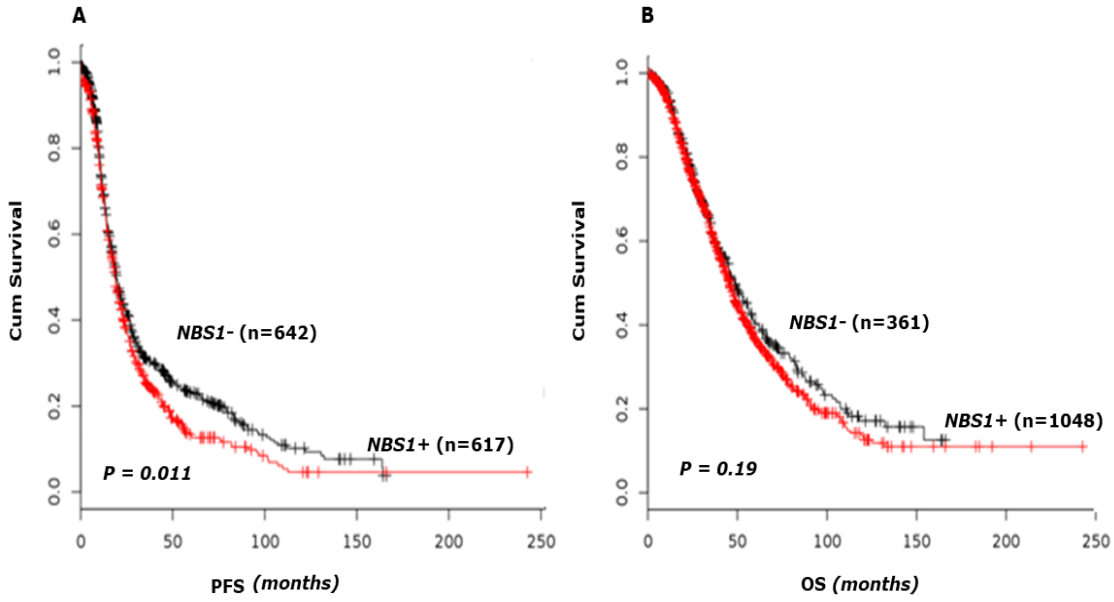

Figure 5.4: The correlation of NBS1 mRNA expression and PFS and OS survivals. A) High NBS1 mRNA expression (Red lines) is significantly associated with poor PFS. B) No significant correlation was associated with OS.

5.3.2 PRE-CLINICAL STUDIES

5.3.2.1 THE DEPLETION OF NBS1 PROMOTES THE CHEMO-SENSITIVITY IN OC CELL LINES

We first tested the baseline level of NBS1 in A2780, A2780cis, PEO1 and PEO4 cell lines. In whole lysate, NBS1 baseline protein level was significantly high in the A2780cis cells compared to the A2780 cells. Similarly, NBS1 baseline protein level was significantly high in the PEO4 cells compared to PEO1 cells (Figure 5.5). Thus, the NBS1 baseline level is high in cisplatin-resistant cells lines A2780cis and PEO4 cells compared to cisplatin-sensitive cell lines A2780 and PEO1 cells.

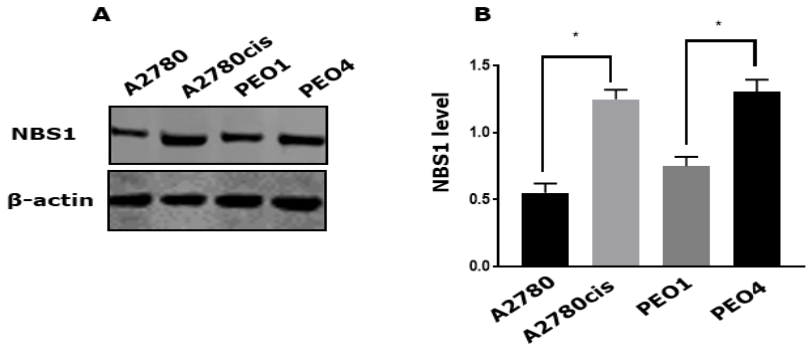

Figure 5.5: Western blot for NBS1 protein levels in A2780, A2780cis, PEO1 and PEO4 cells. A) High NBS1 protein level in cisplatin-resistant A2780cis and PEO4 cells compared to platinum-sensitive A2780 and PEO1 cells. B) The quantification of NBS1 levels in four ovarian cell lines. The detected band intensity for NBS1 as well as β-actin band intensity were quantified in LI-COR software. The readings for NBS1 were normalised to β-actin reading. Microsoft Excel 2010 was used for normalization. The P value was calculated by student's t-test; * $p<0.05$. Data presentation and statistical analysis were performed using GraphPad Prism, version 7.

To examine the alteration in sub-cellular localization of NBS1, we took nuclear and cytoplasmic extracts from A2780, A2780cis, PEO1 and PEO4 cell lines before and after 5 μM cisplatin treatment. Although after 24 hours of cisplatin treatment, there was no significant differences, at 48 hours, significantly increased NBS1 nuclear sub-cellular localisation in A2780cis and PEO4 cells were evident compared to A2780 and PEO1 cells. No significant changes were observed for NBS1 cytoplasmic expression (Figure 5.6-5.7). The data suggests that NBS1 nuclear accumulation could promote

repair of platinum induced DNA damage and lead to resistance in A2780cis and PEO4 cells.

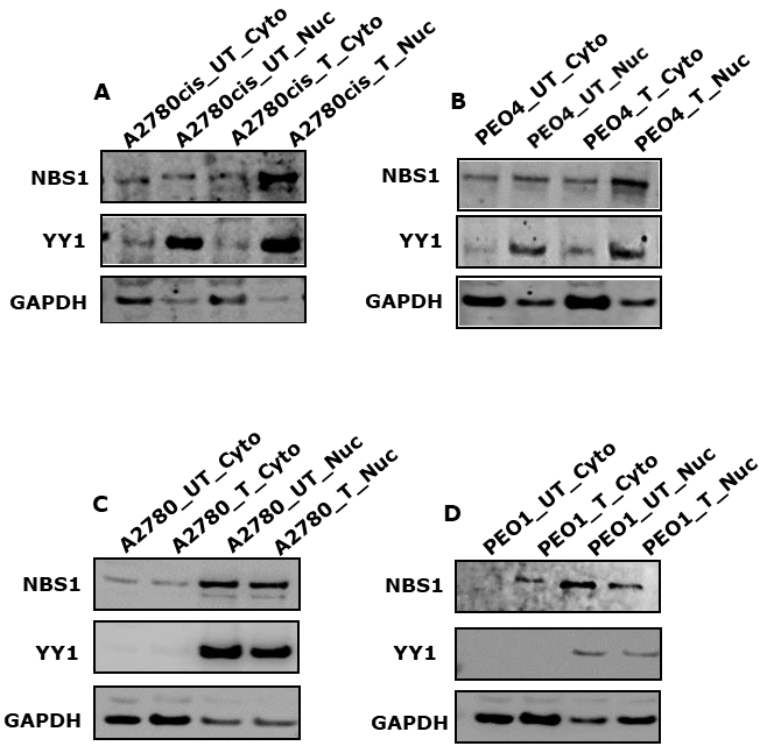

Figure 5.6: Representative western blot of nuclear and cytoplasmic levels of NBS1. For nuclear and cytoplasmic extraction protocol see chapter two (P.107-108). NBS1 nuclear expressions were normalised to YY1 levels. NBS1 cytoplasmic expressions were normalised to GADPH levels. Microsoft Excel 2010 was used for normalization. A) NBS1 nuclear expression in A2780cis cells was significantly increased after 5 μM cisplatin therapy for 48 hours, while no difference was observed in NBS1 cytoplasmic expression before and after cisplatin treatment. B) NBS1 nuclear expression in PEO4 cells was significantly increased after 5 μM cisplatin treatment for 48 hours, while no significant difference was seen in NBS1 cytoplasmic expression. C) NBS1 nuclear and cytoplasmic expression in A2780 cells did not change after 48 hour of cisplatin therapy. D) Cisplatin treatment for 48 hours did not change NBS1 nuclear and cytoplasmic levels in PEO1 cells (Mesquita et al., 2019).

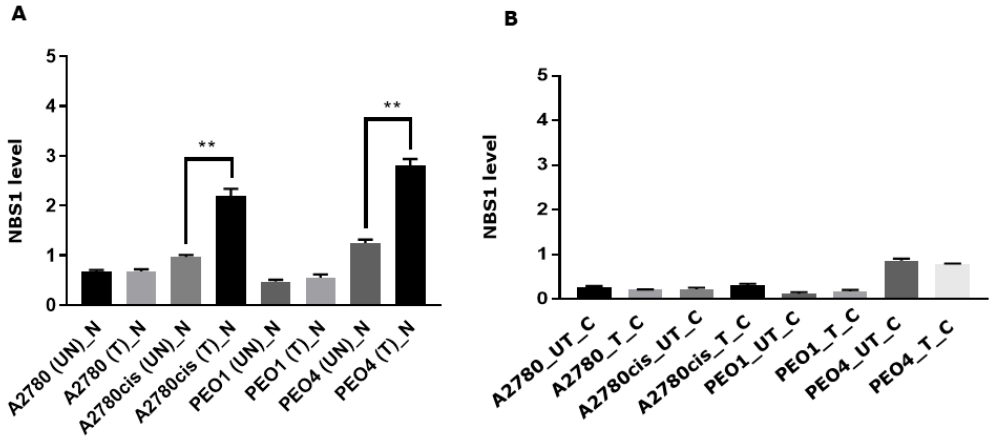

Figure 5.7: The quantification of NBS1 nuclear and cytoplasmic expression levels. A) NBS1 nuclear levels A2780, A2780cis, PEO1 and PEO4. NBS1 expression level in untreated A2780cis and PEO4 cells was high compared with untreated A2780 and PEO1. NBS1 nuclear expression level was significantly increased after cisplatin treatment in A2780cis and PEO4 cells compared the same cells before treatment. B) NBS1 cytoplasmic levels in A2780, A2780cis, PEO1 and PEO4. The P value was calculated by student's t-test, ** p>0.01. Data presentation and statistical analysis were performed using GraphPad Prism, version 7.

We then studied NBS1 depletion in A2780cis and PEO4 cells for platinum sensitivity. Downregulation of genes that are upregulated in resistance cell lines using siRNA is a useful approach to study resistance mechanism (Ganesh et al., 2013). We generated transient knockdown (KD) of NBS1 by siRNA in A2780cis cell line. NBS1 was successfully knocked down by day three and persistent on day five in A2780cis cells (Figure 5.8).

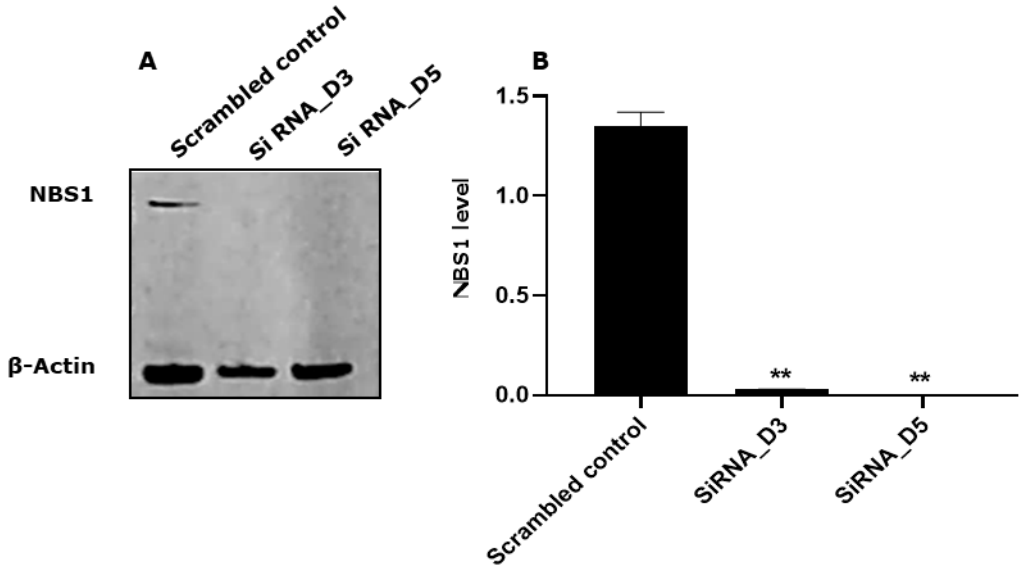

Figure 5.8: NBS1 knock down in A2780cis cells using siRNA. Cells were seeded at 60-70% confluency in T25 flasks overnight. Cells were transfected with mNBS1 siRNA oligonucleotide or scrambled siRNA oligonucleotide control in Opti-MEM media. Transfection process was preformed using lipofectamine 3000 regent (Mesquita et al., 2019). See chapter two (P.97) for more details. Transfection efficiency was confirmed using western blot. A) Representative western blot which shows NBS1 protein level in A2780cis control and silenced cells. MRE11 was successfully knocked down in day 3 and day 5 in A2780cis cells. B) The quantification analysis of NBS1 depletion in A2780cis scrambled control and silenced cells. The P value was calculated by student's t-test, ** $p<0.01$. D3=day 3, D5=day 5. Data presentation and statistical analysis were performed using GraphPad Prism, version 7.

In clonogenic assays, NBS1_KD_A2780cis cells were significantly sensitive to cisplatin treatment than were the control cells (Figure 5.9). We then conducted functional studies using fluorescence-activated cell sorting (FACS) to investigate the impact of NBS1 KD scrambled control cells. After 24 hours of 5 μM cisplatin treatment, NBS1 depleted cells showed a significant accumulation of γH2AX, which is a surrogate marker of DSB accumulation in nucleus (Figure 5.10). Accumulation of DSBs induce cell cycle checkpoint activation leading on cell cycle arrest to allow time for cells to repair DNA damage. If the damages were unrepairable, cells undergo apoptosis. Therefore, we investigated the effect of NBS1 KD on cell cycle and apoptosis after 24 hours of 5 μM cisplatin treatment in NBS1-deficient and proficient cells. S-phase cell cycle arrest and increased apoptotic cells population was evident in NBS1_KD cells compared with scrambled controls (Figure 5.10).

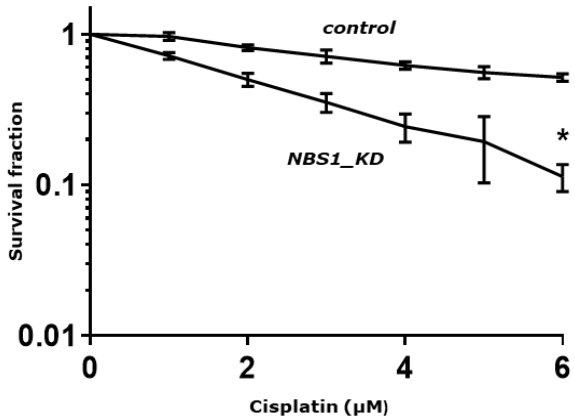

Figure 5.9: Clonogenic assay showing cisplatin sensitivity in A2780cis and NBS1_KD_A2780cis cells. Cells transfected as described in figure 5.8. Control cells and transfected cells (NBS1_KD) were seeded in six-well plates and left in the incubator overnight. The following day, increased doses of cisplatin were added. Cells were then left in the incubator for two weeks (Ali et al., 2019a). Microsoft Excel 2010 was used to determine plating efficiency and survival fraction, see chapter two page (100-101) for more details. NBS1 depletion increased cisplatin sensitivity in A2780cis cells. The P value was calculated by student's t-test, * $p<0.050$.

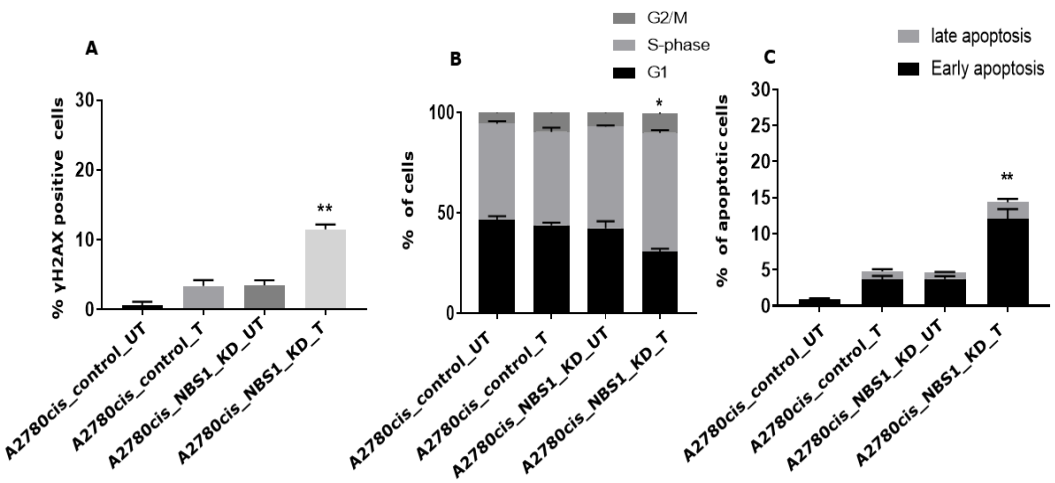

Figure 5.10: Functional studies of A2780cis cells using flow cytometry. Cells transfected as described in figure 5.8. On day two, A2780cis siRNA control and transfected NBS1 siRNA cells were trypsinized and re-plated in six-well plates. The following day, 5 μM of cisplatin was added for 24 hours. Cells were then collected (Ali et al., 2018); Protocols are described in chapter 2 (P.102-106). A) The percentage of γH2Ax positive cells, statistical analysis determined by one-way ANOVA. A2780cis_NBS1_KD treated cells revealed significant accumulation of yH2AX positive cells. B) Cell cycle analysis in UT and treated cells, from two way-ANOVA. A2780cis_NBS1_KD treated cells showed S-phase cell cycle arrest. C) Annexin V analysis in UT and treated cells, from two way-ANOVA. A2780cis_NBS1_KD treated cells demonstrated significant increased apoptotic cells. Weasel Software Version 3.0.2 (The Walter and Eliza Hall Institute of Medical Research, Australia) was used for all flow cytometry analyses. * $p<0.050$ and ** $P < 0.01$. UT= untreated cells, T= treated cells, T= treated cells. Data presentation and statistical analysis were performed using GraphPad Prism, version 7.

We next generated transient (KD) of NBS1 using siRNA in another platinum-resistant PEO4 cells (Figure 5.11). NBS1 was successfully knocked down by day three and persistent on day five in PEO4 cells. In clonogenic assays, NBS1_KD_PEO4 cells were significantly more

sensitive to cisplatin treatment than were the scrambled controls (Figure 5.12).

We then preformed functional studies in NBS1_KD_PEO4 cells and PEO4 scrambled control cells. DSB accumulation, S-phase cell cycle arrest and apoptosis was evident in NBS1_KD cells compared to scrambled controls (Figure 5.13).

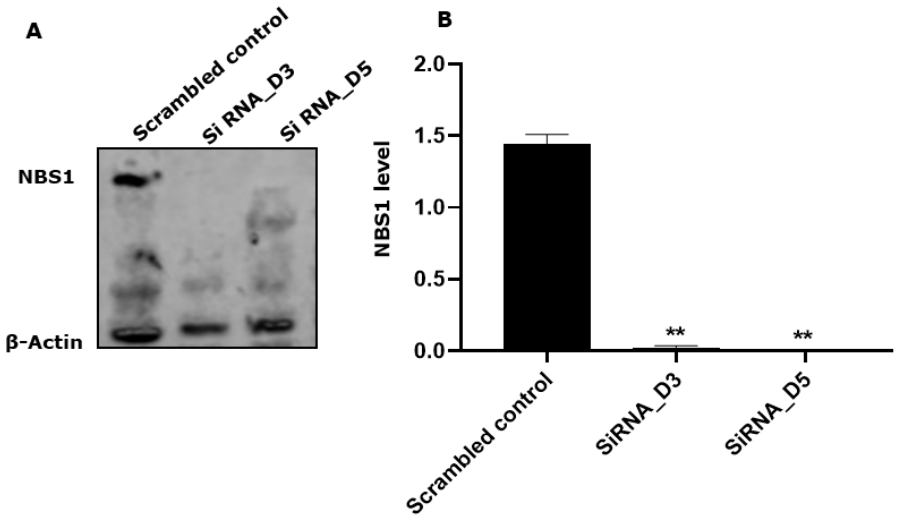

Figure 5.11: NBS1 knock down in PEO4 cells using siRNA. A) Representative western blot which shows NBS1 protein level in PEO4 scrambled control and silenced cells. NBS1 was successfully knocked down in day 3 and day 5 in PEO4 cells. B) The quantification analysis of NBS1 reduction in PEO4 scrambled control and silenced cells. P value was calculated by student's t-test, * $p<0.050$ and ** $p<0.01$. D3=day 3, D5=day 5. Data presentation and statistical analysis were performed using GraphPad Prism, version 7.

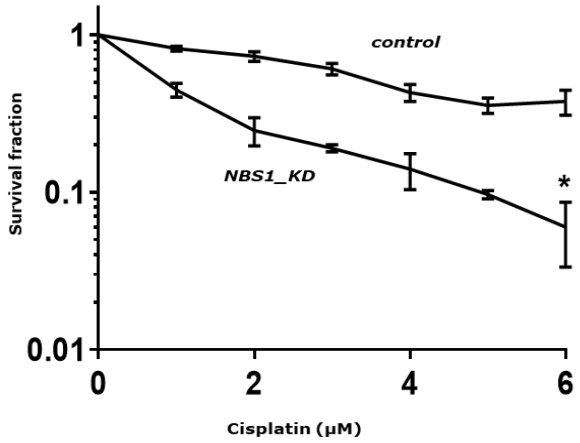

Figure 5.12: Clonogenic assay showing cisplatin sensitivity in PEO4 and NBS1_KD_PEO4 cells. Cells transfected as described in figure 5.8. Control cells and transfected cells (NBS1_KD) were seeded in six-well plates and left in incubator overnight. The following day, increased doses of cisplatin were added. Cells were then left in the incubator for two weeks (Ali et al., 2019a). NBS1 depletion increased toxicity of PEO4 cells to cisplatin. The P value was calculated by student's t-test, * $p<0.050$. Data presentation and statistical analysis were performed using GraphPad Prism, version 7.

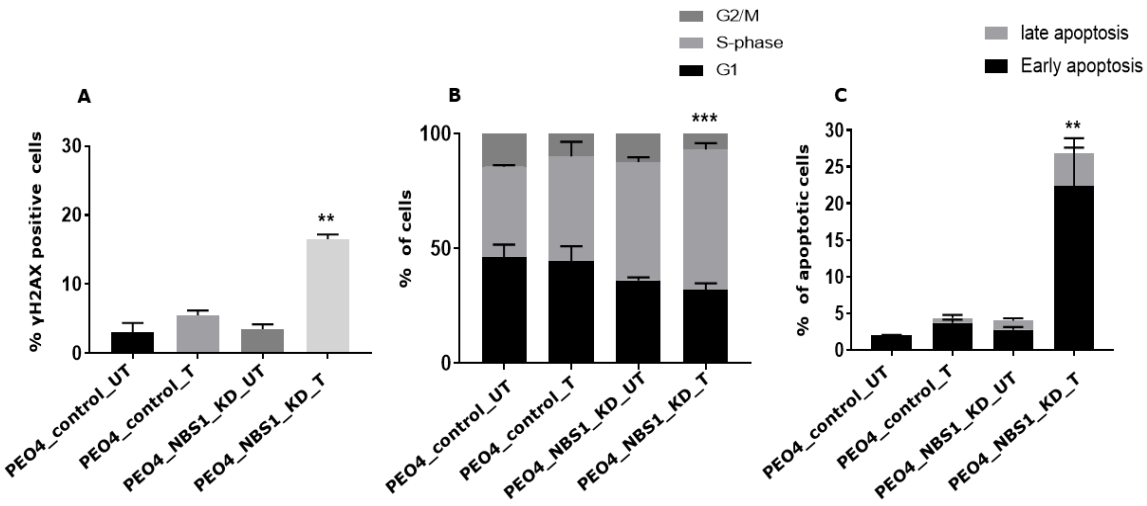

Figure 5.13: Functional studies of PEO4 cells using flow cytometry. A) The percentage of γH2Ax positive cells in UT and treated cells. PEO4_NBS1_KD treated cells revealed significant accumulation of γH2AX positive cells. B) Cell cycle analysis in UT and treated cells. PEO4_NBS1_KD treated cells showed S-phase cell cycle arrest. C) Annexin V analysis of UT and treated cells. PEO4_NBS1_KD treated cells demonstrated significant increased apoptotic cells. The P-value was calculated by one way-ANOVA or two way-ANOVA, **P < 0.01 and ***p<0.001. Data presentation and statistical analysis were performed using GraphPad Prism, version 7.

The results were validated using another siRNA construct for NBS1 (Figure 5.14). Cisplatin sensitization was evident in NBS1_KD_A2780cis cells compared to that in scrambled control cells (Figure 5.15).

Taken together, the clinical and pre-clinical results provide evidence that NBS1 is a biomarker of platinum sensitivity in EOC.

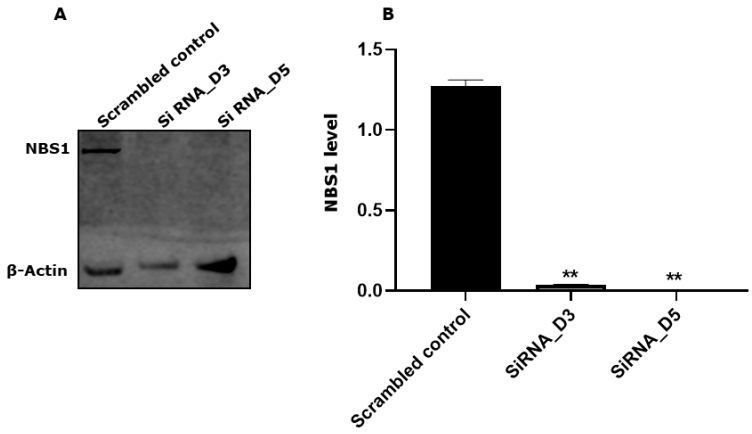

Figure 5.14: NBS1 knock down in A2780cis cells using a second siRNA construct. A) Representative western blot which revels NBS1 protein level in A2780cis control cells and silenced cells. NBS1 was successfully knocked down in day 3 and day 5 in A2780cis cells. B) The quantification analysis of NBS1 reduction in A2780cis scrambled control and silenced cells. The P value was calculated by student's t-test, ** $p<0.01$. D3=day 3, D5=day 5. Data presentation and statistical analysis were performed using GraphPad Prism, version 7.

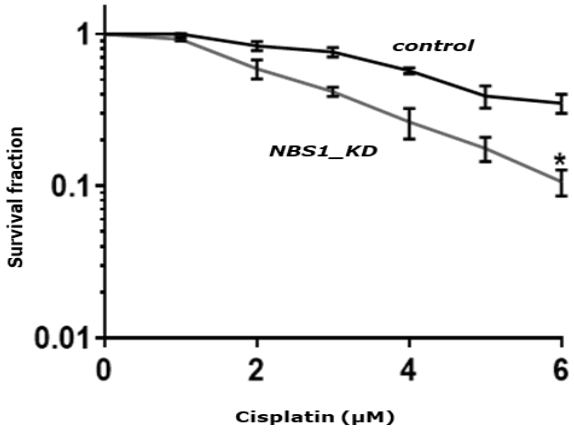

Figure 5.15: Clonogenic assay showing cisplatin sensitivity in A2780cis and NBS1_KD_A2780cis cells. We used a second siRNA construct to validate our previous results. See chapter two (P.97) for transfection methods. Scrambled control cells and transfected cells (NBS1_KD) were seeded in six-well plates overnight. The following day, increased dose of cisplatin was added. Cells were then left in the incubator for two weeks (Ali et al., 2019a). NBS1 depletion increased cisplatin sensitivity in A2780cis cells. The P value was calculated by student's t-test, * $p<0.050$.

5.4 RESULTS SUMMARY

- Clinical data showed that high cytoplasmic NBS1 protein level was linked with serous cystadenocarcinoma (p=0.00004). High nuclear NBS1 protein levels were significantly associated with poor PFS (p=0.003) and poor OS (p=0.035). The cytoplasmic expression of NBS1 did not influence survival.
- Clinical data revealed that high NBS1 mRNA expressions levels were significantly associated with PFS (p=0.011) but has no influence on OS.
- Preclinical studies demonstrated that NBS1 depletion sensitized A2780cis and PEO4 cells to platinum therapy. Increases sensitivity was correlated with DSB accumulation, S-phase cell cycle arrest and apoptosis when compared with scrambled controls.

5.5 DISCUSSION

Platinum drugs (cisplatin and carboplatin) are affective agents commonly used as a first-line treatment for different malignancies (head and neck, lung, colon and ovarian). However, acquired resistance of these agents remains challenging despite the high response rate after surgery and platinum treatment (Raja et al., 2012).

Resistance to platinum agents has been linked to several mechanisms mentioned in chapter 1. Considering that the target of these agents is DNA, the sensitivity and resistance to platinum drugs is affected/ modulated by the capability of cells to recognize and repair the DNA damaged induced by these agents. In particular, there is a strong preclinical evidence indicating how the presence or the absence of a particular DNA repair mechanism (because of mutations, knockdown or knockout, epigenetic changes of genes involved in DNA repair) is correlated with sensitivity/ resistance to platinating agents (Deans and West, 2011, Darzynkiewicz et al., 2009, Dai et al., 2015). NBS1 is a critical DNA repair gene that plays an important role in sensing and repairing DSBs and participates in telomere maintenance and integrity (Stavridi and Halazonetis, 2005, Difilippantonio et al., 2005, Zhang et al., 2006). Therefore, NBS1

targeting might disturb DBSs repair and may contribute to sensitizing resistance OC cells to platinum agents.

In this work, we provided comprehensive clinical and preclinical evidence that NBS1 could be a predictor of platinum resistance and could also be a promising drug target for chemo-sensitization. We clinically demonstrated that high nuclear NBS1 is not statistically significant in terms of clinicopathological characteristics, but it was significantly associated with poor survivals outcomes in EOC patients an evident by poor PFS. That may be due to the sample size, which was small to show significance in terms of clinicopathological parameters. Alternatively, it might be that NBS1 has role as a late event in increasing invasiveness and metastasis in EOC. Previous study showed that high NBS1 is linked to aggressive clinicopathological characteristics and poor prognosis for the recurrence of EOC (Lee et al., 2015). A recent study has demonstrated that low NBS1 expression was observed in low-grade EOC (Brandt et al., 2017). NBS1 overexpression was observed in a significant proportion (45%) of advanced head and neck squamous cell carcinoma (HNSCC) patients and correlated with a worse prognosis. Increased NBS1 expression enhanced the transformation activity of HNSCC cells via the activation of PI3K/AKT pathway (Yang et al., 2006a). The activation of PI3K/AKT pathway increases

tumorigenesis, tumour metastasis, and chemotherapeutic resistance (West et al., 2002).

Interestingly, NBS1 overexpression was correlated with metastasis of HNSCC patients. The Induction of Epithelial-mesenchymal transition (EMT) was seen in NBS1 overexpression HNSCC cell line (FADUNBS), while NBS1 siRNA reversed the shift of EMT markers. Increased invasiveness/migration of FADUNBS was reported *in vitro* and *in vivo* assay. High NBS1 upregulated the Snail (an EMT regulator) and its downstream target MMP-2 (Yang et al., 2007). High NBS1 in both the protein and mRNA levels were associated with tumour severity and metastatic death in uveal melanomas. However, similar NBS1 expression in class 1 (good prognosis) normal and tumour uveal melanocytes suggests NBS1 overexpression might be a late event in the progression of melanoma (Ehlers and Harbour, 2005). Hsu et al found that strong NBS1 expression was significantly associated with a poor overall survivals in oral squamous cell carcinoma (OSCC) patients (Hsu et al., 2010). In addition, overexpression of NBS1 is a poor prognostic factor in prostate cancer and acute myeloid leukaemia (Grupp et al., 2014, Kefala et al., 2013). In gastric cancer (GC) high NBS1 was independent predictor of recurrence after surgery (Altan et al., 2016).

Our pre-clinical data showed that basal levels of NBS1 was high in A2780cis and PEO4 cells compared to A2780 and PEO1 cells. Overexpression of NBS1 in resistance cell lines could increase DNA repair capacity and promote resistance to platinum therapy. We also revealed that NBS1 depletion caused a significant platinum sensitization A2780cis and PEO4 cells, and was associated with increased DSB accumulation, S-phase arrest and increased apoptotic cells. However, the protein level of MRE11 (chapter 3), RAD50 (chapter 4) and NBS1 in resistance cell lines (A2780cis and PEO4) may not necessarily reflect proteins activity in these cell lines. The functional assessment of MRE11 or RAD50 or NBS1 deficient cells can be confirmed using homologous recombination deficient (HRD) assays such as DR-GFP and RAD51 focus formation assay (Nakanishi et al., 2011, Mukhopadhyay et al., 2010).

A Previous study designed an adenoviral vector containing mutant cDNA for C-terminal 300 amino acids of NBS1, thus maintaining the hMRE11 interaction domain. The resulting mutant NBS1 (Ad-NBS1) significantly sensitized cisplatin, increased DSBs and inhibited tumour cell growth in HNSCC cell lines (Tran et al., 2004).

Another study using the same adenoviral vector (Ad-NBS1) showed that Ad-NBS1 effectively suppressed the function of MRN complex in infected HNSCC cells and increased cisplatin chemosensitization *in vitro* and in a mouse model with human HNSCC (Araki et al., 2010). This could be due to the molecular disruption of MRN complex via the mutant NBS1 expression and loss of c-terminal that contains multiple phosphorylation sites by ATR and ATM kinases and the forkhead-associated and BRCA1 c-terminus domains.

These lost regions of NBS1 provide the functions of H2AX phosphorylation, ATM activation, MRN complex recruitment to DSBs sites, cell cycle arrest and initiation of DSB repair (Kobayashi et al., 2004, Czornak et al., 2008).

Fibroblasts NBS1-deficient cells showed profound sensitivity to PARP inhibition compared to Fibroblasts NBS1-proficinet cells (McCabe et al., 2006). In addition, deficiency in NBS1 sensitized breast cancer cells to PARP1 inhibitor (Oplustilova et al., 2012).

In conclusion, the present study reveals high expression levels of NBS1 to be related to a worse response towards platinum-based chemotherapy in advanced EOC. Furthermore, our *in-vitro* data shows that NBS1 targeting in EOC increased sensitization to platinum-based chemotherapy, which could be a promising approach

for personalization of EOC therapy. However, there are some limitations in current work, for example, only two resistance ovarian cancer cell lines were used (A2780cis and PEO4 cells), the functional studies were not repeated on the second NBS1 siRNA construct, CRISPER-cas9 can be used to validate siRNA results and Comet assay or other DNA damage makers could be performed to measure DNA damage. The development of potent compounds to inhibit NBS1 is justified.

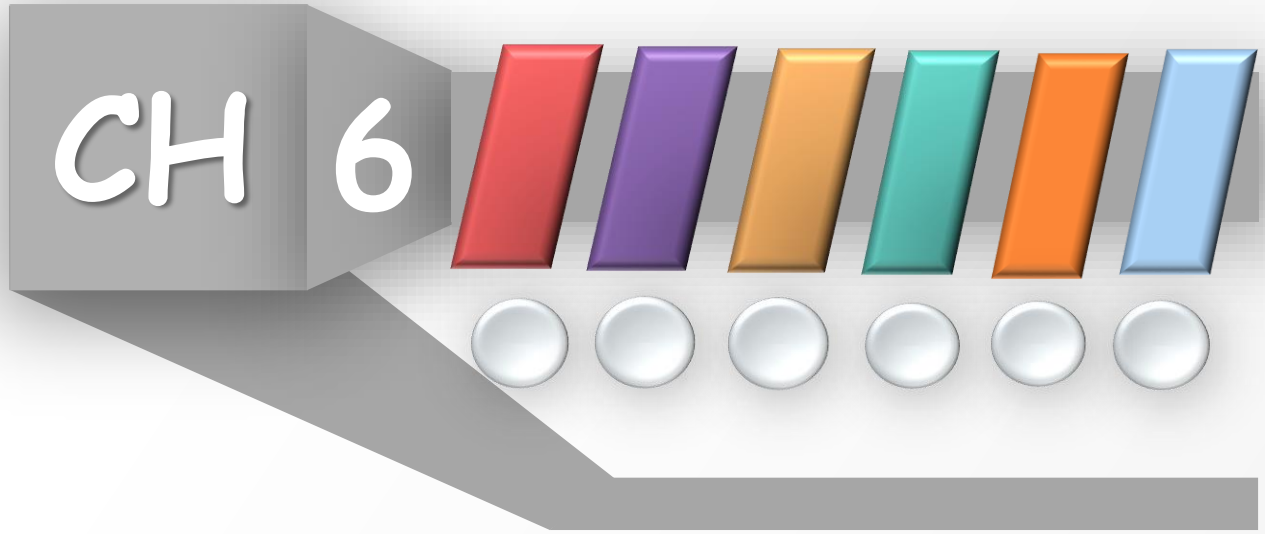

EXPANDING THE SYNTHETIC LETHAL STRATEGY BEYOND PARP INHIBITORS



6. EXPANDING THE SYNTHETIC LETHAL STRATEGY BEYOND PARP INHIBITORS

6.1 INTRODUCTION

6.2 SYNTHETIC LETHALITY

Platinum agents have been used as a first line therapy to treat ovarian cancer (OC) patients for many years. However, the overall survival (OS) for patients with advances OC remains poor. The cytotoxicity of platinum drugs (cisplatin, carboplatin) directly create intra-strand and inter-strand DNA adducts, which contribute to double strand breaks (DSBs) during replication (Lord and Ashworth, 2017, van Zyl et al., 2018). Platinum-DNA adducts can be detected and processed via the DNA repair pathways. Development of personalized therapy approach targeting DNA repair mechanisms is an exciting new strategy in OC (Gavande et al., 2016).

Synthetic lethality (SL) is where the effects of two non-lethal genetic alterations can contribute to lethality together. This lethality might be from genes involved in the same or other related pathways, suggesting that a deficiency in both genes significantly disturbs their signalling and function (Hosoya and Miyagawa, 2014). The possibility to particularly target cancer cells via inhibition of a gene known to

be in a synthetic lethal association with a mutated tumour suppressor gene has been proposed.

Poly-(ADP)-ribose polymerase 1 (PARP1) is an enzyme that plays a critical role in DNA repair. BRCA1 and BRCA2 proteins are critically involved in DSBs via homologous recombination (HR). Women carrying harmful germline alterations in the *BRCA1/2* genes have a high risk of developing OC (Walsh, 2015). The SL approach using PARP inhibitors (PARPi) in BRCA deficient OC patients was revealed to considerably improve progression-free survival (Lord and Ashworth, 2017, Walsh, 2015). However, 40 – 70% of BRCA1/2-mutated OCs have shown a resistance to PARPi treatment (Jiang et al., 2019). To overcome this resistance, the development of alternative SL targets is urgently required in OC therapy. MRE11 is critically involved in HR, non-homologous and joining (NHEJ) and telomere maintenance (Lamarche et al., 2010a). Mirin is a small molecule that inhibits MRE11 exonuclease activity. Mirin was shown to sensitise resistance OC cell lines and increased DSBs, S-phase arrest and apoptosis in these cells (see chapter 3). The first question in this chapter is whether mirin would be synthetically lethal in BRCA2 deficient cells.

The X-ray repair cross-complementing gene 1 (XRCC1) protein is importantly involved in BER and single stand break repair (SSBR)

pathways. XRCC1 has no identified enzymatic activity, but it acts as a scaffold protein interacted with several proteins involved in BER and SSBR such as PARP1 and Ligase III (LIG III). XRCC1 plays role in repairing DSBs through an alternative non-homologous end joining (alt-NHEJ) mechanism. Two recent studies showed that there was significant correlation between two XRCC1 polymorphisms XRCC1 (Arg399Gln and XRCC1 Arg194Trp) and clinical outcomes in OC patients. XRCC1 deficiency in OC cells potentially increased the sensitivity to platinum agents (Ali et al., 2019a, Abdel-Fatah et al., 2013, Sultana et al., 2013b, London, 2015). The second question in this chapter is whether mirin would be synthetically lethal in XRCC1 deficient cells.

6.3 MIRIN RESISTANT IN PEO1 CELLS

Almost half of OC patients have mutations in HR pathway namely *BRCA1/2* alterations. PARPi are highly effective targeted therapy in HR-deficient OC patients. Unfortunately, PARPi resistance have recently shown to be a major issue in the clinic (Bitler et al., 2017, Noordermeer and van Attikum, 2019).

Studies about PARPi resistance in BRCA-deficient cells are expending rapidly, showing several mechanisms leading to resistance including restoration of stalled replication fork protection and, most widely,

restoration of HR pathway [reactivation of BRCA1/2, loss of 53BP1 and down-regulation of PARP] (Kim et al., 2017b, Noordermeer and van Attikum, 2019). Generation of mirin resistant BRCA-deficient OC cells to investigate mechanism of resistance are needed and could pave the road for new treatment options to overcome resistance.

The establishment of chemoresistant cancer cells could be a powerful system to investigate the molecular mechanism contributing to chemotherapeutic resistance. PEO1 cells poses a *BRCA2* mutation [5193C>G (Y1655X)] and are hypersensitive to cisplatin and olaparib. A secondary BRCA2 mutation that restores BRCA2 function is the main reason for the acquired resistance to cisplatin and PARPi (Sakai et al., 2009, Barber et al., 2013, Edwards et al., 2008, Norquist et al., 2011, Swisher et al., 2008). We exposed PEO1 cells to stepwise increasing concentrations of mirin over a period of 210 days to establish a mirin-resistant cell line, PEO1R (see Chapter 2 page 108).

6.4 CHAPTER AIMS

In chapter 3, 4 and 5, we demonstrated that MRN complex was a predictor of platinum agent sensitivity and that MRE11 blockade increased the sensitization to platinum in resistance OC cell lines. Therefore, the aims of this chapter were 1) to study if MRE11 inhibition by mirin could induce synthetic lethality in BRCA2-deficient and XRCC1-deficient ovarian cancers, 2) to investigate the role of DNA repair mechanisms in PEO1R cells and 3) to study whether similar or different mechanisms are involved in cisplatin and PARPi resistance can be found in PEO1R cells. Particularly, the experimental goals were as follow:

- Study whether MRE11 blockade could be synthetically lethal in BRCA2-deficient OC cells in 2D and 3D models systems.
- Investigate whether MRE11 inhibition could be synthetically lethal in XRCC1-deficient OC cells in 2D and 3D models systems.
- Treat PEO1 cells with stepwise increasing concentration of mirin over a period of 210 days to determine if PEO1R cells can be established.
- Evaluate the possible mechanism of resistance in PEO1R cells.
- Investigate the role of MRE11 in invasion, epithelial to mesenchymal transition (EMT) and stem-cell like phenotype.

- Identify any possible molecular target in PEO1R for future consideration.

6.5 RESULTS

6.5.1 MIRIN IS SYNTHETICALLY LETHAL IN BRCA2-DEFECIENT CANCER CELLS

BRCA2 has a key role in repairing DSBs through HR. BRCA2 binds to RAD51 via BRC repeats, mobilises it to the DNA damage and then aids the RAD51 nucleoprotein filaments, which in turns help in searching for homologous sequence to use it as a template (Gudmundsdottir and Ashworth, 2006). The BRCA2 C-terminus involved in RAD50 filaments stabilization. This stabilization is vital to protect stalled replication fork. MRE11, besides its crucial role in HR, is needed during restart of stalled replication forks and the activation of checkpoints. MRE11 nuclease activity can prevent replication collapse during replication stress (Schlacher et al., 2011b, Ying et al., 2012). In BRCA2-deficient cells that accumulate replication fork intermediates, inhibition of MRE11 nuclease activity will lead to accumulation of toxic intermediates that eventually become DSBs contributing to apoptosis.

We investigated whether the treatment of mirin, an MRE11 inhibitor, is synthetically lethal in BRCA2-deficient OC cells. We started by checking BRCA2 protein level in PEO1 and PEO4 cells (Figure 6.1). We then preformed clonogenic assays to determine the sensitivity of

the cells to mirin treatment. We found that BRCA2-deficent PEO1 cells were significantly sensitive to mirin compared to PEO4 Cells (Figure 6.1). All figures and statistical analyses in this chapter were performed by GraphPad Prism, version 7, unless otherwise stated. All results in this chapter are expressed as means ± standard deviation (S.D.) of three independent experiments, unless otherwise stated.

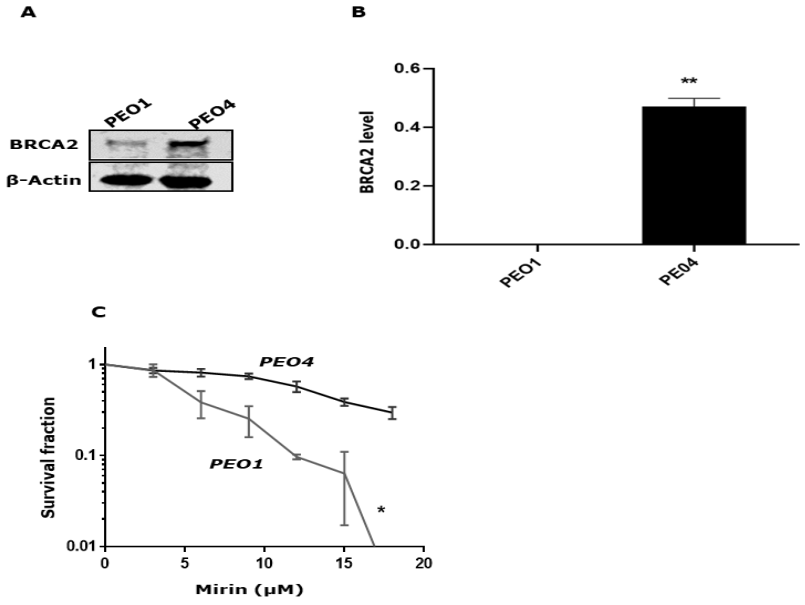

Figure 6.1: Effects of mirin on PEO1 and PEO4 cells. A) Representative western blot showing BRCA2 level in PEO1 and PEO4 cells. PEO1 is a BRCA2-deficent cell line while PEO4 is a BRCA2-proficient cell line. B) Quantification of BRCA2 levels in PEO1 and PEO4 cells. C) Clonogenic assay showing mirin sensitivity in PEO1 and PEO4 cells. Cells were trypsinised and plated into six-well plates overnight. On the following day, cells were treated with various doses of mirin. Cells were then incubated for 14 days (Ali et al., 2019a). PEO1 cells were significantly sensitive to mirin compared to PEO4 cells. The P value was calculated by student's t-test, * $p<0.050$. Data presentation and statistical analysis were performed using GraphPad Prism, version 7.

To test whether mirin could induce DSBs in PEO1 (BRCA2-deficient cells), we conducted a fluorescence-activated cell sorting (FACS) analysis to monitor the accumulation of γH2AX which is a surrogate marker of DSB accumulation in nuclei. Mirin treatment significantly increased the accumulation of DSBs in PEO1 cells (Figure 6.2).

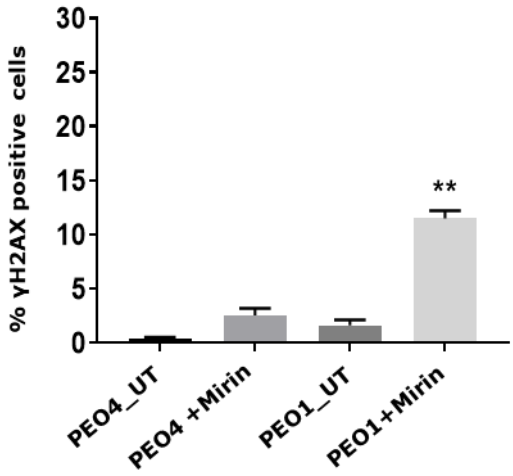

Figure 6.2: The percentage of γH2Ax positive cells in mirin-treated PEO1 and PEO4 cells using FACS. 18μM of Mirin for 24 hours significantly increased the accumulation of γH2Ax in PEO1 cells compared to PE04 cells. ** $p<0.01$ as determined by one-way ANOVA. Weasel Software Version 3.0.2 (The Walter and Eliza Hall Institute of Medical Research, Australia) was used for all FACS analyses. Data presentation and statistical analysis were performed using GraphPad Prism, version 7. UT= untreated cells.

To further validate the accumulation of DSB, we checked the accumulation of 53BP1 foci and γH2AX foci by immunofluorescence (IF) staining. 53BP1 is a nuclear protein that is crucially involved in signalling and repairing DSBs in mammalian cells. 53BP1 is main regulator for DSB repair choice (Panier and Boulton, 2014). IF staining showed that mirin treatment significantly increased 53BP1 and γH2AX foci accumulation in PEO1 cells compared to those in PE04 cells (Figure 6.3).

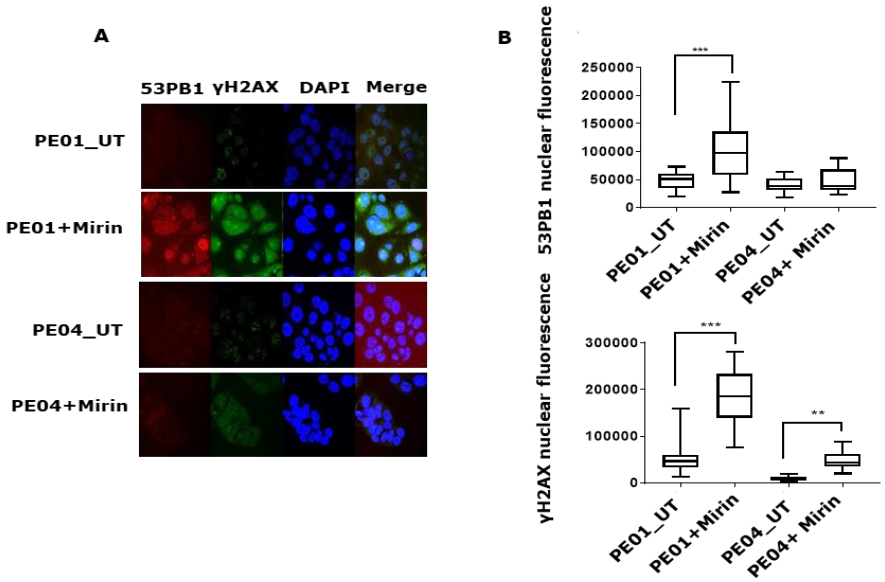

Figure 6.3: Immunofluorescence staining for 53BP1 and γH2AX in PEO1 and PEO4 cells untreated (UT) and treated with mirin (18μMol/L) for 24 hours. Protocol is described in chapter 2 (P.108-109). A) Immunofluorescent images of mirin-treated and UT cells. Mirin treatment significantly increased γH2Ax foci and 53BP1 foci in PEO1 cells compared to PE04 cells. The analysis of images was performed by ImageJ software. B) Quantification of γH2Ax and 53BP1 nuclear fluorescence. ** $p<0.01$, *** $p<0.001$, determined by student's t-test. Data presentation and statistical analysis were performed using GraphPad Prism, version 7. UT= untreated cells.

We then conducted FACS to monitor the effects of mirin therapy on cell cycle and apoptosis in PEO1 and PEO4 cells. Mirin treatment correlated with G2/M cell cycle arrest and increased apoptosis (Figure 6.4)

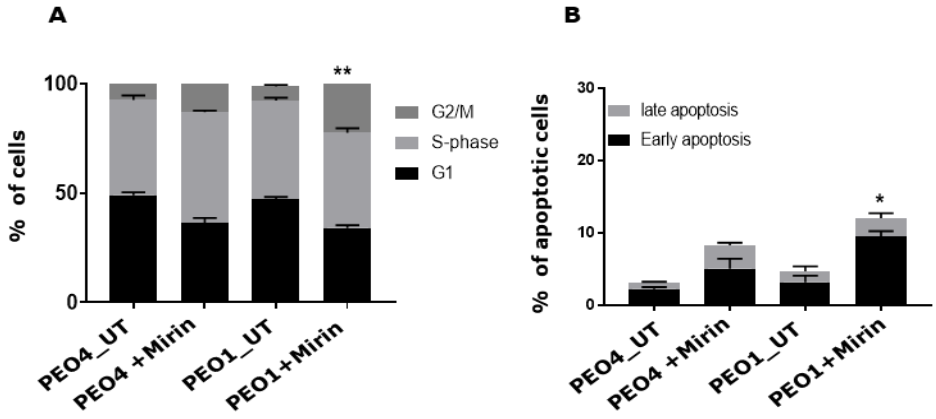

Figure 6.4: Functional studies of PEO4 and PEO1 cells using FACS. A) In PEO1 cells, mirin treatment (18 μM for 24 hours) was significantly associated with G2/M cell cycle arrest. B) In PEO1 cells, annexin V analysis showed that mirin treatment (18 μM for 24 hours) increased the apoptotic population. *$p<0.05$, ** $p<0.01$, determined by two way-ANOVA. UT= untreated cells. Data presentation and statistical analysis were performed using GraphPad Prism, version 7.

Three-dimensional culture (3D)-spheroids models is interesting. OC cells form spheroids like what is closely seen in tumours with hypoxic centre and complex structures. It is not always what is shown in 2D can be shown in 3D spheroids model. So, it is important to validate 2D results with 3D spheroids models. We tested mirin sensitivity in PEO1 and PEO4 spheroids structures. As in the two-dimensional (2D) model, mirin treatment significantly increased dead cells in PEO1 spheroids compare to mirin treated PEO4 spheroids (Figure 6.5).

To validate the data further, we tested the effects of mirin treatment on HeLa control and BRCA2-deficient HeLa cells. In clonogenic assays, BRCA2-deficient HeLa cells were highly sensitive to mirin therapy when compared with HeLa control cells (Figure 6.6). We then preformed FACS to assess the impact of mirin therapy on DSB, cell cycle arrest and apoptosis. Mirin treatment led to increased DSB accumulation, to G2/M cell cycle arrest and to increased apoptosis (Figure 6.7).

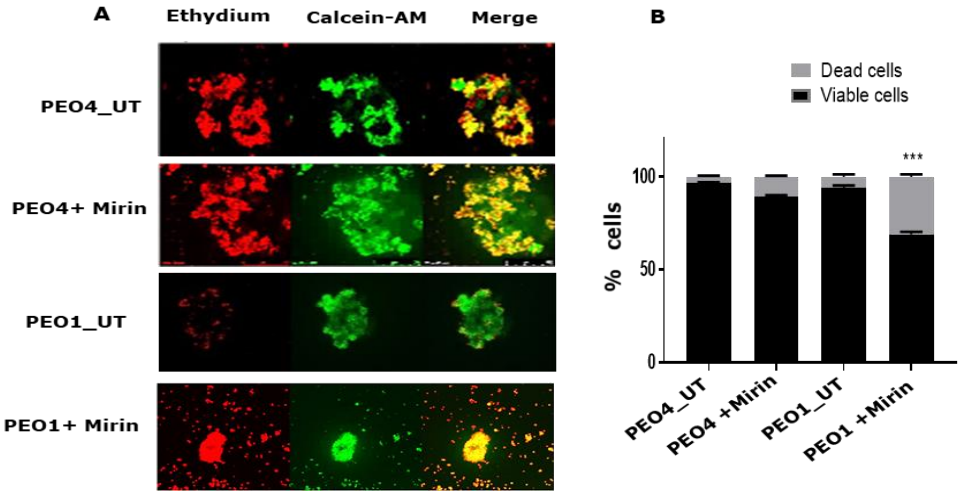

Figure 6.5: Spheroids of PEO1 and PEO4 cells untreated (UT) and treated with 18μM mirin for 48 hours. 4 × 10^4 cells were seeded in ultra-low attachment 6-well plates, and tumour spheres media was used every 4 days. After spheres formation, spheres were treated with mirin for 48 hours. Spheres then fixed with 37% formaldehyde and stained with calcein (2.5μM) and ethidium homodimer (1.5μM). A) Representative photomicrographic images of mirin untreated and treated PEO4 and PEO1 spheroids. The size of spheroids formed by PEO1 and PEO4 cell lines were different. Images were taken by confocal microscopy. Mirin therapy substantially increased dead cells in PEO1 spheroids compare to mirin treatment in PEO4 spheroids. All spheroids Images were analysed by ImageJ software. B) FACS analysis of PEO1 and PEO4 cells viability. *** $p<0.001$, calculated by two-way ANOVA. Weasel Software Version 3.0.2 (The Walter and Eliza Hall Institute of Medical Research, Australia) was used for flow cytometry analyses. Data presentation and statistical analysis were performed using GraphPad Prism, version 7.

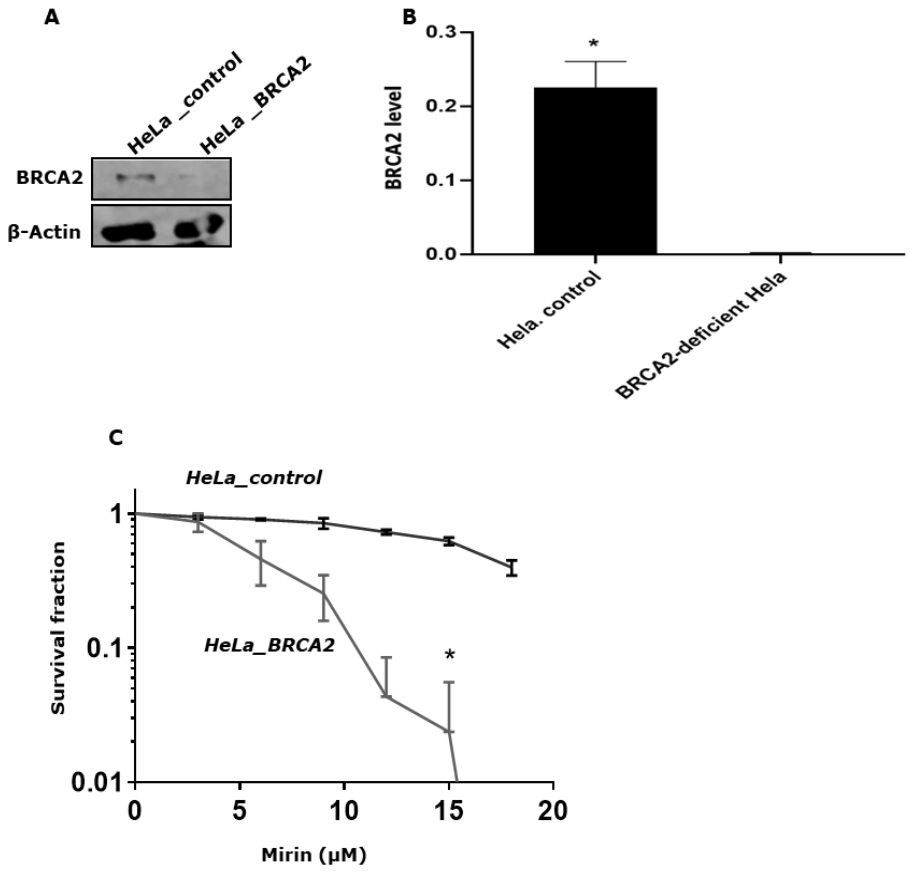

Figure 6.6: Effects of mirin on BRAC2-deficient HeLa cells. A) Representative western blotting showing BRCA2 levels in HeLa control cells and BRCA2-deficient HeLa cells. BRCA2 levels are detected in Hela control whereas no detected BRCA2 level in BRCA2-deficient HeLa cells. The detected band intensity for BRCA2 as well as B-actin band intensity were quantified in LI-COR software. The readings for BRCA2 were normalised to B-actin reading. B) Quantification of BRCA2 levels control and BRCA2-deficient HeLa cells. C) Clonogenic assay showing Mirin sensitivity in Hela control and BRCA2-deficient HeLa cells. Cells were trypsinized and plated into six-well plates overnight. On the following day, cells were treated with various doses of mirin. Cells were incubated for 14 days (Ali et al., 2019a). BRCA2-deificent HeLa cells were significantly more sensitive to mirin treatment than were the HeLa control cells. * $p<0.050$, calculated by student's t-test. Data presentation and statistical analysis were performed using GraphPad Prism, version 7.

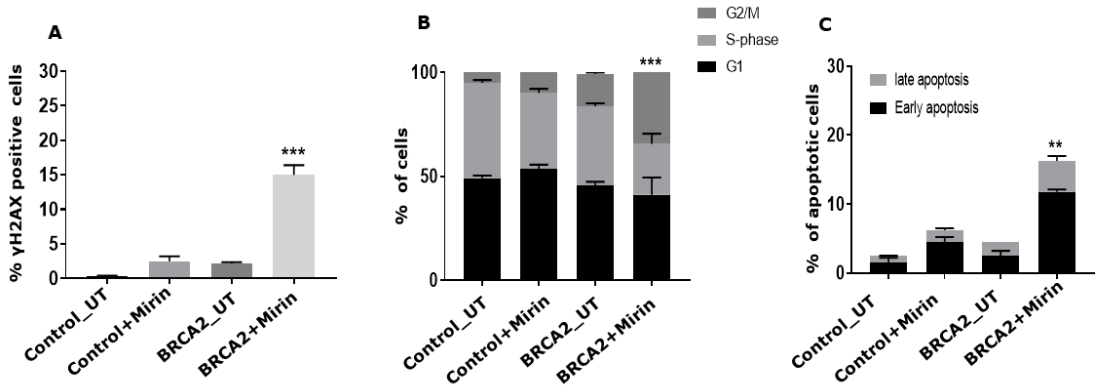

Figure 6.7: Functional studies of mirin-treated and untreated (UT) control and BRCA2-deficient HeLa cells. Cells were trypsinized and plated into six-well plates. On the following day, cells were treated with 18μM mirin for 24 hours and then collected. Protocols are described in chapter 2 page 102-106. A) The percentage of γH2Ax positive cells; statistical analysis determined by one-way ANOVA. BRCA2 +mirin revealed significant accumulation of γH2AX positive cells. B) Cell cycle analysis in UT and treated cells, from two way-ANOVA. BRCA2 +mirin showed G2/M cell cycle arrest. C) Annexin V analysis in UT and treated cells, from two way-ANOVA. BRCA2 +mirin demonstrated significant increased apoptotic cells. **P<0.01, *** P < 0.001.

In the 3D spheroids models, BRCA2-deficient HeLa spheroids were more sensitive to mirin therapy compared with HeLa control spheroids (Figure 6.8). Altogether, the results provide evident that targeting MRE11 exonuclease activity is a promising strategy for SL in BRCA2-deficient cancer cells.

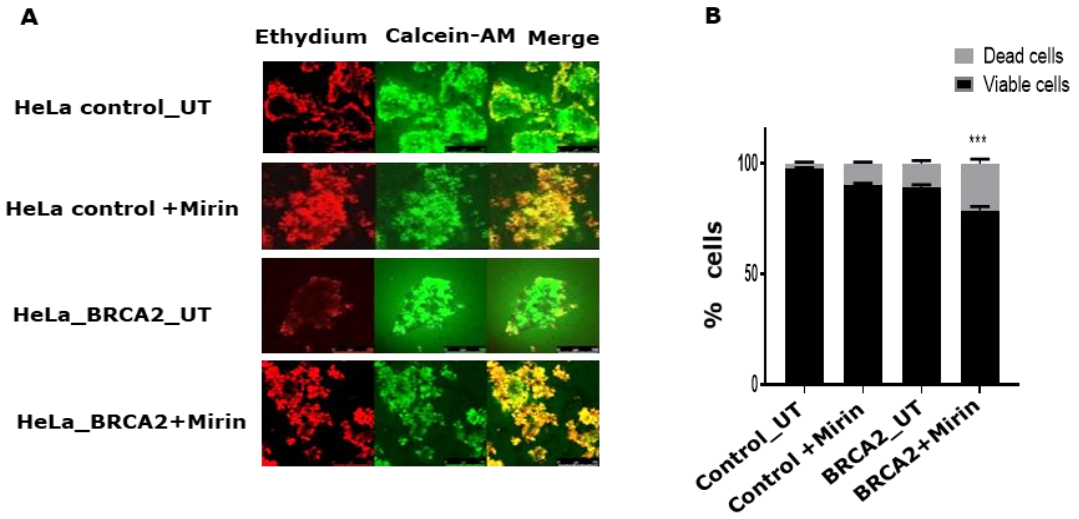

Figure 6.8: Spheroids of HeLa control and BRCA2-deficient HeLa cells untreated (UT) and treated with 18μM mirin for 48 hours. A) Representative photomicrographic images of UT and treated spheroids. Mirin treatment increased dead cells in BRCA2-deficient HeLa spheroids compared to HeLa control spheroids. Hela control spheroids were larger in size than Hela_BRCA2 spheroids. B) Analysis of control and BRCA2-deficient HeLa cell viability. *** $p<0.001$, calculated two-way ANOVA.

To examine the clinicopathological significance of BRCA2 and MRE11 co-expression, we preformed immunohistochemical studies (IHC) in OC clinical cohorts. Patients with tumours had high BRCA2 and high MRE11 co-expression had worse PFS (P=0.005) and poor OS (p=0.001) compared to tumours that were low BRCA2 and low MRE11 co-expression (Figure 6.9).

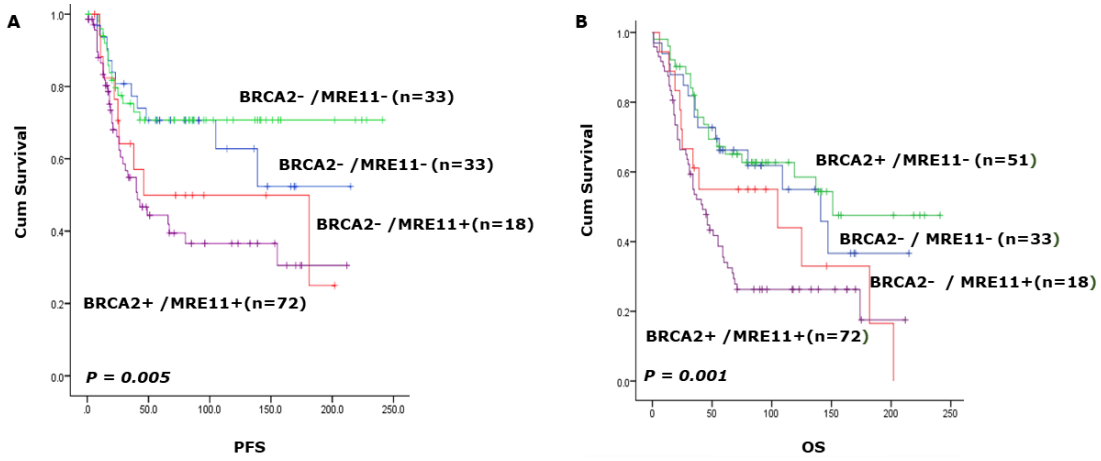

Figure 6.9: Kaplan Meier survival curves for BRCA2 and MRE11 co-expression. Kaplan Meier statistical analysis was used to conduct a univariate analysis of OS and PFS against BRCA2 and MRE11 expression. A) Progression-free survival (PFS)**.** High BRCA2/high MRE11 expression (purple line) was significantly associated with poor PFS, defined as the time between treatment initiation and subsequent tumour progression. B) Overall survival (OS). High BRCA2/high MRE11 expression (purple line) was significantly associated with poor OS. OS was calculated from the day of diagnosis or time of treatment initiation to the time where patients were still alive.

6.5.2 MIRIN IS SYNTHETICALLY LETHAL IN XRCC1-DEFICIENT CANCER CELLS

XRCC1 play vital role in BER, SSBR and alt-NHEJ DNA repair pathways (Ali et al., 2019a). Moreover, XRCC1, along with MRE11, has a role in replication fork stability maintenance (Ying et al., 2016). Our lab previously demonstrated that XRCC1-defieciency is a predictor of platinum sensitivity in OC (Abdel-Fatah et al., 2013). We thus tested whether mirin is synthetic lethal in XRCC1-deficient cells. We used A2780_XRCC1_KO cells (knocked-out by CRISPR) to compare with A2780 control cells. In clonogenic assays, A2780_XRCC1_KO cells were significantly sensitive to mirin treatment compared to A2780 control cells (Figure 6.10). We then preformed FACS to monitor DSB accumulation, cell cycle arrest and apoptosis. FACS data showed that mirin therapy in A2780_XRCC1_KO cells was associated with increased the accumulation of DSB, S-phase arrest and increased apoptosis population (Figure 6.11). Next, we moved to 3D spheroid models. Similar to results in a 2D system, A2780_XRCC1_KO spheroids were extremely sensitive to mirin treatment compared to A2780 control spheroids (Figure 6.12).

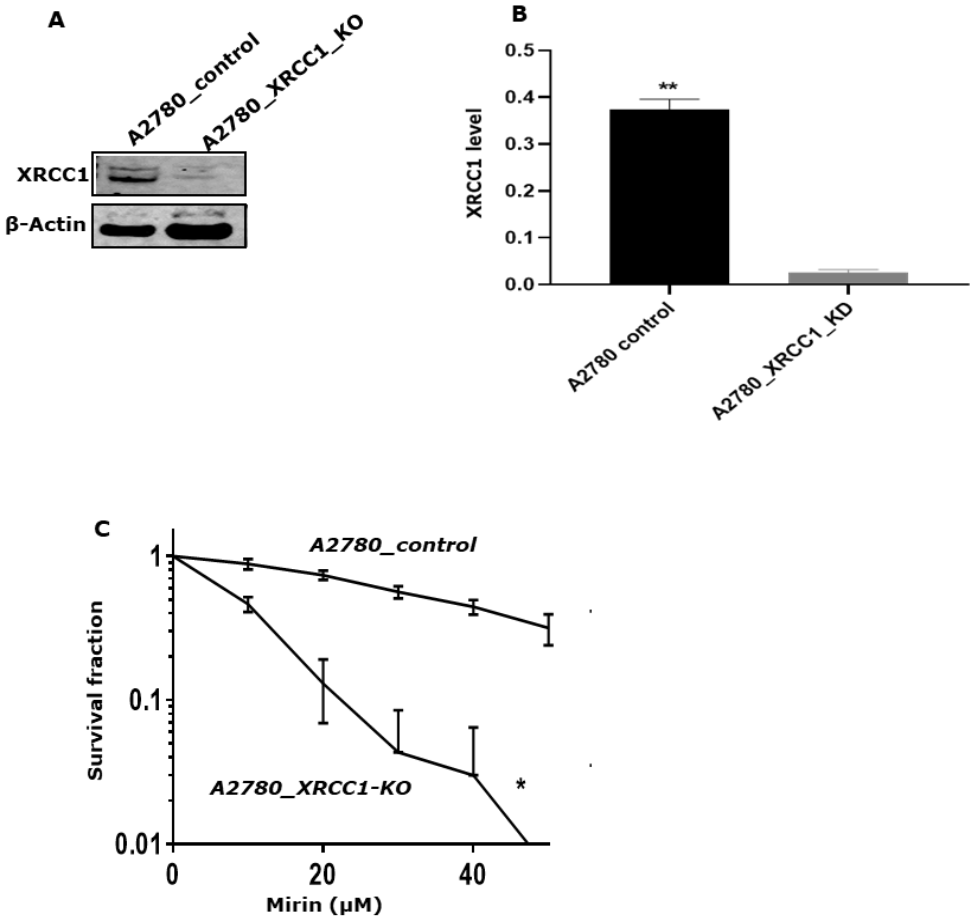

Figure 6.10: Mirin sensitivity in XRCC1 knockout cells. A) Representative western blot showing XRCC1 levels in A2780 control cells and A2780_XRCC1-KO cells. XRCC1 levels are detected in A2780C cells while week XRCC1 levels were detected in A2780_XRCC1_KO cells. The detected band intensity for XRCC1 as well as B-actin band intensity were quantified in LI-COR software. The readings for XRCC1 were normalised to B-actin reading. B) Quantification of XRCC1 levels in A2780 control cells and A2780_XRCC1-KO cells. C) Clonogenic assay showing mirin sensitivity in A2780 control cells and A2780_XRCC1-KO cells. Cells were trypsinised and plated into six-well plates overnight. On the following day, cells were treated with various doses of mirin. Cells were incubated for two weeks (Ali et al., 2019a). A2780_XRCC1_KO cells were significantly sensitive to mirin treatment compared to mirin treatment in A2780 control cells. * $p<0.050$, **$p<0.01$, calculated by student's t-test.

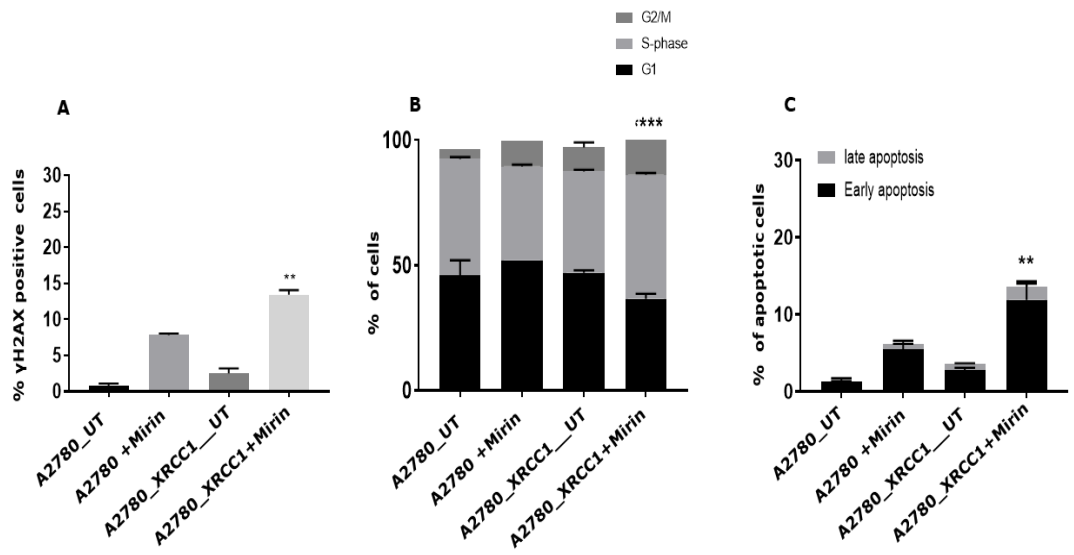

Figure 6.11: Functional studies of A2780 control and A2780_XRCC1-KO cells using FACS. Cells were trypsinised and plated into six-well plates overnight. On the following day, cells were untreated (UT) or treated with 25μM mirin for 24 hours. Cells were then collected; Protocols are described in chapter 2 (P.102-106). A) The percentage of γH2Ax positive cells; statistical analysis determined by one-way ANOVA. A2780_XRCC1+mirin revealed significant accumulation of γH2AX positive cells. B) Cell cycle analysis in UT and treated cells, from two way-ANOVA. A2780_XRCC1+mirin showed S-phase cell cycle arrest. C) Annexin V analysis in UT and treated cells, from two way-ANOVA. A2780_XRCC1+mirin demonstrated significant increased apoptotic cells. **P<0.01, *** P < 0.001.

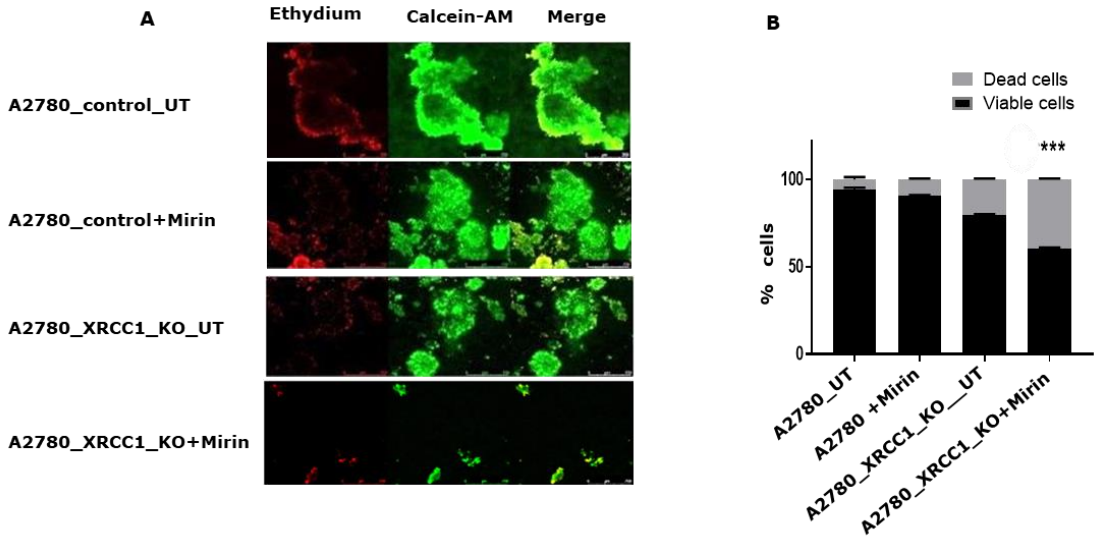

Figure 6.12: Spheroids of A2780 control and A2780_XRCC1-KO cells untreated (UT) and treated with 25μM mirin for 48 hours. A) Representative photomicrographic images of mirin untreated and treated A2780 control and A2780_XRCC1_KO spheroids. Mirin therapy significantly reduced the cells viability in A2780_XRCC1_KO spheroids compare to mirin treatment in A2780 control spheroids. A2780 control spheroids were larger in size than A2780_XRCC1 spheroids. B) FACS analysis of cell viability. *** $p<0.001$, calculated by two-way ANOVA.

To further validate our data, we tested the effects of mirin treatment on HeLa control and XRCC1-deficient HeLa cells. In clonogenic assays, XRCC1-deficient HeLa cells were significantly sensitive to mirin treatment compared with HeLa control cells (Figure 6.13). We then conducted FACS to assess the effects of mirin treatment on DSB, cell cycle arrest and apoptosis in the Hela cells. Mirin therapy led to increased DSB accumulation, S-phase cell cycle arrest and increased apoptosis (Figure 6.14).

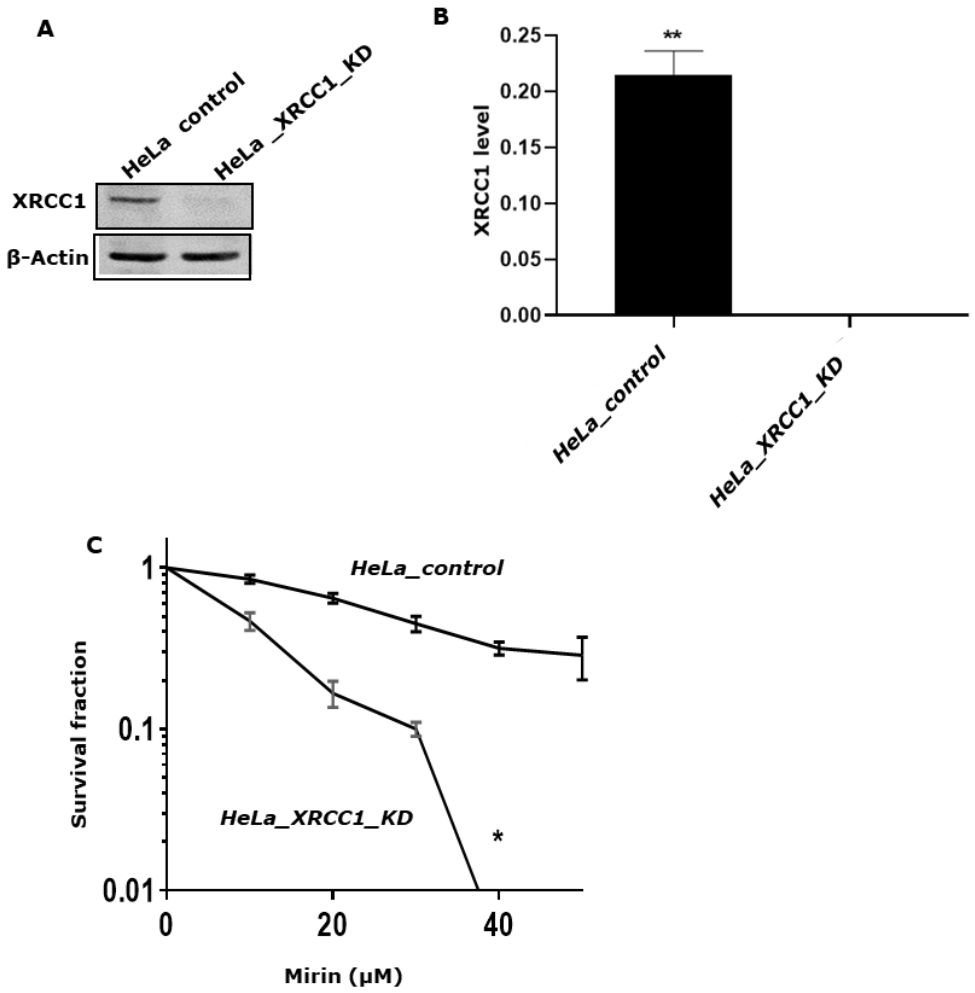

Figure 6.13: Mirin sensitivity of XRCC1-deficient cells. A) Representative western blot showing XRCC1 protein levels in HeLa control cells and XRCC1-deficent HeLa cells. XRCC1 levels were detected in Hela control whereas no detected XRCC1 level in XRCC1-deficient HeLa cells. The detected band intensity for XRCC1 as well as B-actin band intensity were quantified in LI-COR software. The readings for XRCC1 were normalised to B-actin reading. B) Quantification of XRCC1 level in HeLa control and XRCC1-deficent HeLa cells. C) Clonogenic assay showing mirin sensitivity in HeLa control cells and HeLa_XRCC1_KD cells. Cells were trypsinized and plated into six-well plates overnight. On the following day, cells were treated with various doses of mirin. Cells were incubated for two weeks (Ali et al., 2019a). XRCC1-deficient HeLa cells were significantly sensitive to mirin compared to HeLa control cells. * $p<0.050$, **$p<0.01$, calculated by student's t-test.

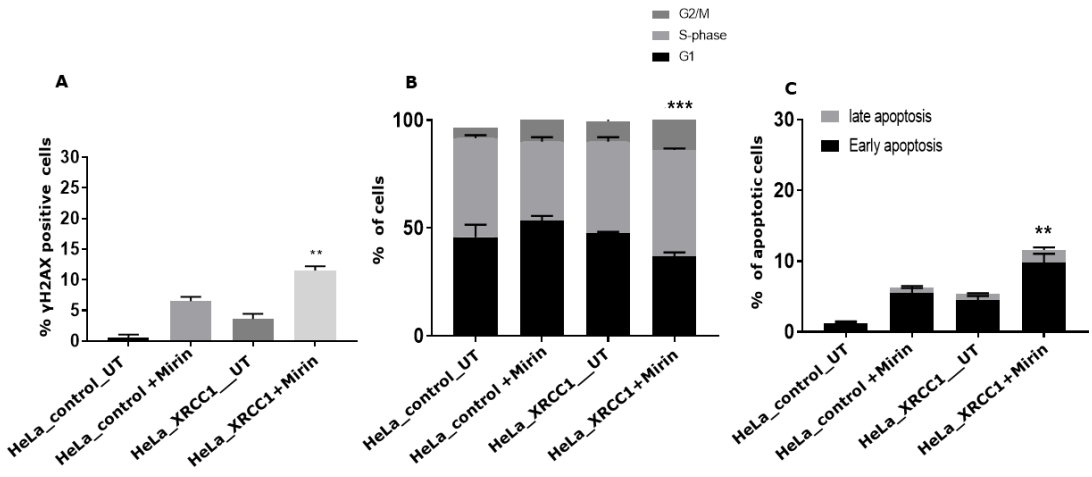

Figure 6.14: Functional studies of HeLa control cells and XRCC1-deificent HeLa cells using FACS. Cells were trypsinised and plated into six-well plates overnight. On the following, day cells were untreated (UT) or treated with 25μM mirin for 24 hours. Cells were then collected. A) The percentage of γH2Ax positive cells; statistical analysis determined by one-way ANOVA. Hela_XRCC1+mirin revealed significant accumulation of γH2AX positive cells. B) Cell cycle analysis of mirin-treated and UT; from two way-ANOVA. Hela_XRCC1+mirin showed S-phase cell cycle arrest C) Annexin V analysis of mirin-treated and UT cells; from two way-ANOVA. Hela_XRCC1+mirin demonstrated significant increased apoptotic cells. **P<0.01, *** P < 0.001.

We then proceeded to 3D spheroid models. Resulting data were similar to those from the 2D system, XRCC1-deficient HeLa spheroids were sensitive to mirin treatment compared to HeLa control spheroids (Figure 6.15).

To evaluate the clinicopathological significance of XRCC1 and MRE11 co-expression, we preformed IHC in OC clinical cohorts. Patients with tumours had high XRCC1 and high MRE11 co-expression showed

poor PFS (P=0.014) and poor OS (p=0.017) compared to tumours that were low XRCC1 and low MRE11 co-expression (Figure 6.16).

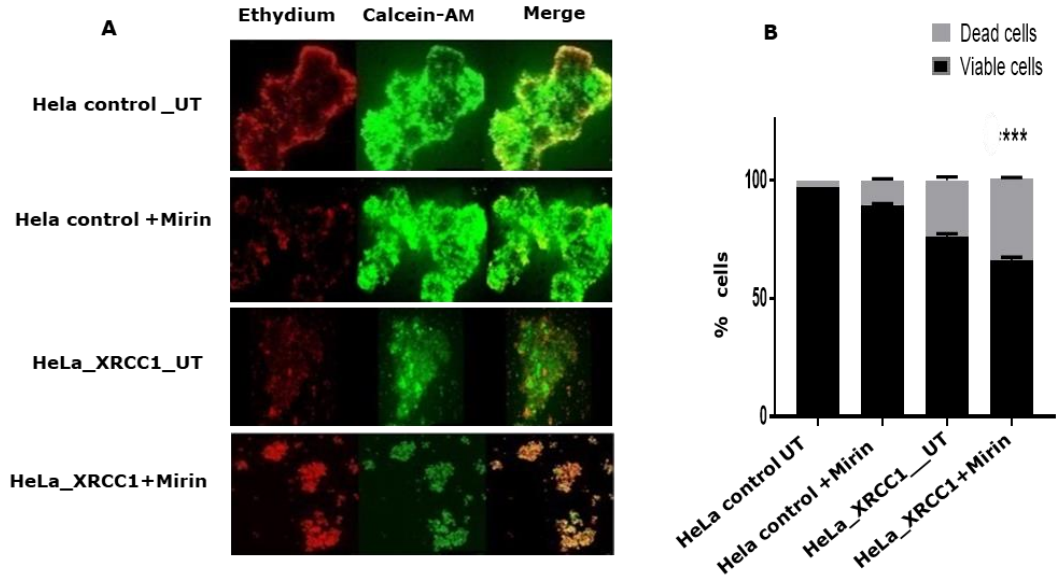

Figure 6.15: Spheroids of HeLa control and XRCC1-deficient HeLa cells untreated (UT) and treated with 25μM mirin for 48 hours. A) Representative photomicrographic images of mirin untreated or treated HeLa control and HeLa_XRCC1-KO spheroids. Mirin treatment was increased dead cells in XRCC1-deficient HeLa spheroids compare to mirin treatment in HeLa control spheroids. Hela control spheroids were larger in size than Hela_XRCC1 spheroids. B) Analysis of cell viability. *** $p<0.001$, calculated two-way ANOVA.

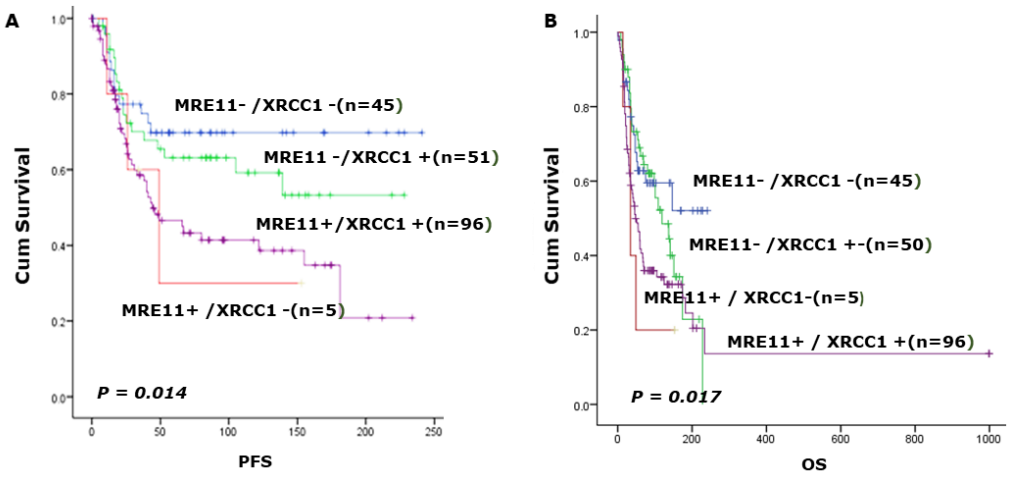

Figure 6.16: Kaplan Meier survival curves for XRCC1 and MRE11 co-expression. Kaplan Meier statistical analysis was used to conduct a univariate analysis of OS and PFS against XRCC1 and MRE11 expression. A) High XRCC1/High MRE11 expression (purple lines) is significantly associated with poor PFS. B) High XRCC1/High MRE11 expression (purple lines) is significantly associated with poor OS.

6.5.3 PEO1R CELLS OVEREXPRESSES MRE11 AND UP-REGULATE SEVERAL DNA REPAIR GENES

PEO1 cells were treated with stepwise increasing concentrations of mirin (5 μM–45 μM) over a period of 210 days to establish the mirin-resistant cell line PEO1R. Clonogenic assays were used to evaluate PEO1R cells sensitivity to mirin and cisplatin. PEO1R cells were significantly resistance to mirin and cisplatin compared to PEO1 cells (Figure 6.17).

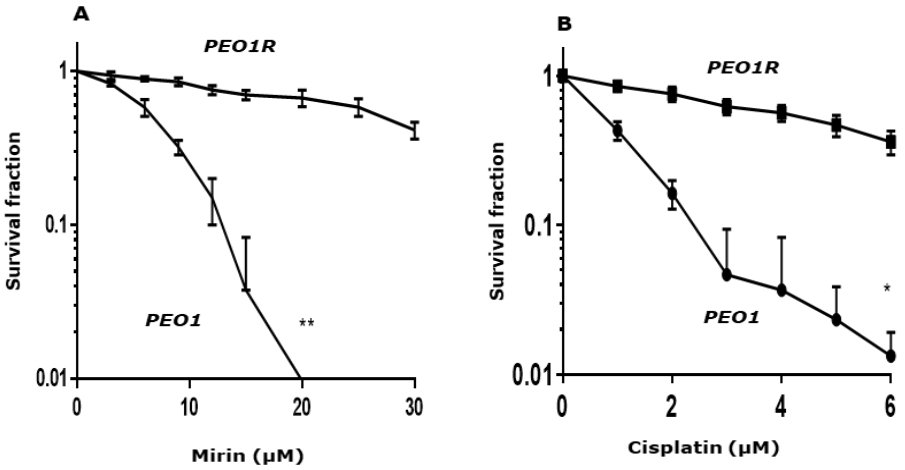

Figure 6.17: Clonogenic assays showing sensitivity to mirin and cisplatin in PEO1 and PEO1R cells. A) PEO1 cells were significantly sensitive to mirin compared to PEO1R cells. B) PEO1 cells were significantly sensitive to cisplatin compared to PEO1R cells. Microsoft Excel 2010 was used to determine plating efficiency and survival fraction, see chapter two page 100-101 for more details. * p<0.050, **<0.001, calculated by student's t-test. Data presentation and statistical analysis were performed using GraphPad Prism, version 7.

In 3D spheroids models, Similar to the results of the 2D system, PEO1R spheroids were resistance to mirin and cisplatin therapy when it compared with PEO1 spheroids (Figure 6.18).

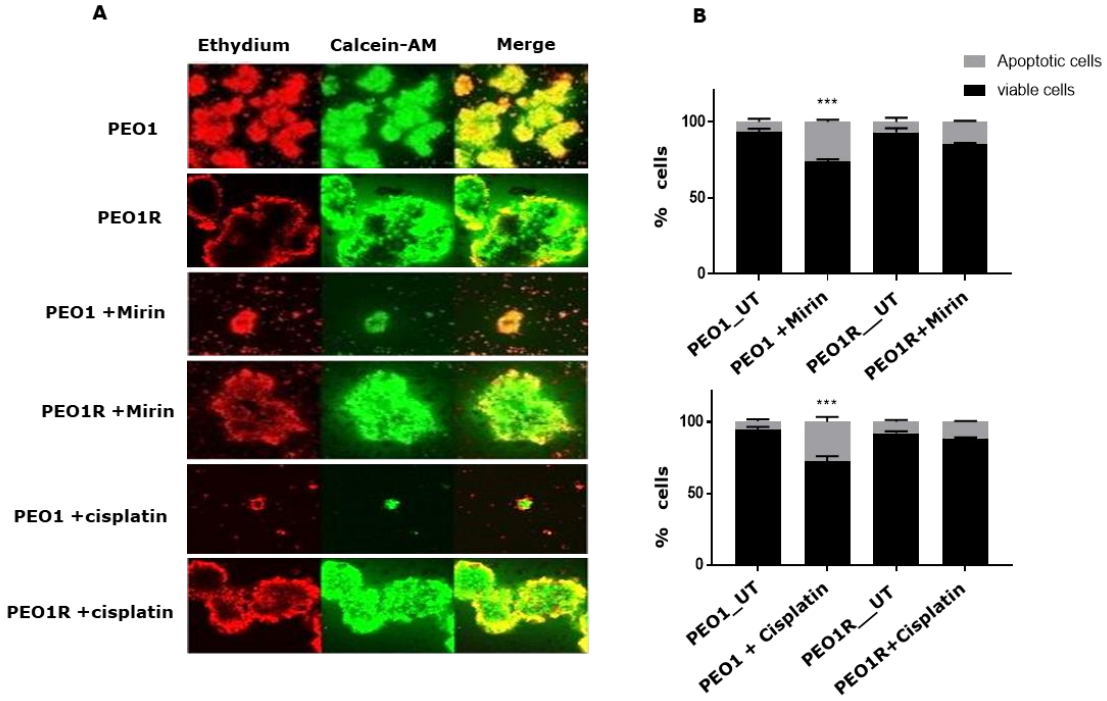

Figure 6.18: Spheroids of PEO1 and PE01R cells untreated (UT) and treated with 18μM mirin or 5μM cisplatin for 48 hours. A) Representative photomicrographic images of mirin-treated, cisplatin-treated and UT PEO1 and PEO1R spheroids. Mirin and cisplatin treatment were increased dead cells in PEO1 spheroids compare to mirin and cisplatin treatment in PEOR spheroids. PEO1R spheroids were also larger in size than PEO1 spheroids. B) Analysis of PEO1 and PEOR cell viability. ***p < 0.001, calculated by two-way ANOVA.

We also tested sensitivity of PEO1R to olaparib. In clonogenic assays, interestingly, PEO1R cells were cross resistance to olaparib treatment (Figure 6.19).

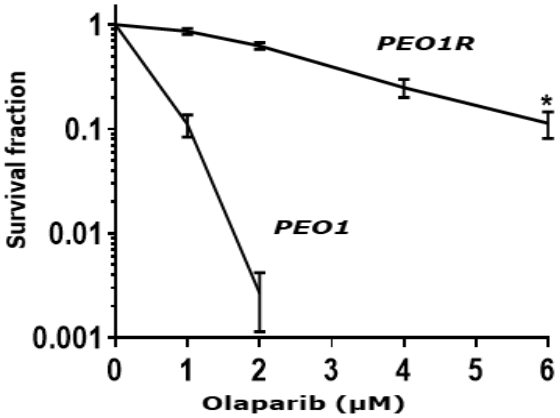

Figure 6.19: Clonogenic assay for Olaparip sensitivity in PEO1 and PEO1R cells. PEO1R cells were significantly resistance to Olaparip compared to PEO1 cells. *p < 0.050, calculated by student's t-test.

Studies of PARPi resistance in BRCA-deficient cells have shown several mechanisms of resistance, including restoration of HR (reactivation of BRCA function, inactivation of 53BP1, down regulation of PARP1) and restoration of stalled replication form protection (Kim et al., 2017b, Noordermeer and van Attikum, 2019). We hypothesised that a similar mechanism of resistance might be operating in PEO1R cells. We preformed western blot in PEO1 and PEO1R lysates to determine if there is a reactivation in BRCA2 in PEO1R cells. As shown in figure 6.20, we did not notice any evidence

of BRCA2 restoration in PEO1R cells. However, loss of 53BP1 was evident in PEO1R cells but 53BP1 still present in PEO1 cells. 53BP1 inactivation in BRCA-deficient cells restores DSB resection and activates HR (Jaspers et al., 2013, Bouwman et al., 2010).

We preformed FACS to monitor the effects of mirin and cisplatin on DSB, cell cycle arrest and apoptosis in PEO1 and PEO1R cells. The data showed that Mirin or cisplatin therapy in PEO1 cells induced significant accumulation of DSB, cell cycle arrest and increased apoptosis compared to PEO1R cells (Figure 6.21-6.22).

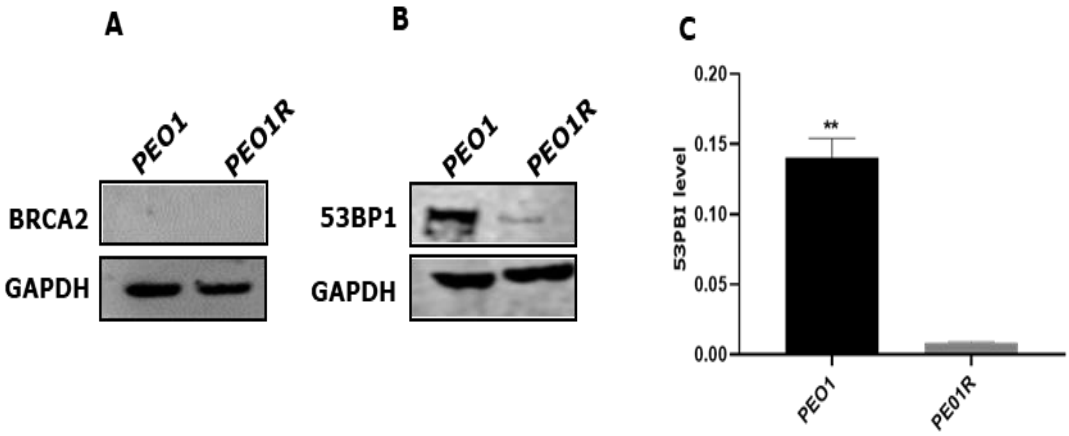

Figure 6.20: BRCA2 and 53BP1 baseline proteins levels in PEO1 and PEO1R cells. A) Representative western blot of BRCA2. BRCA2 was undetectable in PEO1 and PEO1R cells. B) Representative western blot of 53BP1. PEO1R cells showed a significantly reduced level of 53BP1 compared to that in PEO1 cells. C) Quantification of 53BP1 levels in PEO1 and PEO1R cells. **p < 0.01, calculated by student's t-test.

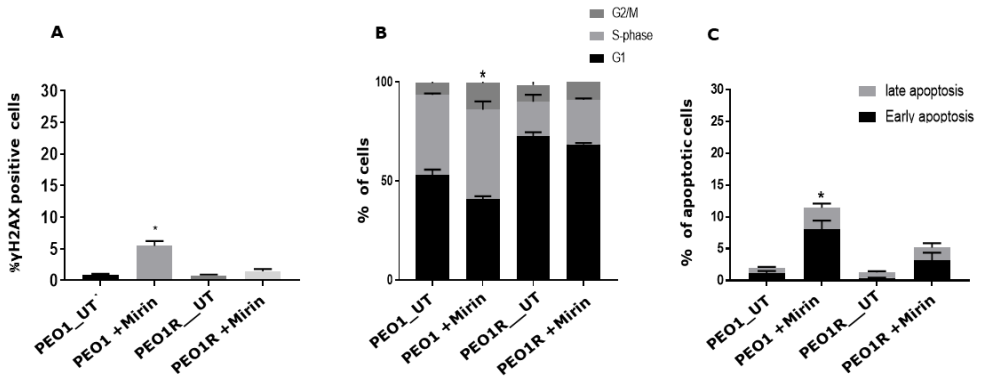

Figure 6.21: Functional studies of mirin-treated PEO1 and PEO1R cells using FACS. Cells were untreated (UT) or treated with 18 μM of mirin for 24 hours. A) Percentage of γH2Ax-positive cells; statistical analysis by one-way ANOVA. PEO1+ mirin revealed significant accumulation of γH2AX positive cells compared to PEO1R+ mirin. B) Cell cycle analysis; statistical analysis by two way-ANOVA. PEO1+ mirin showed G2/M cell cycle arrest. C) Annexin V analysis; statistical analysis by two way-ANOVA. PEO1+ mirin distracted significant increase apoptotic cells. *$p < 0.05$.

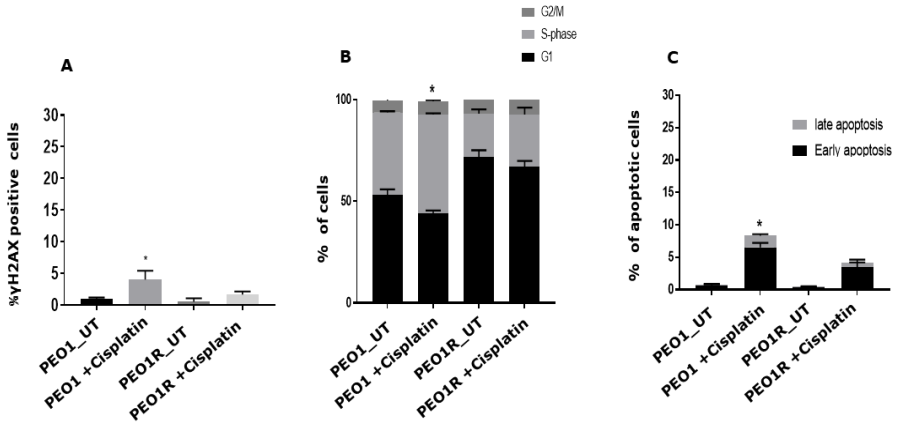

Figure 6.22: Functional studies of cisplatin-treated PEO1 and PEO1R cells using FACS. Cells were untreated (UT) or treated with 5 μM of cisplatin for 24 hours. A) Percentage of γH2Ax-positive cells increase in PEO1+ cisplatin, statistical analysis by one-way ANOVA. B) PEO1+ cisplatin showed S-phase analysis; statistical analysis by two way-ANOVA. C) PEO1+ cisplatin significant increased apoptotic cells; statistical analysis by two way-ANOVA. *$p < 0.05$.

These data seem to support HR activation in PEO1R cells. To further validate this result, we then assessed MRN complex expression in PEO1 and PEO1R cells. MRE11 was highly expressed in PEO1R cells compare to PEO1 cells. We then preformed IF staining to confirm the overexpression of MRE11 in PEO1R. The results showed that MRE11 unclear expression was increased in PEO1R cells compared to PEO1 cells (Figure 6.23). Increased MRE11 protein expression was also correlated with significant increased *MRE11* mRNA expression, as determined by real-time PCR (Figure 6.23).

MRE11 interacts with both NBS1 and RAD50 and enhances MRN complex stability. Even Though RAD50 and NBS1 do not directly interact with each other, they dependent on MRE11 for stability. MRE11 alterations that disrupts RAD50 and/or NBS1 interactions can destabilise and decrease the level of MRN complex (Lamarche et al., 2010b, Syed and Tainer, 2018b). Therefore, we also examined NBS1 and RAD50 protein levels in lysates from PEO1 cells and PEO1R cells. As expected, NBS1 and RAD50 protein levels were increased in PEO1R cells compared to PEO1 cells (Figure 6.24). When MRE11 was knocked down by siRNA in PEO1R cells (PEO1R_MRE11_KD), we observed a significant decreased in NBS1 and RAD50 protein levels (Figure 6.25).

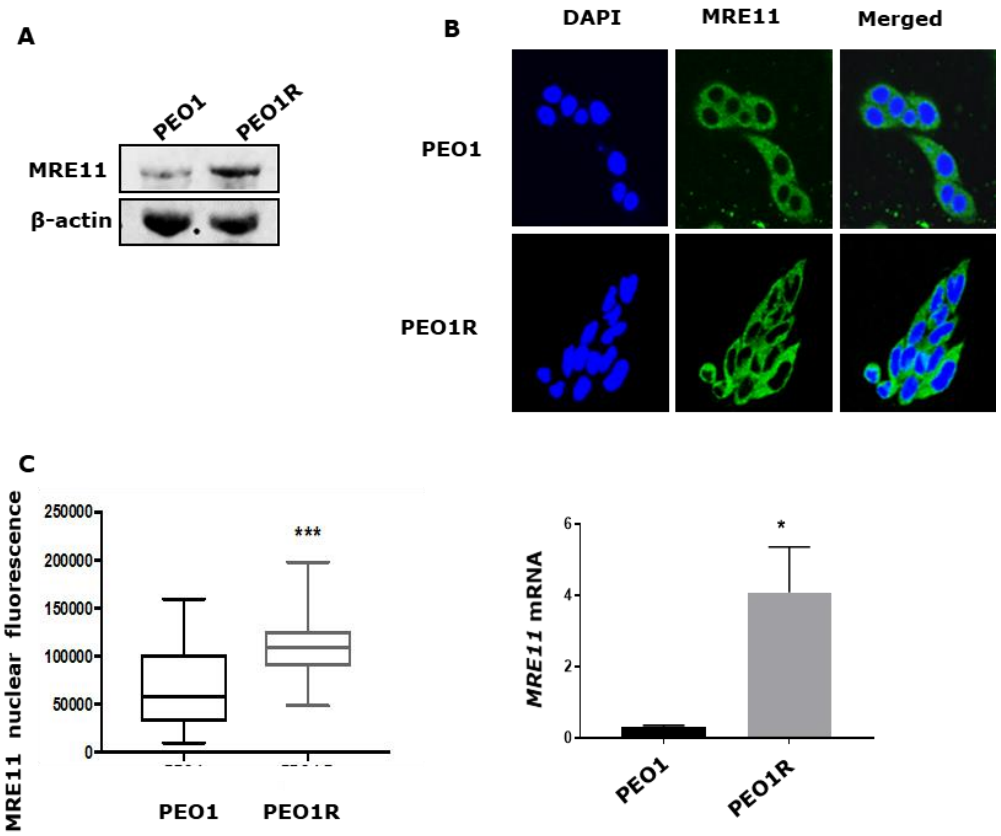

Figure 6.23: MRE11 levels in PEO1 and PEO1R cells. A) Representative western blot showing MRE11 protein levels in PEO1 and PEO1R cells. MRE11 overexpressed in PEO1R cells compared to PEO1 cells. B) Immunofluorescence staining for MRE11 in PEO1 and PEO1R cells. MRE11 nuclear expression was increased in PEO1R cells compared to PE01 cells. The analysis of images was performed by ImageJ software. C) Quantification of MRE11 nuclear fluorescence was performed by GraphPad Prism, version 7. D) Relative MRE11 mRNA in PEO1 and PEO1R cells assessed by real time PCR. *$p < 0.05$; ***$p < 0.001$, determined by student's t-test.

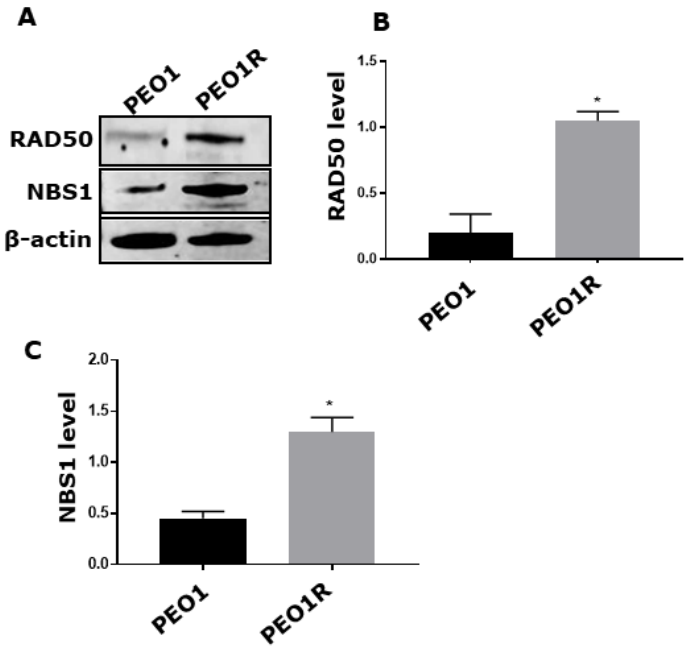

Figure 6.24: RAD50 and NSB1 levels in PEO1 and PEO1R cells. A) Representative western bolt of RAD50 and NBS1. RAD50 and NBS1 were overexpressed in PEO1R cells compare to PEO1 cells. RAD50, NBS1 and B-actin band intensities were quantified in LI-COR software. The readings for RAD50 and NBS1 were normalised to B-actin readings. B) Quantification of RAD50 levels in PEO1 cells and PEO1R cells. C) Quantification of and NBS1 levels in PEO1 cells and PEO1R cells. *$p < 0.05$, calculated by student's t-test.

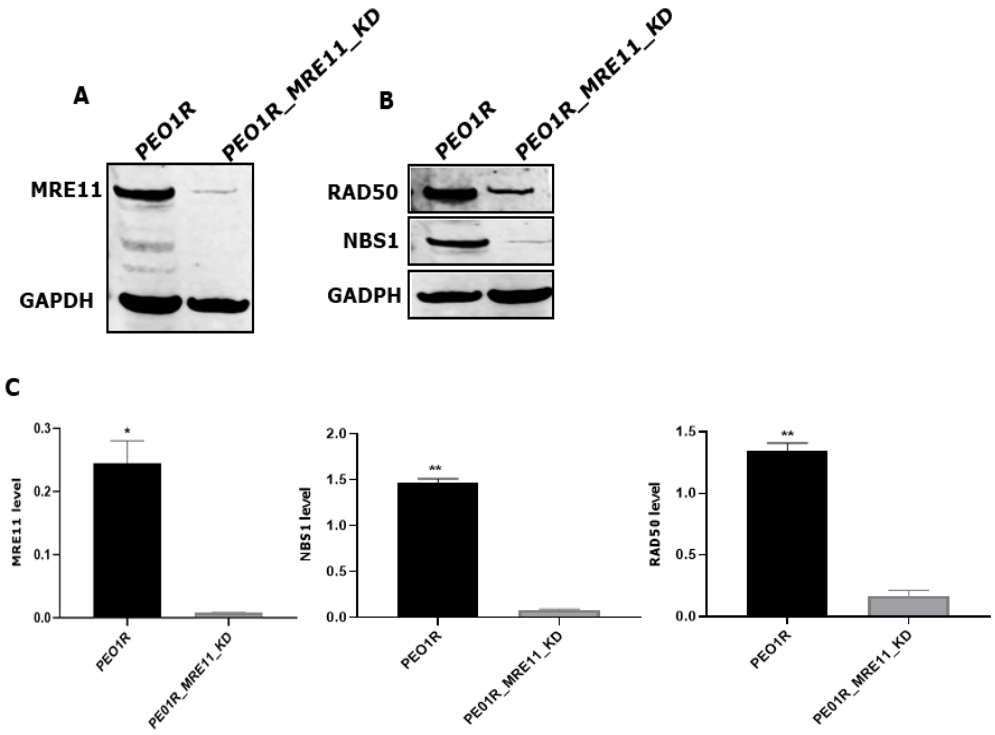

Figure 6.25: MRE11, RAD50 and NBS1 levels in PEO1R and PEO1R_MRE11_KD cells. A) Representative western bolt of MRE11. This showed a successful knockdown of MRE11 in PEO1R cells. Cell lyases we used here were taken from MRE 11 KD cells in day three. B) Representative western blot of RAD50 and NBS1. PEO1R_MRE11-KD cells revealed a significant reduction in RAD50 and NBS1 protein levels C) Quantification of MRE11, RAD50 and NBS1 levels in PEO1R and PEO1R_MRE11-KD cells. *p < 0.05; **p < 0.01, calculated by student's t-test.

To study the role of MRE11 in the acquired resistance in PEO1R cells, we knocked-down MRE11 in PEO1R cell by siRNA, and then preformed clonogenic assays to test the sensitivity of PEO1R_MRE11_KD to cisplatin and mirin treatment. Interestingly, PEO1R-MRE11_KD cells partially restored cisplatin and mirin sensitivity (Figure 6.26).

Taken together, the results provide evidence that high expression of MRE11 leads to the development of mirin resistant in PEO1R cells. As MRE11_KD partially restored mirin and cisplatin sensitivity, we asked whether additional upregulation of other DNA repair genes might lead to resistance. To answer this question, we preformed real time PCR using RT^2 Profiler PCR Array for 84 DNA repair genes in PEO1 and PEO1R cells. The PCR data demonstrated that, in addition to MRE11, PEO1R cell overexpress a number of genes involved in DDR signalling (*ATM, RPA1*), DSB repair (*RAD51B, RAD51C, RAD51D, RAD23B, RAD52, XRCC5, XRCC6BP1, LIG1,LIG3, LIG4, TOP3A, TOP3B*), nucleotide excision repair (*DDB1, DMC1, XPA, ERCC1, ERCC2, ERCC4, ERCC8 and XAB2*), mismatch repair (*MSH3, MSH5, PMS2*), base excision repair (*APEX1, TDG, NEIL1, NEIL2, MPG, MUTYH, PARP1, Polβ*) and MGMT (Figure 6.27).

To further validate these results, we used a panel of antibodies to confirm overexpression at the protein level of RPA1, ATM, RAD51C,

XRCC1, PARP1, PARP2, LIG1, LIG3 and ERCC1 in PEO1R compared to PE01 cells (Figure 6.28).

Collectively, the data provides evidence that up-regulation of DNA repair could be a key mechanism for the acquired resistance to Mirin.

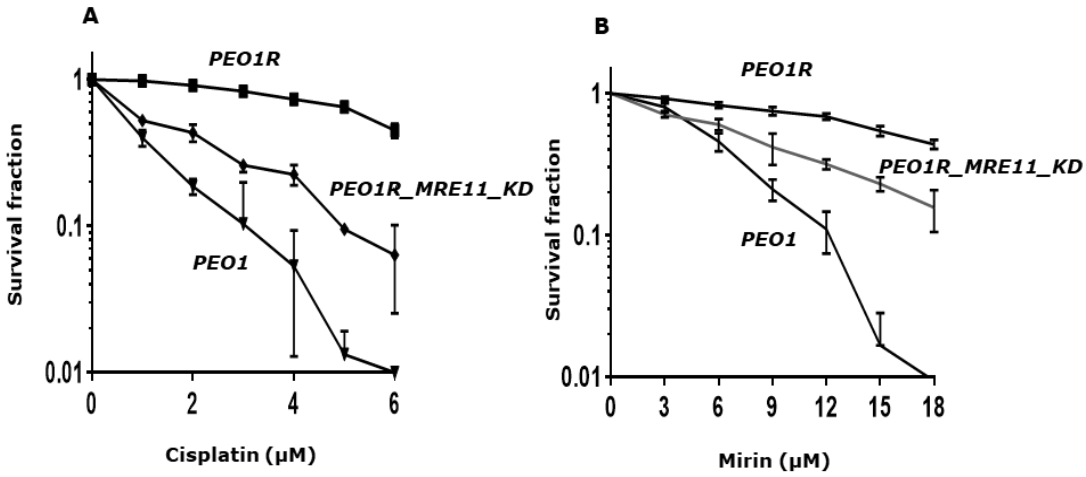

Figure 6.26: Clonogenic assays showing cisplatin and mirin sensitivity in PEO1, PEO1R and PEO1R_MRE11_KD cells. Cells were trypsinised and plated into six-well plates overnight. On the following day, cells were treated with various doses of mirin or cisplatin. Cells were incubated for 14 days. A) Cisplatin sensitivity. PEO1R_MRE11_KD cells partially restored sensitivity to cisplatin compared to PEO1R. B) Mirin sensitivity. PEO1R_MRE11_KD cells partially restored sensitivity to mirin compared to PEO1R cells.

A

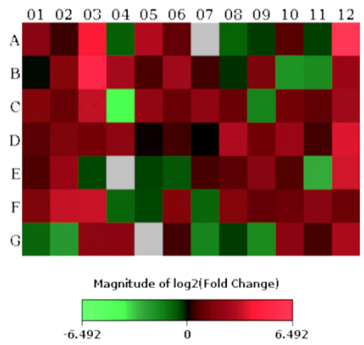

B

Position	Upregulated gene	Position	Upregulated gene
A01	APEX1	C03	MGMT
A03	ATM	C05	MLH3
A05	ATXN3	C06	MM319
A12	DDB1	C07	MPG
B01	DMC1	C08	MRE11
B03	ERCC1	C10	MSH3
B04	ERCC2	C12	MSH5
B06	ERCC4	D02	MUTYH
B09	ERCC8	D03	NEIL1
B12	LIG1	D04	NEIL2
C01	LIG3	D08	PARP1
CO2	LIG4	D09	PARP2

Position	Upregulated gene	Position	Upregulated gene
D10	PARP3	F08	SLK
D12	PM52	F10	TDG
E02	POLB	F11	TOP3A
E09	RAD23B	F12	TOP3B
E12	RAD51B	G03	XAB2
F01	RAD51C	G04	XPA
F02	RAD51D	G10	XRCC5
F03	RAD52	G12	XRCC6BP1
F06	RPA1		

C

Position	Down-regulated gene	Position	Down-regulated gene
A4	ATR	E6	RAD18
A8	BRIP1	E11	RAD51
A9	CCNH	F4	RAD54L
A11	CDK7	F5	RFC1
B10	EX01	F7	RPA3
B11	FEN1	G1	TREX1
C4	MLH1	G2	UNG
C9	MSH2	G7	XRCC1
E3	POLD3	G8	XRCC3
E5	PRKDC	G9	XRCC6

Figure 6.27: Expression of DNA repair genes. A) Heat map showing DNA repair gene expression by RT2 profiler in PEO1 and PEO1R cells. B) List of up-regulated genes in PEO1 and PEO1R cells. C) List of down-regulated genes in PEO1 and PEO1R cells. Red colors in the heat map indicate up-regulated genes, while green indicate down-regulated genes.

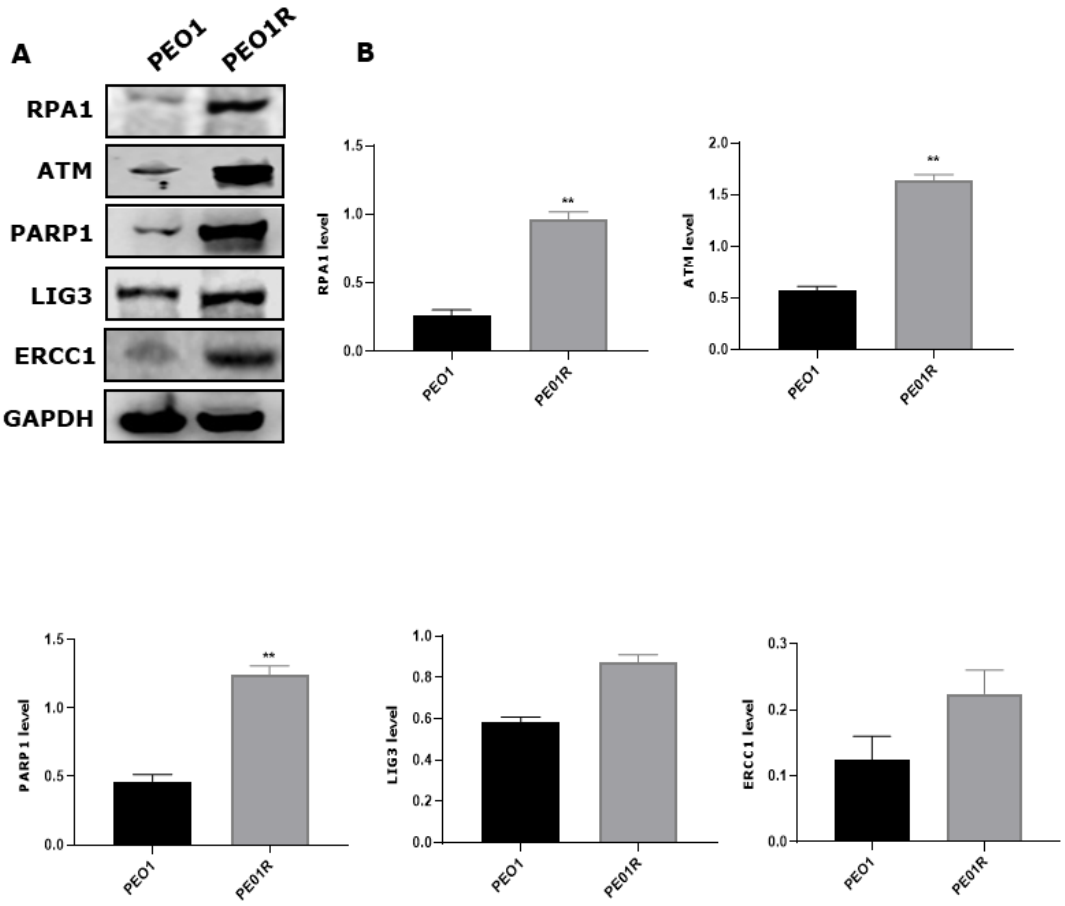

Figure 6.28: DNA repair protein levels in PEO1 and PEO1R cells. A) Representative western bolt. RPA1, ATM, PARP1, LIG3 and ERCC1 were overexpressed in PEO1R cells compared to PEO1 cells. B) Quantification of RPA1, ATM, PARP1, LIG3 and ERCC1 levels in PEO1 cells and PEO1R cells. **p < 0.01, calculated by student's t-test.

6.5.4 MRE11 PHYSICALLY INTERACTS WITH AND PROMOTES OCT4 STABILITY

The data presented so far suggests that the development of resistance to a chemical inhibitor of MRE11 leads to transcriptional up-regulation of DNA repair genes. OCT4 is a POU-homeodomain transcription factor which can be recruited to sites of DNA damage and regulate the expression of DNA repair genes. In addition, a previous bioinformatics study showed that the expression of several DNA repair genes, including MRE11, were associated with OCT4 activity (Campbell et al., 2007). We asked whether OCT4 interacts physically with MRE11. To answer this question, we used a co-immunoprecipitation assay to test whether there is a physical interaction between OCT4 and MRE11. PEO1R and PEO1R_MRE11_KD cells lysates were incubated with MRE11 antibody overnight, then conjugated to A/G magnetic beads, washed and eluted and OCT detected by western blot. OCT4 and MRE11 physically interacted with each other (Figure 6.29).

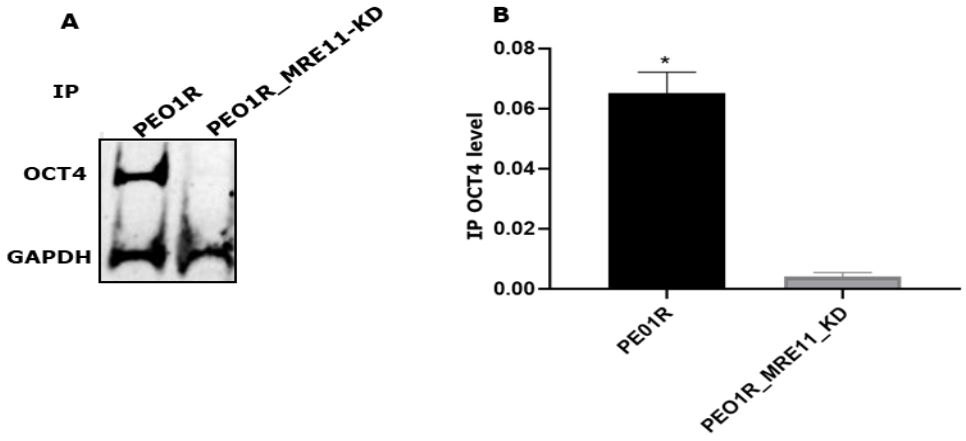

Figure 6.29: Physical interaction between MRE11 and OCT4. A) Representative western blot with co-immunoprecipitation of OCT4 and MRE11. OCT4 interacted with MRE11 in PEO1R cells, while no interaction was detected in PEO1R_MRE11_KD cells. B) Quantification of OCT4 in PEO1R and PEO1R_MRE11_KD cells. *$p < 0.05$, calculated by student's t-test.

When MRE11 was depleted in PEO1R cells using siRNA and checked the protein levels of OCT4, we surprisingly observed a remarkable decreased in OCT4 in PEO1R_MRE11_KD compared to scrambled controls (Figure 6.31), which was also correlated with reduced expression of CD44, RPA1, ATM, PARP1, LIG3 and ERCC1 compared to PEO1R cells (Figure 6.32).

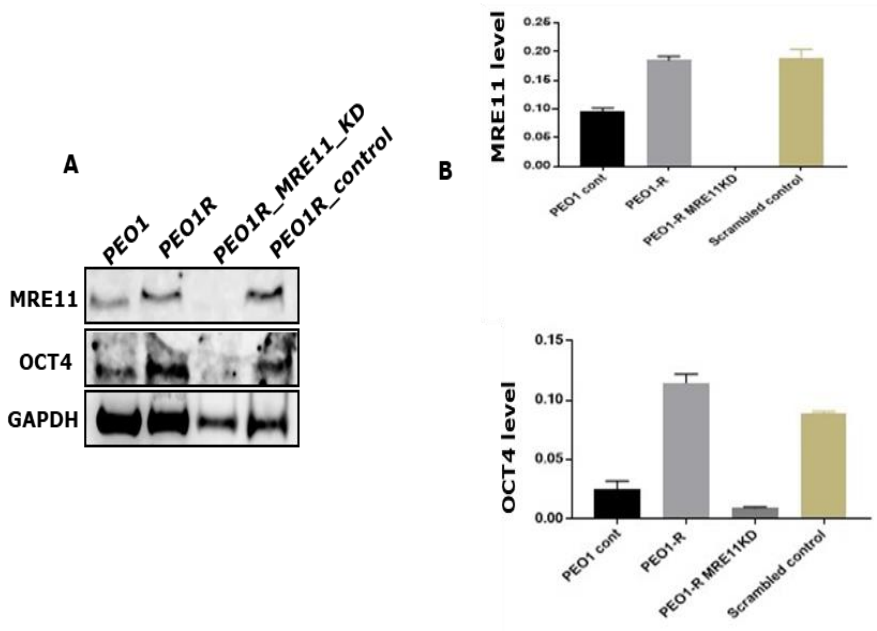

Figure 6.30: MRE11 and OCT4 protein levels in PEO1, PEO1R, PEO1R_MRE11-KD and PEO1_scramble cells. A) Representative western blot. Low expression of MRE11 and OCT4 were seen in PEO1 cells, with high expression of MRE11 and OCT4 in PEO1R cells compared to PEO1 cells. The knockdown of MRE11 in PEO1R_MRE11_KD cells decreased the OCT4 level. The PEO1R scrambled control showed high MRE11 and OCT4 level. B) Quantification of MRE11 and OCT4 levels.

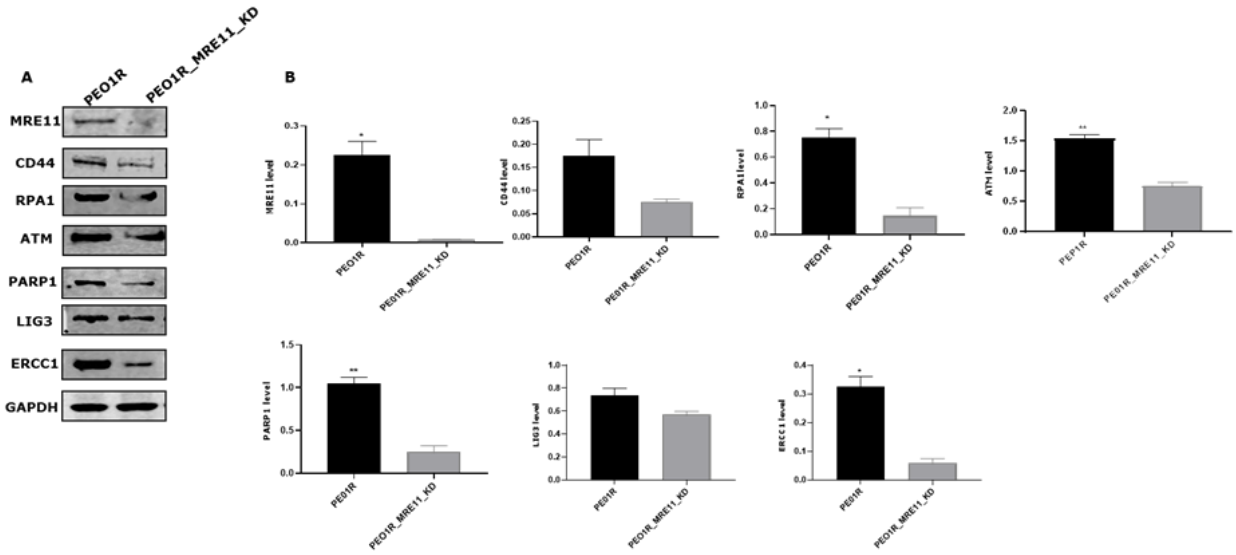

Figure 6.31: MRE11, CD44, RPA1, ATM, PARP1, LIG3 and ERCC1 protein levels in PEO1R and PEO1R_MRE11_KD cells. A) Representative western blot. MRE11, CD44, RPA1, ATM, PARP1, LIG3 and ERCC1 had reduced levels in PEO1_MRE11_KD cells compered to PEO1R cells. B) Quantification of MRE11, CD44, RPA1, ATM, PARP1, LIG3 and ERCC1 levels. *p < 0.05; **p < 0.01, calculated by student's t-test.

The data indicated that MRE11 could promote OCT4 stability and regulate DNA repair gene expression. To evaluate whether OCT4 stability is impaired through proteasome mediated degradation in PEO1R _MRE11 KD cells, we preformed protein degradation assay. PEO1R and PEO1R_MRE11_KD cells were seeded overnight. In the following day, cells were treated with 100 µg/mL Cycloheximide (protein synthesis inhibitor) for 4 hours and then treated with MG123 inhibitor (proteasome inhibitor) at several time points. In untreated cells, at baseline, OCT4 levels were low in PEO1R_MRE11_ KD cells

compared to PEO1R control cells. After 4 hours of cycloheximide treatment followed by MG132 treatment, accumulation of OCT4 levels was evident at 1 hour and 3 hours in PEO1R_MRE11_ KD cells compared to PEO1R control cells. Polyubiquitination of OCT4 may result in proteasome mediated degradation of OCT4 protein (Figure 6-33). We therefore performed an ubiquitination assay to investigate whether MRE11 knockdown induces polyubiquitination of OCT4. For ubiquitination assay PEO1R control cells and PEO1R_MRE11_KD cells were transfected with a plasmid carrying ubiquitin tagged HA as described previously (Ali et al., 2019b). Lysates were then incubated with OCT4 antibody, conjugated with A/G magnetic beads, protein eluted and immunoblotted with anti-HA antibody (Figure 6-34). MRE11 knock down in PEO1R_MRE11_KD cells resulted in greater polyubiquitination of OCT4 compared to control PEO1R cells.

To evaluate the clinicopathological significance of OCT4 and MRE11 co-expression, we preformed IHC in OC clinical cohorts. Patients with tumours had high OCT4 and high MRE11 co-expression showed poor OS ($p=0.021$) compared to tumours that were low OCT4 and low MRE11 co-expression (Figure 6.35).

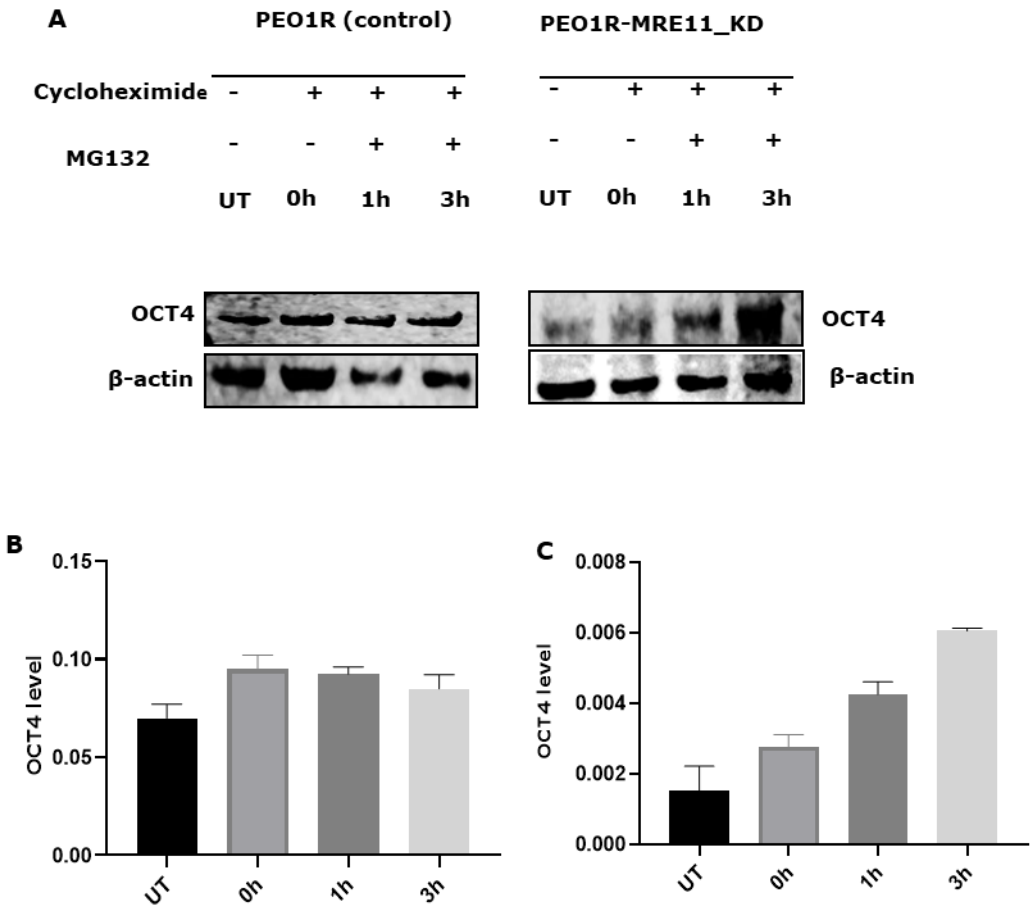

Figure 6.32: Proteasome mediated OCT4 degradation in PEO1R control and PEO1R_MRE11_KD cells. A) Protein stability assay in PEO1R and PEO1R_MRE11_KD cells. In untreated cells, at baseline, OCT4 levels were high in PEO1R control cells compared to PEO1R_MRE11_ KD cells. In PEO1R cells, no change in OCT4 baseline level was observed either before or after MG123 treatment. While in PEO1R_MRE11_KD cells, there was a notable accumulation of OCT4 base line level after one and three hours of MG123 treatment. B) Quantification of OCT4 levels in PEO1R cells. C) Quantification of OCT4 levels in PEO1R_MRE11_KD cells. UT= untreated cells

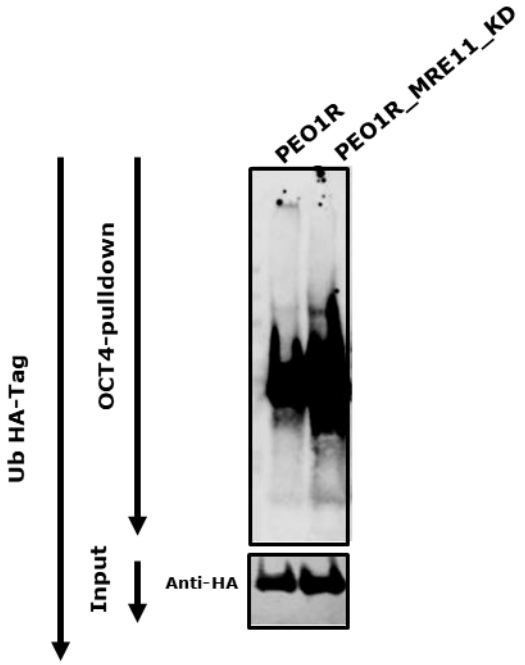

Figure 6.33: Ubiquitination assay in PEO1R control and PEO1R_MRE11_KD cells. Cells were transfected with a plasmid carrying ubiquitin tagged HA (see chapter two Page 119 for more details). Lysates were then incubated with OCT4 antibody, conjugated with A/G magnetic beads, protein eluted and immunoblotted with anti-HA antibody.

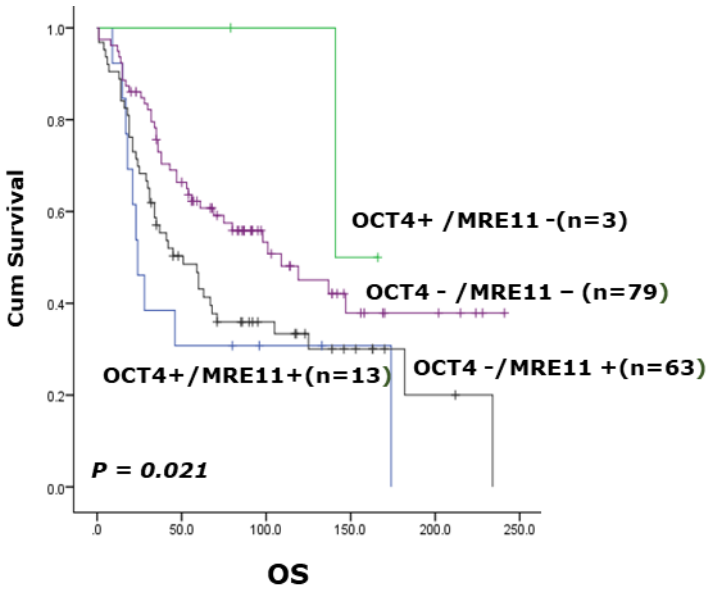

Figure 6.34: Kaplan Meier survival curve for OCT4 and MRE11 co-expression. Kaplan Meier statistical analysis was used to conduct a univariate analysis of OS against OCT4and MRE11 expression. In OS, High OCT/High MRE11 expression (blue lines) is significantly associated with poor OS.

Collectively, the data provides evidence that MRE11 not only physically interacts with OCT4 and regulate proteasome mediated degradation of OCT4 but MRE11-OCT4 co-expression could have prognostic significance in EOC patients.

6.5.5 THE OVEREXPRESSION OF MRE11-OCT4 ENHANCES A CANCER STEM CELL-LIKE AGGRESSIVE PHENOTYPE

Cancer stem cells (CSCs) have increased proliferative potential (Yu et al., 2012). OCT4 has vital roles in self renewal, maintenance of stem cell pluripotency and lineage commitment (Shi and Jin, 2010). During the work with PEO1R cells, we speculate that PEO1R cells would have a CSC phenotype. We investigated the expression of key stem cell markers (SOX2, ALDHA1, NANOG, CD44 and OCT4) in PEO1 and PEO1R cells. While SOX2 or ALDH1 or NANOG levels were not changed, we observed significant overexpression in CD44 and OCT4 transcription factor in PEO1R cells compared to PEO1 cells (Figure 6.36). To confirm CD44 overexpression in PEO1R, we preformed FACS to monitor CD44 expression. FACS data confirmed that CD44 overexpressed in PEO1R cells compared to PEO1 cells (Figure 6.37). To also confirm the expression of OCT4, we conducted IF microscopy. Results showed that nuclear OCT4 overexpression in PEO1R cells compared to PEO1 cells (Figure 6.38).

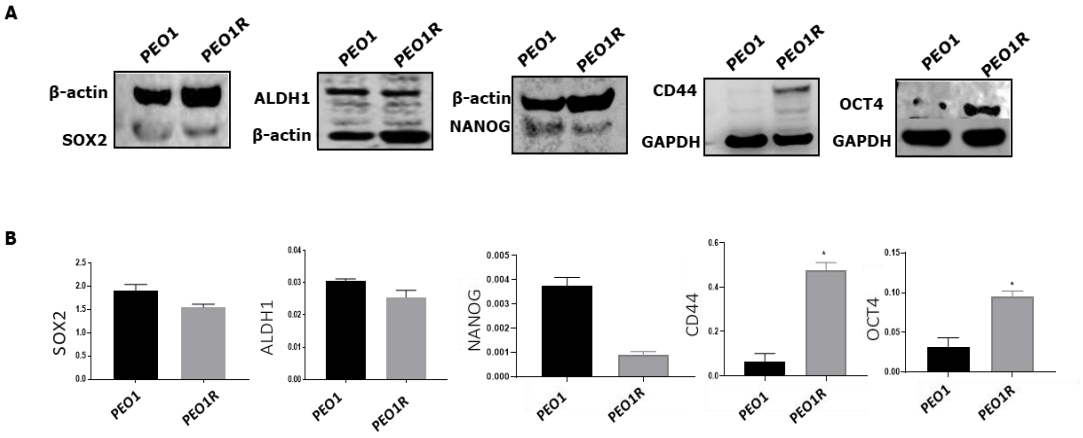

Figure 6.35: SOX2, ALDH1, NANG, CD44 and OCT4 protein levels in PEO1 and PEO1R cells. A) Representative western bolt. No difference was observed in SOX2, ALDH. NANOG levels decreased in PEO1R cells compared to PEO1 cells. CD44 and OCT4 were overexpressed in PEO1R cells compared to PEO1 cells. B) Quantification of SOX2, ALDH1, NANG, CD44 and OCT4. *p < 0.05, calculated by student's t-test.

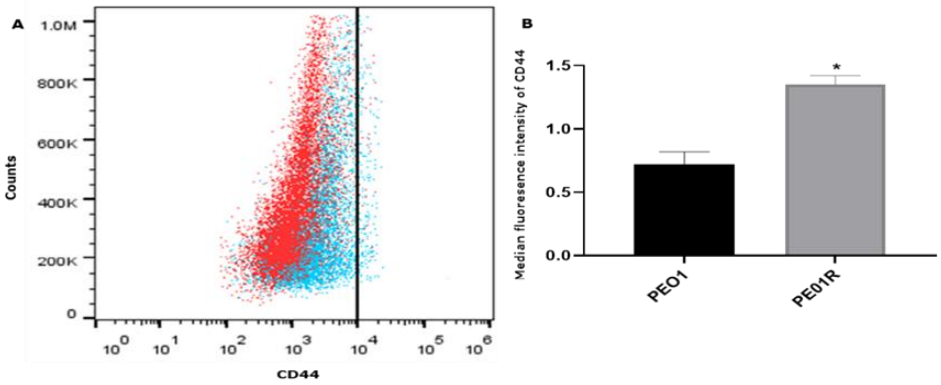

Figure 6.36: FACS analysis of CD44 expression in PEO1 and PEO1R cells. A) CD44 expression in PEO1R cells (blue) and PEO1 cells (red). Unconjugated C44 primary antibody and anti-rabbit IgG secondary antibody (Alexa Fluor® 488) were used. B) Quantification of median fluorescence intensity of CD44. Figure was generated using FlowJo software. *p < 0.05, calculated by student's t-test.

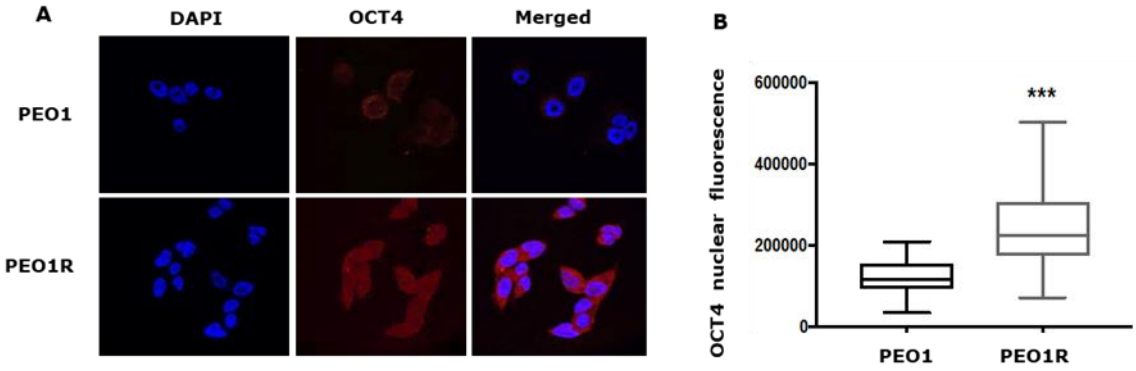

Figure 6.37: Immunofluorescence staining for OCT4 in PEO1 and PEO1R cells. A) Images of OCT4 nuclear expression. OCT4 nuclear expression was significantly increased in PEO1R cells compared to PE01 cells. B) Quantification of OCT4 nuclear fluorescence. ***p < 0.001, calculated by student's t-test.

PEO1R was highly proliferated during the experiments compared the parental cell line, PEO1. A proliferation assay demonstrated that PEO1R cells had a significantly higher proliferative capacity than that of PEO1 cells (Figure 6.39), a phenotype consistent with CSCs.

In 3D spheroids models, which enrich for cells with CSCs-like phonotype, we noticed not only vigorous spheroid forming capacity in PEO1R cells, but PEO1R spheroids were also significantly larger in size than PEO1 spheroids (Figure 6.40).

While controversial, aberrantly the activation of EMT might be a marker of a CSC phenotype (Kong et al., 2011, Shibue and Weinberg, 2017). Phenotypically, PEO1R showed spindle-shaped cells with elongated cellular process compared to PEO1 cells (Figure 6.41).

We tested EMT in PEO1 cells and PEO1R cells. In invasion assay, PEO1R cells were significantly more invasive than PEO1 cells (Figure 6.42). The switching of cadherin, a hallmark of EMT, was evident in PEO1R cells. N-cadherin was upregulated while E-cadherin was downregulated in PEO1R cells compared to PEO1 cells (Figure 6.43).

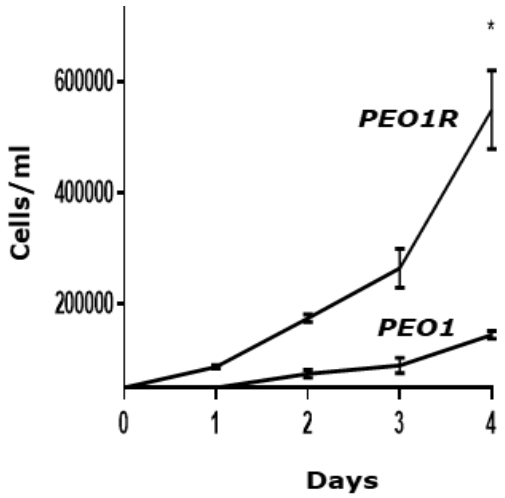

Figure 6.38: Proliferation capacity of PEO1 and PEOR cells. 5x10^4 of PE01 and PE01R cells were seeded in duplicates into 6-well plates overnight. Cells were trypsinized and counted each day for 4 days. *p < 0.05, calculated by student's t-test.

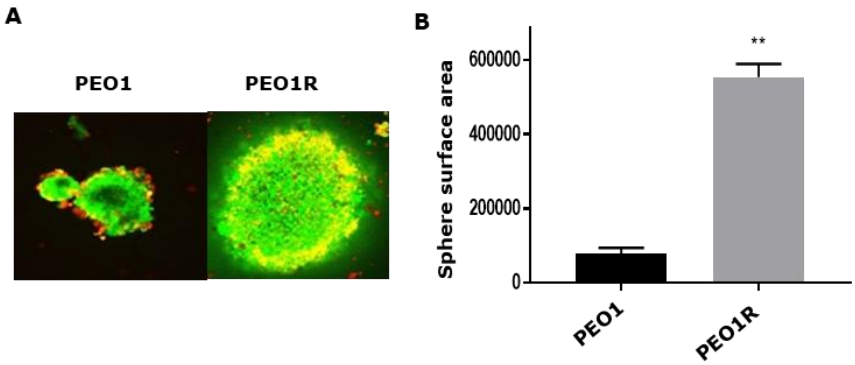

Figure 6.39: Representative photomicrographic images of PEO1 and PEO1R spheroids. A) PEO1R spheroids were robust spheroids and larger in size compared to PEO1 spheroids. B) The measurement of sphere surface was done by imageJ software, and graph was generated by GraphPad Prism. **p < 0.01, calculated by student's t-test.

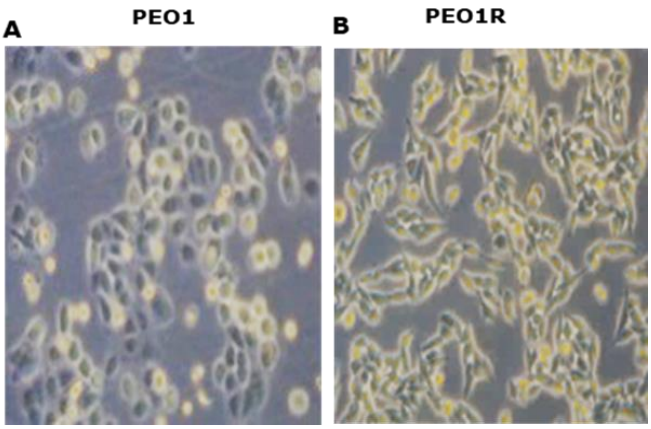

Figure 6.40: PEO1 and PEO1R Morphology. Cells were photographed growing in 2D attached culture conditions and visualized under 20× magnification. A) PEO1 cells showed islands of uniform polygonal cells. B) PEO1R cells were spindle-shaped cells with elongated cellular process (a feature of EMT).

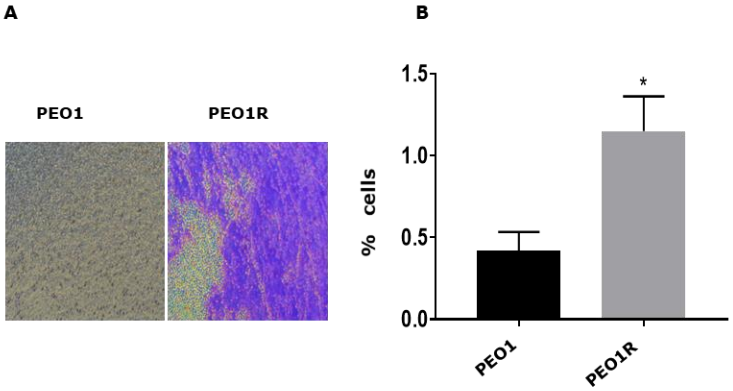

Figure 6.41: Invasion assay showing of PEO1 and PEO1R cells. Invasive cells were stained by crystal violet, extracted and then read at wavelength 560 nm for more details see chapter 2 (P.112-112). A) Representative photomicrographic images of invasion assay. PEO1R cells more invasive compared to PEO1 cells. Images were taken by a light microscope. B) Quantification of invasive cells in PEO1 and PEO1R. *$p < 0.05$, calculated by student's t-test.

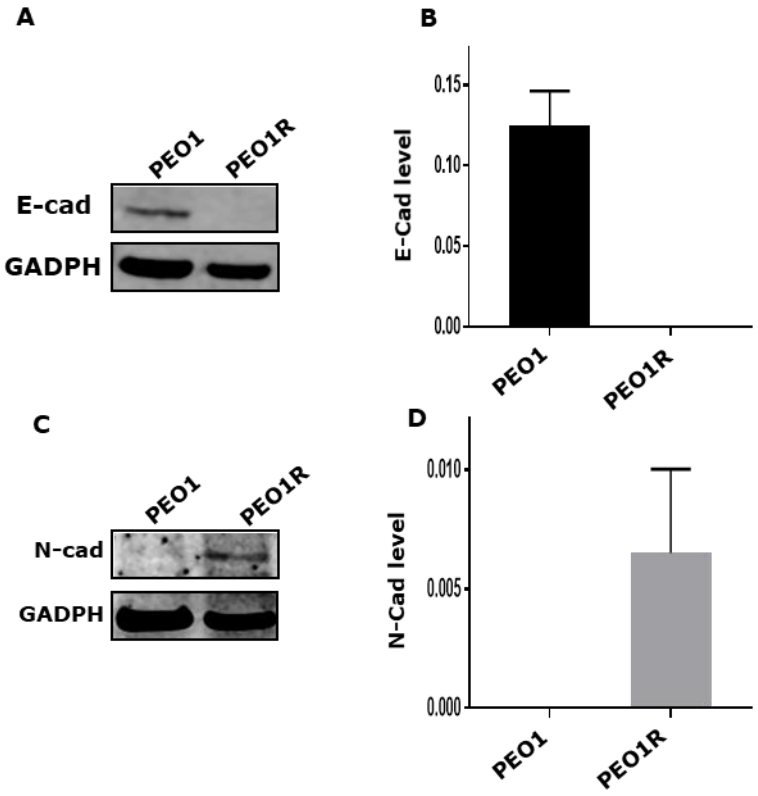

Figure 6.42: E-cadherin and N-cadherin levels in PEO1 and PEO1R cells. A) Representative western bolt showing E-cadherin (E-cad). E-cad levels were presented in PEO1 cells while was low or undetectable levels in PEO1R cells. B) Quantification of E-cad in PEO1 and PEO1R cells. C) Representative western blot of N-cadherin (N-cad). N-cadherin levels were detectable in PEO1R cells but undetectable in PEO1 cells. D) Quantification of N-cadherin in PEO1 and PEO1R cells.

To further validate these results, we performed RT-PCR to evaluate gene expression of several EMT markers. Data showed a significant reduction in *CDH1* (the gene that encodes E-cadherin), increased *VIM* (the gene that encodes vimentin) and increased *ZEB1* mRNA levels in PEO1R cells compared to those in PEO1 cells (Figure 6.44). ZEB1, in addition to its role in EMT, has been shown to promote CSC properties. We observed a 300-fold increase in the expression of *ZEB1* mRNA in PEO1R compared to parental PEO1 cells.

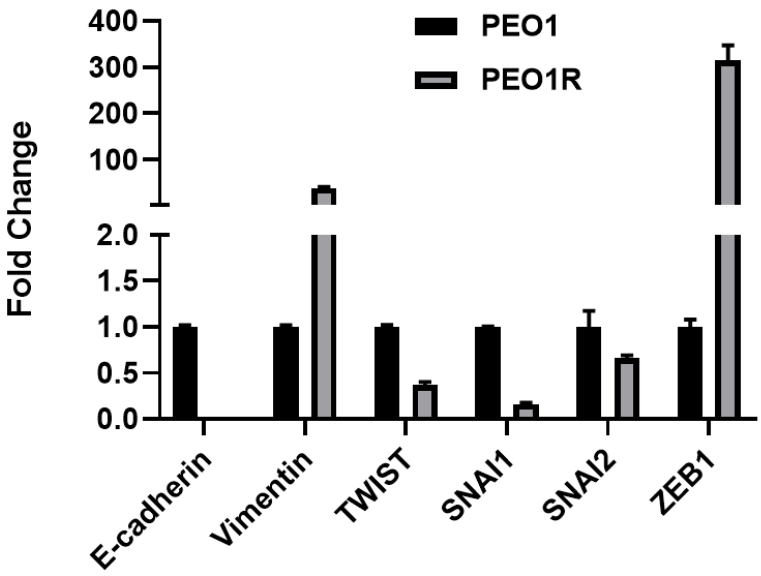

Figure 6.43: Gene expression analysis of EMT markers assessed by RT-PCR. Protocol is described in chapter 2 page 113-118. PEO1R cells had a significant reduction of *E-cad* mRNA. *TWIST*, *SNAL1* and *SNAL2* mRNA levels decreased in PEO1R cells compared to PEO1 cells. *Vimentin* and *ZEB1* mRNA levels significantly increased in PEO1R cells compared to PEO1 cells.

We then conducted *in vivo* tumorigenicity xenograft studies to confirm CSC phenotype. PEO1 and PEO1R cells were subcutaneous injected into the left flank of immunodeficient CD-1 NuNu mice at three dose levels of 2 x 10^{5} cells SC, 1 x 10^{6} cells SC and 2 x 10^{6} cells SC. Three mice were implanted per cell concentration for each of the two cell lines. Tumour establishment and growth was measured twice weekly and animals weighed weekly. As shown in Figure 6.45, the tumour volume was substantially higher in PEO1R bearing immunodeficient CD-1 NuNu mice compared to PEO1 bearing immunodeficient CD-1 NuNu mice. We also confirmed transcriptional overexpression of *E-cadherin*, *Vimentin*, *ZEB1* and *OCT4* in PEO1R bearing SCID mice compared to PEO1 bearing SCID mice (Figure 6.46).

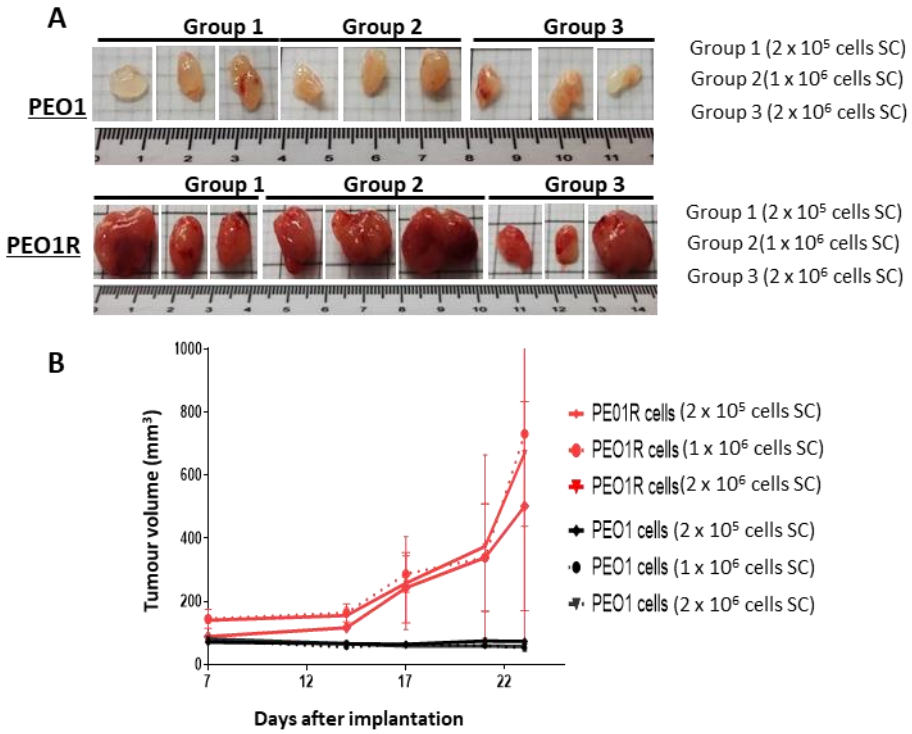

Figure 6.44: PEO1 and PEO1R tumors in immunodeficient mice. A) Isolated tumors. Tumour volume was monitored after injecting mice with PEO1 and PEO1R cells. The tumour volumes were substantially greater in PEO1R bearing immunodeficient CD-1 NuNu mice compared to PEO1 bearing immunodeficient CD-1 NuNu mice. B) Comparison of tumour progression.

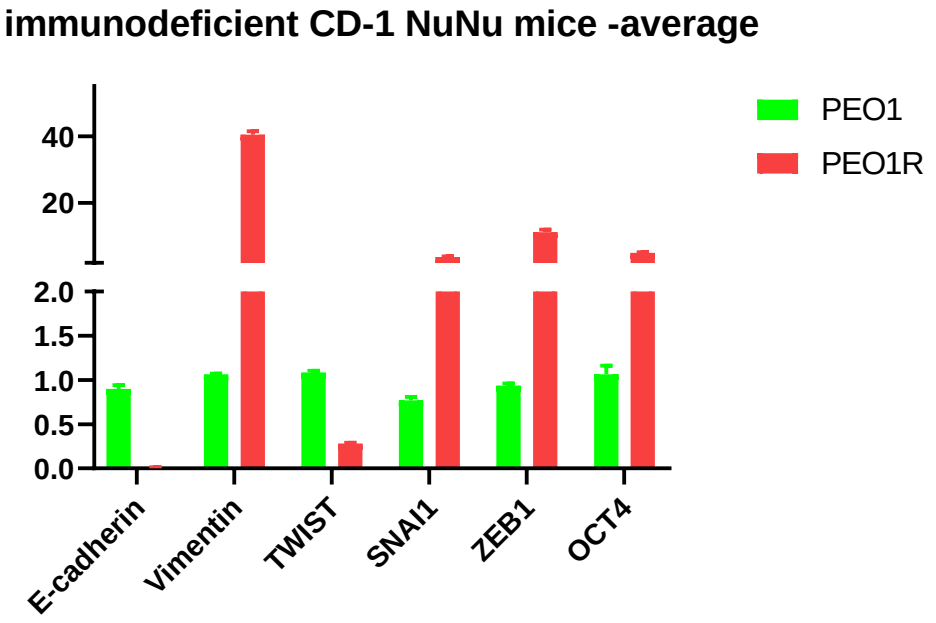

Figure 6.45: Gene expression analysis of E-cadherin, Vimentin,Twist, Snal1, ZEB1 and OCT4 assessed by RT-PCR. *E-cadherin* was signifcanlyly decreased in PEO1R bearing immunodeficient CD-1 NuNu mice compared to PEO1 bearing immunodeficient CD-1 NuNu mice, while *Vimentin*, *Snal1*, *ZEB1* and *OCT4* significantly overexpressed in PEO1R bearing immunodeficient CD-1 NuNu mice compared to PEO1 bearing immunodeficient CD-1 NuNu mice.

6.6 RESULTS SUMMARY

- Pre-clinical data revealed that the blockade of MRE11 exo-nuclease activity is a promising strategy for SL in 2D and 3D BRCA2-deficient cancers.
- Clinical data showed that OC Patients whose tumours had high BRCA2 and high MRE11 co-expression had the poor PFS (p=0.005) and poor OS (p= 0.001) compared to tumours that had low BRCA2 and low MRE11 co-expression.
- Pre-clinical results demonstrated that mirin is synthetically lethal in 2D and 3D XRCC1-deficient cancer cells.
- Clinical data showed that OC Patients whose tumours had high XRCC1 and high MRE11 co-expression had the short PFS (p=0.014) poor OS (p= 0.017) compared to tumours that had low XRCC1 and low MRE11 co-expression.
- We successfully established a stable mirin-resistant PEO1 cells (PEO1R).
- PEO1R cells were cross resistance to cisplatin and olaparib.
- PEO1R cells were overexpress MRE11 and several DNA repair genes.
- OCT4 interacts with MRE11 (MRE11 promotes OCT4 stability and aggressive human ovarian cancers), regulates DNA repair expression, influences platinum/mirin sensitivity and is a feature of aggressive human OCs.

- MRE11-OCT4 overexpression in PEO1R cells promotes a cancer stem cell-like aggressive phenotype.

6.7 DISCUSSION

The recent approval of PARPi for clinical application in breast and OC patients that harbour BRCA mutations has re-energized the DNA repair treatments field. However, the acquired resistance to PAPRi will also impact the clinical use of PARPi. Hence, the development of an alternative SL strategy is crucial. ATM kinase inhibitor, WEE1 inhibitor and ATR kinase inhibitor are currently in early phase in clinical trials (Alblihy et al., 2019).

In this study we provide a comprehensive preclinical evidence that mirin treatment is selective toxic in BRCA2-deficient OC cells including 3D-spheriods models. This toxicity was correlated with accumulation of DSB, cell cycle arrest and increased apoptosis. We proposed here a working model for MRE11 blockade as SL strategy in BRCA2-defecient OC cells as follows: First, the DNA repair in BRCA2-deficent cells will be dependent on MRE11-ATM pathway as an alternative pathway for DSB repair to survive. MRE11 inhibition using mirin will prevent the activation of ATM (Dupre et al., 2008), leading to a block of the alternative pathway for DSB repair. This will result in increased DSB accumulation, cell cycle arrest and increased apoptosis. Second, MRE11 play pivotal role during restart of stalled replication forks. BRCA2 also has role in protecting stalled replication fork from degradation by MRE11 exonuclease activity (Ying et al.,

2012). MRE11 is hyperactivated in BRCA2-deficient cells to promote survivals (Schlacher et al., 2011b). Mirin inhibit MRE11 exonuclease activity leading to replication stress, DSB accumulation and apoptosis. Ying et al. reported that mirin selectively killed BRCA2-deficent Chinese hamster cells compared to same cells that were BRCA2-proficent (Ying et al., 2012). MRE11 was found to be hyperactive in BRCA2-defecient and PARP-inhibited cells due to the failure in protecting stalled replication fork by BRCA2 and PARP, which opens new doors for blocking MRE11 to target cancers (Ying et al., 2012, Schlacher et al., 2011b).

We also showed that mirin therapy selectively killed XRCC1-deficient OC cells including 3D-spheriods models. Mirin toxicity in XRCC1-deficient OC cells was correlated with accumulation of DSB, cell cycle arrest and increased apoptosis. A model for SL interaction between XRCC1 and MRE11 is suggested as follow: First, XRCC1 functions as a scaffold protein interacted with several proteins involved in BER and SSBR such as PARP1 and LIG III (Ali et al., 2019a). XRCC1 is needed for the repair of unresected stalled replication forks which enhanced cell survivals (Ying et al., 2016). MRE11 recruitment is mediated by PARP1 in stalled replication forks that require XRCC1 mediated repair (Ying et al., 2012, Ying et al., 2016). Therefore, MRE11 inhibition in XRCC1-defiecent cells might enhanced replication stress, accumulation of DSB and apoptosis.

Second, XRCC1-deficient cells generate single strand breaks (SSBs) which eventually converted to DSB during replication (Sultana et al., 2013a). MRE11 is required for DSBs repair. Accordingly, MRE11 inhibition will lead to DSB accumulation, cell cycle arrest and increased apoptosis.

The potential of a 3D spheroids system for the development of novel anticancer approaches has been shown overtime (Hirschhaeuser et al., 2010). However, the variation of spheroids sizes formed by different cell lines could affect data interpretation specifically in relation to drug response where drug penetration may differ. Using large spheroids (>500 μm in diameter) for drug toxicity studies could help increasing the accuracy of data. Large spheroids consist of an outer proliferating zone, an internal quiescent zone resulting from limited oxygen, nutrients and metabolites distributions and a necrotic core resembling the heterogeneity in solid in vivo tumours. Large spheroids were shown to be more resistant due to the hypoxic centres that lead to decreased drug diffusion, and altered PH which might change drug activity and increased efflux pump. For these reasons careful attention should be paid in designing 3D spheroids experiments. There are several 3D culture methods and cytotoxicity assays can be applied based on the researcher's needs (Zanoni et al., 2016, Mehta et al., 2012).

Development of primary or acquired resistance to PARP inhibitors (such as olaparib, talazoparib, niraparib, rucaparib) is an emerging clinical problem in BRCA germ-line deficient or platinum sensitive ovarian cancers. Restoration of homologous recombination (HR) [reactivation of BRCA function, inactivation of 53BP1, down regulation of PARP1] and restoration of stalled replication fork protection are important mechanisms of PARP inhibitor resistance. As additional DNA repair inhibitors (such as those targeting MRE11) evolve in cancer therapeutics, evaluation of mechanisms of resistance to newer class of DNA repair inhibitors become a high priority (Sakai et al., 2009, Barber et al., 2013, Edwards et al., 2008, Norquist et al., 2011, Swisher et al., 2008, Bitler et al., 2017, Noordermeer and van Attikum, 2019, Kim et al., 2017b). We made several novel observation in PEO1R cells compared with PEO1 cells. Interstingly, no restoration of BRCA2 expression in PEO1R cells was observed. MRE11 overexpression and 53BP1 incativation were an essential driver for the acquired ressitace in PEO1R cells. It has been shown that loss of 53BP1 lead to PARPi resistance in BRCA1-deficient mouse mammary tumours (Jaspers et al., 2013). Moreover, up-regulation of multiple genes invloved in BER, NER, MMR and HR pathways was observed in PEO1R cells compared to PEO1 cells.

More importantly, PEO1R cells were also cross resistance to cisplatinand and PARP inhibitor olaparib.This new finding suggests that the development of cross resistance might be a significant clinical issue as new DNA repair inhibitors enter clinical trails beyond PAPRi.

Cancer stem cell (CSC) comprise a subgroup of cancer cells that can self-renew, initiate tumours *in vivo,* and dictate invasion and metastasis. Several cell-surface markers have been reported that may help in identifying CSC including CD44, CD24, CD133 and CD177 (Pattabiraman and Weinberg, 2014, Jaggupilli and Elkord, 2012). Tissue culture derived or patient derived CSCs manifest an enhanced DNA repair capacity and thus resistance to chemotherapy and radiotherapy (Phi et al., 2018). Lung cancer CSCs and glioblastoma CSCs have been demonstrated to promote the capacity of HR and NHEJ (Vitale et al., 2017). Furthermore, glioblastoma CSCs showed increased PARP1 activity (Venere et al., 2014). Breast CSCs were associated with APE1 up-regulation (Karimi-Busheri et al., 2010). In addition, CD117/CD44 CSCs ovarian cancer CSCs showed promoted DNA polymerase eta (POLH) (Srivastava et al., 2015). In this work, we showed that the isolation of mirin and cisplatin resistance PEO1R cells manifest a stem cell-like phonotype. CSCs phenotype of PEO1R is supported by CD44 expression.

PE01R cells demonstrate a low level of NANOG. NANOG is a transcriptional factor which has a role in ensuring self-renewal of embryonic stem cells and maintaining pluripotency (Pan and Thomson, 2007). It is interesting to note that there was a differential expression of stem cell markers but in the literature, such expression is quite commonly reported. For example, clonogenic potential and tumour formation capacity of CSCs in human colorectal cancer (CRC) could be promoted by increased NANOG1 expression (Ibrahim et al., 2012a, Zhang et al., 2013b). The variation in the expression of cancer stem cell markers reflects the complex interaction happening in the cells which determent stem cell phenotype.

More importantly, PEO1R cells overexpress OCT4. OCT4 is a transcriptional factor which has a vital role in self-renewal, pluripotency and lineage commitment (Han et al., 2014). A recent study showed that OCT4 has a key role in tumorigenesis, treatment resistant and prognosis (Villodre et al., 2016). Several studies showed that OCT4 is correlated with DNA damage response (DDR) of cancer cells towards irradiation (Ventela et al., 2015, Shen et al., 2014). A previous bioinformatics study showed that the expression of several DNA repair genes including MRE11, to be associated with OCT4 (Campbell et al., 2007).

In the current study, a novel observation was that OCT4 physically interacted with MRE11. MRE11 also stabilised OCT4 expression and MRE11 depletion promoted proteasome mediated OCT4 degradation. Human WWP2, an E3 ubiquitin ligase has been shown to interact with OCT4 to regulate OCT4 protein level through proteasome mediated degradation in human embryonic stem (Xu et al., 2009). Whether MRE11 operates at this interface will be an interesting area for future investigation. The depletion of MRE11 in PEO1R cells also reduced expression of several DNA repair protein involved in HR and BER. It would be interesting to study whether OCT4 depletion using siRNA could lead to decrease the expression of MRE11 and other DNA repair genes.

Collectively, the data would support our hypothesis that PEO1R cells not only overexpress MRE11 and other DNA repair genes but also OCT4 which enhances the development of a CSCs phenotype.

PEO1R cells had a significantly higher proliferative capacity than that of PEO1 cells, a phenotype consistent with CSCs. PEO1R spheroids were also significantly larger in size than PEO1 spheroids. PEO1R cells were also significantly more invasive than PEO1 cells. However, the invasion assay did not take account of the different proliferation rates of the two cell lines. To accurately assess the invasion capacity

of PEO1 and PEO1R cells, we should perform the invasion assay below the doubling time of these cells, such as at 6-8 hours.

PEO1R cells also displayed a significant reduction in mRNA level of *E-cadherin* and low levels of *Twist* and *SNAIL1/2*. *In vivo*, *SNAIL1* was significantly higher in PEO1R bearing immunodeficient CD-1 NuNu mice compared to PEO1 bearing immunodeficient CD-1 NuNu mice. We did not confirm the mRNA level of *SANIL2* in vivo. It is worth checking. The mRNA level of *Twist* was lower in PEO1R bearing immunodeficient CD-1 NuNu mice compared to PEO1 bearing immunodeficient CD-1 NuNu mice. The variable expression in *Twist* might reflect the complex interaction occur in the cells which switch of the EMT program. Further investigations are needed to illustrate the low levels of Twist PEO1R cells. PEO1R cells showed increased ZEB1 and increased Vimentin. Reduction of E-cadherin is a critical event for EMT in the development of embryonic and cancer progression. Up-regulation of ZEB1 coincided with E-cadherin downregulation in both mRNA level and protein level during EMT (Eger et al., 2005). Owing to the crucial role of ZEB1 in the suppression of E-cadherin, ZEB1 functions as a key driver of EMT and cancer progression (Zhang et al., 2014, Peinado et al., 2007). Overexpression of ZEB1 has been reported in several cancers including pancreatic cancer (Wellner et al., 2010), uterine cancer (Spoelstra et al., 2006), lung cancer (Zhang et al., 2013c), breast

cancer (Eger et al., 2005), colon cancer (Zhang et al., 2013a) and gastric cancer (Okugawa et al., 2012). ZEB1 expression in these tumours associates with E-cadherin reduction and with advanced stages or metastasis, which show the relevance of ZEB1 and cancer progression. ZEB1 overexpression enhanced radioresistant in breast cell lines *in vitro* and *in vivo* (Zhang et al., 2014)

Vimentin overexpression has been reported in several epithelial cancers including gastrointestinal tumours, prostate cancer, breast cancer, CNS tumours, malignant melanoma and lung cancer. This overexpression in cancer was associated with increased tumour growth, invasion and poor prognosis (Satelli and Li, 2011).

A recent study has shown that OCT4 could upregulate the expression of ZEB1 and then enhance the EMT process in human rectal carcinoma cells (SW480). Depletion of ZEB1 can reverse the radiation-resistant of SW480 cells which induced by the overexpression of OCT4 (Shao et al., 2018). PEO1R cells also showed high expression of OCT4 and ZEB1. It would be interesting to explore the OCT4/ZEB1 interaction mechanism in OC cell lines and how this mechanism might play a role in the resistance in PEO1R cells.

In conclusion, the development of cross-resistance to olaparib inhibitor via the overexpression of HR proteins and the evolution of a CSC like-phenotype in PEO1R cells propose critical mechanistic insights into the development of resistance to emerging DNA repair targets such as those targeting MRE11 for personalization of OC therapy. However, more preclinical and xenograft experiments are required to validate mirin-BRCA2 and mirin-XRCC1 synthetic lethality approaches. In addition, further studies will be conducted to further elucidate the molecular interaction between MRE11 and OCT4 and how this interaction could lead to high tumour proliferation, invasion and resistance in PEO1R cells. Further experiments are also needed to highlight the possible molecular interaction between OCT4 and ZEB1.

CH 7

GENERAL DISCUSSION AND FUTURE DIRECTION



7. GENERAL DISCUSSION AND FUTURE DIRECTION

Epithelial ovarian cancer (EOC) is not a single disease, and it consists of different group of tumours that are classified based on distinguishing morphologic and genetic characteristics (Kim et al., 2012). As we began to comprehensively understand the aetiology and molecular mechanisms of EOC, the hope of a single agent that can effectively increase patients' survivals dissipates. A formidable clinical issue for EOC treatment is it is the presentation at advanced stage (Coleman et al., 2013). The search for clinically applicable screening tools has failed to identify factors that can accurately lead to early stage identification. As a result, women will continue to show non-specific symptoms at an advanced stage of EOC. We should realistically aim to change EOC from a silent killer to a chronic disease.

Surgery plays a vital role in EOC management, and it should be performed when complete cytoreduction can be achieved. Surgery is followed by the combination of platinum-taxane agents, and more recently, bevacizumab was added (Oza et al., 2015). However, patients with relapse still presented in the clinic due to the acquired resistance, which limits the available choice of agents. Polypharmacy with secondary agents has not revealed to be effective because of the toxic profile of most of these agents and advanced age and several comorbidities of patients lead to

reduce the use of the polypharmacy (Woopen et al., 2016, Oldak et al., 2019).

An effective treatment approach would be to select patient's treatment in the appropriate stage of EOC, and this selection is based on biomarkers for response. However, the implementation of this strategy is highly restricted due to our limited capability to precisely predict a treatment response and the availability of effectiveness agents. A deep understanding of response and resistance mechanisms to the standard chemotherapy and novel agents would not only facilitate our ability to predict and monitor the development of resistance and clinical relapse but also would help in the selecting of the most suitable novel agents for treatment, which might benefit survivals.

Platinum-based chemotherapy has been used as a first-line treatment for EOC. Although initial responsiveness to platinum-based treatment is high (60-80%), more than 70% of advanced stage EOC patients relapse, and even in stage I or II the relapse rate is 20%-25% due to platinum resistant (Huntoon et al., 2013, van Zyl et al., 2018, Ushijima, 2010b). The recent approval of PARP inhibitors (PARPi) for use in a clinical setting in BRCA mutated ovarian cancer (OC) has re-energised DNA repair targeted therapy field. However, 40%-70% of patients do not respond to PARPi, which makes an adverse clinical impact (Jiang et al., 2019). Therefore, the development of alternative DNA

repair targets is crucial. The MRN complex is a key sensor of double strand break (DSBs) and is essential for the coordination of DNA damage response, DNA repair, cell cycle regulation and apoptosis (Syed and Tainer, 2018b). In this thesis, we provide comprehensive clinical and pre-clinical evidence that MRN complex targeting could a promising new approach to personalise EOC therapy.

7.1 MRN COMPLEX ASSOCIATES WITH PLATINUM RESISTANT IN EOC

In this work, we showed that the overexpression of MRE11, RAD50 and NBS1 was linked to aggressive OC with short progression free survival (PFS). However, we used tissue microarray (TMA) cores rather than full-face sections during the staining of MRN complex, but our cohort has been studied with different markers and using full-face and TMA sections. The concordance between full-face and TMAs sections was excellent (Abdel-Fatah et al., 2014c, Abdel-Fatah et al., 2013). Additionally, a validation slide had multiple pre-case TMA cores showing excellent concordance.

In colorectal cancer, MRN complex overexpression was linked to a poor response to radiotherapy and worse survival (Ho et al., 2018).

In gastric cancer patients receiving platinum therapy, overexpression of MRN complex was associated with a poor response and worse survival in patients (Altan et al., 2016). Similarly, Elevated MRE11 expression has been correlated with more malignant behaviour than normal MRE11 expression in breast cancer patients (Yuan et al., 2012).

Collectively, the clinical data provides evidence that MRN complex is a promising prognostic and predictive factor in cancer.

7.2 MOLECULAR DISRUPTION OF MRN COMPLEX ENHANCES PLATINUM CHEMO-SENSITIVITY IN OC CELL LINES

In whole lysate, MRN complex baseline level was significantly high in resistance cell lines (i.e. A2780cis and PEO4 cells) compared to sensitive cell lines (i.e. A2780 and PEO1 cells). We then preformed nuclear and cytoplasmic extraction to investigate the alteration in sub-cellular localization of MRN complex (see chapter 3, 4 and 5). The data indicate that the expression of MRN complex is subjected to sub-cellular localisation upon treatment of cisplatin in A2780cis and PEO4 cells.

Using siRNA to knockdown MRE11, RAD50 or NBS1 in A2780cis and PEO4 cells, we observed substantial sensitization to platinum chemotherapy. Increased sensitization was correlated with DSBs, cell cycle arrest and apoptosis.

Similarly, *in vitro*, cisplatin chemo-sensitization has also been observed in MRN depleted in cancer cells with increase DNA damage and the toxicity in cancer cells (Bian et al., 2019). Radio-sensitization was also evident in RAD50 depleted colorectal cancer cell lines (Chen et al., 2018).

To strengthen our results further, we should expand the screening for MRN complex levels, nuclear and cytoplasmic extraction, and the depletion experiments to other ovarian resistance cell lines including PEO6, OVCAR3 and SKOV3 cells. Furthermore, it is worth examining CRISPR-CAS9 to knockout MRN complex in A2780cis and PEO4 cells to validate our results. After obtaning a stable knockout of MRE11, RAD50 or NBS1, we then could progress to xengrafit mouse studies and 3D tumour spheroid models.

7.3 MRE11 BLOCKADE BY MIRIN INCREASES PLATINUM SENSITIVITY IN OC CELL LINES

Mirin, a small molecule inhibitor of 3’-5’ exonuclease activity of MRE11, blocks ATM activation without affecting ATM kinase activity

(Dupre et al., 2008, Shibata et al., 2014). We show that mirin treatment sensitized A2780cis and PEO4 cells to cisplatin. This sensitization was associated with DSBs, cell cycle arrest and apoptosis.

Previous study demonstrated that mirin can effectively increase radio-sensitivity in human glioblastoma cells, which suggest that mirin could be a potent radiosensitizer for glioma cells treatment (Mishima et al., 2014). In prostate cancer, mirin showed to inhibit the androgen-dependent transcription and cancer cells growth (Jividen et al., 2018). Recent study demonstrated that mirin promotes alkylating drug's efficacy in glioblastoma cells (Berte et al., 2016).

It would be interesting to conduct 3D tumour spheroid models from A2780cis and PEO4 cells and then monitor the effect of mirin and cisplatin combination therapy compared to cisplatin monotherapy on these spheroids. We can also preform xengrafit mouse studies using mirin in combination with cisplatin and cisplatin monotherapy by injecting A2780cis and PEO4 spheroids into mice. The study can be used alongside with MRE11 knockout xengrafit studies.

7.4 MIRIN IS SYNTHETICALLY LETHAL IN BRCA2-DEFICENT CELLS

Mirin therapy is selective toxic in BRCA2 deficient OC cell and BRCA2-deficient HeLa cells in both 2D cell lines model and 3D-spheroid models. Increased sensitivity was associated with DSB accumulation, cell cycle arrest and apoptosis. A model for synthetic lethal interaction between BRCA2 and MRE11 is proposed here as follows. First, BRCA2-deficient cells will be reliant on MRE11-ATM dependent alternative DSB repair pathways for survival. MRE11 blockade by mirin prevents ATM activation and block compensatory DSB repair leading onto DSB accumulation, cell cycle arrest and cell death. Second, MRE11 has an important role during re-initiation restart of stalled replication forks. BRCA2 also protects stalled replication forks from degradation by MRE11 exonuclease. In BRCA2-deficient cells, MRE11 is hyper-activated to promote survival (Schlacher et al., 2011b). MRE11 exonuclease blockade in BRCA2-deficient cells results in replication stress, DSB accumulation and cell death.

Additionally, PARP1 has an important role in the protection of stalled replication forks, which explains the molecular mechanism of synthetic lethality between PAPR1 and BRCA2. Interestingly, in PARP-inhibited cells, MRE11 is hyper-activated to promote survival (Ying et al., 2012, Schlacher et al., 2011a), which highlights the

importance of MRE11 nuclease activity blockade. Furthermore, whether combinatorial approaches targeting variable DNA repair pathway could be a viable approach is also an area of intense investigation.

7.5 MIRIN IS SYNTHETICALLY LETHAL IN XRCC1-DEFICENT CELLS

Mirin treatment is also selective toxic in XRCC1-deficient OC cells and XRCC1-deficient HeLa cells in both 2D cell lines models and 3D-spheroid models. Increased sensitivity was correlated with DSB accumulation, cell cycle arrest and apoptosis.

The MRN complex has recognised roles during base excision (Sagan et al., 2009). XRCC1 interacts with PARP1 during base excision repair (BER) and single strand break repair (SSBR) (Ali et al., 2019a). Emerging evidence also implicates a key role for XRCC1 in replication fork stability. XRCC1 is involved in the repair of certain unresected stalled replication forks. PARP1 mediated MRE11 recruitment has also been shown in stalled replication forks that require XRCC1 mediated repair (Ying et al., 2012, Ying et al., 2016). Therefore, MRE11 blockade in XRCC1-deficient cells may promote replication stress, DSB accumulation and cell death. Alternatively, XRCC1-deficient cells accumulate SSB, which get converted to DSBs during replication (Sultana et al., 2013a), and DSBs require MRE11 mediated repair.

We already have a stable polβ knockout in A2780 and A2780cis cells and FEN1 knockout in A2780cis, and a PhD student is currently working on an RPA1 knockout in OVCR3 cells. It would be interesting

to treat these cell lines with mirin to examine a possible synthetic lethality interaction.

7.6 MIRIN-RESISTANT PEO1R CELLS OVEREXPRESS MRE11 AND UPREGULATE SEVERAL DNA REPAIR GENES

Studies of PARP inhibitor resistance in BRCA-deficient cells have revealed several mechanisms of resistance including restoration of homologous recombination (HR) [reactivation of BRCA function, inactivation of 53BP1, down regulation of PARP1] and restoration of stalled replication fork protection. To evaluate whether similar mechanisms may evolve during the development of mirin-resistant cells line PEO1R, we made several novel observations in PEO1R cells compared to the parent PEO1 cells. There was no re-expression of BRCA2 gene, and 53BP1 inactivation and MRE11 overexpression was an important driver for acquired resistance to mirin. Moreover, we observed upregulation of several genes involved in multiple DNA repair pathways in PEO1R cells compared to PEO1 cells. More Importantly, PEO1R cells were also cross-resistant to cisplatin and olaparib compared to parental PEO1 cells. This new finding indicates that the development of cross-resistance may be significant clinical problem, as new DNA repair targeted inhibitors enter clinical trials beyond PARP inhibitors.

The data would support HR activation in PEO1R cells. PEO1R cells also overexpressed MRE11, RAD50 and NBS1 protein levels. PEO1R increased the mRNA and protein expression of several DNA repair genes that involved in multiple DNA repair pathways. Interestingly, the knockdown of MRE11 in PEO1R cell reduced the level of these DNA repair proteins and partially restored the sensitivity to mirin and cisplatin.

Collectively, the data provide evidence that MRE11 overexpression contributes to the development of mirin-resistant in PEO1R cells.

7.7 PEO1R CELLS OVEREXPRESS OCT4 AND MANIFEST AN AGGRESSIVE PHENOTYPE WITH CANCER STEM CELL-LIKE FEATURES

In the current study, we describe the isolation of mirin and cisplatin-resistant PEO1R cells with a stem cell like phenotype. The cancer stem cells (CSCs) phenotype of PEO1R is supported by expression of CD44 and OCT4. OCT4 is a transcription factor that has key roles in self renewal, pluripotency and lineage commitment. A previous bioinformatics study described several DNA repair genes, including MRE11, were correlated with OCT4 (Campbell et al., 2007).

In our study, a novel observation was that OCT4 physically interacted with MRE11. MRE11 also stabilised OCT4 expression. When MRE11 was depleted in PEO1R cells, OCT4 was also reduced.

Taken together, the data support our hypothesis that mirin resistant PEO1R cells not only overexpress MRE11 but also OCT4, which promotes the development of a CSC phenotype. Interestingly PEO1R cells displayed an EMT phenotype with ZEB1, vimentin, N-cadherin upregulation and down-regulation of E-cadherin *in vitro* and *in vivo*.

7.8 STRENGTHS AND WEAKNESSES OF THIS PROJECT

One strength of this study in terms of clinical investigation is that immunohistochemistry (IHC) was performed in 331 EOC patients and validated by evaluating MRE11 mRNA in publicly available online gene expression dataset.

In pre-clinical studies, all the knockdown experiments were validated by other siRNA constructs. The synthetic lethality studies were also validated by 3D system to mimic *in vivo* system.

This project adds to the understanding of cisplatin and PARP resistance mechanisms by highlighting a further resistance mechanism in addition to the published mechanisms.

The first limitation of this project is the use of only two ovarian resistance cell lines to show the effect of the knockdown of MRN complex in increasing platinum sensitivity. The second limitation is the use of only siRNA constructs, which have been shown to have off-target effects. Third, the suggested mechanism in PEO1R cells is based on one cell line. Fourth, the assessment of the resistance mechanism in chapter 6 need to be further investigated. The reason why I did not explore the proposed resistance mechanism further is due to time limitation, as the generation of the resistance in PEO1 cells took long time.

7.9 FUTURE DIRECTIONS

This work adds to the growing evidence of the significant role of MRN complex in the resistance of EOC. However, it has generated quite a few further questions. To answer these questions, several future projects are being considered. The immediate plan is to assess the role of MRE11 knocking out to platinum sensitization by knocking out MRE11 using CRISPER-CAS9 in A2780cis and PEO4 cells and inject these cell lines in mice. To test the effect of mirin on increasing the sensitivity of A2780cis and PEO4 cells to platinum agents, A2780cis and PEO4 cells will be injected in mice and then treated with cisplatin monotherapy or cisplatin and mirin combination therapy. This study

will confirm the proposed efficacy of the combinations and show their specificity to cancer cells by studying the toxicity of the combination.

To further investigate the results of the resistance mechanism study, multiple experiments are planned.

- The interaction between MRE11 and OCT4 will be investigated further *in silico* approaches, such as domain-Pairs-Based approach, to potentially identify drug targets.
- The effect of OCT4 knockout by CRISPR-CAS9 in PEO1R cells on DNA repair expressions, the high proliferation capability of PEO1R cells, and the expression of EMT markers will be examined.
- Intensive investigations will be performed in PEO1 and PEO1R cells derived from xenograft mouse models (CDX). At the histopathology level, MRE11, OCT4, KI-67, ZEB1, E-cadherin, and N-cadherin will be stained using IHC. To study the transcriptome of gene expression pattern in PEO1 and PEO1R cells, RNA-seq will be performed. RNA will be extracted from both cell lines and CDX and then samples will send to Novagene Company in Cambridge to do the analysis.
- A single clonal analysis will be performed to show that a single cell of a PEO1R CDX tumour can lead to a highly proliferative, aggressive, and drug resistant tumour. This experiment will be

followed by functional analysis including tumorigenicity, proliferation, and drug response, and genomic studies, including gene expression analysis and pathways analysis.

- ZEB1 downstream interactions involved in tumour progression, such as cumbs3, HUGL2, and PATJ, will be investigate

CH. 8

REFERENCES



REFERENCES

ABBOTTS, R. & MADHUSUDAN, S. 2010. Human AP endonuclease 1 (APE1): from mechanistic insights to druggable target in cancer. *Cancer Treat Rev,* 36**,** 425-35.

ABDEL-FATAH, T., SULTANA, R., ABBOTTS, R., HAWKES, C., SEEDHOUSE, C., CHAN, S. & MADHUSUDAN, S. 2013. Clinicopathological and functional significance of XRCC1 expression in ovarian cancer. *Int J Cancer,* 132**,** 2778-86.

ABDEL-FATAH, T. M., RUSSELL, R., ALBARAKATI, N., MALONEY, D. J., DORJSUREN, D., RUEDA, O. M., MOSELEY, P., MOHAN, V., SUN, H., ABBOTTS, R., MUKHERJEE, A., AGARWAL, D., ILLUZZI, J. L., JADHAV, A., SIMEONOV, A., BALL, G., CHAN, S., CALDAS, C., ELLIS, I. O., WILSON, D. M., 3RD & MADHUSUDAN, S. 2014a. Genomic and protein expression analysis reveals flap endonuclease 1 (FEN1) as a key biomarker in breast and ovarian cancer. *Mol Oncol,* 8**,** 1326-38.

ABDEL-FATAH, T. M. A., ARORA, A., MOSELEY, P., COVENEY, C., PERRY, C., JOHNSON, K., KENT, C., BALL, G., CHAN, S. & MADHUSUDAN, S. 2014b. ATM, ATR and DNA-PKcs expressions correlate to adverse clinical outcomes in epithelial ovarian cancers. *BBA clinical,* 2**,** 10-17.

ABDEL-FATAH, T. M. A., RUSSELL, R., ALBARAKATI, N., MALONEY, D. J., DORJSUREN, D., RUEDA, O. M., MOSELEY, P., MOHAN, V., SUN, H., ABBOTTS, R., MUKHERJEE, A., AGARWAL, D., ILLUZZI, J. L., JADHAV, A., SIMEONOV, A., BALL, G., CHAN, S., CALDAS, C., ELLIS, I. O., WILSON, D. M., 3RD & MADHUSUDAN, S. 2014c. Genomic and protein expression analysis reveals flap endonuclease 1 (FEN1) as a key biomarker in breast and ovarian cancer. *Molecular oncology,* 8**,** 1326-1338.

ABUZEID, W. M., JIANG, X., SHI, G., WANG, H., PAULSON, D., ARAKI, K., JUNGREIS, D., CARNEY, J., O'MALLEY, B. W., JR. & LI, D. 2009. Molecular disruption of RAD50 sensitizes human tumor cells to cisplatin-based chemotherapy. *J Clin Invest,* 119**,** 1974-85.

AGHAJANIAN, C., BLANK, S. V., GOFF, B. A., JUDSON, P. L., TENERIELLO, M. G., HUSAIN, A., SOVAK, M. A., YI, J. & NYCUM, L. R. 2012. OCEANS: a randomized, double-blind, placebo-controlled phase III trial of chemotherapy with or

without bevacizumab in patients with platinum-sensitive recurrent epithelial ovarian, primary peritoneal, or fallopian tube cancer. *J Clin Oncol,* 30**,** 2039-45.

AL-ATTAR, A., GOSSAGE, L., FAREED, K. R., SHEHATA, M., MOHAMMED, M., ZAITOUN, A. M., SOOMRO, I., LOBO, D. N., ABBOTTS, R., CHAN, S. & MADHUSUDAN, S. 2010. Human apurinic/apyrimidinic endonuclease (APE1) is a prognostic factor in ovarian, gastro-oesophageal and pancreatico-biliary cancers. *British journal of cancer,* 102**,** 704-709.

AL-SUBHI, N., ALI, R., ABDEL-FATAH, T., MOSELEY, P. M., CHAN, S. Y. T., GREEN, A. R., ELLIS, I. O., RAKHA, E. A. & MADHUSUDAN, S. 2018. Targeting ataxia telangiectasia-mutated- and Rad3-related kinase (ATR) in PTEN-deficient breast cancers for personalized therapy. *Breast cancer research and treatment,* 169**,** 277-286.

AL RAWAHI, T., LOPES, A. D., BRISTOW, R. E., BRYANT, A., ELATTAR, A., CHATTOPADHYAY, S. & GALAAL, K. 2013. Surgical cytoreduction for recurrent epithelial ovarian cancer. *Cochrane Database Syst Rev***,** Cd008765.

ALBLIHY, A., MESQUITA, K. A., SADIQ, M. T. & MADHUSUDAN, S. 2019. Development and implementation of precision therapies targeting base-excision DNA repair in BRCA1-associated tumors. *Expert Review of Precision Medicine and Drug Development,* 4**,** 11-25.

ALI, R., AL-KAWAZ, A., TOSS, M. S., GREEN, A. R., MILIGY, I. M., MESQUITA, K. A., SEEDHOUSE, C., MIRZA, S., BAND, V., RAKHA, E. A. & MADHUSUDAN, S. 2018. Targeting PARP1 in XRCC1-Deficient Sporadic Invasive Breast Cancer or Preinvasive Ductal Carcinoma In Situ Induces Synthetic Lethality and Chemoprevention. *Cancer Res,* 78**,** 6818-6827.

ALI, R., ALABDULLAH, M., ALBLIHY, A., MILIGY, I., MESQUITA, K. A., CHAN, S. Y., MOSELEY, P., RAKHA, E. A. & MADHUSUDAN, S. 2019a. PARP1 blockade is synthetically lethal in XRCC1 deficient sporadic epithelial ovarian cancers. *Cancer Lett*.

ALI, R., ALABDULLAH, M., MILIGY, I., NORMATOVA, M., BABAEI-JADIDI, R., NATERI, A. S., RAKHA, E. A. & MADHUSUDAN, S. 2019b. ATM Regulated PTEN Degradation Is XIAP E3 Ubiquitin Ligase Mediated in p85alpha Deficient Cancer Cells and Influence Platinum Sensitivity. *Cells,* 8.

ALTAN, B., YOKOBORI, T., IDE, M., BAI, T., YANOMA, T., KIMURA, A., KOGURE, N., SUZUKI, M., BAO, P., MOCHIKI, E., OGATA, K., HANDA, T., KAIRA, K., NISHIYAMA, M., ASAO, T., OYAMA, T. & KUWANO, H. 2016. High Expression of MRE11-RAD50-NBS1 Is Associated with Poor Prognosis and Chemoresistance in Gastric Cancer. *Anticancer Res,* 36**,** 5237-5247.

ANNETT, S. & ROBSON, T. 2018. Targeting cancer stem cells in the clinic: Current status and perspectives. *Pharmacol Ther,* 187**,** 13-30.

ARAKI, K., YAMASHITA, T., REDDY, N., WANG, H., ABUZEID, W. M., KHAN, K., O'MALLEY, B. W., JR. & LI, D. 2010. Molecular disruption of NBS1 with targeted gene delivery enhances chemosensitisation in head and neck cancer. *Br J Cancer,* 103**,** 1822-30.

AUBREY, B. J., KELLY, G. L., JANIC, A., HEROLD, M. J. & STRASSER, A. 2018. How does p53 induce apoptosis and how does this relate to p53-mediated tumour suppression? *Cell death and differentiation,* 25**,** 104-113.

AUDEBERT, M., SALLES, B. & CALSOU, P. 2004. Involvement of poly(ADP-ribose) polymerase-1 and XRCC1/DNA ligase III in an alternative route for DNA double-strand breaks rejoining. *J Biol Chem,* 279**,** 55117-26.

AWASTHI, P., FOIANI, M. & KUMAR, A. 2015. ATM and ATR signaling at a glance. *Journal of Cell Science,* 128**,** 4255-4262.

BARBER, L. J., SANDHU, S., CHEN, L., CAMPBELL, J., KOZAREWA, I., FENWICK, K., ASSIOTIS, I., RODRIGUES, D. N., REIS FILHO, J. S., MORENO, V., MATEO, J., MOLIFE, L. R., DE BONO, J., KAYE, S., LORD, C. J. & ASHWORTH, A. 2013. Secondary mutations in BRCA2 associated with clinical resistance to a PARP inhibitor. *J Pathol,* 229**,** 422-9.

BARLOW, J. H., LISBY, M. & ROTHSTEIN, R. 2008. Differential regulation of the cellular response to DNA double-strand breaks in G1. *Mol Cell,* 30**,** 73-85.

BEAUFORT, C. M., HELMIJR, J. C., PISKORZ, A. M., HOOGSTRAAT, M., RUIGROK-RITSTIER, K., BESSELINK, N., MURTAZA, M., VAN, I. W. F., HEINE, A. A., SMID, M., KOUDIJS, M. J., BRENTON, J. D., BERNS, E. M. & HELLEMAN, J. 2014. Ovarian cancer cell line panel (OCCP): clinical importance of in vitro morphological subtypes. *PLoS One,* 9**,** e103988.

BERKOVICH, E., MONNAT, R. J., JR. & KASTAN, M. B. 2007. Roles of ATM and NBS1 in chromatin structure modulation and DNA double-strand break repair. *Nat Cell Biol,* 9**,** 683-90.

BERNSTEIN, C., BERNSTEIN, H., PAYNE, C. M. & GAREWAL, H. 2002. DNA repair/pro-apoptotic dual-role proteins in five major DNA repair pathways: fail-safe protection against carcinogenesis. *Mutat Res,* 511**,** 145-78.

BERTE, N., PIÉE-STAFFA, A., PIECHA, N., WANG, M., BORGMANN, K., KAINA, B. & NIKOLOVA, T. 2016. Targeting Homologous Recombination by Pharmacological Inhibitors Enhances the Killing Response of Glioblastoma Cells Treated with Alkylating Drugs. *Molecular Cancer Therapeutics,* 15**,** 2665.

BHASKARA, V., DUPRE, A., LENGSFELD, B., HOPKINS, B. B., CHAN, A., LEE, J. H., ZHANG, X., GAUTIER, J., ZAKIAN, V. & PAULL, T. T. 2007. Rad50 adenylate kinase activity regulates DNA tethering by Mre11/Rad50 complexes. *Mol Cell,* 25**,** 647-61.

BHAT, R. A., CHIA, Y. N., LIM, Y. K., YAM, K. L., LIM, C. & TEO, M. 2015. Survival Impact of Secondary Cytoreductive Surgery for Recurrent Ovarian Cancer in an Asian Population. *Oman medical journal,* 30**,** 344-352.

BIAN, L., MENG, Y., ZHANG, M. & LI, D. 2019. MRE11-RAD50-NBS1 complex alterations and DNA damage response: implications for cancer treatment. *Molecular Cancer,* 18**,** 169.

BISHOP, A. J. & SCHIESTL, R. H. 2002. Homologous Recombination and Its Role in Carcinogenesis. *J Biomed Biotechnol,* 2**,** 75-85.

BITLER, B. G., WATSON, Z. L., WHEELER, L. J. & BEHBAKHT, K. 2017. PARP inhibitors: Clinical utility and possibilities of overcoming resistance. *Gynecol Oncol,* 147**,** 695-704.

BOOKMAN, M. A., GREER, B. E. & OZOLS, R. F. 2003. Optimal therapy of advanced ovarian cancer: carboplatin and paclitaxel versus cisplatin and paclitaxel (GOG158) and an update on GOG0182-ICON5. *Int J Gynecol Cancer,* 13 Suppl 2**,** 149-55.

BORDE, V. & COBB, J. 2009. Double functions for the Mre11 complex during DNA double-strand break repair and replication. *Int J Biochem Cell Biol,* 41**,** 1249-53.

BOUWMAN, P., ALY, A., ESCANDELL, J. M., PIETERSE, M., BARTKOVA, J., VAN DER GULDEN, H., HIDDINGH, S., THANASOULA, M., KULKARNI, A., YANG, Q., HAFFTY, B. G., TOMMISKA, J., BLOMQVIST, C., DRAPKIN, R., ADAMS, D. J.,

NEVANLINNA, H., BARTEK, J., TARSOUNAS, M., GANESAN, S. & JONKERS, J. 2010. 53BP1 loss rescues BRCA1 deficiency and is associated with triple-negative and BRCA-mutated breast cancers. *Nature structural & molecular biology,* 17**,** 688-695.

BRANDT, S., SAMARTZIS, E. P., ZIMMERMANN, A. K., FINK, D., MOCH, H., NOSKE, A. & DEDES, K. J. 2017. Lack of MRE11-RAD50-NBS1 (MRN) complex detection occurs frequently in low-grade epithelial ovarian cancer. *BMC Cancer,* 17**,** 44.

BRANZEI, D. & FOIANI, M. 2008. Regulation of DNA repair throughout the cell cycle. *Nat Rev Mol Cell Biol,* 9**,** 297-308.

BRYANT, H. E., SCHULTZ, N., THOMAS, H. D., PARKER, K. M., FLOWER, D., LOPEZ, E., KYLE, S., MEUTH, M., CURTIN, N. J. & HELLEDAY, T. 2005. Specific killing of BRCA2-deficient tumours with inhibitors of poly(ADP-ribose) polymerase. *Nature,* 434**,** 913-7.

BUIS, J., WU, Y., DENG, Y., LEDDON, J., WESTFIELD, G., ECKERSDORFF, M., SEKIGUCHI, J. M., CHANG, S. & FERGUSON, D. O. 2008. Mre11 nuclease activity has essential roles in DNA repair and genomic stability distinct from ATM activation. *Cell,* 135**,** 85-96.

BUISSON, R., DION-COTE, A. M., COULOMBE, Y., LAUNAY, H., CAI, H., STASIAK, A. Z., STASIAK, A., XIA, B. & MASSON, J. Y. 2010. Cooperation of breast cancer proteins PALB2 and piccolo BRCA2 in stimulating homologous recombination. *Nat Struct Mol Biol,* 17**,** 1247-54.

BURGER, R. A., BRADY, M. F., BOOKMAN, M. A., FLEMING, G. F., MONK, B. J., HUANG, H., MANNEL, R. S., HOMESLEY, H. D., FOWLER, J., GREER, B. E., BOENTE, M., BIRRER, M. J. & LIANG, S. X. 2011. Incorporation of bevacizumab in the primary treatment of ovarian cancer. *N Engl J Med,* 365**,** 2473-83.

BUSCHTA-HEDAYAT, N., BUTERIN, T., HESS, M. T., MISSURA, M. & NAEGELI, H. 1999. Recognition of nonhybridizing base pairs during nucleotide excision repair of DNA. *Proceedings of the National Academy of Sciences,* 96**,** 6090-6095.

CAMPBELL, P. A., PEREZ-IRATXETA, C., ANDRADE-NAVARRO, M. A. & RUDNICKI, M. A. 2007. Oct4 targets regulatory nodes to modulate stem cell function. *PLoS One,* 2**,** e553.

CAPP, J. P., BOUDSOCQ, F., BERTRAND, P., LAROCHE-CLARY, A., POURQUIER, P., LOPEZ, B. S., CAZAUX, C., HOFFMANN, J. S. & CANITROT, Y. 2006. The DNA polymerase lambda is required for the repair of non-compatible DNA double strand breaks by NHEJ in mammalian cells. *Nucleic Acids Res,* 34**,** 2998-3007.

CHAI, W., SFEIR, A. J., HOSHIYAMA, H., SHAY, J. W. & WRIGHT, W. E. 2006. The involvement of the Mre11/Rad50/Nbs1 complex in the generation of G-overhangs at human telomeres. *EMBO reports,* 7**,** 225-230.

CHAKRABORTY, A., TAPRYAL, N., VENKOVA, T., HORIKOSHI, N., PANDITA, R. K., SARKER, A. H., SARKAR, P. S., PANDITA, T. K. & HAZRA, T. K. 2016. Classical non-homologous end-joining pathway utilizes nascent RNA for error-free double-strand break repair of transcribed genes. *Nature Communications,* 7**,** 13049.

CHALHOUB, N. & BAKER, S. J. 2009. PTEN and the PI3-kinase pathway in cancer. *Annual review of pathology,* 4**,** 127-150.

CHANG, L., HUANG, J., WANG, K., LI, J., YAN, R., ZHU, L., YE, J., WU, X., ZHUANG, S., LI, D. & ZHANG, G. 2016. Targeting Rad50 sensitizes human nasopharyngeal carcinoma cells to radiotherapy. *BMC cancer,* 16**,** 190-190.

CHEAIB, B., AUGUSTE, A. & LEARY, A. 2015. The PI3K/Akt/mTOR pathway in ovarian cancer: therapeutic opportunities and challenges. *Chin J Cancer,* 34**,** 4-16.

CHEN, C., WANG, Y., MEI, J. F., LI, S. S., XU, H. X., XIONG, H. P., WANG, X. H. & HE, X. 2018. Targeting RAD50 increases sensitivity to radiotherapy in colorectal cancer cells. *Neoplasma,* 65**,** 75-80.

CHEN, V. W., RUIZ, B., KILLEEN, J. L., COTE, T. R., WU, X. C. & CORREA, C. N. 2003. Pathology and classification of ovarian tumors. *Cancer,* 97**,** 2631-42.

CHOUDHURY, A., NELSON, L. D., TEO, M. T., CHILKA, S., BHATTARAI, S., JOHNSTON, C. F., ELLIOTT, F., LOWERY, J., TAYLOR, C. F., CHURCHMAN, M., BENTLEY, J., KNOWLES, M. A., HARNDEN, P., BRISTOW, R. G., BISHOP, D. T. & KILTIE, A. E. 2010. MRE11 expression is predictive of cause-specific survival following radical radiotherapy for muscle-invasive bladder cancer. *Cancer Res,* 70**,** 7017-26.

CHRISTMANN, M., TOMICIC, M. T., ROOS, W. P. & KAINA, B. 2003. Mechanisms of human DNA repair: an update. *Toxicology,* 193**,** 3-34.

CHRZANOWSKA, K. H., GREGOREK, H., DEMBOWSKA-BAGIŃSKA, B., KALINA, M. A. & DIGWEED, M. 2012. Nijmegen breakage syndrome (NBS). *Orphanet journal of rare diseases,* 7**,** 13-13.

CHUNG, D. C. & RUSTGI, A. K. 2003. The hereditary nonpolyposis colorectal cancer syndrome: genetics and clinical implications. *Ann Intern Med,* 138**,** 560-70.

COLEMAN, R. L., MONK, B. J., SOOD, A. K. & HERZOG, T. J. 2013. Latest research and treatment of advanced-stage epithelial ovarian cancer. *Nature reviews. Clinical oncology,* 10**,** 211-224.

COLOMBO, N., GUTHRIE, D., CHIARI, S., PARMAR, M., QIAN, W., SWART, A. M., TORRI, V., WILLIAMS, C., LISSONI, A. & BONAZZI, C. 2003. International Collaborative Ovarian Neoplasm trial 1: a randomized trial of adjuvant chemotherapy in women with early-stage ovarian cancer. *J Natl Cancer Inst,* 95**,** 125-32.

CORTIZAS, E. M., ZAHN, A., HAJJAR, M. E., PATENAUDE, A. M., DI NOIA, J. M. & VERDUN, R. E. 2013. Alternative end-joining and classical nonhomologous end-joining pathways repair different types of double-strand breaks during class-switch recombination. *J Immunol,* 191**,** 5751-63.

CORY, A. H., OWEN, T. C., BARLTROP, J. A. & CORY, J. G. 1991. Use of an aqueous soluble tetrazolium/formazan assay for cell growth assays in culture. *Cancer Commun,* 3**,** 207-12.

COUEDEL, C., MILLS, K. D., BARCHI, M., SHEN, L., OLSHEN, A., JOHNSON, R. D., NUSSENZWEIG, A., ESSERS, J., KANAAR, R., LI, G. C., ALT, F. W. & JASIN, M. 2004. Collaboration of homologous recombination and nonhomologous end-joining factors for the survival and integrity of mice and cells. *Genes Dev,* 18**,** 1293-304.

CRUET-HENNEQUART, S., GLYNN, M. T., MURILLO, L. S., COYNE, S. & CARTY, M. P. 2008. Enhanced DNA-PK-mediated RPA2 hyperphosphorylation in DNA polymerase eta-deficient human cells treated with cisplatin and oxaliplatin. *DNA Repair (Amst),* 7**,** 582-96.

CZORNAK, K., CHUGHTAI, S. & CHRZANOWSKA, K. H. 2008. Mystery of DNA repair: the role of the MRN complex and ATM kinase in DNA damage repair. *J Appl Genet,* 49**,** 383-96.

D'AMOURS, D. & JACKSON, S. P. 2002. The Mre11 complex: at the crossroads of dna repair and checkpoint signalling. *Nat Rev Mol Cell Biol,* 3**,** 317-27.

DAEMEN, A., WOLF, D. M., KORKOLA, J. E., GRIFFITH, O. L., FRANKUM, J. R., BROUGH, R., JAKKULA, L. R., WANG, N. J., NATRAJAN, R., REIS-FILHO, J. S., LORD, C. J., ASHWORTH, A., SPELLMAN, P. T., GRAY, J. W. & VAN'T VEER, L. J. 2012. Cross-platform pathway-based analysis identifies markers of response to the PARP inhibitor olaparib. *Breast Cancer Res Treat,* 135**,** 505-17.

DAI, C. H., LI, J., CHEN, P., JIANG, H. G., WU, M. & CHEN, Y. C. 2015. RNA interferences targeting the Fanconi anemia/BRCA pathway upstream genes reverse cisplatin resistance in drug-resistant lung cancer cells. *J Biomed Sci,* 22**,** 77.

DAMIA, G. & BROGGINI, M. 2019. Platinum Resistance in Ovarian Cancer: Role of DNA Repair. *Cancers,* 11**,** 119.

DARZYNKIEWICZ, Z., TRAGANOS, F. & WLODKOWIC, D. 2009. Impaired DNA damage response--an Achilles' heel sensitizing cancer to chemotherapy and radiotherapy. *Eur J Pharmacol,* 625**,** 143-50.

DAVIS, A. J. & CHEN, D. J. 2013. DNA double strand break repair via non-homologous end-joining. *Translational cancer research,* 2**,** 130-143.

DEANS, A. J. & WEST, S. C. 2011. DNA interstrand crosslink repair and cancer. *Nature reviews. Cancer,* 11**,** 467-480.

DEBNATH, J., MUTHUSWAMY, S. K. & BRUGGE, J. S. 2003. Morphogenesis and oncogenesis of MCF-10A mammary epithelial acini grown in three-dimensional basement membrane cultures. *Methods,* 30**,** 256-68.

DELLA PEPA, C., TONINI, G., PISANO, C., DI NAPOLI, M., CECERE, S. C., TAMBARO, R., FACCHINI, G. & PIGNATA, S. 2015. Ovarian cancer standard of care: are there real alternatives? *Chinese Journal of Cancer,* 34**,** 17-27.

DEMUTH, I., FRAPPART, P. O., HILDEBRAND, G., MELCHERS, A., LOBITZ, S., STOCKL, L., VARON, R., HERCEG, Z., SPERLING, K., WANG, Z. Q. & DIGWEED, M. 2004. An inducible null

mutant murine model of Nijmegen breakage syndrome proves the essential function of NBS1 in chromosomal stability and cell viability. *Hum Mol Genet,* 13**,** 2385-97.

DENG, J., WANG, L., CHEN, H., HAO, J., NI, J., CHANG, L., DUAN, W., GRAHAM, P. & LI, Y. 2016. Targeting epithelial-mesenchymal transition and cancer stem cells for chemoresistant ovarian cancer. *Oncotarget,* 7**,** 55771-55788.

DEVOUASSOUX-SHISHEBORAN, M. & GENESTIE, C. 2015. Pathobiology of ovarian carcinomas. *Chinese journal of cancer,* 34**,** 50-55.

DIANOV, G. L. 2011. Base excision repair targets for cancer therapy. *American journal of cancer research,* 1**,** 845-851.

DIBIASE, S. J., ZENG, Z. C., CHEN, R., HYSLOP, T., CURRAN, W. J., JR. & ILIAKIS, G. 2000. DNA-dependent protein kinase stimulates an independently active, nonhomologous, end-joining apparatus. *Cancer Res,* 60**,** 1245-53.

DIFILIPPANTONIO, S., CELESTE, A., FERNANDEZ-CAPETILLO, O., CHEN, H. T., REINA SAN MARTIN, B., VAN LAETHEM, F., YANG, Y. P., PETUKHOVA, G. V., ECKHAUS, M., FEIGENBAUM, L., MANOVA, K., KRUHLAK, M., CAMERINI-OTERO, R. D., SHARAN, S., NUSSENZWEIG, M. & NUSSENZWEIG, A. 2005. Role of Nbs1 in the activation of the Atm kinase revealed in humanized mouse models. *Nat Cell Biol,* 7**,** 675-85.

DIMITROVA, N. & DE LANGE, T. 2009. Cell Cycle-Dependent Role of MRN at Dysfunctional Telomeres: ATM Signaling-Dependent Induction of Nonhomologous End Joining (NHEJ) in G₁ and Resection-Mediated Inhibition of NHEJ in G₂. *Molecular and Cellular Biology,* 29**,** 5552-5563.

DMITRIEVA, N. I., MALIDE, D. & BURG, M. B. 2011. Mre11 is expressed in mammalian mitochondria where it binds to mitochondrial DNA. *American journal of physiology. Regulatory, integrative and comparative physiology,* 301**,** R632-R640.

DOUBENI, C. A., DOUBENI, A. R. & MYERS, A. E. 2016. Diagnosis and Management of Ovarian Cancer. *Am Fam Physician,* 93**,** 937-44.

DUPRE, A., BOYER-CHATENET, L., SATTLER, R. M., MODI, A. P., LEE, J. H., NICOLETTE, M. L., KOPELOVICH, L., JASIN, M., BAER,

R., PAULL, T. T. & GAUTIER, J. 2008. A forward chemical genetic screen reveals an inhibitor of the Mre11-Rad50-Nbs1 complex. *Nat Chem Biol,* 4**,** 119-25.

EDWARDS, S. L., BROUGH, R., LORD, C. J., NATRAJAN, R., VATCHEVA, R., LEVINE, D. A., BOYD, J., REIS-FILHO, J. S. & ASHWORTH, A. 2008. Resistance to therapy caused by intragenic deletion in BRCA2. *Nature,* 451**,** 1111-5.

EGER, A., AIGNER, K., SONDEREGGER, S., DAMPIER, B., OEHLER, S., SCHREIBER, M., BERX, G., CANO, A., BEUG, H. & FOISNER, R. 2005. DeltaEF1 is a transcriptional repressor of E-cadherin and regulates epithelial plasticity in breast cancer cells. *Oncogene,* 24**,** 2375-85.

EHLERS, J. P. & HARBOUR, J. W. 2005. NBS1 expression as a prognostic marker in uveal melanoma. *Clin Cancer Res,* 11**,** 1849-53.

ELATTAR, A., BRYANT, A., WINTER-ROACH, B. A., HATEM, M. & NAIK, R. 2011. Optimal primary surgical treatment for advanced epithelial ovarian cancer. *Cochrane Database of Systematic Reviews*.

ESSERS, J., VAN STEEG, H., DE WIT, J., SWAGEMAKERS, S. M., VERMEIJ, M., HOEIJMAKERS, J. H. & KANAAR, R. 2000. Homologous and non-homologous recombination differentially affect DNA damage repair in mice. *Embo j,* 19**,** 1703-10.

ESTRELA, J. M., ORTEGA, A. & OBRADOR, E. 2006. Glutathione in cancer biology and therapy. *Crit Rev Clin Lab Sci,* 43**,** 143-81.

FAN, C. H., LIU, W. L., CAO, H., WEN, C., CHEN, L. & JIANG, G. 2013. O6-methylguanine DNA methyltransferase as a promising target for the treatment of temozolomide-resistant gliomas. *Cell Death &Amp; Disease,* 4**,** e876.

FANNING, E., KLIMOVICH, V. & NAGER, A. R. 2006. A dynamic model for replication protein A (RPA) function in DNA processing pathways. *Nucleic Acids Res,* 34**,** 4126-37.

FARMER, H., MCCABE, N., LORD, C. J., TUTT, A. N., JOHNSON, D. A., RICHARDSON, T. B., SANTAROSA, M., DILLON, K. J., HICKSON, I., KNIGHTS, C., MARTIN, N. M., JACKSON, S. P., SMITH, G. C. & ASHWORTH, A. 2005. Targeting the DNA repair defect in BRCA mutant cells as a therapeutic strategy. *Nature,* 434**,** 917-21.

FATTAH, F., LEE, E. H., WEISENSEL, N., WANG, Y., LICHTER, N. & HENDRICKSON, E. A. 2010. Ku regulates the non-homologous end joining pathway choice of DNA double-strand break repair in human somatic cells. *PLoS Genet,* 6**,** e1000855.

FERNALD, K. & KUROKAWA, M. 2013. Evading apoptosis in cancer. *Trends in cell biology,* 23**,** 620-633.

FLORES-PEREZ, A., RAFAELLI, L. E., RAMIREZ-TORRES, N., ARECHAGA-OCAMPO, E., FRIAS, S., SANCHEZ, S., MARCHAT, L. A., HIDALGO-MIRANDA, A., QUINTANAR-JURADO, V., RODRIGUEZ-CUEVAS, S., BAUTISTA-PINA, V., CARLOS-REYES, A. & LOPEZ-CAMARILLO, C. 2014. RAD50 targeting impairs DNA damage response and sensitizes human breast cancer cells to cisplatin therapy. *Cancer Biol Ther,* 15**,** 777-88.

FREEMAN, A. K. & MONTEIRO, A. N. A. 2010. Phosphatases in the cellular response to DNA damage. *Cell Communication and Signaling,* 8**,** 27.

GALLUZZI, L., SENOVILLA, L., VITALE, I., MICHELS, J., MARTINS, I., KEPP, O., CASTEDO, M. & KROEMER, G. 2012. Molecular mechanisms of cisplatin resistance. *Oncogene,* 31**,** 1869-83.

GANESH, S., IYER, A. K., WEILER, J., MORRISSEY, D. V. & AMIJI, M. M. 2013. Combination of siRNA-directed Gene Silencing With Cisplatin Reverses Drug Resistance in Human Non-small Cell Lung Cancer. *Molecular therapy. Nucleic acids,* 2**,** e110-e110.

GATEI, M., JAKOB, B., CHEN, P., KIJAS, A. W., BECHEREL, O. J., GUEVEN, N., BIRRELL, G., LEE, J.-H., PAULL, T. T., LERENTHAL, Y., FAZRY, S., TAUCHER-SCHOLZ, G., KALB, R., SCHINDLER, D., WALTES, R., DÖRK, T. & LAVIN, M. F. 2011. ATM protein-dependent phosphorylation of Rad50 protein regulates DNA repair and cell cycle control. *The Journal of biological chemistry,* 286**,** 31542-31556.

GAVANDE, N. S., VANDERVERE-CAROZZA, P. S., HINSHAW, H. D., JALAL, S. I., SEARS, C. R., PAWELCZAK, K. S. & TURCHI, J. J. 2016. DNA repair targeted therapy: The past or future of cancer treatment? *Pharmacology & therapeutics,* 160**,** 65-83.

GAYMES, T. J., MOHAMEDALI, A. M., PATTERSON, M., MATTO, N., SMITH, A., KULASEKARARAJ, A., CHELLIAH, R., CURTIN, N., FARZANEH, F., SHALL, S. & MUFTI, G. J. 2013. Microsatellite instability induced mutations in DNA repair genes CtIP and MRE11 confer hypersensitivity to poly (ADP-ribose)

polymerase inhibitors in myeloid malignancies. *Haematologica,* 98**,** 1397-1406.

GEORGESCU, M.-M. 2010. PTEN Tumor Suppressor Network in PI3K-Akt Pathway Control. *Genes & cancer,* 1**,** 1170-1177.

GHOSAL, G. & CHEN, J. 2013. DNA damage tolerance: a double-edged sword guarding the genome. *Translational cancer research,* 2**,** 107-129.

GHOSH, R., GILDA, J. E. & GOMES, A. V. 2014. The necessity of and strategies for improving confidence in the accuracy of western blots. *Expert review of proteomics,* 11**,** 549-560.

GIANNINI, G., RISTORI, E., CERIGNOLI, F., RINALDI, C., ZANI, M., VIEL, A., OTTINI, L., CRESCENZI, M., MARTINOTTI, S., BIGNAMI, M., FRATI, L., SCREPANTI, I. & GULINO, A. 2002. Human MRE11 is inactivated in mismatch repair-deficient cancers. *EMBO Rep,* 3**,** 248-54.

GILLET, L. C. J. & SCHÄRER, O. D. 2006. Molecular Mechanisms of Mammalian Global Genome Nucleotide Excision Repair. *Chemical Reviews,* 106**,** 253-276.

GRUPP, K., BOUMESLI, R., TSOURLAKIS, M. C., KOOP, C., WILCZAK, W., ADAM, M., SAUTER, G., SIMON, R., IZBICKI, J. R., GRAEFEN, M., HULAND, H., STEURER, S., SCHLOMM, T., MINNER, S. & QUAAS, A. 2014. The prognostic impact of high Nijmegen breakage syndrome (NBS1) gene expression in ERG-negative prostate cancers lacking PTEN deletion is driven by KPNA2 expression. *Int J Cancer,* 135**,** 1399-407.

GUDMUNDSDOTTIR, K. & ASHWORTH, A. 2006. The roles of BRCA1 and BRCA2 and associated proteins in the maintenance of genomic stability. *Oncogene,* 25**,** 5864-74.

GYORFFY, B., LÁNCZKY, A. & SZÁLLÁSI, Z. 2012. Implementing an online tool for genome-wide validation of survival-associated biomarkers in ovarian-cancer using microarray data from 1287 patients. *Endocr Relat Cancer,* 19**,** 197-208.

HAINCE, J. F., MCDONALD, D., RODRIGUE, A., DERY, U., MASSON, J. Y., HENDZEL, M. J. & POIRIER, G. G. 2008. PARP1-dependent kinetics of recruitment of MRE11 and NBS1 proteins to multiple DNA damage sites. *J Biol Chem,* 283**,** 1197-208.

HAN, G., SIDHU, D., DUGGAN, M. A., ARSENEAU, J., CESARI, M., CLEMENT, P. B., EWANOWICH, C. A., KALLOGER, S. E. &

KOBEL, M. 2013. Reproducibility of histological cell type in high-grade endometrial carcinoma. *Mod Pathol,* 26**,** 1594-604.

HAN, S.-M., HAN, S.-H., COH, Y.-R., JANG, G., CHAN RA, J., KANG, S.-K., LEE, H.-W. & YOUN, H.-Y. 2014. Enhanced proliferation and differentiation of Oct4- and Sox2-overexpressing human adipose tissue mesenchymal stem cells. *Experimental & molecular medicine,* 46**,** e101-e101.

HANAWALT, P. C. 2002. Subpathways of nucleotide excision repair and their regulation. *Oncogene,* 21**,** 8949-56.

HASHIMOTO, Y., RAY CHAUDHURI, A., LOPES, M. & COSTANZO, V. 2010. Rad51 protects nascent DNA from Mre11-dependent degradation and promotes continuous DNA synthesis. *Nature Structural &Amp; Molecular Biology,* 17**,** 1305.

HEIKKINEN, K., RAPAKKO, K., KARPPINEN, S.-M., ERKKO, H., KNUUTILA, S., LUNDÁN, T., MANNERMAA, A., BØRRESEN-DALE, A.-L., BORG, A., BARKARDOTTIR, R. B., PETRINI, J. & WINQVIST, R. 2006. RAD50 and NBS1 are breast cancer susceptibility genes associated with genomic instability. *Carcinogenesis,* 27**,** 1593-1599.

HELLEDAY, T., PETERMANN, E., LUNDIN, C., HODGSON, B. & SHARMA, R. A. 2008. DNA repair pathways as targets for cancer therapy. *Nat Rev Cancer,* 8**,** 193-204.

HELMINK, B. A., BREDEMEYER, A. L., LEE, B.-S., HUANG, C.-Y., SHARMA, G. G., WALKER, L. M., BEDNARSKI, J. J., LEE, W.-L., PANDITA, T. K., BASSING, C. H. & SLECKMAN, B. P. 2009. MRN complex function in the repair of chromosomal Rag-mediated DNA double-strand breaks. *The Journal of experimental medicine,* 206**,** 669-679.

HELT, C. E., CLIBY, W. A., KENG, P. C., BAMBARA, R. A. & O'REILLY, M. A. 2005. Ataxia telangiectasia mutated (ATM) and ATM and Rad3-related protein exhibit selective target specificities in response to different forms of DNA damage. *J Biol Chem,* 280**,** 1186-92.

HENNESSY, B. T., COLEMAN, R. L. & MARKMAN, M. 2009. Ovarian cancer. *Lancet,* 374**,** 1371-82.

HIENTZ, K., MOHR, A., BHAKTA-GUHA, D. & EFFERTH, T. 2016. The role of p53 in cancer drug resistance and targeted chemotherapy. *Oncotarget,* 8**,** 8921-8946.

HIGGINS, C. F. 2007. Multiple molecular mechanisms for multidrug resistance transporters. *Nature,* 446**,** 749-57.

HIRSCHHAEUSER, F., MENNE, H., DITTFELD, C., WEST, J., MUELLER-KLIESER, W. & KUNZ-SCHUGHART, L. A. 2010. Multicellular tumor spheroids: an underestimated tool is catching up again. *J Biotechnol,* 148**,** 3-15.

HO, V., CHUNG, L., SINGH, A., LEA, V., ABUBAKAR, A., LIM, S. H., NG, W., LEE, M., DE SOUZA, P., SHIN, J. S. & LEE, C. S. 2018. Overexpression of the MRE11-RAD50-NBS1 (MRN) complex in rectal cancer correlates with poor response to neoadjuvant radiotherapy and prognosis. *BMC Cancer,* 18**,** 869.

HO, V., CHUNG, L., SINGH, A., LEA, V., REVOLTAR, M., LIM, S. H., TUT, T.-G., NG, W., LEE, M., DE SOUZA, P., SHIN, J.-S. & SOON LEE, C. 2017. Early Postoperative Low Expression of RAD50 in Rectal Cancer Patients Associates with Disease-Free Survival. *Cancers,* 9**,** 163.

HOLZER, A. K., MANOREK, G. H. & HOWELL, S. B. 2006. Contribution of the major copper influx transporter CTR1 to the cellular accumulation of cisplatin, carboplatin, and oxaliplatin. *Mol Pharmacol,* 70**,** 1390-4.

HOPFNER, K. P., CRAIG, L., MONCALIAN, G., ZINKEL, R. A., USUI, T., OWEN, B. A., KARCHER, A., HENDERSON, B., BODMER, J. L., MCMURRAY, C. T., CARNEY, J. P., PETRINI, J. H. & TAINER, J. A. 2002. The Rad50 zinc-hook is a structure joining Mre11 complexes in DNA recombination and repair. *Nature,* 418**,** 562-6.

HOPFNER, K. P., KARCHER, A., SHIN, D. S., CRAIG, L., ARTHUR, L. M., CARNEY, J. P. & TAINER, J. A. 2000. Structural biology of Rad50 ATPase: ATP-driven conformational control in DNA double-strand break repair and the ABC-ATPase superfamily. *Cell,* 101**,** 789-800.

HOPKINS, B. B. & PAULL, T. T. 2008. The P. furiosus mre11/rad50 complex promotes 5' strand resection at a DNA double-strand break. *Cell,* 135**,** 250-260.

HOSOYA, N. & MIYAGAWA, K. 2014. Targeting DNA damage response in cancer therapy. *Cancer science,* 105**,** 370-388.

HSU, D. S., CHANG, S. Y., LIU, C. J., TZENG, C. H., WU, K. J., KAO, J. Y. & YANG, M. H. 2010. Identification of increased NBS1

expression as a prognostic marker of squamous cell carcinoma of the oral cavity. *Cancer Sci,* 101**,** 1029-37.

HUNTOON, C. J., FLATTEN, K. S., WAHNER HENDRICKSON, A. E., HUEHLS, A. M., SUTOR, S. L., KAUFMANN, S. H. & KARNITZ, L. M. 2013. ATR inhibition broadly sensitizes ovarian cancer cells to chemotherapy independent of BRCA status. *Cancer research,* 73**,** 3683-3691.

IBRAHIM, E. E., BABAEI-JADIDI, R., SAADEDDIN, A., SPENCER-DENE, B., HOSSAINI, S., ABUZINADAH, M., LI, N., FADHIL, W., ILYAS, M., BONNET, D. & NATERI, A. S. 2012a. Embryonic NANOG activity defines colorectal cancer stem cells and modulates through AP1- and TCF-dependent mechanisms. *Stem Cells,* 30**,** 2076-87.

IBRAHIM, Y. H., GARCIA-GARCIA, C., SERRA, V., HE, L., TORRES-LOCKHART, K., PRAT, A., ANTON, P., COZAR, P., GUZMAN, M., GRUESO, J., RODRIGUEZ, O., CALVO, M. T., AURA, C., DIEZ, O., RUBIO, I. T., PEREZ, J., RODON, J., CORTES, J., ELLISEN, L. W., SCALTRITI, M. & BASELGA, J. 2012b. PI3K inhibition impairs BRCA1/2 expression and sensitizes BRCA-proficient triple-negative breast cancer to PARP inhibition. *Cancer Discov,* 2**,** 1036-47.

ILIAKIS, G., WANG, H., PERRAULT, A. R., BOECKER, W., ROSIDI, B., WINDHOFER, F., WU, W., GUAN, J., TERZOUDI, G. & PANTELIAS, G. 2004. Mechanisms of DNA double strand break repair and chromosome aberration formation. *Cytogenet Genome Res,* 104**,** 14-20.

JACKSON, S. P. & BARTEK, J. 2009. The DNA-damage response in human biology and disease. *Nature,* 461**,** 1071-1078.

JAGGUPILLI, A. & ELKORD, E. 2012. Significance of CD44 and CD24 as cancer stem cell markers: an enduring ambiguity. *Clin Dev Immunol,* 2012**,** 708036.

JAMIESON, E. R. & LIPPARD, S. J. 1999. Structure, Recognition, and Processing of Cisplatin-DNA Adducts. *Chem Rev,* 99**,** 2467-98.

JASPERS, J. E., KERSBERGEN, A., BOON, U., SOL, W., VAN DEEMTER, L., ZANDER, S. A., DROST, R., WIENTJENS, E., JI, J., ALY, A., DOROSHOW, J. H., CRANSTON, A., MARTIN, N. M., LAU, A., O'CONNOR, M. J., GANESAN, S., BORST, P., JONKERS, J. & ROTTENBERG, S. 2013. Loss of 53BP1 causes PARP inhibitor resistance in Brca1-mutated mouse mammary tumors. *Cancer Discov,* 3**,** 68-81.

JAZAYERI, A., BALESTRINI, A., GARNER, E., HABER, J. E. & COSTANZO, V. 2008. Mre11-Rad50-Nbs1-dependent processing of DNA breaks generates oligonucleotides that stimulate ATM activity. *Embo j,* 27**,** 1953-62.

JIANG, X., LI, X., LI, W., BAI, H. & ZHANG, Z. 2019. PARP inhibitors in ovarian cancer: Sensitivity prediction and resistance mechanisms. *Journal of cellular and molecular medicine,* 23**,** 2303-2313.

JIRICNY, J. 2006. The multifaceted mismatch-repair system. *Nat Rev Mol Cell Biol,* 7**,** 335-46.

JIVIDEN, K., KEDZIERSKA, K. Z., YANG, C.-S., SZLACHTA, K., RATAN, A. & PASCHAL, B. M. 2018. Genomic analysis of DNA repair genes and androgen signaling in prostate cancer. *BMC cancer,* 18**,** 960-960.

KARIMI-BUSHERI, F., RASOULI-NIA, A., MACKEY, J. R. & WEINFELD, M. 2010. Senescence evasion by MCF-7 human breast tumor-initiating cells. *Breast Cancer Res,* 12**,** R31.

KEFALA, M., PAPAGEORGIOU, S. G., KONTOS, C. K., ECONOMOPOULOU, P., TSANAS, A., PAPPA, V., PANAYIOTIDES, I. G., GORGOULIS, V. G., PATSOURIS, E. & FOUKAS, P. G. 2013. Increased expression of phosphorylated NBS1, a key molecule of the DNA damage response machinery, is an adverse prognostic factor in patients with de novo myelodysplastic syndromes. *Leuk Res,* 37**,** 1576-82.

KHANNA, K. K. & JACKSON, S. P. 2001. DNA double-strand breaks: signaling, repair and the cancer connection. *Nat Genet,* 27**,** 247-54.

KHOURY, K. & DOMLING, A. 2012. P53 mdm2 inhibitors. *Curr Pharm Des,* 18**,** 4668-78.

KIM, A., UEDA, Y., NAKA, T. & ENOMOTO, T. 2012. Therapeutic strategies in epithelial ovarian cancer. *Journal of experimental & clinical cancer research : CR,* 31**,** 14-14.

KIM, J. H., GROSBART, M., ANAND, R., WYMAN, C., CEJKA, P. & PETRINI, J. H. J. 2017a. The Mre11-Nbs1 Interface Is Essential for Viability and Tumor Suppression. *Cell Rep,* 18**,** 496-507.

KIM, Y., KIM, A., SHARIP, A., SHARIP, A., JIANG, J., YANG, Q. & XIE, Y. 2017b. Reverse the Resistance to PARP Inhibitors. *International journal of biological sciences,* 13**,** 198-208.

KIM, Y. J. & WILSON, D. M., 3RD 2012. Overview of base excision repair biochemistry. *Curr Mol Pharmacol,* 5**,** 3-13.

KOBAYASHI, J., ANTOCCIA, A., TAUCHI, H., MATSUURA, S. & KOMATSU, K. 2004. NBS1 and its functional role in the DNA damage response. *DNA Repair (Amst),* 3**,** 855-61.

KODAZ, H., HACIBEKIROGLU, I., TURKMEN, E., ERDOGAN, B., ELPEN, C., UZUNOGLU, S. & CICIN, I. 2015. Increased dose single-agent gemcitabine in platinum-taxane resistant metastatic ovarian cancer. *Tumori,* 101**,** 36-40.

KONG, D., LI, Y., WANG, Z. & SARKAR, F. H. 2011. Cancer Stem Cells and Epithelial-to-Mesenchymal Transition (EMT)-Phenotypic Cells: Are They Cousins or Twins? *Cancers,* 3**,** 716-729.

KONONEN, J., BUBENDORF, L., KALLIONIEMI, A., BARLUND, M., SCHRAML, P., LEIGHTON, S., TORHORST, J., MIHATSCH, M. J., SAUTER, G. & KALLIONIEMI, O. P. 1998. Tissue microarrays for high-throughput molecular profiling of tumor specimens. *Nat Med,* 4**,** 844-7.

KONSTANTINOPOULOS, P. A., CECCALDI, R., SHAPIRO, G. I. & D'ANDREA, A. D. 2015. Homologous Recombination Deficiency: Exploiting the Fundamental Vulnerability of Ovarian Cancer. *Cancer discovery,* 5**,** 1137-1154.

KOOPMAN, G., REUTELINGSPERGER, C. P., KUIJTEN, G. A., KEEHNEN, R. M., PALS, S. T. & VAN OERS, M. H. 1994. Annexin V for flow cytometric detection of phosphatidylserine expression on B cells undergoing apoptosis. *Blood,* 84**,** 1415-20.

KOPPENSTEINER, R., SAMARTZIS, E. P., NOSKE, A., VON TEICHMAN, A., DEDES, I., GWERDER, M., IMESCH, P., IKENBERG, K., MOCH, H., FINK, D., STUCKI, M. & DEDES, K. J. 2014. Effect of MRE11 loss on PARP-inhibitor sensitivity in endometrial cancer in vitro. *PLoS One,* 9**,** e100041.

KOTHANDAPANI, A., DANGETI, V. S., BROWN, A. R., BANZE, L. A., WANG, X. H., SOBOL, R. W. & PATRICK, S. M. 2011. Novel role of base excision repair in mediating cisplatin cytotoxicity. *J Biol Chem,* 286**,** 14564-74.

KRUGER, I., ROTHKAMM, K. & LOBRICH, M. 2004. Enhanced fidelity for rejoining radiation-induced DNA double-strand breaks in

the G2 phase of Chinese hamster ovary cells. *Nucleic Acids Res,* 32**,** 2677-84.

LALWANI, N., PRASAD, S. R., VIKRAM, R., SHANBHOGUE, A. K., HUETTNER, P. C. & FASIH, N. 2011. Histologic, molecular, and cytogenetic features of ovarian cancers: implications for diagnosis and treatment. *Radiographics,* 31**,** 625-46.

LAMARCHE, B. J., ORAZIO, N. I. & WEITZMAN, M. D. 2010a. The MRN complex in double-strand break repair and telomere maintenance. *FEBS letters,* 584**,** 3682-3695.

LAMARCHE, B. J., ORAZIO, N. I. & WEITZMAN, M. D. 2010b. The MRN complex in double-strand break repair and telomere maintenance. *FEBS Lett,* 584**,** 3682-95.

LAURBERG, J. R., BREMS-ESKILDSEN, A. S., NORDENTOFT, I., FRISTRUP, N., SCHEPELER, T., ULHOI, B. P., AGERBAEK, M., HARTMANN, A., BERTZ, S., WITTLINGER, M., FIETKAU, R., RODEL, C., BORRE, M., JENSEN, J. B., ORNTOFT, T. & DYRSKJOT, L. 2012. Expression of TIP60 (tat-interactive protein) and MRE11 (meiotic recombination 11 homolog) predict treatment-specific outcome of localised invasive bladder cancer. *BJU Int,* 110**,** E1228-36.

LAVIN, M. F. 2007. ATM and the Mre11 complex combine to recognize and signal DNA double-strand breaks. *Oncogene,* 26**,** 7749-58.

LEE, G. S., NEIDITCH, M. B., SALUS, S. S. & ROTH, D. B. 2004. RAG proteins shepherd double-strand breaks to a specific pathway, suppressing error-prone repair, but RAG nicking initiates homologous recombination. *Cell,* 117**,** 171-84.

LEE, J. H. & PAULL, T. T. 2005. ATM activation by DNA double-strand breaks through the Mre11-Rad50-Nbs1 complex. *Science,* 308**,** 551-4.

LEE, J. H. & PAULL, T. T. 2007. Activation and regulation of ATM kinase activity in response to DNA double-strand breaks. *Oncogene,* 26**,** 7741-8.

LEE, Y. J., LEE, M. Y., RUAN, A., CHEN, C. K., LIU, H. P., WANG, C. J., CHAO, W. R. & HAN, C. P. 2016. Multipoint Kras oncogene mutations potentially indicate mucinous carcinoma on the entire spectrum of mucinous ovarian neoplasms. *Oncotarget,* 7**,** 82097-82103.

LEE, Y. K., PARK, N. H. & LEE, H. 2015. Clinicopathological values of NBS1 and DNA damage response genes in epithelial ovarian cancers. *Exp Mol Med,* 47**,** e195.

LEHMANN, S., BYKOV, V. J., ALI, D., ANDREN, O., CHERIF, H., TIDEFELT, U., UGGLA, B., YACHNIN, J., JULIUSSON, G., MOSHFEGH, A., PAUL, C., WIMAN, K. G. & ANDERSSON, P. O. 2012. Targeting p53 in vivo: a first-in-human study with p53-targeting compound APR-246 in refractory hematologic malignancies and prostate cancer. *J Clin Oncol,* 30**,** 3633-9.

LHEUREUX, S., GOURLEY, C., VERGOTE, I. & OZA, A. M. 2019. Epithelial ovarian cancer. *Lancet,* 393**,** 1240-1253.

LI, G. M. 2008. Mechanisms and functions of DNA mismatch repair. *Cell Res,* 18**,** 85-98.

LIEBER, M. R. 2010a. The mechanism of double-strand DNA break repair by the nonhomologous DNA end-joining pathway. *Annu Rev Biochem,* 79**,** 181-211.

LIEBER, M. R. 2010b. The mechanism of double-strand DNA break repair by the nonhomologous DNA end-joining pathway. *Annual review of biochemistry,* 79**,** 181-211.

LLORENTE, B. & SYMINGTON, L. S. 2004. The Mre11 nuclease is not required for 5' to 3' resection at multiple HO-induced double-strand breaks. *Mol Cell Biol,* 24**,** 9682-94.

LLOYD, J., CHAPMAN, J. R., CLAPPERTON, J. A., HAIRE, L. F., HARTSUIKER, E., LI, J., CARR, A. M., JACKSON, S. P. & SMERDON, S. J. 2009. A supramodular FHA/BRCT-repeat architecture mediates Nbs1 adaptor function in response to DNA damage. *Cell,* 139**,** 100-11.

LONDON, R. E. 2015. The structural basis of XRCC1-mediated DNA repair. *DNA Repair (Amst),* 30**,** 90-103.

LORD, C. J. & ASHWORTH, A. 2017. PARP inhibitors: Synthetic lethality in the clinic. *Science,* 355**,** 1152-1158.

LORET, N., DENYS, H., TUMMERS, P. & BERX, G. 2019. The Role of Epithelial-to-Mesenchymal Plasticity in Ovarian Cancer Progression and Therapy Resistance. *Cancers (Basel),* 11.

LORUSSO, D., MANCINI, M., DI ROCCO, R., FONTANELLI, R. & RASPAGLIESI, F. 2012. The role of secondary surgery in recurrent ovarian cancer. *International journal of surgical oncology,* 2012**,** 613980-613980.

LOU, Z., MINTER-DYKHOUSE, K., FRANCO, S., GOSTISSA, M., RIVERA, M. A., CELESTE, A., MANIS, J. P., VAN DEURSEN, J., NUSSENZWEIG, A., PAULL, T. T., ALT, F. W. & CHEN, J. 2006. MDC1 maintains genomic stability by participating in the amplification of ATM-dependent DNA damage signals. *Mol Cell,* 21**,** 187-200.

LU, M., LU, J., YANG, X., YANG, M., TAN, H., YUN, B. & SHI, L. 2009. Association between the NBS1E185Q polymorphism and cancer risk: a meta-analysis. *BMC Cancer,* 9**,** 124.

LUO, M., HE, H., KELLEY, M. R. & GEORGIADIS, M. M. 2010. Redox regulation of DNA repair: implications for human health and cancer therapeutic development. *Antioxidants & redox signaling,* 12**,** 1247-1269.

MABUCHI, S., KURODA, H., TAKAHASHI, R. & SASANO, T. 2015. The PI3K/AKT/mTOR pathway as a therapeutic target in ovarian cancer. *Gynecologic Oncology,* 137**,** 173-179.

MAHAJAN, K. N., NICK MCELHINNY, S. A., MITCHELL, B. S. & RAMSDEN, D. A. 2002. Association of DNA polymerase mu (pol mu) with Ku and ligase IV: role for pol mu in end-joining double-strand break repair. *Mol Cell Biol,* 22**,** 5194-202.

MANTOVANI, F., COLLAVIN, L. & DEL SAL, G. 2019. Mutant p53 as a guardian of the cancer cell. *Cell death and differentiation,* 26**,** 199-212.

MAO, Z., BOZZELLA, M., SELUANOV, A. & GORBUNOVA, V. 2008. Comparison of nonhomologous end joining and homologous recombination in human cells. *DNA Repair (Amst),* 7**,** 1765-71.

MARÉCHAL, A. & ZOU, L. 2013. DNA damage sensing by the ATM and ATR kinases. *Cold Spring Harbor perspectives in biology,* 5**,** a012716.

MARKMAN, M., KENNEDY, A., WEBSTER, K., KULP, B., PETERSON, G. & BELINSON, J. 2000. Phase 2 evaluation of topotecan administered on a 3-day schedule in the treatment of platinum- and paclitaxel-refractory ovarian cancer. *Gynecol Oncol,* 79**,** 116-9.

MARKMAN, M., WEBSTER, K., ZANOTTI, K., ROHL, J. & BELINSON, J. 2004. Use of tamoxifen in asymptomatic patients with recurrent small-volume ovarian cancer. *Gynecol Oncol,* 93**,** 390-3.

MATOS, L. L. D., TRUFELLI, D. C., DE MATOS, M. G. L. & DA SILVA PINHAL, M. A. 2010. Immunohistochemistry as an important tool in biomarkers detection and clinical practice. *Biomarker insights,* 5**,** 9-20.

MAZIN, A. V., MAZINA, O. M., BUGREEV, D. V. & ROSSI, M. J. 2010. Rad54, the motor of homologous recombination. *DNA Repair (Amst),* 9**,** 286-302.

MCCABE, N., TURNER, N. C., LORD, C. J., KLUZEK, K., BIALKOWSKA, A., SWIFT, S., GIAVARA, S., O'CONNOR, M. J., TUTT, A. N., ZDZIENICKA, M. Z., SMITH, G. C. & ASHWORTH, A. 2006. Deficiency in the repair of DNA damage by homologous recombination and sensitivity to poly(ADP-ribose) polymerase inhibition. *Cancer Res,* 66**,** 8109-15.

MCKINNON, P. J. 2009. DNA repair deficiency and neurological disease. *Nat Rev Neurosci,* 10**,** 100-12.

MCPHERSON, L. A., SHEN, Y. & FORD, J. M. 2014. Poly (ADP-ribose) polymerase inhibitor LT-626: Sensitivity correlates with MRE11 mutations and synergizes with platinums and irinotecan in colorectal cancer cells. *Cancer Lett,* 343**,** 217-23.

MEHTA, G., HSIAO, A. Y., INGRAM, M., LUKER, G. D. & TAKAYAMA, S. 2012. Opportunities and challenges for use of tumor spheroids as models to test drug delivery and efficacy. *Journal of controlled release : official journal of the Controlled Release Society,* 164**,** 192-204.

MESQUITA, K. A., ALABDULLAH, M., GRIFFIN, M., TOSS, M. S., FATAH, T., ALBLIHY, A., MOSELEY, P., CHAN, S. Y. T., RAKHA, E. A. & MADHUSUDAN, S. 2019. ERCC1-XPF deficiency is a predictor of olaparib induced synthetic lethality and platinum sensitivity in epithelial ovarian cancers. *Gynecol Oncol,* 153**,** 416-424.

MIMITOU, E. P. & SYMINGTON, L. S. 2009. DNA end resection: many nucleases make light work. *DNA Repair (Amst),* 8**,** 983-95.

MINCHOM, A., AVERSA, C. & LOPEZ, J. 2018. Dancing with the DNA damage response: next-generation anti-cancer therapeutic strategies. *Therapeutic advances in medical oncology,* 10**,** 1758835918786658-1758835918786658.

MISHIMA, K., MISHIMA-KANEKO, M., SAYA, H., ISHIMARU, N., YAMADA, K., FUKADA, J., NISHIKAWA, R. & KAWATA, T. 2014. RT-21Mre11-Rad50-Nbs1 COMPLEX INHIBITOR MIRIN

ENHANCES RADIOSENSITIVITY IN HUMAN GLIOBLASTOMA CELLS. *Neuro-Oncology,* 16**,** v192-v192.

MOHIUDDIN, I. S., WEI, S. J. & KANG, M. H. 2019. Role of OCT4 in cancer stem-like cells and chemotherapy resistance. *Biochim Biophys Acta Mol Basis Dis*.

MOMENIMOVAHED, Z., TIZNOBAIK, A., TAHERI, S. & SALEHINIYA, H. 2019. Ovarian cancer in the world: epidemiology and risk factors. *International journal of women's health,* 11**,** 287-299.

MONK, B. J., PUJADE-LAURAINE, E. & BURGER, R. A. 2013. Integrating bevacizumab into the management of epithelial ovarian cancer: the controversy of front-line versus recurrent disease. *Ann Oncol,* 24 Suppl 10**,** x53-x58.

MOORMAN, P. G., CALINGAERT, B., PALMIERI, R. T., IVERSEN, E. S., BENTLEY, R. C., HALABI, S., BERCHUCK, A. & SCHILDKRAUT, J. M. 2008. Hormonal risk factors for ovarian cancer in premenopausal and postmenopausal women. *American journal of epidemiology,* 167**,** 1059-1069.

MORALES, J., LI, L., FATTAH, F. J., DONG, Y., BEY, E. A., PATEL, M., GAO, J. & BOOTHMAN, D. A. 2014. Review of poly (ADP-ribose) polymerase (PARP) mechanisms of action and rationale for targeting in cancer and other diseases. *Critical reviews in eukaryotic gene expression,* 24**,** 15-28.

MOYNAHAN, M. E. & JASIN, M. 2010. Mitotic homologous recombination maintains genomic stability and suppresses tumorigenesis. *Nat Rev Mol Cell Biol,* 11**,** 196-207.

MUKHOPADHYAY, A., ELATTAR, A., CERBINSKAITE, A., WILKINSON, S. J., DREW, Y., KYLE, S., LOS, G., HOSTOMSKY, Z., EDMONDSON, R. J. & CURTIN, N. J. 2010. Development of a functional assay for homologous recombination status in primary cultures of epithelial ovarian tumor and correlation with sensitivity to poly(ADP-ribose) polymerase inhibitors. *Clin Cancer Res,* 16**,** 2344-51.

MURALI, R., DAVIDSON, B., FADARE, O., CARLSON, J. A., CRUM, C. P., GILKS, C. B., IRVING, J. A., MALPICA, A., MATIAS-GUIU, X., MCCLUGGAGE, W. G., MITTAL, K., OLIVA, E., PARKASH, V., RUTGERS, J. K. L., STAATS, P. N., STEWART, C. J. R., TORNOS, C. & SOSLOW, R. A. 2019. High-grade Endometrial Carcinomas: Morphologic and Immunohistochemical Features, Diagnostic Challenges and Recommendations. *International journal of gynecological pathology : official journal of the*

International Society of Gynecological Pathologists, 38 Suppl 1**,** S40-S63.

MUSA, F. & SCHNEIDER, R. 2015. Targeting the PI3K/AKT/mTOR pathway in ovarian cancer. *Translational Cancer Research,* 4**,** 97-106.

MUSELLA, A., BARDHI, E., MARCHETTI, C., VERTECHY, L., SANTANGELO, G., SASSU, C., TOMAO, F., RECH, F., D'AMELIO, R., MONTI, M., PALAIA, I., MUZII, L. & BENEDETTI PANICI, P. 2018. Rucaparib: An emerging parp inhibitor for treatment of recurrent ovarian cancer. *Cancer Treat Rev,* 66**,** 7-14.

MYLAVARAPU, S., DAS, A. & ROY, M. 2018. Role of BRCA Mutations in the Modulation of Response to Platinum Therapy. *Frontiers in oncology,* 8**,** 16-16.

NAGARAJU, G., ODATE, S., XIE, A. & SCULLY, R. 2006. Differential Regulation of Short- and Long-Tract Gene Conversion between Sister Chromatids by Rad51C. *Molecular and Cellular Biology,* 26**,** 8075-8086.

NAKANISHI, K., CAVALLO, F., BRUNET, E. & JASIN, M. 2011. Homologous recombination assay for interstrand cross-link repair. *Methods in molecular biology (Clifton, N.J.),* 745**,** 283-291.

NANAYAKKARA, A. K., FOLLIT, C. A., CHEN, G., WILLIAMS, N. S., VOGEL, P. D. & WISE, J. G. 2018. Targeted inhibitors of P-glycoprotein increase chemotherapeutic-induced mortality of multidrug resistant tumor cells. *Scientific reports,* 8**,** 967-967.

NEFF, R. T., SENTER, L. & SALANI, R. 2017. BRCA mutation in ovarian cancer: testing, implications and treatment considerations. *Therapeutic advances in medical oncology,* 9**,** 519-531.

NIMONKAR, A. V., GENSCHEL, J., KINOSHITA, E., POLACZEK, P., CAMPBELL, J. L., WYMAN, C., MODRICH, P. & KOWALCZYKOWSKI, S. C. 2011. BLM-DNA2-RPA-MRN and EXO1-BLM-RPA-MRN constitute two DNA end resection machineries for human DNA break repair. *Genes & development,* 25**,** 350-362.

NIU, H., RAYNARD, S. & SUNG, P. 2009. Multiplicity of DNA end resection machineries in chromosome break repair. *Genes Dev,* 23**,** 1481-6.

NOORDERMEER, S. M. & VAN ATTIKUM, H. 2019. PARP Inhibitor Resistance: A Tug-of-War in BRCA-Mutated Cells. *Trends Cell Biol,* 29**,** 820-834.

NORQUIST, B., WURZ, K. A., PENNIL, C. C., GARCIA, R., GROSS, J., SAKAI, W., KARLAN, B. Y., TANIGUCHI, T. & SWISHER, E. M. 2011. Secondary somatic mutations restoring BRCA1/2 predict chemotherapy resistance in hereditary ovarian carcinomas. *J Clin Oncol,* 29**,** 3008-15.

O'BRYAN, J. P. 2019. Pharmacological targeting of RAS: Recent success with direct inhibitors. *Pharmacological research,* 139**,** 503-511.

O'NEILL, C. J., MCBRIDE, H. A., CONNOLLY, L. E., DEAVERS, M. T., MALPICA, A. & MCCLUGGAGE, W. G. 2007. High-grade ovarian serous carcinoma exhibits significantly higher p16 expression than low-grade serous carcinoma and serous borderline tumour. *Histopathology,* 50**,** 773-9.

OKUGAWA, Y., TOIYAMA, Y., TANAKA, K., MATSUSITA, K., FUJIKAWA, H., SAIGUSA, S., OHI, M., INOUE, Y., MOHRI, Y., UCHIDA, K. & KUSUNOKI, M. 2012. Clinical significance of Zinc finger E-box Binding homeobox 1 (ZEB1) in human gastric cancer. *J Surg Oncol,* 106**,** 280-5.

OLDAK, S., IOANNOU, S., KAMATH, P., HUANG, M., GEORGE, S., SLOMOVITZ, B. & SCHLUMBRECHT, M. 2019. Polypharmacy in Patients with Ovarian Cancer. *Oncologist,* 24**,** 1201-1208.

OPLUSTILOVA, L., WOLANIN, K., MISTRIK, M., KORINKOVA, G., SIMKOVA, D., BOUCHAL, J., LENOBEL, R., BARTKOVA, J., LAU, A., O'CONNOR, M. J., LUKAS, J. & BARTEK, J. 2012. Evaluation of candidate biomarkers to predict cancer cell sensitivity or resistance to PARP-1 inhibitor treatment. *Cell Cycle,* 11**,** 3837-50.

OZA, A. M., COOK, A. D., PFISTERER, J., EMBLETON, A., LEDERMANN, J. A., PUJADE-LAURAINE, E., KRISTENSEN, G., CAREY, M. S., BEALE, P., CERVANTES, A., PARK-SIMON, T. W., RUSTIN, G., JOLY, F., MIRZA, M. R., PLANTE, M., QUINN, M., POVEDA, A., JAYSON, G. C., STARK, D., SWART, A. M., FARRELLY, L., KAPLAN, R., PARMAR, M. K. & PERREN, T. J. 2015. Standard chemotherapy with or without bevacizumab for women with newly diagnosed ovarian cancer (ICON7): overall survival results of a phase 3 randomised trial. *Lancet Oncol,* 16**,** 928-36.

PAN, G. & THOMSON, J. A. 2007. Nanog and transcriptional networks in embryonic stem cell pluripotency. *Cell Research,* 17**,** 42-49.

PANIER, S. & BOULTON, S. J. 2014. Double-strand break repair: 53BP1 comes into focus. *Nature Reviews Molecular Cell Biology,* 15**,** 7-18.

PANNUNZIO, N. R., LI, S., WATANABE, G. & LIEBER, M. R. 2014. Non-homologous end joining often uses microhomology: implications for alternative end joining. *DNA repair,* 17**,** 74-80.

PARDO, B., GOMEZ-GONZALEZ, B. & AGUILERA, A. 2009. DNA repair in mammalian cells: DNA double-strand break repair: how to fix a broken relationship. *Cell Mol Life Sci,* 66**,** 1039-56.

PARMAR, M. K., LEDERMANN, J. A., COLOMBO, N., DU BOIS, A., DELALOYE, J. F., KRISTENSEN, G. B., WHEELER, S., SWART, A. M., QIAN, W., TORRI, V., FLORIANI, I., JAYSON, G., LAMONT, A. & TROPE, C. 2003. Paclitaxel plus platinum-based chemotherapy versus conventional platinum-based chemotherapy in women with relapsed ovarian cancer: the ICON4/AGO-OVAR-2.2 trial. *Lancet,* 361**,** 2099-106.

PATTABIRAMAN, D. R. & WEINBERG, R. A. 2014. Tackling the cancer stem cells - what challenges do they pose? *Nature reviews. Drug discovery,* 13**,** 497-512.

PAVELITZ, T., RENFRO, L., FOSTER, N. R., CARACOL, A., WELSCH, P., LAO, V. V., GRADY, W. B., NIEDZWIECKI, D., SALTZ, L. B., BERTAGNOLLI, M. M., GOLDBERG, R. M., RABINOVITCH, P. S., EMOND, M., MONNAT, R. J., JR. & MAIZELS, N. 2014. MRE11-deficiency associated with improved long-term disease free survival and overall survival in a subset of stage III colon cancer patients in randomized CALGB 89803 trial. *PloS one,* 9**,** e108483-e108483.

PEINADO, H., OLMEDA, D. & CANO, A. 2007. Snail, Zeb and bHLH factors in tumour progression: an alliance against the epithelial phenotype? *Nat Rev Cancer,* 7**,** 415-28.

PELTOMAKI, P. 2003. Role of DNA mismatch repair defects in the pathogenesis of human cancer. *J Clin Oncol,* 21**,** 1174-9.

PERREN, T. J., SWART, A. M., PFISTERER, J., LEDERMANN, J. A., PUJADE-LAURAINE, E., KRISTENSEN, G., CAREY, M. S., BEALE, P., CERVANTES, A., KURZEDER, C., DU BOIS, A., SEHOULI, J., KIMMIG, R., STAHLE, A., COLLINSON, F., ESSAPEN, S., GOURLEY, C., LORTHOLARY, A., SELLE, F.,

MIRZA, M. R., LEMINEN, A., PLANTE, M., STARK, D., QIAN, W., PARMAR, M. K. & OZA, A. M. 2011. A phase 3 trial of bevacizumab in ovarian cancer. *N Engl J Med,* 365**,** 2484-96.

PHI, L. T. H., SARI, I. N., YANG, Y. G., LEE, S. H., JUN, N., KIM, K. S., LEE, Y. K. & KWON, H. Y. 2018. Cancer Stem Cells (CSCs) in Drug Resistance and their Therapeutic Implications in Cancer Treatment. *Stem Cells Int,* 2018**,** 5416923.

PICCART, M. J., BERTELSEN, K., JAMES, K., CASSIDY, J., MANGIONI, C., SIMONSEN, E., STUART, G., KAYE, S., VERGOTE, I., BLOM, R., GRIMSHAW, R., ATKINSON, R. J., SWENERTON, K. D., TROPE, C., NARDI, M., KAERN, J., TUMOLO, S., TIMMERS, P., ROY, J. E.-A., LHOAS, F. O., LINDVALL, B., BACON, M., BIRT, A., ANDERSEN, J. E., ZEE, B., PAUL, J., BARON, B. T. & PECORELLI, S. 2000. Randomized Intergroup Trial of Cisplatin–Paclitaxel Versus Cisplatin–Cyclophosphamide in Women With Advanced Epithelial Ovarian Cancer: Three-Year Results. *JNCI: Journal of the National Cancer Institute,* 92**,** 699-708.

PRAT, J. 2012. New insights into ovarian cancer pathology. *Annals of Oncology,* 23**,** x111-x117.

PUJADE-LAURAINE, E., HILPERT, F., WEBER, B., REUSS, A., POVEDA, A., KRISTENSEN, G., SORIO, R., VERGOTE, I., WITTEVEEN, P., BAMIAS, A., PEREIRA, D., WIMBERGER, P., OAKNIN, A., MIRZA, M. R., FOLLANA, P., BOLLAG, D. & RAY-COQUARD, I. 2014. Bevacizumab combined with chemotherapy for platinum-resistant recurrent ovarian cancer: The AURELIA open-label randomized phase III trial. *J Clin Oncol,* 32**,** 1302-8.

QIAO, G. B., WU, Y. L., YANG, X. N., ZHONG, W. Z., XIE, D., GUAN, X. Y., FISCHER, D., KOLBERG, H. C., KRUGER, S. & STUERZBECHER, H. W. 2005. High-level expression of Rad51 is an independent prognostic marker of survival in non-small-cell lung cancer patients. *British Journal of Cancer,* 93**,** 137-143.

RABIK, C. A. & DOLAN, M. E. 2007. Molecular mechanisms of resistance and toxicity associated with platinating agents. *Cancer treatment reviews,* 33**,** 9-23.

RAI, R., ZHENG, H., HE, H., LUO, Y., MULTANI, A., CARPENTER, P. B. & CHANG, S. 2010. The function of classical and alternative non-homologous end-joining pathways in the fusion of dysfunctional telomeres. *Embo j,* 29**,** 2598-610.

RAJA, F. A., CHOPRA, N. & LEDERMANN, J. A. 2012. Optimal first-line treatment in ovarian cancer. *Ann Oncol.* England.

RASS, E., GRABARZ, A., PLO, I., GAUTIER, J., BERTRAND, P. & LOPEZ, B. S. 2009. Role of Mre11 in chromosomal nonhomologous end joining in mammalian cells. *Nat Struct Mol Biol,* 16**,** 819-24.

REID, B. M., PERMUTH, J. B. & SELLERS, T. A. 2017. Epidemiology of ovarian cancer: a review. *Cancer Biol Med,* 14**,** 9-32.

REIN, K. & STRACKER, T. H. 2014. The MRE11 complex: an important source of stress relief. *Exp Cell Res,* 329**,** 162-9.

RICCARDI, C. & NICOLETTI, I. 2006. Analysis of apoptosis by propidium iodide staining and flow cytometry. *Nat Protoc,* 1**,** 1458-61.

RICCI, F., AFFATATO, R., CARRASSA, L. & DAMIA, G. 2018. Recent Insights into Mucinous Ovarian Carcinoma. *International journal of molecular sciences,* 19**,** 1569.

RICHARD, D. J., SAVAGE, K., BOLDERSON, E., CUBEDDU, L., SO, S., GHITA, M., CHEN, D. J., WHITE, M. F., RICHARD, K., PRISE, K. M., SCHETTINO, G. & KHANNA, K. K. 2011. hSSB1 rapidly binds at the sites of DNA double-strand breaks and is required for the efficient recruitment of the MRN complex. *Nucleic acids research,* 39**,** 1692-1702.

RIHA, K., HEACOCK, M. L. & SHIPPEN, D. E. 2006. The role of the nonhomologous end-joining DNA double-strand break repair pathway in telomere biology. *Annu Rev Genet,* 40**,** 237-77.

ROBERT, I., DANTZER, F. & REINA-SAN-MARTIN, B. 2009. Parp1 facilitates alternative NHEJ, whereas Parp2 suppresses IgH/c-myc translocations during immunoglobulin class switch recombination. *J Exp Med,* 206**,** 1047-56.

ROSEN, D. G., YANG, G., LIU, G., MERCADO-URIBE, I., CHANG, B., XIAO, X. S., ZHENG, J., XUE, F.-X. & LIU, J. 2009. Ovarian cancer: pathology, biology, and disease models. *Frontiers in bioscience (Landmark edition),* 14**,** 2089-2102.

ROSEN, D. G., ZHANG, Z., SHAN, W. & LIU, J. 2010. Morphological and molecular basis of ovarian serous carcinoma. *Journal of biomedical research,* 24**,** 257-263.

ROSIDI, B., WANG, M., WU, W., SHARMA, A., WANG, H. & ILIAKIS, G. 2008. Histone H1 functions as a stimulatory factor in backup pathways of NHEJ. *Nucleic acids research,* 36**,** 1610-1623.

SAGAN, D., MULLER, R., KROGER, C., HEMATULIN, A., MORTL, S. & ECKARDT-SCHUPP, F. 2009. The DNA repair protein NBS1 influences the base excision repair pathway. *Carcinogenesis,* 30**,** 408-15.

SAITO, Y., FUJIMOTO, H. & KOBAYASHI, J. 2013. Role of NBS1 in DNA damage response and its relationship with cancer development. *Translational Cancer Research; Vol 2, No 3 (June 2013): Translational Cancer Research (DNA Damage and Repair)*.

SAKAI, W., SWISHER, E. M., JACQUEMONT, C., CHANDRAMOHAN, K. V., COUCH, F. J., LANGDON, S. P., WURZ, K., HIGGINS, J., VILLEGAS, E. & TANIGUCHI, T. 2009. Functional restoration of BRCA2 protein by secondary BRCA2 mutations in BRCA2-mutated ovarian carcinoma. *Cancer Res,* 69**,** 6381-6.

SAMIMI, G., KATANO, K., HOLZER, A. K., SAFAEI, R. & HOWELL, S. B. 2004. Modulation of the cellular pharmacology of cisplatin and its analogs by the copper exporters ATP7A and ATP7B. *Mol Pharmacol,* 66**,** 25-32.

SATELLI, A. & LI, S. 2011. Vimentin in cancer and its potential as a molecular target for cancer therapy. *Cell Mol Life Sci,* 68**,** 3033-46.

SCHAETZLEIN, S., KODANDARAMIREDDY, N. R., JU, Z., LECHEL, A., STEPCZYNSKA, A., LILLI, D. R., CLARK, A. B., RUDOLPH, C., KUHNEL, F., WEI, K., SCHLEGELBERGER, B., SCHIRMACHER, P., KUNKEL, T. A., GREENBERG, R. A., EDELMANN, W. & RUDOLPH, K. L. 2007. Exonuclease-1 deletion impairs DNA damage signaling and prolongs lifespan of telomere-dysfunctional mice. *Cell,* 130**,** 863-77.

SCHARER, O. D. 2003. Chemistry and biology of DNA repair. *Angew Chem Int Ed Engl,* 42**,** 2946-74.

SCHÄRER, O. D. 2013. Nucleotide excision repair in eukaryotes. *Cold Spring Harbor perspectives in biology,* 5**,** a012609-a012609.

SCHLACHER, K., CHRIST, N., SIAUD, N., EGASHIRA, A., WU, H. & JASIN, M. 2011a. Double-strand break repair-independent role for BRCA2 in blocking stalled replication fork degradation by MRE11. *Cell,* 145**,** 529-42.

SCHLACHER, K., CHRIST, N., SIAUD, N., EGASHIRA, A., WU, H. & JASIN, M. 2011b. Double-strand break repair-independent role for BRCA2 in blocking stalled replication fork degradation by MRE11. *Cell,* 145**,** 529-542.

SHAO, M., BI, T., DING, W., YU, C., JIANG, C., YANG, H., SUN, X. & YANG, M. 2018. OCT4 Potentiates Radio-Resistance and Migration Activity of Rectal Cancer Cells by Improving Epithelial-Mesenchymal Transition in a ZEB1 Dependent Manner. *Biomed Res Int,* 2018**,** 3424956.

SHAROM, F. J. 2008. ABC multidrug transporters: structure, function and role in chemoresistance. *Pharmacogenomics,* 9**,** 105-27.

SHEN, L., HUANG, X., XIE, X., SU, J., YUAN, J. & CHEN, X. 2014. High Expression of SOX2 and OCT4 Indicates Radiation Resistance and an Independent Negative Prognosis in Cervical Squamous Cell Carcinoma. *The journal of histochemistry and cytochemistry : official journal of the Histochemistry Society,* 62**,** 499-509.

SHI, G. & JIN, Y. 2010. Role of Oct4 in maintaining and regaining stem cell pluripotency. *Stem cell research & therapy,* 1**,** 39-39.

SHIBATA, A., MOIANI, D., ARVAI, A. S., PERRY, J., HARDING, S. M., GENOIS, M. M., MAITY, R., VAN ROSSUM-FIKKERT, S., KERTOKALIO, A., ROMOLI, F., ISMAIL, A., ISMALAJ, E., PETRICCI, E., NEALE, M. J., BRISTOW, R. G., MASSON, J. Y., WYMAN, C., JEGGO, P. A. & TAINER, J. A. 2014. DNA double-strand break repair pathway choice is directed by distinct MRE11 nuclease activities. *Mol Cell,* 53**,** 7-18.

SHIBUE, T. & WEINBERG, R. A. 2017. EMT, CSCs, and drug resistance: the mechanistic link and clinical implications. *Nature reviews. Clinical oncology,* 14**,** 611-629.

SHIMIZU, M., TOKI, T., TAKAGI, Y., KONISHI, I. & FUJII, S. 2000. Immunohistochemical detection of the Wilms' tumor gene (WT1) in epithelial ovarian tumors. *Int J Gynecol Pathol,* 19**,** 158-63.

SHIN, D. S., CHAHWAN, C., HUFFMAN, J. L. & TAINER, J. A. 2004. Structure and function of the double-strand break repair machinery. *DNA Repair (Amst),* 3**,** 863-73.

SHIOTANI, B. & ZOU, L. 2009. Single-stranded DNA orchestrates an ATM-to-ATR switch at DNA breaks. *Mol Cell,* 33**,** 547-58.

SIDDIK, Z. H. 2003. Cisplatin: mode of cytotoxic action and molecular basis of resistance. *Oncogene,* 22**,** 7265-79.

SIEGEL, R. L., MILLER, K. D. & JEMAL, A. 2018. Cancer statistics, 2018. *CA Cancer J Clin,* 68**,** 7-30.

SITU, Y., CHUNG, L., LEE, C. S. & HO, V. 2019. MRN (MRE11-RAD50-NBS1) Complex in Human Cancer and Prognostic Implications in Colorectal Cancer. *International journal of molecular sciences,* 20**,** 816.

SKIRNISDOTTIR, I., BJERSAND, K., AKERUD, H. & SEIDAL, T. 2013. Napsin A as a marker of clear cell ovarian carcinoma. *BMC cancer,* 13**,** 524-524.

SMOLLE, E., TAUCHER, V., PICHLER, M., PETRU, E., LAX, S. & HAYBAECK, J. 2013. Targeting signaling pathways in epithelial ovarian cancer. *International journal of molecular sciences,* 14**,** 9536-9555.

SODANI, K., PATEL, A., KATHAWALA, R. J. & CHEN, Z.-S. 2012. Multidrug resistance associated proteins in multidrug resistance. *Chinese journal of cancer,* 31**,** 58-72.

SODERLUND, K., STAL, O., SKOOG, L., RUTQVIST, L. E., NORDENSKJOLD, B. & ASKMALM, M. S. 2007. Intact Mre11/Rad50/Nbs1 complex predicts good response to radiotherapy in early breast cancer. *Int J Radiat Oncol Biol Phys,* 68**,** 50-8.

SONG, I. S., SAVARAJ, N., SIDDIK, Z. H., LIU, P., WEI, Y., WU, C. J. & KUO, M. T. 2004. Role of human copper transporter Ctr1 in the transport of platinum-based antitumor agents in cisplatin-sensitive and cisplatin-resistant cells. *Mol Cancer Ther,* 3**,** 1543-9.

SORENSEN, C. S., HANSEN, L. T., DZIEGIELEWSKI, J., SYLJUASEN, R. G., LUNDIN, C., BARTEK, J. & HELLEDAY, T. 2005. The cell-cycle checkpoint kinase Chk1 is required for mammalian homologous recombination repair. *Nat Cell Biol,* 7**,** 195-201.

SPOELSTRA, N. S., MANNING, N. G., HIGASHI, Y., DARLING, D., SINGH, M., SHROYER, K. R., BROADDUS, R. R., HORWITZ, K. B. & RICHER, J. K. 2006. The transcription factor ZEB1 is aberrantly expressed in aggressive uterine cancers. *Cancer Res,* 66**,** 3893-902.

SRIVASTAVA, A. K., HAN, C., ZHAO, R., CUI, T., DAI, Y., MAO, C., ZHAO, W., ZHANG, X., YU, J. & WANG, Q. E. 2015. Enhanced

expression of DNA polymerase eta contributes to cisplatin resistance of ovarian cancer stem cells. *Proc Natl Acad Sci U S A,* 112**,** 4411-6.

SRIVASTAVA, M. & RAGHAVAN, S. C. 2015. DNA double-strand break repair inhibitors as cancer therapeutics. *Chem Biol,* 22**,** 17-29.

STAVRIDI, E. S. & HALAZONETIS, T. D. 2005. Nbs1 moving up in the world. *Nat Cell Biol.* England.

STEINKE, V., ENGEL, C., BÜTTNER, R., SCHACKERT, H. K., SCHMIEGEL, W. H. & PROPPING, P. 2013. Hereditary nonpolyposis colorectal cancer (HNPCC)/Lynch syndrome. *Deutsches Arzteblatt international,* 110**,** 32-38.

STORDAL, B., TIMMS, K., FARRELLY, A., GALLAGHER, D., BUSSCHOTS, S., RENAUD, M., THERY, J., WILLIAMS, D., POTTER, J., TRAN, T., KORPANTY, G., CREMONA, M., CAREY, M., LI, J., LI, Y., ASLAN, O., O'LEARY, J. J., MILLS, G. B. & HENNESSY, B. T. 2013. BRCA1/2 mutation analysis in 41 ovarian cell lines reveals only one functionally deleterious BRCA1 mutation. *Mol Oncol,* 7**,** 567-79.

STRACKER, T. H. & PETRINI, J. H. J. 2011. The MRE11 complex: starting from the ends. *Nature reviews. Molecular cell biology,* 12**,** 90-103.

STRAUSS, H. G., HEMSEN, A., KARBE, I., LAUTENSCHLAGER, C., PERSING, M. & THOMSSEN, C. 2008. Phase II trial of biweekly pegylated liposomal doxorubicin in recurrent platinum-refractory ovarian and peritoneal cancer. *Anticancer Drugs,* 19**,** 541-5.

SULTANA, R., ABDEL-FATAH, T., ABBOTTS, R., HAWKES, C., ALBARAKATI, N., SEEDHOUSE, C., BALL, G., CHAN, S., RAKHA, E. A., ELLIS, I. O. & MADHUSUDAN, S. 2013a. Targeting XRCC1 deficiency in breast cancer for personalized therapy. *Cancer Res,* 73**,** 1621-34.

SULTANA, R., ABDEL-FATAH, T., PERRY, C., MOSELEY, P., ALBARAKTI, N., MOHAN, V., SEEDHOUSE, C., CHAN, S. & MADHUSUDAN, S. 2013b. Ataxia telangiectasia mutated and Rad3 related (ATR) protein kinase inhibition is synthetically lethal in XRCC1 deficient ovarian cancer cells. *PLoS One,* 8**,** e57098.

SWISHER, E. M., SAKAI, W., KARLAN, B. Y., WURZ, K., URBAN, N. & TANIGUCHI, T. 2008. Secondary BRCA1 mutations in BRCA1-mutated ovarian carcinomas with platinum resistance. *Cancer Res,* 68**,** 2581-6.

SYED, A. & TAINER, J. A. 2018a. The MRE11-RAD50-NBS1 Complex Conducts the Orchestration of Damage Signaling and Outcomes to Stress in DNA Replication and Repair. *Annual review of biochemistry,* 87**,** 263-294.

SYMINGTON, L. S. 2002. Role of RAD52 epistasis group genes in homologous recombination and double-strand break repair. *Microbiol Mol Biol Rev,* 66**,** 630-70, table of contents.

TAO, Y., LI, H., HUANG, R., MO, D., ZENG, T., FANG, M. & LI, M. 2018. Clinicopathological and Prognostic Significance of Cancer Stem Cell Markers in Ovarian Cancer Patients: Evidence from 52 Studies. *Cell Physiol Biochem,* 46**,** 1716-1726.

TAUCHI, H., KOBAYASHI, J., MORISHIMA, K., VAN GENT, D. C., SHIRAISHI, T., VERKAIK, N. S., VANHEEMS, D., ITO, E., NAKAMURA, A., SONODA, E., TAKATA, M., TAKEDA, S., MATSUURA, S. & KOMATSU, K. 2002. Nbs1 is essential for DNA repair by homologous recombination in higher vertebrate cells. *Nature,* 420**,** 93-8.

TEO, M. T., DYRSKJOT, L., NSENGIMANA, J., BUCHWALD, C., SNOWDEN, H., MORGAN, J., JENSEN, J. B., KNOWLES, M. A., TAYLOR, G., BARRETT, J. H., BORRE, M., ORNTOFT, T. F., BISHOP, D. T. & KILTIE, A. E. 2014. Next-generation sequencing identifies germline MRE11A variants as markers of radiotherapy outcomes in muscle-invasive bladder cancer. *Ann Oncol,* 25**,** 877-83.

THAVARAMARA, T., TANGJITGAMOL, S., MANUSIRIVITHAYA, S. & LEELAHAKORN, S. 2009. Oral etoposide for refractory or recurrent epithelial ovarian cancer. *J Med Assoc Thai,* 92**,** 1397-405.

THOMPSON, L. H. & SCHILD, D. 2002. Recombinational DNA repair and human disease. *Mutat Res,* 509**,** 49-78.

THOMS, K. M., KUSCHAL, C. & EMMERT, S. 2007. Lessons learned from DNA repair defective syndromes. *Exp Dermatol,* 16**,** 532-44.

TOMIMATSU, N., MUKHERJEE, B., CATHERINE HARDEBECK, M., ILCHEVA, M., VANESSA CAMACHO, C., LOUISE HARRIS, J., PORTEUS, M., LLORENTE, B., KHANNA, K. K. & BURMA, S. 2014. Phosphorylation of EXO1 by CDKs 1 and 2 regulates DNA end resection and repair pathway choice. *Nature Communications,* 5**,** 3561.

TOSS, A., TOMASELLO, C., RAZZABONI, E., CONTU, G., GRANDI, G., CAGNACCI, A., SCHILDER, R. J. & CORTESI, L. 2015. Hereditary ovarian cancer: not only BRCA 1 and 2 genes. *BioMed research international,* 2015**,** 341723-341723.

TRAN, H. M., SHI, G., LI, G., CARNEY, J. P., O'MALLEY, B. & LI, D. 2004. Mutant Nbs1 enhances cisplatin-induced DNA damage and cytotoxicity in head and neck cancer. *Otolaryngol Head Neck Surg,* 131**,** 477-84.

TRAVERSO, N., RICCIARELLI, R., NITTI, M., MARENGO, B., FURFARO, A. L., PRONZATO, M. A., MARINARI, U. M. & DOMENICOTTI, C. 2013. Role of glutathione in cancer progression and chemoresistance. *Oxid Med Cell Longev,* 2013**,** 972913.

TREVIÑO, L. S., BUCKLES, E. L. & JOHNSON, P. A. 2012. Oral contraceptives decrease the prevalence of ovarian cancer in the hen. *Cancer prevention research (Philadelphia, Pa.),* 5**,** 343-349.

TRIMBOS, J. B., VERGOTE, I., BOLIS, G., VERMORKEN, J. B., MANGIONI, C., MADRONAL, C., FRANCHI, M., TATEO, S., ZANETTA, G., SCARFONE, G., GIURGEA, L., TIMMERS, P., COENS, C. & PECORELLI, S. 2003. Impact of adjuvant chemotherapy and surgical staging in early-stage ovarian carcinoma: European Organisation for Research and Treatment of Cancer-Adjuvant ChemoTherapy in Ovarian Neoplasm trial. *J Natl Cancer Inst,* 95**,** 113-25.

TSENG, S. F., CHANG, C. Y., WU, K. J. & TENG, S. C. 2005. Importin KPNA2 is required for proper nuclear localization and multiple functions of NBS1. *J Biol Chem,* 280**,** 39594-600.

USHIJIMA, K. 2010a. Treatment for recurrent ovarian cancer-at first relapse. *J Oncol,* 2010**,** 497429.

USHIJIMA, K. 2010b. Treatment for recurrent ovarian cancer-at first relapse. *Journal of oncology,* 2010**,** 497429-497429.

VALERIE, K. & POVIRK, L. F. 2003. Regulation and mechanisms of mammalian double-strand break repair. *Oncogene,* 22**,** 5792-812.

VAN ZYL, B., TANG, D. & BOWDEN, N. A. 2018. Biomarkers of platinum resistance in ovarian cancer: what can we use to improve treatment. *Endocr Relat Cancer,* 25**,** R303-r318.

VANG, R., SHIH, I.-M. & KURMAN, R. J. 2009. Ovarian low-grade and high-grade serous carcinoma: pathogenesis, clinicopathologic and molecular biologic features, and diagnostic problems. *Advances in anatomic pathology,* 16**,** 267-282.

VAZ, B., POPOVIC, M. & RAMADAN, K. 2017. DNA-Protein Crosslink Proteolysis Repair. *Trends Biochem Sci,* 42**,** 483-495.

VENERE, M., HAMERLIK, P., WU, Q., RASMUSSEN, R. D., SONG, L. A., VASANJI, A., TENLEY, N., FLAVAHAN, W. A., HJELMELAND, A. B., BARTEK, J. & RICH, J. N. 2014. Therapeutic targeting of constitutive PARP activation compromises stem cell phenotype and survival of glioblastoma-initiating cells. *Cell Death Differ,* 21**,** 258-69.

VENTELA, S., SITTIG, E., MANNERMAA, L., MAKELA, J. A., KULMALA, J., LOYTTYNIEMI, E., STRAUSS, L., CARPEN, O., TOPPARI, J., GRENMAN, R. & WESTERMARCK, J. 2015. CIP2A is an Oct4 target gene involved in head and neck squamous cell cancer oncogenicity and radioresistance. *Oncotarget,* 6**,** 144-58.

VERGOTE, I., TROPE, C. G., AMANT, F., KRISTENSEN, G. B., EHLEN, T., JOHNSON, N., VERHEIJEN, R. H., VAN DER BURG, M. E., LACAVE, A. J., PANICI, P. B., KENTER, G. G., CASADO, A., MENDIOLA, C., COENS, C., VERLEYE, L., STUART, G. C., PECORELLI, S. & REED, N. S. 2010. Neoadjuvant chemotherapy or primary surgery in stage IIIC or IV ovarian cancer. *N Engl J Med,* 363**,** 943-53.

VILAR, E., BARTNIK, C. M., STENZEL, S. L., RASKIN, L., AHN, J., MORENO, V., MUKHERJEE, B., INIESTA, M. D., MORGAN, M. A., RENNERT, G. & GRUBER, S. B. 2011. MRE11 deficiency increases sensitivity to poly(ADP-ribose) polymerase inhibition in microsatellite unstable colorectal cancers. *Cancer research,* 71**,** 2632-2642.

VILLODRE, E. S., KIPPER, F. C., PEREIRA, M. B. & LENZ, G. 2016. Roles of OCT4 in tumorigenesis, cancer therapy resistance and prognosis. *Cancer Treat Rev,* 51**,** 1-9.

VITALE, I., MANIC, G., DE MARIA, R., KROEMER, G. & GALLUZZI, L. 2017. DNA Damage in Stem Cells. *Mol Cell,* 66**,** 306-319.

WALKER, J. R., CORPINA, R. A. & GOLDBERG, J. 2001. Structure of the Ku heterodimer bound to DNA and its implications for double-strand break repair. *Nature,* 412**,** 607-14.

WALSH, C. S. 2015. Two decades beyond BRCA1/2: Homologous recombination, hereditary cancer risk and a target for ovarian cancer therapy. *Gynecol Oncol,* 137**,** 343-50.

WALTES, R., KALB, R., GATEI, M., KIJAS, A. W., STUMM, M., SOBECK, A., WIELAND, B., VARON, R., LERENTHAL, Y., LAVIN, M. F., SCHINDLER, D. & DORK, T. 2009a. Human RAD50 deficiency in a Nijmegen breakage syndrome-like disorder. *Am J Hum Genet,* 84**,** 605-16.

WALTES, R., KALB, R., GATEI, M., KIJAS, A. W., STUMM, M., SOBECK, A., WIELAND, B., VARON, R., LERENTHAL, Y., LAVIN, M. F., SCHINDLER, D. & DÖRK, T. 2009b. Human RAD50 deficiency in a Nijmegen breakage syndrome-like disorder. *American journal of human genetics,* 84**,** 605-616.

WANG, J., XU, W.-H., WEI, Y., ZHU, Y., QIN, X.-J., ZHANG, H.-L. & YE, D.-W. 2019. Elevated MRE11 expression associated with progression and poor outcome in prostate cancer. *Journal of Cancer,* 10**,** 4333-4340.

WANG, M., WU, W., WU, W., ROSIDI, B., ZHANG, L., WANG, H. & ILIAKIS, G. 2006. PARP-1 and Ku compete for repair of DNA double strand breaks by distinct NHEJ pathways. *Nucleic acids research,* 34**,** 6170-6182.

WANG, Y., GUDIKOTE, J., GIRI, U., YAN, J., DENG, W., YE, R., JIANG, W., LI, N., HOBBS, B. P., WANG, J., SWISHER, S. G., FUJIMOTO, J., WISTUBA, II, KOMAKI, R., HEYMACH, J. V. & LIN, S. H. 2018. RAD50 Expression Is Associated with Poor Clinical Outcomes after Radiotherapy for Resected Non-small Cell Lung Cancer. *Clin Cancer Res,* 24**,** 341-350.

WELLNER, U., BRABLETZ, T. & KECK, T. 2010. ZEB1 in Pancreatic Cancer. *Cancers,* 2**,** 1617-1628.

WEST, K. A., CASTILLO, S. S. & DENNIS, P. A. 2002. Activation of the PI3K/Akt pathway and chemotherapeutic resistance. *Drug Resist Updat,* 5**,** 234-48.

WILLIAMS, R. S., WILLIAMS, J. S. & TAINER, J. A. 2007. Mre11-Rad50-Nbs1 is a keystone complex connecting DNA repair

machinery, double-strand break signaling, and the chromatin template. *Biochem Cell Biol,* 85**,** 509-20.

WOOD, R. D. 1999. DNA damage recognition during nucleotide excision repair in mammalian cells. *Biochimie,* 81**,** 39-44.

WOOPEN, H., RICHTER, R., ISMAEEL, F., CHEKEROV, R., ROOTS, I., SIEPMANN, T. & SEHOULI, J. 2016. The influence of polypharmacy on grade III/IV toxicity, prior discontinuation of chemotherapy and overall survival in ovarian cancer. *Gynecol Oncol,* 140**,** 554-8.

WU, D., TOPPER, L. M. & WILSON, T. E. 2008. Recruitment and dissociation of nonhomologous end joining proteins at a DNA double-strand break in Saccharomyces cerevisiae. *Genetics,* 178**,** 1237-49.

WU, Y., XIAO, S. & ZHU, X. D. 2007. MRE11-RAD50-NBS1 and ATM function as co-mediators of TRF1 in telomere length control. *Nat Struct Mol Biol,* 14**,** 832-40.

XU, H., WANG, W., LI, C., YU, H., YANG, A., WANG, B. & JIN, Y. 2009. WWP2 promotes degradation of transcription factor OCT4 in human embryonic stem cells. *Cell Research,* 19**,** 561-573.

YAJIMA, H., LEE, K. J. & CHEN, B. P. 2006. ATR-dependent phosphorylation of DNA-dependent protein kinase catalytic subunit in response to UV-induced replication stress. *Mol Cell Biol,* 26**,** 7520-8.

YANG, M.-H., CHIANG, W.-C., CHOU, T.-Y., CHANG, S.-Y., CHEN, P.-M., TENG, S.-C. & WU, K.-J. 2006a. Increased NBS1 Expression Is a Marker of Aggressive Head and Neck Cancer and Overexpression of NBS1 Contributes to Transformation. *Clinical Cancer Research,* 12**,** 507.

YANG, M. H., CHANG, S. Y., CHIOU, S. H., LIU, C. J., CHI, C. W., CHEN, P. M., TENG, S. C. & WU, K. J. 2007. Overexpression of NBS1 induces epithelial-mesenchymal transition and co-expression of NBS1 and Snail predicts metastasis of head and neck cancer. *Oncogene,* 26**,** 1459-67.

YANG, M. H., CHIANG, W. C., CHOU, T. Y., CHANG, S. Y., CHEN, P. M., TENG, S. C. & WU, K. J. 2006b. Increased NBS1 expression is a marker of aggressive head and neck cancer and overexpression of NBS1 contributes to transformation. *Clin Cancer Res,* 12**,** 507-15.

YANG, Y.-G., SAIDI, A., FRAPPART, P.-O., MIN, W., BARRUCAND, C., DUMON-JONES, V., MICHELON, J., HERCEG, Z. & WANG, Z.-Q. 2006c. Conditional deletion of Nbs1 in murine cells reveals its role in branching repair pathways of DNA double-strand breaks. *The EMBO journal,* 25**,** 5527-5538.

YING, S., CHEN, Z., MEDHURST, A. L., NEAL, J. A., BAO, Z., MORTUSEWICZ, O., MCGOURAN, J., SONG, X., SHEN, H., HAMDY, F. C., KESSLER, B. M., MEEK, K. & HELLEDAY, T. 2016. DNA-PKcs and PARP1 Bind to Unresected Stalled DNA Replication Forks Where They Recruit XRCC1 to Mediate Repair. *Cancer research,* 76**,** 1078-1088.

YING, S., HAMDY, F. C. & HELLEDAY, T. 2012. Mre11-dependent degradation of stalled DNA replication forks is prevented by BRCA2 and PARP1. *Cancer Res,* 72**,** 2814-21.

YOO, S. Y. & KWON, S. M. 2013. Angiogenesis and Its Therapeutic Opportunities. *Mediators of Inflammation,* 2013**,** 11.

YU, Y., MAHANEY, B. L., YANO, K., YE, R., FANG, S., DOUGLAS, P., CHEN, D. J. & LEES-MILLER, S. P. 2008. DNA-PK and ATM phosphorylation sites in XLF/Cernunnos are not required for repair of DNA double strand breaks. *DNA Repair (Amst),* 7**,** 1680-92.

YU, Z., PESTELL, T. G., LISANTI, M. P. & PESTELL, R. G. 2012. Cancer stem cells. *The international journal of biochemistry & cell biology,* 44**,** 2144-2151.

YUAN, S. S., HOU, M. F., HSIEH, Y. C., HUANG, C. Y., LEE, Y. C., CHEN, Y. J. & LO, S. 2012. Role of MRE11 in cell proliferation, tumor invasion, and DNA repair in breast cancer. *J Natl Cancer Inst,* 104**,** 1485-502.

YUN, M. H. & HIOM, K. 2009. CtIP-BRCA1 modulates the choice of DNA double-strand-break repair pathway throughout the cell cycle. *Nature,* 459**,** 460-3.

ZANONI, M., PICCININI, F., ARIENTI, C., ZAMAGNI, A., SANTI, S., POLICO, R., BEVILACQUA, A. & TESEI, A. 2016. 3D tumor spheroid models for in vitro therapeutic screening: a systematic approach to enhance the biological relevance of data obtained. *Scientific Reports,* 6**,** 19103.

ZHANG, G. J., ZHOU, T., TIAN, H. P., LIU, Z. L. & XIA, S. S. 2013a. High expression of ZEB1 correlates with liver metastasis and poor prognosis in colorectal cancer. *Oncol Lett,* 5**,** 564-568.

ZHANG, J., ESPINOZA, L. A., KINDERS, R. J., LAWRENCE, S. M., PFISTER, T. D., ZHOU, M., VEENSTRA, T. D., THORGEIRSSON, S. S. & JESSUP, J. M. 2013b. NANOG modulates stemness in human colorectal cancer. *Oncogene,* 32**,** 4397-405.

ZHANG, J., LU, C., KANG, J., CAO, C. & LI, M. 2013c. Involvement of ZEB1 and E-cadherin in the invasion of lung squamous cell carcinoma. *Mol Biol Rep,* 40**,** 949-56.

ZHANG, P., WEI, Y., WANG, L., DEBEB, B. G., YUAN, Y., ZHANG, J., YUAN, J., WANG, M., CHEN, D., SUN, Y., WOODWARD, W. A., LIU, Y., DEAN, D. C., LIANG, H., HU, Y., ANG, K. K., HUNG, M. C., CHEN, J. & MA, L. 2014. ATM-mediated stabilization of ZEB1 promotes DNA damage response and radioresistance through CHK1. *Nat Cell Biol,* 16**,** 864-75.

ZHANG, Q., BYKOV, V. J. N., WIMAN, K. G. & ZAWACKA-PANKAU, J. 2018. APR-246 reactivates mutant p53 by targeting cysteines 124 and 277. *Cell Death Dis,* 9**,** 439.

ZHANG, Y., LIM, C. U., WILLIAMS, E. S., ZHOU, J., ZHANG, Q., FOX, M. H., BAILEY, S. M. & LIBER, H. L. 2005. NBS1 knockdown by small interfering RNA increases ionizing radiation mutagenesis and telomere association in human cells. *Cancer Res,* 65**,** 5544-53.

ZHANG, Y., ZHOU, J. & LIM, C. U. 2006. The role of NBS1 in DNA double strand break repair, telomere stability, and cell cycle checkpoint control. *Cell Res,* 16**,** 45-54.

ZHENG, H.-C. 2017. The molecular mechanisms of chemoresistance in cancers. *Oncotarget,* 8**,** 59950-59964.

ZHU, H., LUO, H., ZHANG, W., SHEN, Z., HU, X. & ZHU, X. 2016. Molecular mechanisms of cisplatin resistance in cervical cancer. *Drug Des Devel Ther,* 10**,** 1885-95.

ZIMMERMANN, M. & DE LANGE, T. 2014. 53BP1: pro choice in DNA repair. *Trends Cell Biol,* 24**,** 108-17.